Journal of Healthcare Engineering

Data and Intelligence in Cyber Health

Lead Guest Editor: Khin wee Lai
Guest Editors: Abhra Roy Chowdhury and Hum Yan Chai

Data and Intelligence in Cyber Health

Journal of Healthcare Engineering

Data and Intelligence in Cyber Health

Lead Guest Editor: Khin wee Lai
Guest Editors: Abhra Roy Chowdhury and Hum Yan Chai

Contents

Retracted: Application of Intelligent Nursing Information System in Emergency Nursing Management
Journal of Healthcare Engineering
Retraction (1 page), Article ID 9875341, Volume 2023 (2023)

A Low-Cost Multistage Cascaded Adaptive Filter Configuration for Noise Reduction in Phonocardiogram Signal
S. Hannah Pauline, Samiappan Dhanalakshmi, R. Kumar, R. Narayanamoorthi, and Khin Wee Lai
Research Article (24 pages), Article ID 3039624, Volume 2022 (2022)

Radiological Analysis of COVID-19 Using Computational Intelligence: A Broad Gauge Study
S. Vineth Ligi, Soumya Snigdha Kundu, R. Kumar, R. Narayanamoorthi, Khin Wee Lai, and Samiappan Dhanalakshmi
Review Article (25 pages), Article ID 5998042, Volume 2022 (2022)

Construction of a Diagnostic Model for Lymph Node Metastasis of the Papillary Thyroid Carcinoma Using Preoperative Ultrasound Features and Imaging Omics
Chao Zhang, Lihua Cheng, Weiwen Zhu, Jian Zhuang, Tong Zhao, Xiaoqin Li, and Wenfeng Wang
Research Article (10 pages), Article ID 1872412, Volume 2022 (2022)

Cloud-Based Fault Prediction Using IoT in Office Automation for Improvisation of Health of Employees
Mudita Uppal, Deepali Gupta, Sapna Juneja, Gaurav Dhiman, and Sandeep Kautish
Review Article (13 pages), Article ID 8106467, Volume 2021 (2021)

Management and Plan of Undergraduates' Mental Health Based on Keyword Extraction
Weifeng Zhang
Research Article (9 pages), Article ID 3361755, Volume 2021 (2021)

[Retracted] Application of Intelligent Nursing Information System in Emergency Nursing Management
Qing Li and Yujie Chen
Research Article (13 pages), Article ID 3998830, Volume 2021 (2021)

5G Edge Computing Enabled Directional Data Collection for Medical Community Electronic Health Records
Xiaoqiang Yan and Xiaogang Ren
Research Article (12 pages), Article ID 5598077, Volume 2021 (2021)

Three-Dimensional Finite Element Analysis of L4-5 Degenerative Lumbar Disc Traction under Different Pushing Heights
Huaili Ding, Lijun Liao, Peichun Yan, Xiaolin Zhao, and Min Li
Research Article (9 pages), Article ID 1322397, Volume 2021 (2021)

Medical Internet of Things to Realize Elderly Stroke Prevention and Nursing Management
Xin Li, Sufen Ren, and Fangqiu Gu
Research Article (12 pages), Article ID 9989602, Volume 2021 (2021)

Artificial Intelligence Analysis of EEG Amplitude in Intensive Heart Care
Junjun Chen, Hong Pu, and Dianrong Wang
Research Article (9 pages), Article ID 6284035, Volume 2021 (2021)

Application of a Computerized Decision Support System to Develop Care Strategies for Elderly Hemodialysis Patients
Yiqiu Zhu and Xiyi Zheng
Research Article (10 pages), Article ID 5060484, Volume 2021 (2021)

Research on Geriatric Care for Equalizing the Topological Layout of Health Care Infrastructure Networks
Rui Liu, Miao Du, Jun Shen, Xiaolan Wang, and Ying Jiang
Research Article (13 pages), Article ID 8306479, Volume 2021 (2021)

Hindawi
Journal of Healthcare Engineering
Volume 2023, Article ID 9875341, 1 page
https://doi.org/10.1155/2023/9875341

Retraction

Retracted: Application of Intelligent Nursing Information System in Emergency Nursing Management

Journal of Healthcare Engineering

Received 17 October 2023; Accepted 17 October 2023; Published 18 October 2023

This article has been retracted by Hindawi following an investigation undertaken by the publisher [1]. This investigation has uncovered evidence of one or more of the following indicators of systematic manipulation of the publication process:

(1) Discrepancies in scope
(2) Discrepancies in the description of the research reported
(3) Discrepancies between the availability of data and the research described
(4) Inappropriate citations
(5) Incoherent, meaningless and/or irrelevant content included in the article
(6) Peer-review manipulation

The presence of these indicators undermines our confidence in the integrity of the article's content and we cannot, therefore, vouch for its reliability. Please note that this notice is intended solely to alert readers that the content of this article is unreliable. We have not investigated whether authors were aware of or involved in the systematic manipulation of the publication process.

In addition, our investigation has also shown that one or more of the following human-subject reporting requirements has not been met in this article: ethical approval by an Institutional Review Board (IRB) committee or equivalent, patient/participant consent to participate, and/or agreement to publish patient/participant details (where relevant).

Wiley and Hindawi regrets that the usual quality checks did not identify these issues before publication and have since put additional measures in place to safeguard research integrity.

We wish to credit our own Research Integrity and Research Publishing teams and anonymous and named external researchers and research integrity experts for contributing to this investigation.

The corresponding author, as the representative of all authors, has been given the opportunity to register their agreement or disagreement to this retraction. We have kept a record of any response received.

References

[1] Q. Li and Y. Chen, "Application of Intelligent Nursing Information System in Emergency Nursing Management," *Journal of Healthcare Engineering*, vol. 2021, Article ID 3998830, 13 pages, 2021.

Hindawi
Journal of Healthcare Engineering
Volume 2022, Article ID 3039624, 24 pages
https://doi.org/10.1155/2022/3039624

Research Article

A Low-Cost Multistage Cascaded Adaptive Filter Configuration for Noise Reduction in Phonocardiogram Signal

S. Hannah Pauline,[1] **Samiappan Dhanalakshmi**,[1] **R. Kumar**,[1] **R. Narayanamoorthi**,[2] **and Khin Wee Lai**[3]

[1]*Department of Electronics and Communication Engineering, College of Engineering and Technology, Faculty of Engineering and Technology, SRM Institute of Science and Technology, SRM Nagar, Kattankulathur 603203, Kanchipuram, Chennai, Tamil Nadu, India*
[2]*Department of Electrical and Electronics Engineering, College of Engineering and Technology, Faculty of Engineering and Technology, SRM Institute of Science and Technology, SRM Nagar, Kattankulathur 603203, Kanchipuram, Chennai, Tamil Nadu, India*
[3]*Department of Biomedical Engineering, Faculty of Engineering, Universit Malaya, Kuala Lumpur 50603, Malaysia*

Correspondence should be addressed to Samiappan Dhanalakshmi; dhanalas@srmist.edu.in and Khin Wee Lai; lai.khinwee@um.edu.my

Received 23 June 2021; Revised 10 August 2021; Accepted 21 March 2022; Published 30 April 2022

Academic Editor: Cosimo Ieracitano

Phonocardiogram (PCG), the graphic recording of heart signals, is analyzed to determine the cardiac mechanical function. In the recording of PCG signals, the major problem encountered is the corruption by surrounding noise signals. The noise-corrupted signal cannot be analyzed and used for advanced processing. Therefore, there is a need to denoise these signals before being employed for further processing. Adaptive Noise Cancellers are best suited for signal denoising applications and can efficiently recover the corrupted PCG signal. This paper introduces an optimal adaptive filter structure using a Sign Error LMS algorithm to estimate a noise-free signal with high accuracy. In the proposed filter structure, a noisy signal is passed through a multistage cascaded adaptive filter structure. The number of stages to be cascaded and the step size for each stage are adjusted automatically. The proposed Variable Stage Cascaded Sign Error LMS (SELMS) adaptive filter model is tested for denoising the fetal PCG signal taken from the SUFHS database and corrupted by Gaussian and colored pink noise signals of different input SNR levels. The proposed filter model is also tested for pathological PCG signals in the presence of Gaussian noise. The simulation results prove that the proposed filter model performs remarkably well and provides 8–10 dB higher SNR values in a Gaussian noise environment and 2-3 dB higher SNR values in the presence of colored noise than the existing cascaded LMS filter models. The MSE values are improved by 75–80% in the case of Gaussian noise. Further, the correlation between the clean signal and its estimate after denoising is more than 0.99. The PSNR values are improved by 7 dB in a Gaussian noise environment and 1-2 dB in the presence of pink noise. The advantage of using the SELMS adaptive filter in the proposed filter model is that it offers a cost-effective hardware implementation of Adaptive Noise Canceller with high accuracy.

1. Introduction

The phonocardiogram signal [1] contains important information about the heart's operations and is used to detect various heart disorders [2]. However, recording PCG signals and other biomedical signals [3, 4] is very challenging since they are susceptible to environmental noise apart from the other noise signals [5]. As a result, denoising of PCG signals is a mandatory requirement before its analysis [6]. Nevertheless, denoising a PCG signal to increase signal quality by removing the background noise is difficult. The accuracy of results is determined by the performance of denoising algorithms used, which diminishes as the noise level rises [7]. Various PCG signal denoising approaches have been

proposed in the literature based on the time and frequency domain [8]. Frequency domain methods are preferred since they contain adequate information on the spectral characteristics of the PCG signal components [9]. Among the frequency domain approaches, the most commonly used techniques are Empirical Mode Decomposition (EMD) [10, 11], Variational Mode Decomposition (VMD) [12], Singular Spectrum Analysis (SSA) [13], and Tunable Q-Wavelet Transform [14]. Although these techniques give an efficient performance, the computational time is high. Compared to all the proposed techniques for PCG signal denoising, the Discrete Wavelet Transform (DWT) [15, 16] is more effective and performs better in a noisy environment. However, it requires a predefined basis function to produce optimal SNR values. In this paper, we have explored the possibility of applying the Adaptive Noise Cancellation technique using adaptive filters, which is predominantly used for signal denoising in telecommunication to PCG signal denoising. Adaptive filters provide the best estimate of clean signals with automatic performance adaptation. Adaptive algorithms employed in adaptive filters track the dynamic variations in the signal and modify their behavior according to the input signal; therefore, they are used in several applications, including echo [17, 18] and noise cancellation [19], noise reduction [20], signal enhancement [21, 22] adaptive equalization [23], and line enhancement [24]. The fundamental Adaptive Noise Canceller is depicted in Figure 1.

The primary input signal provided to the ANC is the noisy signal $d(n)$ defined as

$$d(n) = s(n) + v(n), \tag{1}$$

where $s(n)$ is the noise-free signal and $v(n)$ is the added noise signal. $s(n)$ and $v(n)$ are not time correlated to each other, and the input signal to the filter $x(n)$ is a noise signal in time correlated to $v(n)$. The adaptive filter gives the replica of the noise signal and $\widehat{v}(n)$ as

$$y(n) = \mathbf{w}^T(n)\mathbf{x}(n), \tag{2}$$

where $\mathbf{w}(n) = [w_0, w_1, \ldots w_{M-1}]^T$ and $\mathbf{x}(n) = [x_0(n), x_1(n-1), \ldots x_{M-1}(n-M+1)]^T$ are weights of the filter and its input, respectively, M is the order of filter, and the error signal is computed as

$$\begin{aligned} e(n) &= d(n) - y(n) \\ &= d(n) - \widehat{v}(n), \end{aligned} \tag{3}$$

such that the effect of noise is minimal. The efficiency of the adaptive filter is improved by using suitable algorithms like LMS and its variants. Due to its feasible implementation and robustness, the LMS adaptive algorithm [25] is commonly used. Sign Error LMS adaptive algorithm has less number of computations than the LMS algorithm but to achieve a good performance, smaller step size should be used. The SE LMS algorithm, however, suffers from low convergence speeds. The convergence speed can be improved and the steady-state MSE minimized by optimizing the adaptive filter structure [26] as suggested by several researchers. The cascaded

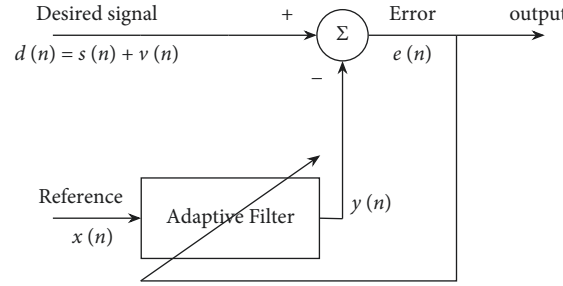

Figure 1: Block representation of ANC.

adaptive filter structure was first proposed by Ahmed et al. [27] for the detection of multiple sinusoids. The cascaded filter structure is effectively employed to enhance and track multiple sinusoids. A cascaded structure of the FIR filter proposed by Prandoni and Vetterli [28] for adaptive linear prediction proves that, compared to a single-stage filter, a cascaded structure converges faster to an optimal predictor. The major advantage pointed out in [28] is the computational efficiency of the cascaded adaptive filter structure. For lossless compression of audio signals, several techniques have been proposed in literature based on Laplacian distribution [29], decoupled approach [30], context model [31], linear transforms [32], and linear prediction [33]. However, the nonstationary feature of audio signals requires the use of an adaptive filtering approach [34] for lossless audio coding since adaptive filters provide good tracking capability. A cascade combination of higher-order LMS filter and lower-order RLS filter proposed by Yu and Ko [35] is used as a predictor for lossless audio coding. This cascaded RLS-LMS predictor provides faster convergence and superior prediction gain as it uses a cascade combination of low complexity LMS filter and high converging RLS filter models. For MPEG-4 lossless audio coding [36], the cascaded RLS-LMS predictor attains the best compression ratio. In ANC (Active Noise Cancellation) systems, the Filtered × Least Mean Square (FxLMS) algorithm [37] is widely applied for efficient noise cancellation. Nevertheless, the FxLMS algorithm's steady-state performance is affected by the presence of uncorrelated noise at the error sensor. The cascaded adaptive filtering approach proposed by [38] is successful in preventing ANC filter coefficient oscillation, thus improving the convergence speed. In mechanical and automobile engineering, denoising engine vibrations and other types of noise are of interest to several researchers. Median filtering [39] and wavelet packet threshold denoising [40] are prominent among the existing noise and vibration denoising techniques. More recently, a combination of median filtering and wavelet packet denoising has been effectively used for vibration signal denoising [41]. Adaptive filtering is applied to active noise and control due to its self-tuning capability. For engine noise suppression [42], the use of cascaded LMS adaptive filter models shows that the adaptation of the filter speed is improved. Recently Multistage Adaptive LMS (MSA-LMS) algorithm proposed by [43] has been applied to active vibration and noise control systems and given remarkable performance for signals with complex frequency spectra. Multilevel Adaptive Noise Cancellers have proven to

be very effective in AE- (Acoustic Emission-) based methods to detect rail defects. The simple wavelet hard threshold denoising method [44] causes a loss of useful information and cannot change according to the noise signal variations. To eliminate complex noise and retain the information signal at fast speeds, multilevel noise cancellation based on SANC (Self-Adaptive Noise Cancellation) and ANC is proposed by Zhang et al. in [45], which proves to provide good noise suppression capabilities. Adaptive filtering plays a significant role in biomedical engineering to remove noise and artifacts from ECG signals. The presence of artifacts is one of the crucial challenges in ambulatory ECG monitory systems. For motion artifact removal, several techniques are proposed, and they can be categorized into two, namely, adaptive filtering and Blind Source Separation (BSS) [46]. Although the BSS approach can provide good filtering performance, the adaptive filtering-based approach has a more practical advantage due to its computational simplicity and adaptability to meet the hardware requirements of the system [47]. The efficient removal of artifacts from ambulatory ECG signals [47] is achieved using a cascaded LMS adaptive filter model. Efficient elimination of multiple noise signals from ECG signal [48] is obtained with high output SNR value and faster convergence speed by using a multistage modified NLMS algorithm. A novel 2-stage cascaded LMS adaptive filter configuration is proposed by Dixit in [49] and a 3-stage [50] cascaded LMS adaptive filter by Maurya for Adaptive Noise Cancellation. The proposed cascaded adaptive filter architectures are tested for denoising sinusoidal signals. It has been proved that, compared to traditional LMS adaptive filters, the 2-stage and 3-stage cascaded LMS adaptive filter architectures proposed for Adaptive Noise Cancellation provide better efficiency in terms of SNR and MSE performance.

The above studies show that, for several applications, including Active Noise Control, signal enhancement, linear prediction, noise cancellation, and suppression, the cascaded adaptive filter model performs better than the conventional single-stage adaptive filter in convergence speed and MSE. The above studies have not explored the possibility of varying the number of cascaded filter stages required for the ANC to reach its optimal performance in terms of MSE and convergence speed. The number of cascaded stages and the step size for each stage are fixed in the above-proposed structures. In this work, we propose a novel Variable Stage Cascaded Sign Error (SE) LMS adaptive filter structure wherein the number of filter stages to be cascaded to give optimal performance in steady-state MSE is selected automatically. In contrast, in the existing cascaded filter models, the number of cascaded stages is fixed. To obtain a faster convergence speed, the step size should be adjusted at each stage. The number of cascaded filter stages and the step size for each stage are adjusted automatically to achieve optimal performance regarding steady-state MSE and convergence speed in the proposed filter structure. We have also analyzed the behavior of the proposed filter model using a fixed step size for all the stages. The novelty of the proposed Variable Stage Cascaded SE LMS adaptive filter model is summarized as follows:

(i) Using Sign Error LMS adaptive filter in a cascaded configuration to denoise PCG signals to reduce the hardware cost.

(ii) Automatic adjustment of an optimal number of stages to obtain efficient performance in terms of convergence speed of steady-state MSE.

(iii) Automatic adjustment of the step size of the adaptive filter at each stage ANC to improve the convergence speed.

Compared to the existing signal denoising techniques, the primary advantage of the proposed filter model is the reduction in computational complexity. The proposed filter model employs the SE LMS [51] algorithm for adaptation, which requires a minimum number of computations and provides a low-cost and straightforward implementation of a hardware processor for efficient denoising of PCG signals. Further, the automatic addition of an optimal number of stages provides a minimum MSE value, and the adjustment of step size at each stage helps achieve faster convergence speeds. The results indicate that the proposed Variable Stage (VS) Cascaded Sign Error LMS adaptive filter model provides minimum steady-state MSE and faster convergence speed. The proposed Variable Stage Cascaded SE LMS adaptive filter model is detailed in Section 2. Section 3 includes the MATLAB simulation results, thus verifying the proposed method's effectiveness, the results are discussed in Section 4, and a conclusion with the future scope is included in Section 5.

2. Proposed Variable Stage (VS) Cascaded Sign Error LMS Adaptive Filter Structure

The use of the LMS adaptive algorithm in conventional ANC systems leads to a computationally simpler structure with superior robustness and stability. LMS algorithm is more suited for software implementation. The Sign Error LMS algorithm, a variant of the LMS algorithm, gives a computationally more straightforward and cost-effective implementation of Adaptive Noise Cancellation. It suffers from slow convergence and large steady-state MSE compared to the LMS algorithm. The performance degradation can be avoided by using a smaller step size than the LMS algorithm. Also, the cascaded adaptive filter structure employed in the ANC system helps to reduce the steady-state MSE and increase its convergence speed. We proposed a multistage cascaded configuration of adaptive filters using the Sign Error LMS adaptation algorithm at each stage. The features of the proposed Variable Stage (VS) Cascaded Sign Error (SE) LMS adaptive filter model are as follows:

(i) The number of stages to be cascaded to provide optimal steady-state MSE and convergence speed is automatically varied.

(ii) The step size of the Sign Error LMS adaptation algorithm is adjusted at each stage automatically to improve the convergence speed of the steady-state MSE.

Figure 2 depicts the block diagram representation of the proposed Variable Stage (VS) Cascaded Sign Error (SE) LMS

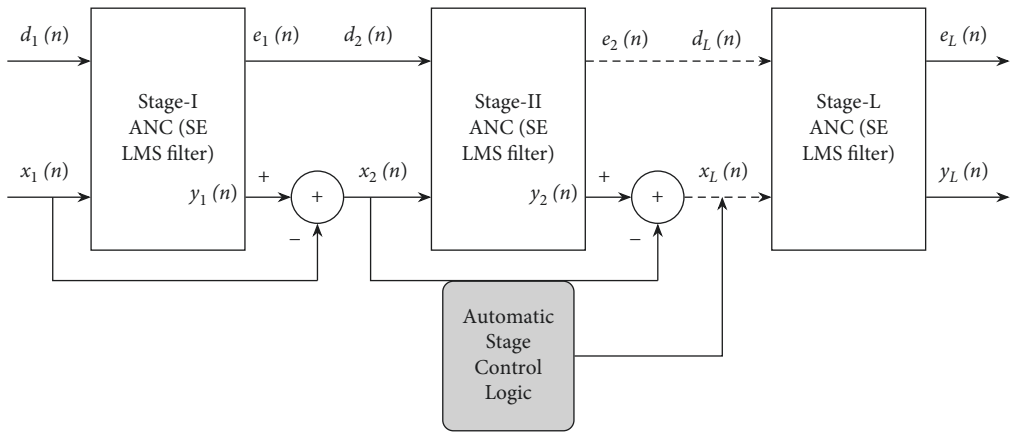

Figure 2: Block diagram of proposed Variable Stage Cascaded SE LMS adaptive filter model.

adaptive filter model, and the schematic diagram is depicted in Figure 3. As depicted in Figure 3, the primary input signal to stage I ANC is the noisy signal $d_1(n) = s(n) + v(n)$, and the reference input signal is the noise signal $v'(n)$ correlated to $v(n)$. The primary input signal to stage II ANC $d_2(n)$ is the output error signal $e_1(n)$ of stage I, and the reference input signal to stage II adaptive filter $x_2(n)$ is the residual reference noise signal from stage I, $x_1(n) - y_1(n)$. In the same way, the error signal of each stage ANC $e_i(n)$ is given to the next stage ANC as its primary input signal $d_{i+1}(n)$, and the reference noise input to the i^{th} stage $x_i(n)$ is the residual reference noise $x_{i-1}(n) - y_{i-1}(n)$ from the preceding $(i-1)^{\text{th}}$ stage ANC. The number of stages to be cascaded to attain optimal performance is adjusted automatically, and the step size of the adaptive filter at each stage is controlled automatically.

The parameters of stage I ANC using the Sign Error LMS algorithm are as follows:

Primary input signal

$$d_1(n) = s(n) + v(n). \tag{4}$$

Reference input signal

$$x_1(n) = v'(n). \tag{5}$$

Filter output

$$\begin{aligned} y_1(n) &= \mathbf{w}_1^T(n)\mathbf{x}_1(n) \\ &= \mathbf{w}_1^T(n)\mathbf{v}'(n) \\ &= \widehat{v}(n), \end{aligned} \tag{6}$$

where $\mathbf{w}_1(n) = [w_0, w_2, \ldots w_{M-1}]^T$ and $\mathbf{x}_1(n) = [x_0(n), x_1(n-1), \ldots x_{M-1}(n-M+1)]^T$ are weights of the filter and its input, respectively, at stage I, and M is the filter order.

Weight update equation

$$\mathbf{w}_1(n+1) = \mathbf{w}_1(n) + \mu_{1\text{SELMS}}\text{sgn}\left[e_1(n)\right]\mathbf{v}'(n), \tag{7}$$

where $\mu_{1\text{SELMS}}$ is the step size of Sign Error LMS filter.

Output error

$$\begin{aligned} e_1(n) &= d_1(n) - y_1(n) \\ &= s(n) + v(n) - \widehat{v}(n) \\ &= s(n) + \Delta v(n), \end{aligned} \tag{8}$$

where $\Delta v(n) = v(n) - \widehat{v}(n)$ is the noise signal to be minimized.

The parameters of stage II ANC are as follows:

Primary input signal

$$\begin{aligned} d_2(n) &= e_1(n) \\ &= d_1(n) - \widehat{v}(n) \\ &= s(n) + \Delta v(n). \end{aligned} \tag{9}$$

Reference input signal

$$x_2(n) = x_1(n) - y_1(n) = v'(n) - \widehat{v}(n) = \Delta v'(n). \tag{10}$$

Filter output

$$\begin{aligned} y_2(n) &= \mathbf{w}_2^T(n)\mathbf{x}_2(n) \\ &= \mathbf{w}_2^T(n)\Delta\mathbf{v}'(n) \\ &= \Delta\widehat{v}(n). \end{aligned} \tag{11}$$

Weight update equation

$$\mathbf{w}_2(n+1) = \mathbf{w}_2(n) + \mu_{2\text{SELMS}}\text{sgn}\left[e_2(n)\right]\Delta\mathbf{v}'(n). \tag{12}$$

Output error

$$e_2(n) = d_2(n) - y_2(n) = s(n) + \Delta v(n) - \Delta\widehat{v}(n) = s(n) + \delta v(n), \tag{13}$$

where $\delta v(n) = \Delta v(n) - \Delta\widehat{v}(n)$ is the remaining noise to be minimized. The number of stages to be cascaded is adjusted till the L^{th} optimal stage is reached. The parameters of stage L ANC are as follows:

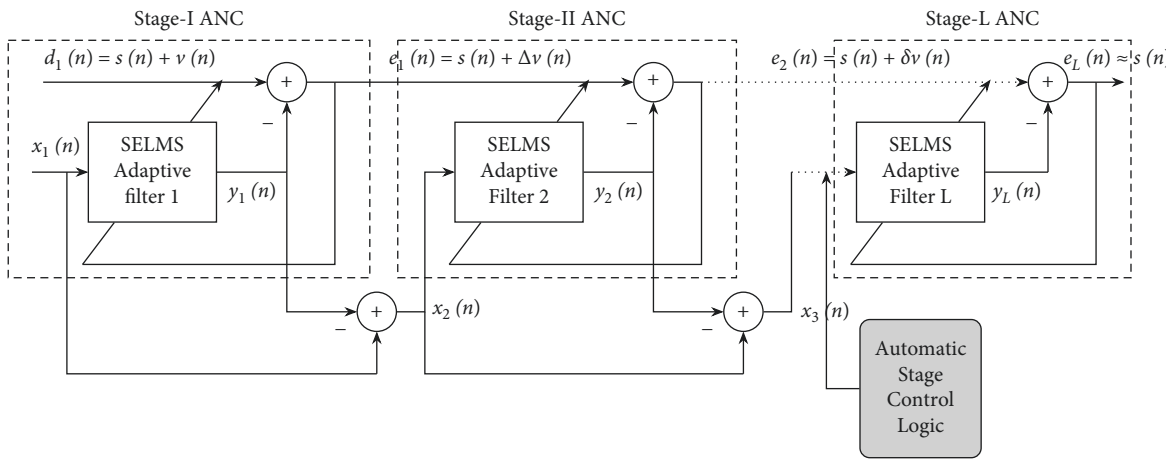

Figure 3: Schematic diagram of proposed Variable Stage Cascaded SE LMS adaptive filter model.

Primary input signal

$$\begin{aligned} d_L(n) &= e_{L-1}(n) \\ &= s(n) + \rho v(n), \end{aligned} \tag{14}$$

where $\rho v(n)$ is a minimal noise.

Reference input signal

$$\begin{aligned} x_L(n) &= x_{L-1}(n) - y_{L-1}(n) \\ &= \rho v'(n). \end{aligned} \tag{15}$$

Filter output

$$\begin{aligned} y_L(n) &= \mathbf{w}_L^T(n)\mathbf{x}_L(n) \\ &= \mathbf{w}_L^T(n)\rho\mathbf{v}'(n) \\ &= \rho\widehat{v}(n). \end{aligned} \tag{16}$$

Weight update equation

$$\mathbf{w}_L(n+1) = \mathbf{w}_L(n) + \mu_{\text{LSELMS}}\operatorname{sgn}\left[e_L(n)\right]\mathbf{x}_L(n). \tag{17}$$

Output error

$$\begin{aligned} e_L(n) &= d_L(n) - y_L(n) \\ &= s(n) + \rho v(n) - \rho\widehat{v}(n) \approx s(n), \end{aligned} \tag{18}$$

where $\rho v(n) - \rho\widehat{v}(n) = \eta v(n)$, where η is a very small quantity. The above analysis ensures that, by adjusting the number of filter stages to its optimum value $L = L_{opt}$, the noise is minimized further, and thus steady-state MSE reduces significantly. The employment of automatic stage selection gives optimal performance in steady-state MSE, and the convergence speed is further improved by using different step size for each stage. The appropriate step size at each stage is also selected automatically. The closest estimate of the noise-free signal is obtained as the filter reaches its optimal stage. This signal $e_L(n) \approx s(n)$ is closely related or in time correlated to the clean signal $s(n)$.

2.1. Mean Square Error (MSE). The error signal at the optimal stage is

$$\begin{aligned} e_L(n) &= d_L(n) - y_L(n) \\ &= s(n) + v(n) - y_1(n) - y_2(n) - \ldots - y_L(n) \\ &= s(n) + v(n) - \left[y_1(n) + y_2(n) + \cdots + y_L(n)\right]. \end{aligned} \tag{19}$$

At the optimal stage L of the ANC, $y_1(n) + y_2(n) + \cdots + y_L(n) = \widetilde{v}(n)$ (replica of $v(n)$) and the MSE is denoted as

$$\begin{aligned} E\left[\left|e_L(n)\right|^2\right] &= E\left[\left|s(n)\right|^2\right] + E\left[\left|v(n) - \widetilde{v}(n)\right|^2\right] \\ &\quad - 2E\left[\left|s(n)\left(v(n) - \widetilde{v}(n)\right)\right|\right] \\ &= E\left[\left|s(n)\right|^2\right] + E\left[\left|v(n) - \widetilde{v}(n)\right|^2\right] \\ &\quad - 2E\left[\left|s(n)v(n)\right|\right] + 2E\left[\left|s(n)\widetilde{v}(n)\right|\right]. \end{aligned} \tag{20}$$

The following equation is obtained due to the uncorrelation between noise $v(n)$ and the information signal $s(n)$.

$$2E\left[\left|s(n)v(n)\right|\right] = 0. \tag{21}$$

Meanwhile, $s(n)$ and output of the adaptive filter $\widehat{v}(n)$ are also uncorrelated; hence, the following is stated:

$$2E\left[\left|s(n)\widetilde{v}(n)\right|\right] = 0. \tag{22}$$

Inserting equations (21) and (22) in (20),

$$E\left[\left|e_L(n)\right|^2\right] = E\left[\left|s(n)\right|^2\right] + E\left[\left|v(n) - \widetilde{v}(n)\right|^2\right]. \tag{23}$$

Further, it is observed that the best replica of the information signal $s(n)$ is achieved as the term $E[|v(n) - \widetilde{v}(n)|^2]$ is minimized. It means that, at the optimal filter stage L, $y_1(n) + y_2(n) + \cdots + y_L(n)$ is as close to $v(n)$ as possible, and hence, $E[|v(n) - \widetilde{v}(n)|^2]$ is minimized. The equation is represented as

$$\left[y_1(n) + y_2(n) + \cdots + y_L(n)\right] \approx v(n). \tag{24}$$

The above analysis proves that the noise signal can be removed from the input signal $d_1(n)$ by adjusting the

number of stages of the filter, and $O(n)$ represents the denoised signal from the ANC.

$$O(n) = e_L(n) \approx s(n). \tag{25}$$

From the above analysis, we infer that the denoised signal $O(n)$ is obtained as the number of stages in the cascaded filter structure approaches its optimal value.

2.2. Automatic Stage Selection Control Logic. The above analysis concludes that the MSE value reaches its minimum only at the filter's optimal stage. To calculate the optimum filter stage, we estimate the Pearson cross-correlation function between the error signal of each stage $e_i(n)$ and the reference input noise signal $v'(n)$. We have assumed that the reference noise signal $v'(n)$ to stage I adaptive filter is correlated to the additive noise signal $v(n)$ but is uncorrelated to the clean signal $s(n)$. The error output of each stage ANC is an estimate of the clean signal; that is, $e_i(n) = \hat{s}(n)$; therefore, the correlation between $e_i(n)$ and $v'(n)$ reduces as the filter reaches its optimal stage. The estimated correlation function between $e_i(n)$ and $v'(n)$ is defined as

$$\rho_{e_i,v'} = \frac{\mathrm{Cov}(e_i, v')}{\sigma_{e_i}\sigma_{v'}}, \tag{26}$$

where $\rho_{e_i,v'}$ is the Pearson product-moment correlation coefficient, $\mathrm{Cov}(e_i, v')$ is the covariance of variables e_i and v', and σ_{e_i} and $\sigma_{v'}$ are the standard deviation of e_i and standard deviation of v'. In the proposed method, $e_i(n)$ is the estimate of the clean signal at each stage and $v'(n)$ is the reference noise signal used at stage I. Since we have presumed that the information signal $s(n)$ and the added noise are uncorrelated, the value of $\rho_{e_i,v'}$ should be low. The estimated correlation function $\rho_{e_i,v'}$ is investigated at each stage, and further adaptive filter stages are added until the value of $\rho_{e_i,v'}$ reaches a minimal threshold value at the optimal cascaded filter stage.

2.3. Variable Step Size for Each Stage. The performance of the Sign Error LMS algorithm can be as good as LMS algorithms if we select a step-size value lower than the LMS algorithm. Thus, the step size of the Sign Error LMS algorithm is selected based on the LMS algorithm. The major challenge with the LMS algorithm is the choice of step size. A significant step size results in fast adaptation but provides a large excess Mean Square Error (excess MSE). A too-large step size will lead to a loss of stability. On the other hand, a too-small step-size result in slow convergence even though the excess MSE is minimum. The upper bound for step size in order to sustain the stability of the LMS algorithm is given by [52]

$$0 < \mu < \frac{2}{\lambda_{\max}}, \tag{27}$$

where μ is the step size and $\lambda_{\max}$ is the largest eigenvalue of the autocorrelation matrix of the input signal $x(n)$. In the proposed filter model, the input to each filter stage is the residual reference noise from the previous stage; hence, different input signal is given to the filter at each stage. Therefore, instead of using the same step-size value for all the stages, using different step size at each stage improves the filter's speed of adaptation. We select a fixed value of step size for stage I adaptive filter by first finding $\mu_{1\max}$ and then selecting the step size for the LMS algorithm using equation (27) as $\mu_{1LMS} \le \mu_{1\max}$. Then, we divide this value by $x = 10$ to obtain the step size of Sign Error LMS at stage I.

$$\begin{aligned} \mu_{1\mathrm{SELMS}} &= \frac{\mu_{1\mathrm{LMS}}}{x} \\ &= \frac{\mu_{1\mathrm{LMS}}}{10}, \end{aligned} \tag{28}$$

where $x = 10$ is selected by using the trial and error method. At stage II, the input to the adaptive filter is $x_2(n) = x_1(n) - y_1(n)$, which means that the input signal to the filter changes at each stage and based on the input, the upper bound for step size also changes. At stage II, we calculate the upper bound of step size $\mu_{2\max}$ for the LMS algorithm using equation (27). Then, the value of $\mu_{2\max}$ is compared with $\mu_{1\max}$. If $\mu_{2\max} > \mu_{1\max}$, then a higher step size is desired for the stage II adaptive filter. Therefore, we set $\mu_{2LMS} = \mu_{1LMS} * k$ and

$$\begin{aligned} \mu_{2\mathrm{SELMS}} &= \frac{\mu_{1\mathrm{LMS}}}{10} * k \\ &= \mu_{1\mathrm{SELMS}} * k, \end{aligned} \tag{29}$$

where k is a constant selected by trial and error method. Otherwise, if $\mu_{2\max} < \mu_{1\max}$, then a smaller step size is required, so we adjust $\mu_{2LMS} = \mu_{1LMS} * 1/k$ and

$$\begin{aligned} \mu_{2\mathrm{SELMS}} &= \frac{\mu_{1\mathrm{LMS}}}{10} * \frac{1}{k} \\ &= \mu_{1\mathrm{SELMS}} * \frac{1}{k}. \end{aligned} \tag{30}$$

In this way, the step size for the filter at each stage is adjusted as

$$\mu_i = \begin{cases} \mu_{i-1} * (k), & \mu_{\max_i} > \mu_{\max_{i-1}}, \\ \mu_{i-1} * \left(\dfrac{1}{k}\right), & \mu_{\max_i} < \mu_{\max_{i-1}}, \end{cases} \tag{31}$$

where μ denotes the step size of SE LMS filter at i^{th} and $(i-1)^{\mathrm{th}}$ stage, $\mu_{\max}$ denotes the upper bound of step size for LMS filter, and $'k'$ is a constant value that varies between 1 and 2; selecting the $'k'$ value is crucial for the convergence of the filter stage. The proposed Variable Stage Cascaded SE LMS adaptive filter model that uses variable step size for each stage has a faster convergence speed than fixed step size for all stages.

By automatically adjusting the number of cascaded stages and the step size at each stage, the steady-state MSE reduces, and convergence speed is improved. Proposed Variable Stage Cascaded SE LMS adaptive filter model used for Adaptive Noise Canceller is summarized in Algorithm 1.

(1) Stage I ANC primary input signal = $d_1(n) = s(n) + v(n)$
(2) Stage I adaptive filter reference input signal = $x_1(n) = v'(n)$
(3) Step-size parameter $\mu_{1\text{SELMS}} = \mu_{1\text{LMS}}/10$ for stage I Sign Error LMS adaptive filter
(4) Filter order = M
(5) Iterations = N
(6) $\rho_{\text{threshold}}$; k
(7) **Outputs**
(8) Stages (L), Error (e), Filter outputs (y), Weights (w)
(9) **Execution**
(10) Compute $\mu_{\max_1} = 2/\lambda_{\max_1}$
(11) Compute the parameters for stage I ANC using SELMS adaptive algorithm.
(12) $y_1(n) = w_1^T x_1$
(13) $w_1(n+1) = w_1(n) + \mu_{1\text{SELMS}}\text{sgn}[e_1(n)]x_1(n)$
(14) $e_1(n) = d_1(n) - y_1(n)$
(15) Calculate the correlation $\rho_{e_i v'}$ between error signal and reference input signal at stage I
(16) $i = 1$
(17) **while** $\rho_{e_i v'} > \rho_{\text{threshold}}$ **do**
(18) $\quad i = i + 1$
(19) $\quad x_i(n) = x_{i-1}(n) - y_{i-1}(n)$
(20) $\quad \mu_{\max_i} = 2/\lambda_{\max_i}$
(21) $\quad d_i(n) = e_{i-1}(n)$
(22) $\quad$ **if** $\mu_{\max_i} < \mu_{\max_{i-1}}$ **then**
(23) $\quad\quad \mu_{\text{iSELMS}} = \mu_{(i-1)\text{SELMS}} * 1/k$;
(24) $\quad$ **else**
(25) $\quad\quad \mu_{i\text{SELMS}} = \mu_{(i-1)\text{SELMS}} * k$
(26) $\quad$ **end**
(27) $\quad y_i(n) = w_i^T x_i$
(28) $\quad w_i(n+1) = w_i(n) + \mu_{i\text{SELMS}}\text{sgn}[e_i(n)]x_i(n)$
(29) $\quad e_i(n) = d_i(n) - y_i(n)$
(30) $\quad \rho_{e_i y_i} = \text{corr}(e_i, v')$
(31) $\quad \mu_{\max_i} = 2/\lambda_{\max_i}$
(32) **end**

Algorithm 1: Proposed Variable Stage Cascaded Sign Error LMS adaptive filter.

3. Results

The performance of the proposed Variable Stage Cascaded SE LMS adaptive filter is tested for fetal PCG (PhonoCardioGram) signal taken from the Shiraz University Fetal Heart Sounds Database (SUFHSDB) [53, 54]. A fetal PCG signal (f1) of duration 2 s was taken from the SUFH database, sampled at 16 kHz. The signal is corrupted by Gaussian and colored (pink) noise of input SNR +4 and −4. It is used to evaluate the signal denoising performance of the proposed filter model. We have also evaluated the proposed filter's performance for two different pathological PCG signals of 2 ms duration taken from the PhysioNet database [55, 56] in the presence of Gaussian noise. The proposed filter output is compared to other recently proposed cascaded filter models objectively in terms of MSE, SNR, ANR, PSNR [57, 58], correlation coefficient (CC) [59, 60], and Mean Absolute Error (MAE) and subjectively in terms of the output signal quality. Simulation parameters are as follows: filter length $M = 2$; the fixed step size used for the adaptive filter is 0.01. The value of parameter k is selected as two. The value of $\rho_{\text{threshold}}$ is appropriately selected depending on the input SNR level, noise added, and output desired. Simulation is conducted in MATLAB version 2017b to extract the clean signal from the noise-corrupted signal.

4. Performance of Proposed Variable Stage Cascaded SE LMS Adaptive Filter for the Fetal PCG Signals

4.1. Subjective Performance Evaluation. The subjective performance evaluation of the proposed Variable Stage Cascaded SE LMS adaptive filter in output signal quality is depicted below. Two different noises are added to the signal, and the performance of the proposed filter is noted in the presence of Gaussian and pink noise.

(a) *Gaussian Noise Environment*. The restoration of clean fetal PCG signal deteriorated by Gaussian noise of input SNR = +4 dB is shown in Figure 4. We infer from Figure 4(d) that the replica of the clean signal is obtained at stage 3 using the proposed filter model. Figure 5 depicts the progressive restoration of the signal at stages 1, 2, and 3. As depicted in Figures 5(b)–5(d), the signal is more corrupted by the noise at stage 1, and progressively, the noise reduces by adding more stages. The best estimate of the clean signal is achieved at stage 3. In Figure 6, the output of the proposed filter is compared with the conventional Sign Error LMS filter and the existing 2-stage [49] and 3-stage [50] cascaded adaptive filter

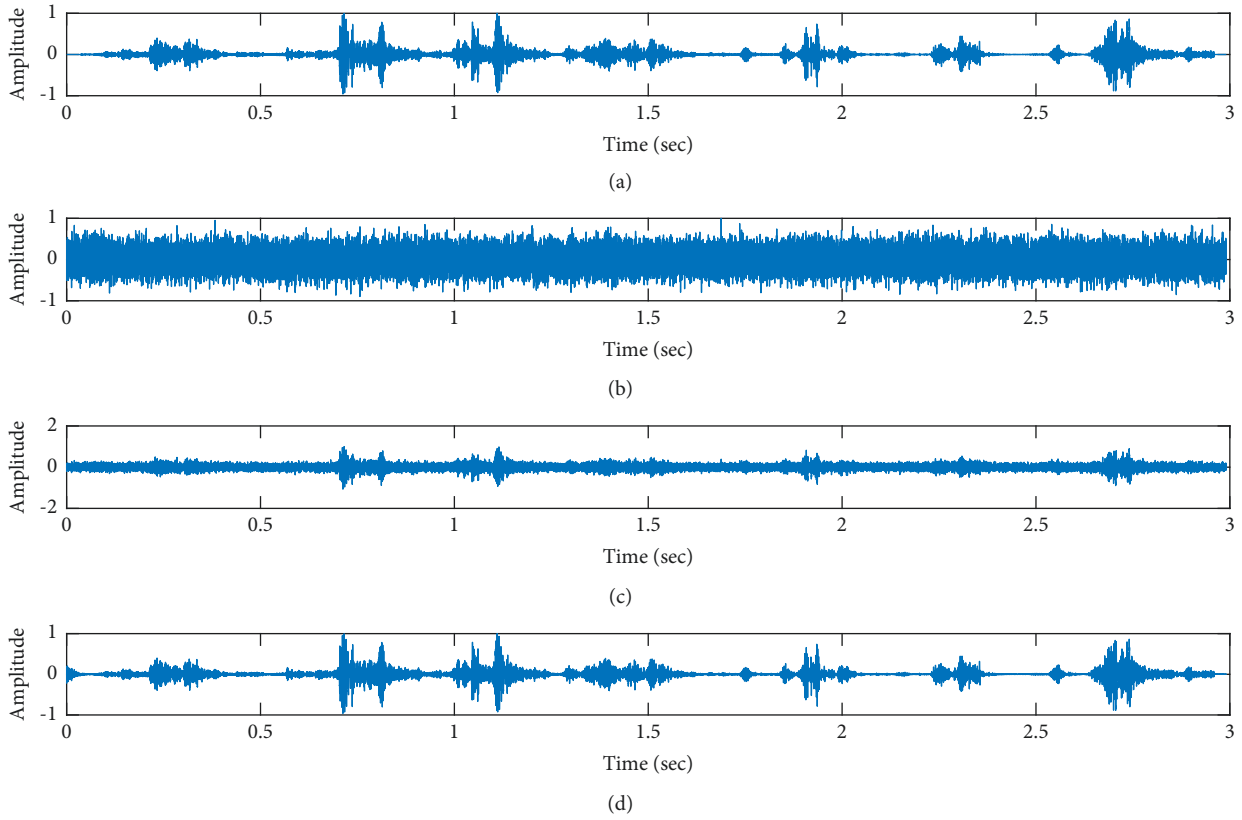

Figure 4: Denoising of FPCG signal corrupted by Gaussian noise of input SNR = +4 dB using the proposed VS Cascaded SE LMS Adaptive Filter output. (a) Clean signal. (b) Additive Gaussian Noise signal. (c) Noisy signal. (d) Proposed VS Cascaded SE LMS Adaptive Filter output.

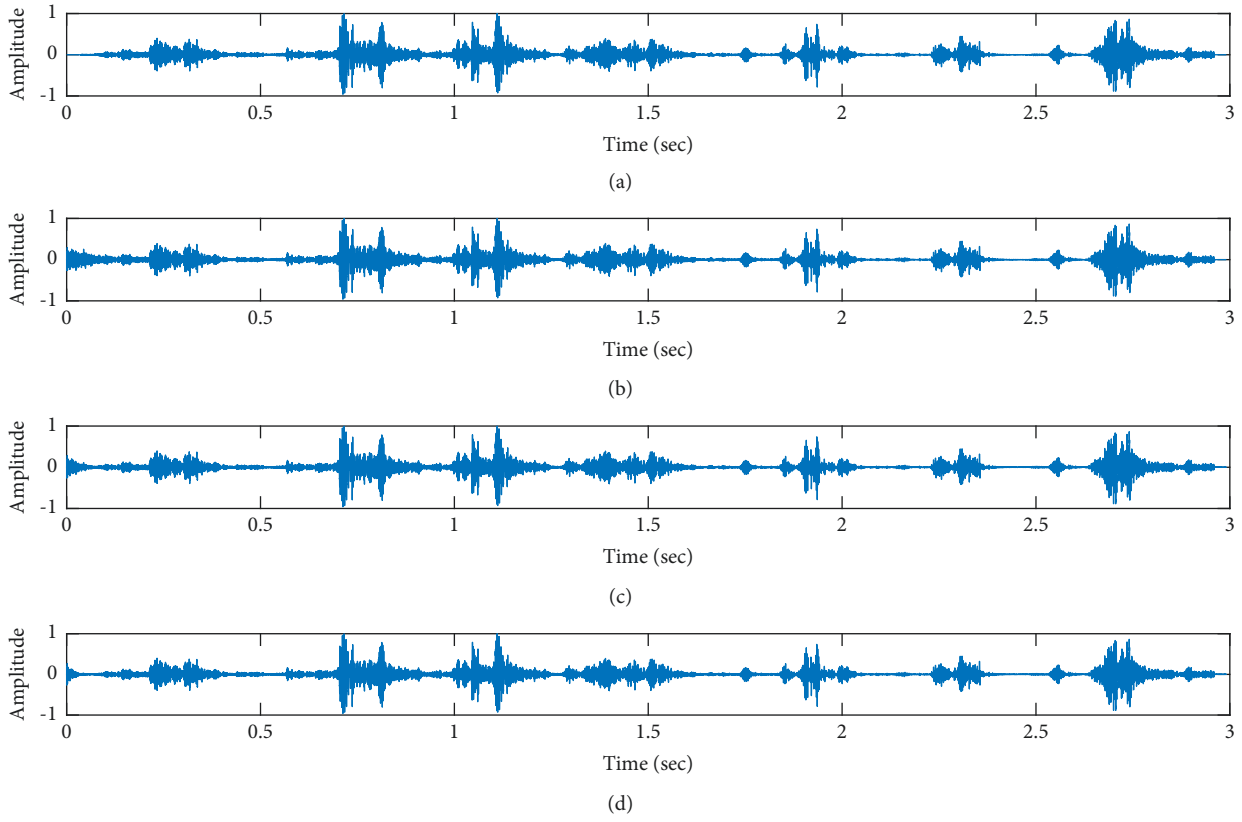

Figure 5: Proposed VS Cascaded SELMS Adaptive Filter stagewise restoration of clean signal (Gaussian noise with input SNR = +4 dB). (a) Clean signal. (b) Proposed VS Cascaded SELMS Adaptive Filter stage 1. (c) Output at stage 2. (d) Output at stage 3.

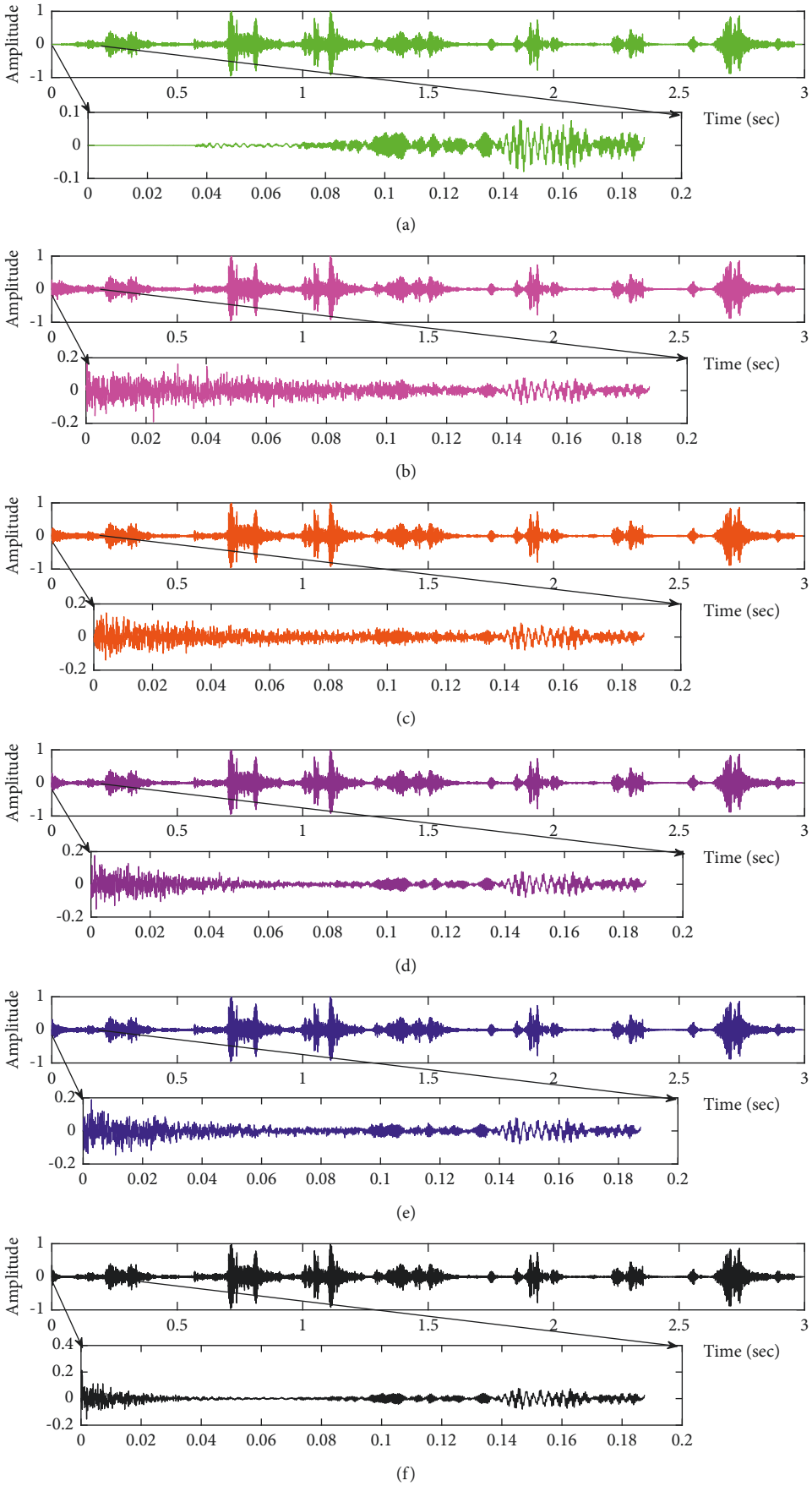

Figure 6: Comparison of proposed VS Cascaded SELMS Adaptive Filter output with various filters (fPCG signal with Gaussian noise input SNR = +4 dB). (a) Clean signal. (b) Conventional SE LMS filter output. (c) Existing 2-stage LMS filter output. (d) Existing 3-stage LMS filter output. (e) Proposed VS Cascaded SELMS Adaptive Filter output (fixed step size). (f) Proposed VS Cascaded SELMS Adaptive Filter output (variable step size).

models. We have also illustrated the performance of the proposed filter model by using a fixed step size for all the stages in Figure 6(e). Figure 7 depicts a high noise scenario where the Gaussian input noise level is set as −4 dB input SNR. As observed in Figure 7(d), the proposed filter performs efficiently and accurately estimates the clean signal even in high noise conditions. Figure 8 shows progressive restoration of the clean fPCG signal at each consecutive stage. This shows that the performance of the proposed VS Cascaded SE LMS Adaptive Filter is better as we increase the number of stages, and as noted in Figure 8(d) at stage 3, the fetal PCG signal is restored with minimum noise. In Figure 9, the performance of the proposed filter for fPCG signal denoising in high noise conditions is compared with the other filter models.

(b) *Pink Noise Environment*. The performance of the proposed filter should be validated in the presence of pink noise, which represents the colored noise scenario. The clean signal is corrupted by the pink noise of input SNR = +4 dB, as depicted in Figure 10(c). Restoration of clean signal with minimum noise is attained using the proposed filter model as depicted in Figure 10(d). Figure 11 shows the performance of the proposed VS Cascaded SE LMS Adaptive Filter at each stage. It can be noted that, at stage 3, the fPCG signal is restored with minimum noise. Figure 12 shows the comparison of the output of existing filter models with the proposed filter. The performance of the proposed filter in a high noise environment is depicted in Figure 13, where the input pink noise level is −4 dB. From Figure 13(d), it is evident that the proposed filter model is effective in minimizing colored noise. Figure 14 shows the stagewise performance of the proposed VS CASCADED SE LMS Adaptive Filter, and Figure 14(d) infers that the fPCG signal is restored with minimum noise at stage 3. The performance of the proposed filter is compared with other existing filter models at high input noise levels in Figure 15.

4.2. Objective Performance Evaluation. In Table 1, the relationship between MSE and correlation between $e_i(n)$ and $v'(n)$ is depicted at each stage. Column 6 of Table 1 shows the different step sizes for each stage. The clean fPCG signal taken from SUFHSDB corrupted by Gaussian and pink noise of input SNR +4 and −4 dB is used to test the performance of the proposed filter. In the field of biomedical engineering, the accuracy of the result is a major criterion for evaluating an algorithm [61, 62] which is verified by objective evaluation. The objective comparison of the proposed filter output with the conventional SE LMS filter and existing 2-stage and 3-stage cascaded filter models is performed in terms of MSE, SNR, ANR, PSNR, CC, and MAE. The results are tabulated in Table 2.

5. Performance of Proposed Variable Stage Cascaded SE LMS Adaptive Filter for the Pathological PCG Signals

5.1. Subjective Performance Evaluation. The subjective performance evaluation of the proposed Variable Stage Cascaded SE LMS adaptive filter is depicted below. Two pathological PCG signals (a0001 and a0115) taken from the PhysioNet database are corrupted by Gaussian noise, and the denoising performance of the proposed filter is noted. The restoration of clean pathological PCG signal from records a0001 and a0115 deteriorated by Gaussian noise of input SNR = +5 dB is shown in Figures 16 and 17, respectively. It is noted from Figures 16(d) and 17(d) that the best estimate of the clean signal is obtained at stage 3 using the proposed filter model. The denoising performance of the proposed filter model at a high Gaussian input noise level of −5 dB SNR is depicted in Figures 18 and 19. We note from Figures 18(d) and 19(d) that, for both the pathological signals (a0001 and a0115), the proposed filter gives an accurate estimate of the clean signal.

5.2. Objective Performance Evaluation. In Table 3, we have compared the performance of the proposed filter model with other cascaded filter models in terms of MSE, SNR, ANR, PSNR, CC, and MAE for both pathological signals (a0001 and a0115) corrupted by Gaussian noise.

5.3. Computational Complexity. The number of multiplications and additions required in one iteration of the algorithm decides the computational complexity. Table 4 presents the number of computations required for the proposed VS Cascaded SE LMS Adaptive Filter model compared to the other recently proposed filter models for Adaptive Noise Cancellation.

6. Discussion

6.1. Performance of Proposed Variable Stage Cascaded SE LMS Adaptive Filter for the Fetal PCG Signals

6.1.1. Subjective Performance Evaluation. In this work, we have proposed an Adaptive Noise Canceller based on the SE LMS algorithm for PCG signal denoising. We have implemented an automatic adjustment of the number of cascaded stages and step size for each stage. We have compared our results with the 2-stage cascaded ANC structure proposed in [49] and with 3-stage cascaded ANC structure proposed in [50]. Also, we have used a fixed step size for the filter at all stage ANCs and compared the results with the proposed self-adjustable step-size filter model.

(a) *Gaussian Noise Environment*. Figures 4 and 5 depict the efficient denoising performance of the proposed filter model in the presence of Gaussian noise of input SNR level +4 dB. From Figure 6, we infer that, compared with the current filter outputs, the proposed filter model with variable step size for each

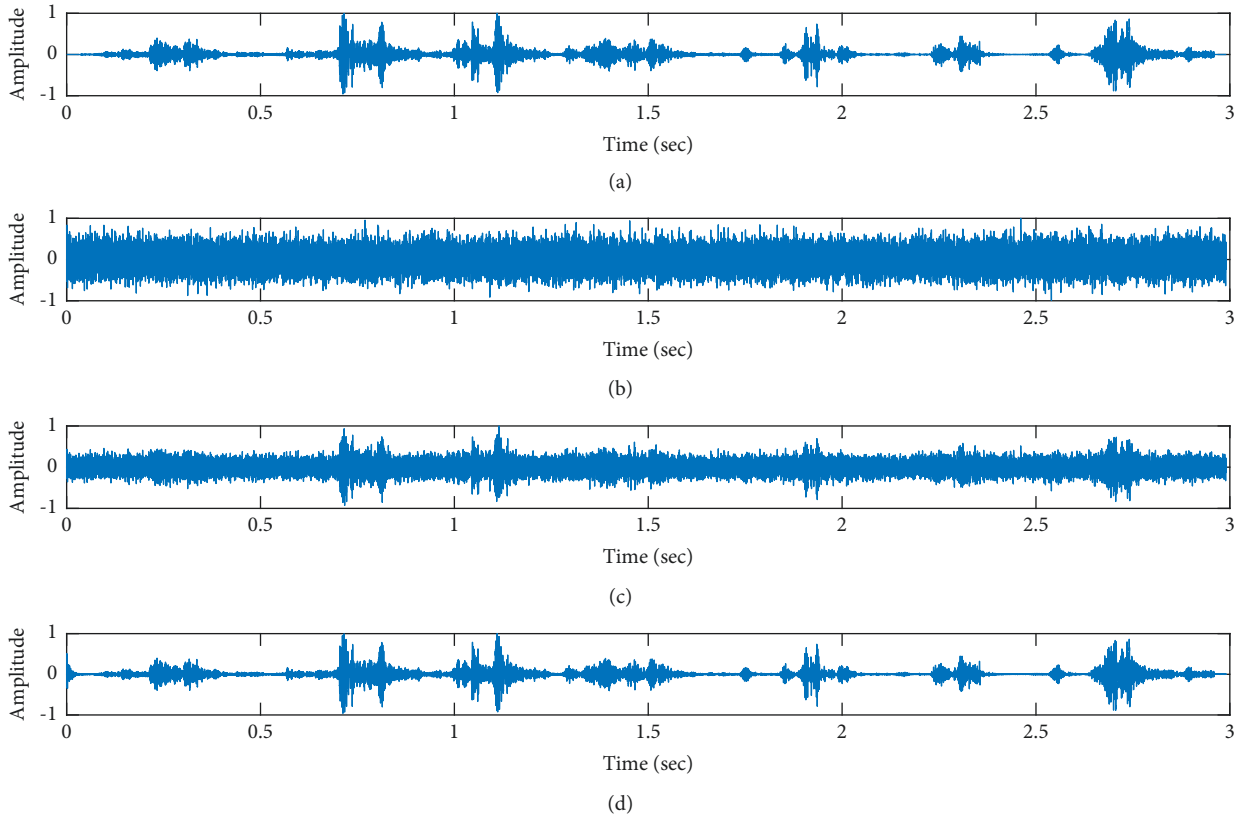

Figure 7: Denoising of fPCG signal corrupted by Gaussian noise of input SNR = −4 dB using the proposed VS Cascaded SE LMS Adaptive Filter output. (a) Clean signal. (b) Additive Gaussian Noise signal. (c) Noisy signal. (d) Proposed VS Cascaded SE LMS Adaptive Filter output.

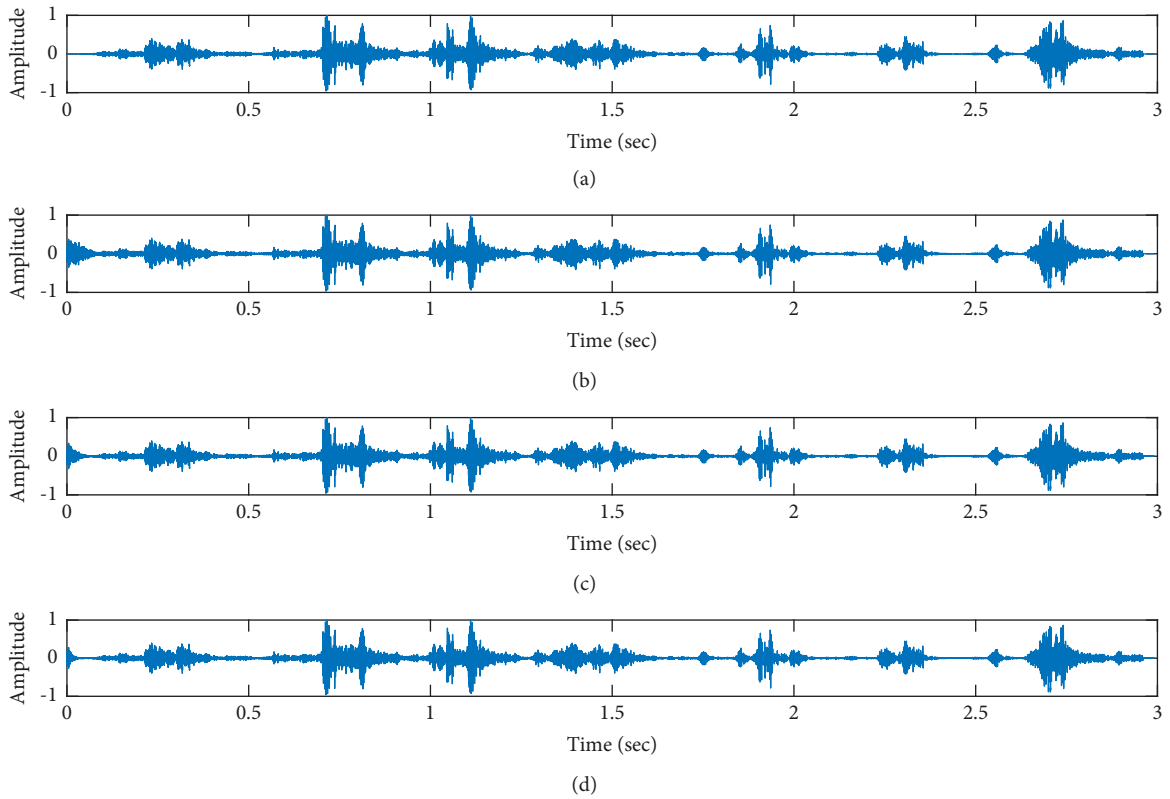

Figure 8: Proposed VS Cascaded SELMS Adaptive Filter stagewise restoration of clean signal (Gaussian noise with input SNR = −4 dB). (a) Clean signal. (b) Proposed VS Cascaded SELMS Adaptive Filter stage 1. (c) Output at stage 2. (d) Output at stage 3.

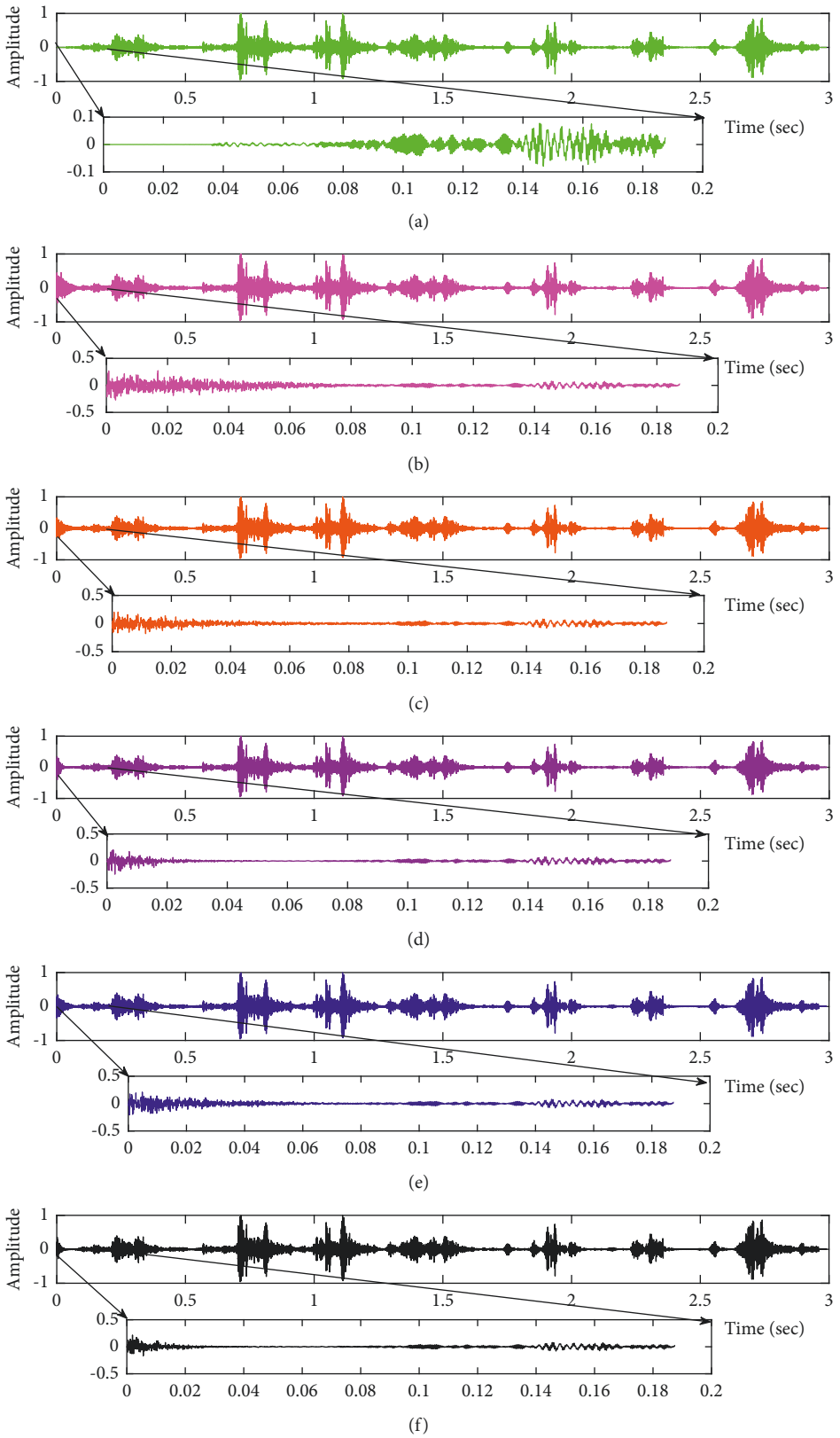

Figure 9: Comparison of proposed VS Cascaded SELMS Adaptive Filter output with various filters (fPCG signal with Gaussian noise input SNR = −4 dB). (a) Clean signal. (b) Conventional SE LMS filter output. (c) Existing 2-stage LMS filter output. (d) Existing 3-stage LMS filter output. (e) Proposed VS Cascaded SELMS Adaptive Filter output (fixed step size). (f) Proposed VS Cascaded SELMS Adaptive Filter output (variable step size).

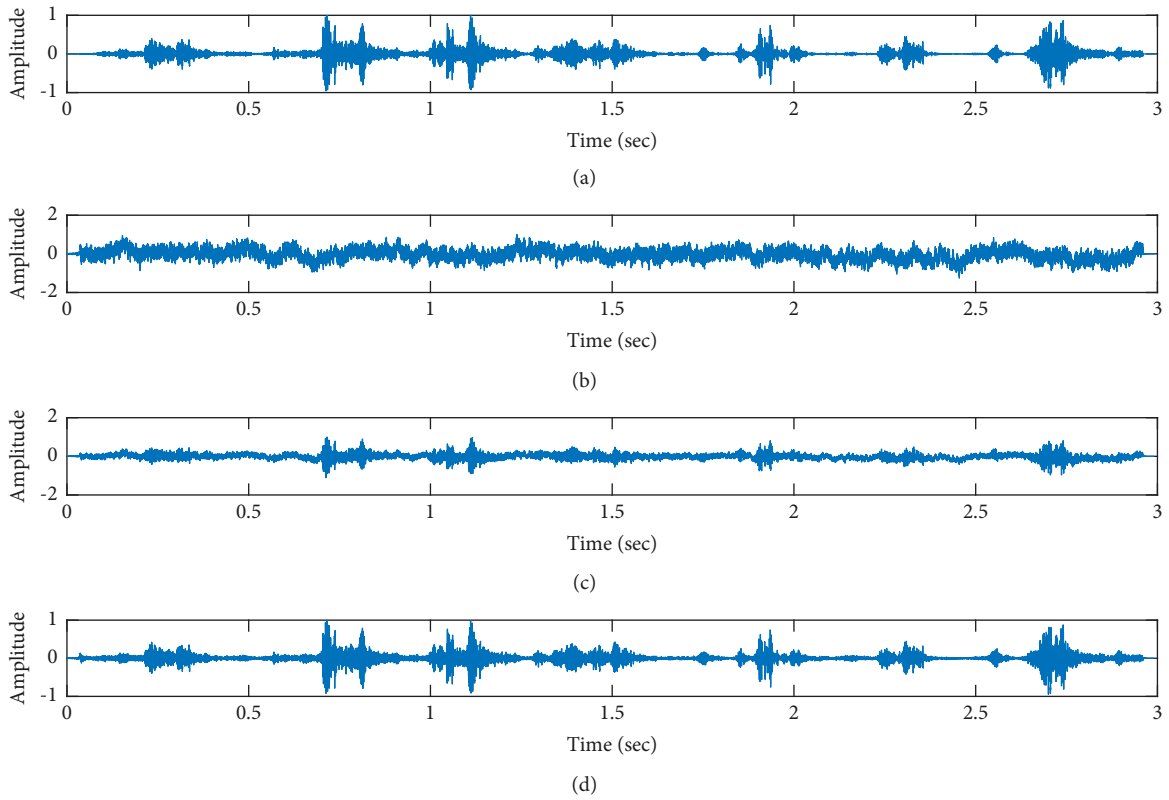

Figure 10: Denoising of fPCG signal corrupted by pink noise input SNR = +4 dB using the proposed VS Cascaded SE LMS Adaptive Filter output. (a) Clean signal. (b) Additive Gaussian Noise signal. (c) Noisy signal. (d) Proposed VS Cascaded SE LMS Adaptive Filter output.

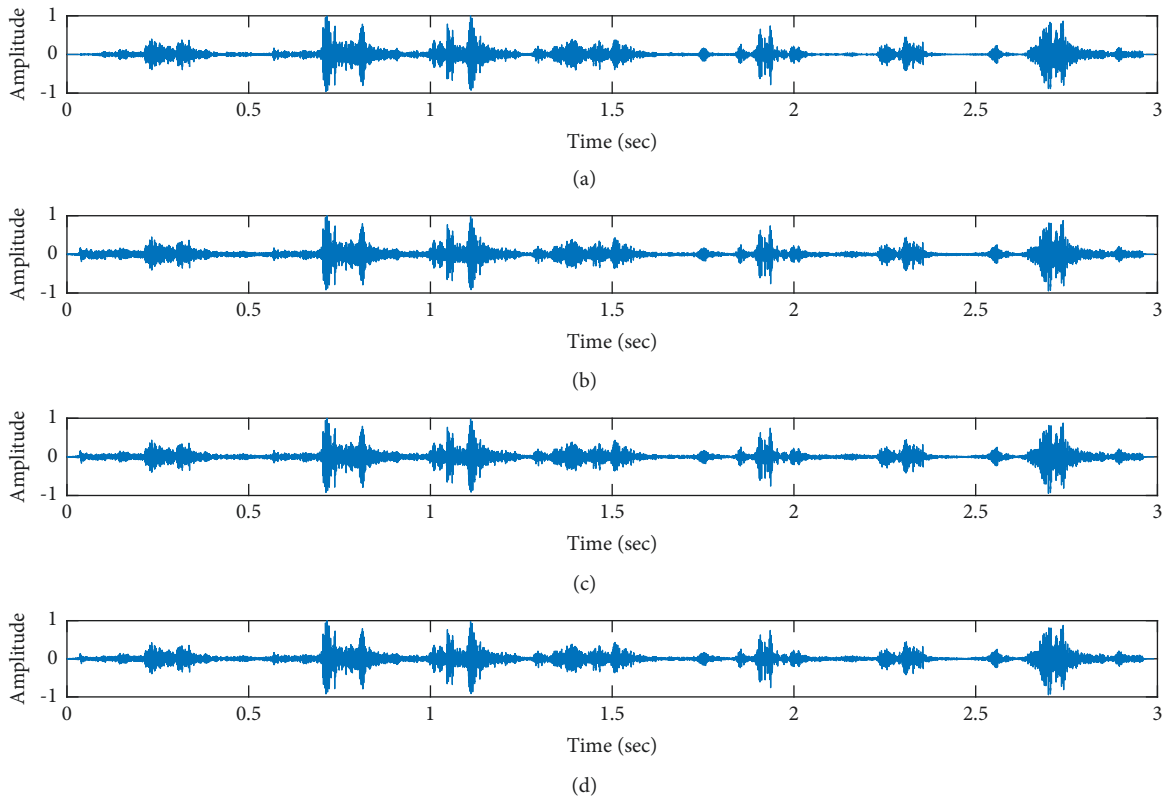

Figure 11: Proposed VS Cascaded SELMS Adaptive Filter stagewise restoration of clean signal (pink noise with input SNR = +4 dB). (a) Clean signal. (b) Proposed VS Cascaded SELMS Adaptive Filter stage 1. (c) Output at stage 2. (d) Output at stage 3.

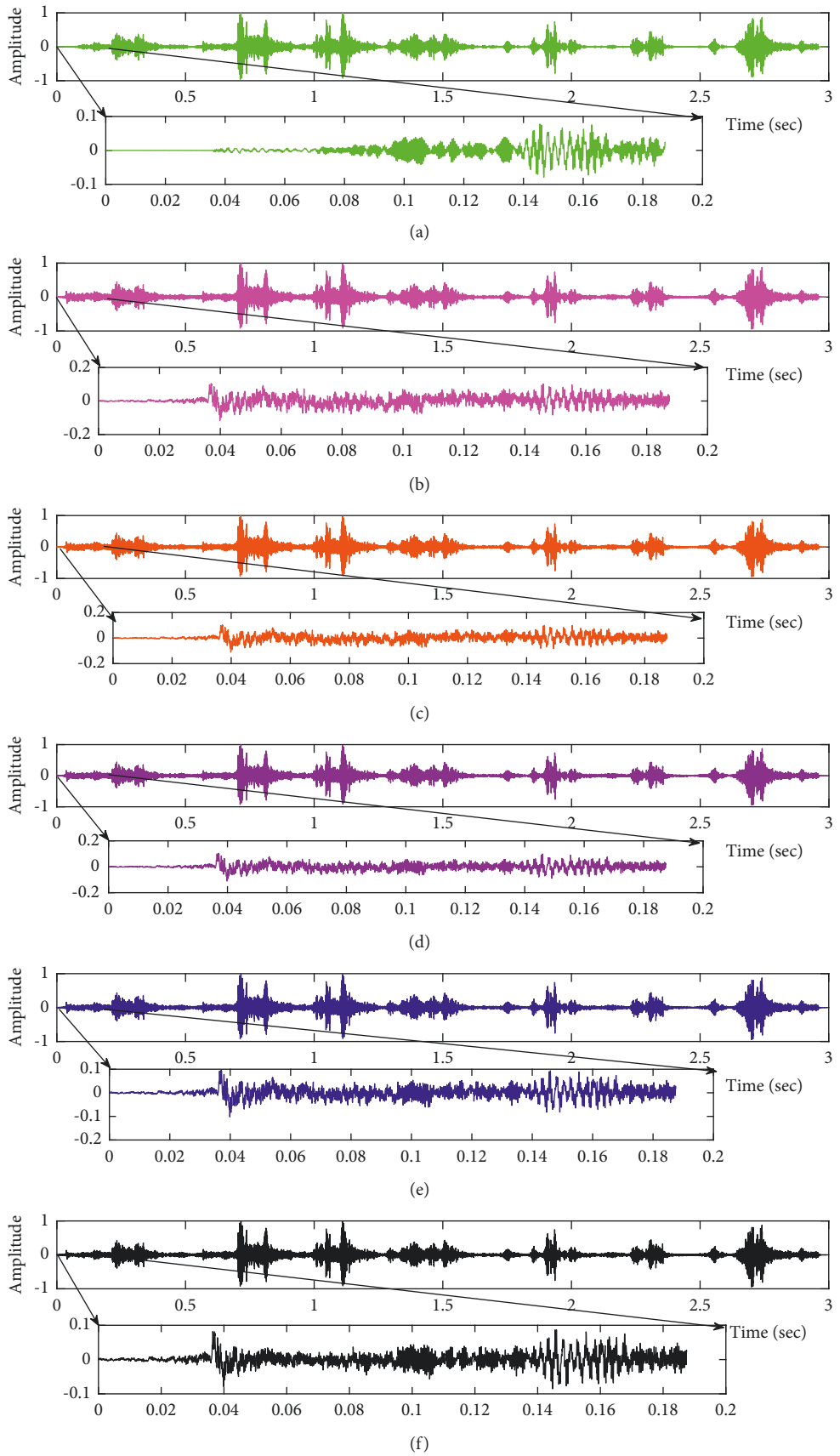

Figure 12: Comparison of proposed VS Cascaded SELMS Adaptive Filter output with various filters (FPCG signal with pink noise input SNR = +4 dB). (a) Clean signal. (b) Conventional SE LMS filter output. (c) Existing 2-stage LMS filter output. (d) Existing 3-stage LMS filter output. (e) Proposed VS Cascaded SELMS Adaptive Filter output (fixed step size). (f) Proposed VS Cascaded SELMS Adaptive Filter output (variable step size).

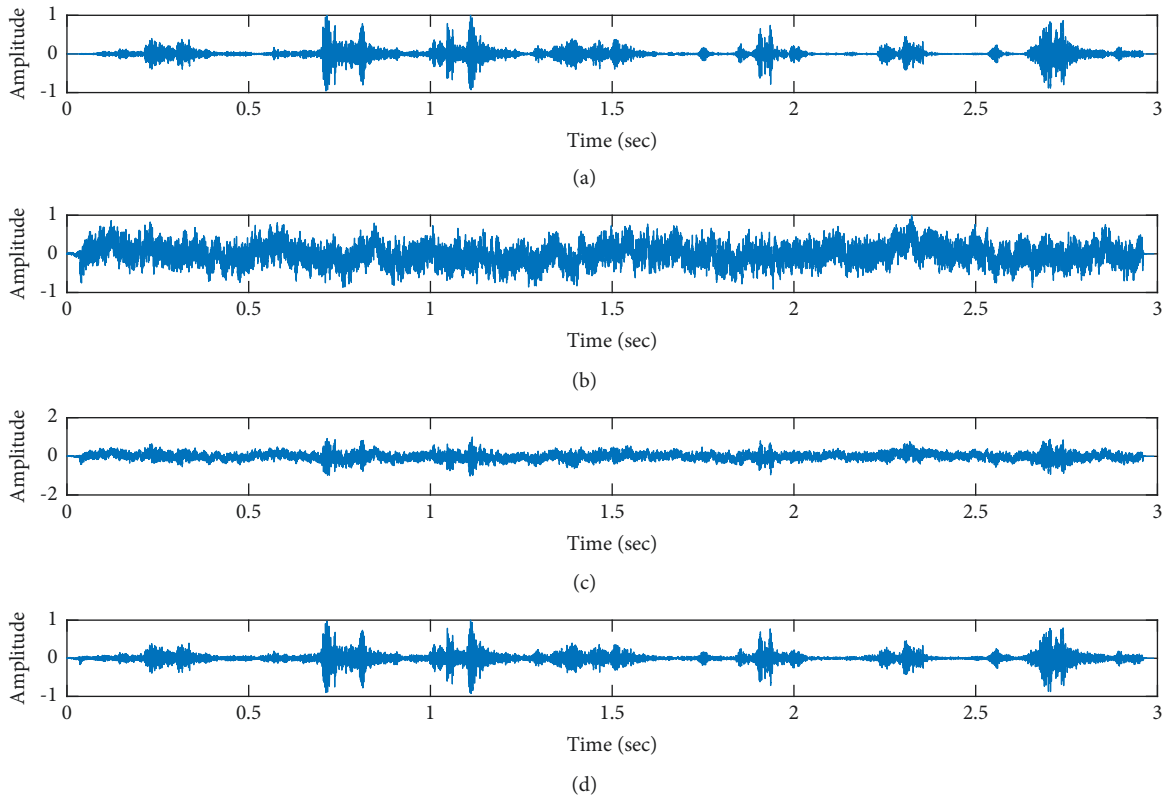

Figure 13: Denoising of fPCG signal corrupted by pink noise input SNR = −4 dB using the proposed VS Cascaded SE LMS Adaptive Filter output. (a) Clean signal. (b) Additive Gaussian Noise signal. (c) Noisy signal. (d) Proposed VS Cascaded SE LMS Adaptive Filter output.

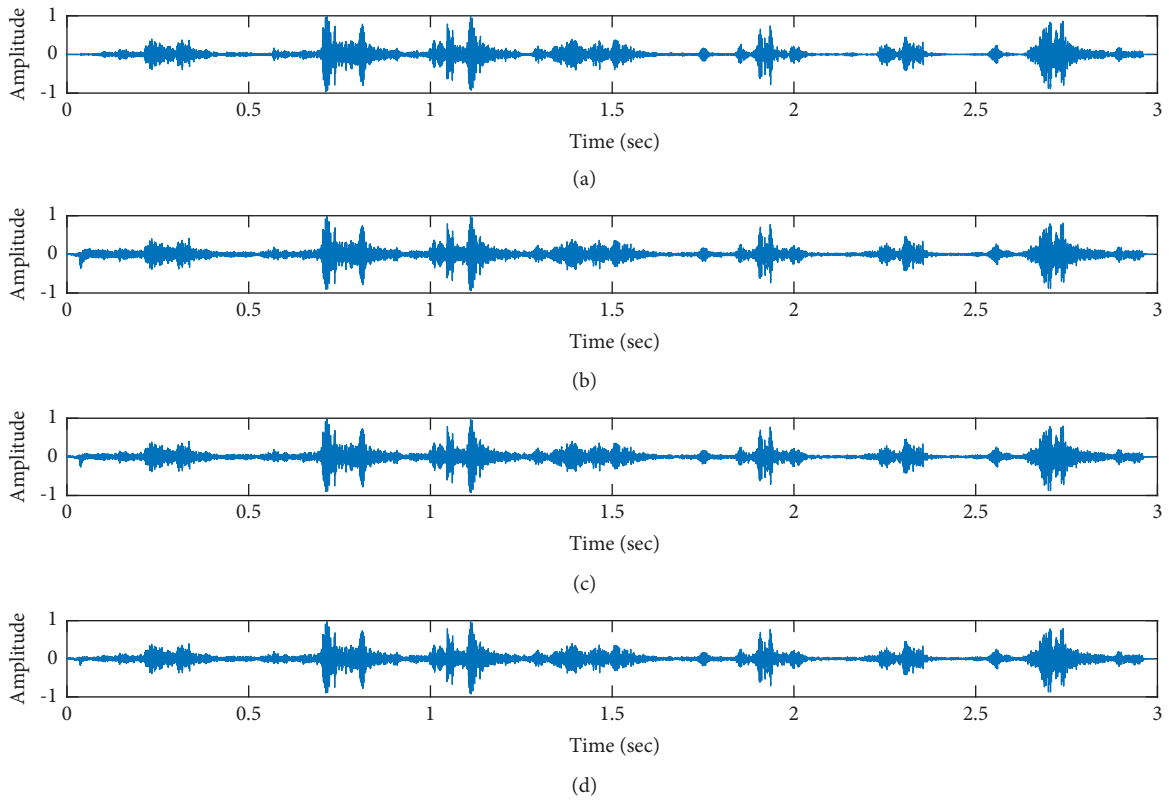

Figure 14: Proposed VS Cascaded SELMS Adaptive Filter stagewise restoration of clean signal (pink noise with input SNR = −4 dB). (a) Clean signal. (b) Proposed VS Cascaded SELMS Adaptive Filter stage 1. (c) Output at stage 2. (d) Output at stage 3.

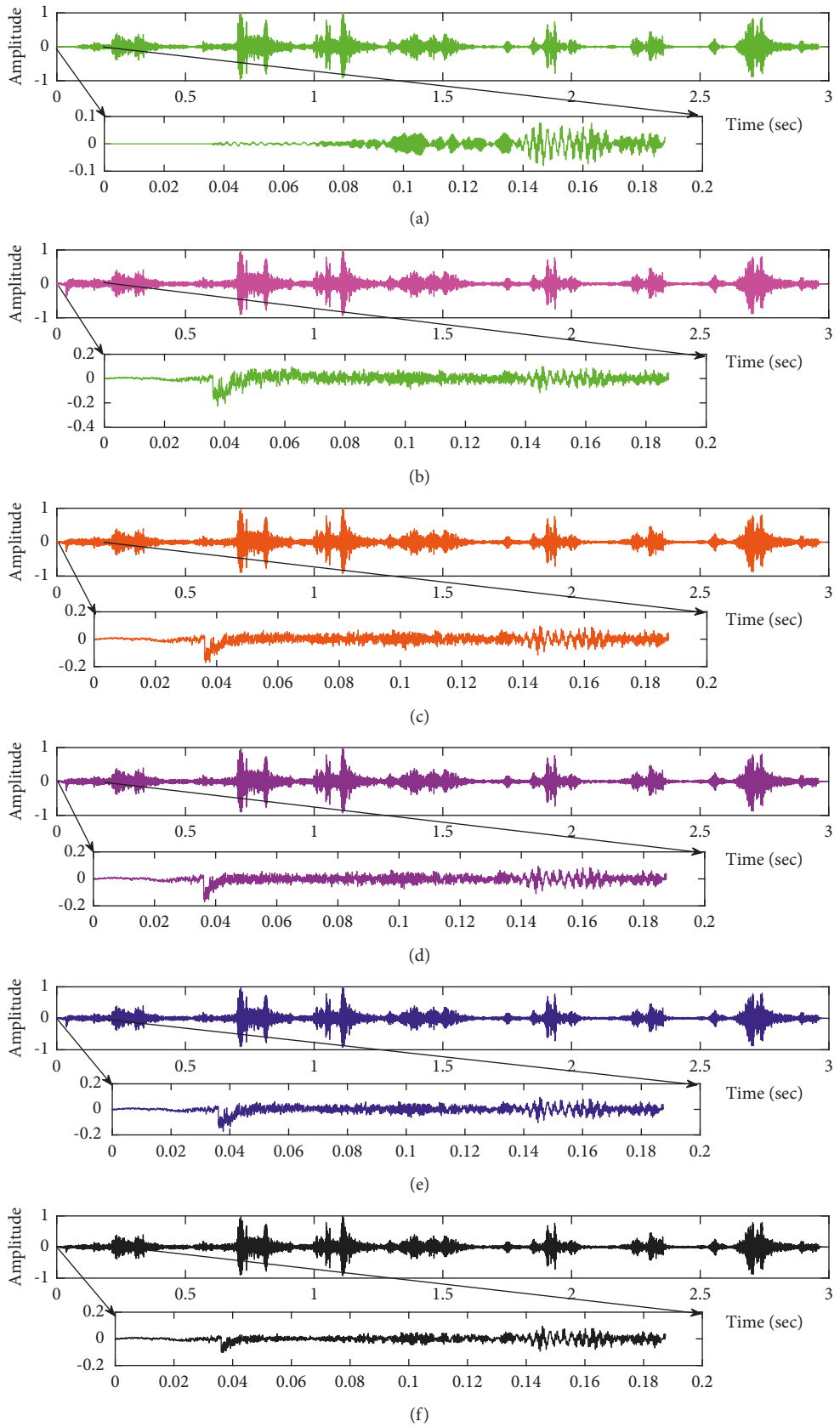

Figure 15: Comparison of proposed VS Cascaded SELMS Adaptive Filter output with various filters (fPCG signal with pink noise input SNR = −4 dB). (a) Clean signal. (b) Conventional SE LMS filter output. (c) Existing 2-stage LMS filter output. (d) Existing 3-stage LMS filter output. (e) Proposed VS Cascaded SELMS Adaptive Filter output (fixed step size). (f) Proposed VS Cascaded SELMS Adaptive Filter output (variable step size).

Table 1: Variation of the correlation function and step size at each stage of proposed VS Cascaded SELMS Adaptive Filter for fPCG input signal corrupted by Gaussian and pink noise.

Noise	Input SNR	Stage	MSE	$\rho_{e_i(n)v'(n)}$	μ_i
Gaussian	+4 dB	I	$5.70E-05$	0.0234	0.01
		II	$2.27E-05$	0.016	0.02
		III	$1.04E-05$	0.0116	0.04
	−4 dB	I	$8.67E-05$	0.0161	0.01
		II	$3.88E-05$	0.0144	0.02
		III	$2.03E-05$	0.0123	0.04
Pink	+4 dB	I	$1.72E-04$	0.014	0.01
		II	$1.45E-04$	0.0043	0.02
		III	$1.36E-04$	0.0001	0.04
	−4 dB	I	$2.98E-04$	0.0192	0.01
		II	$2.50E-04$	0.0014	0.02
		III	$2.36E-04$	0.0001	0.04

Table 2: Comparison of MSE, SNR, ANR, PSNR, CC, and MAE performance of the proposed VS Cascaded SELMS Adaptive Filter with the various existing filter models for fPCG signals.

Noise	Input SNR	Filter Structure	MSE	SNR (dB)	ANR (dB)	PSNR (dB)	CC	MAE
Gaussian	+4 dB	Conventional SELMS adaptive filter	$5.45E-05$	45.5658	50.6788	42.2838	0.9946	0.002
		Existing 2-S cascaded LMS adaptive filter	$3.58E-05$	50.2054	50.3086	44.49	0.9967	0.0017
		Existing 3-S cascaded LMS adaptive filter	$2.71E-05$	52.9885	53.0913	45.6369	0.9975	0.0015
		Proposed VS Cascaded SELMS Adaptive Filter (FSS)	$2.59E-05$	53.1973	53.2649	45.7548	0.9976	0.0011
		Proposed VS Cascaded SELMS Adaptive Filter (VSS)	$1.04E-05$	62.5934	62.6348	49.0503	0.9989	$7.42E-04$
Gaussian	−4 dB	Conventional SELMS adaptive filter	$8.14E-05$	41.8965	51.0083	40.7003	0.9923	0.0024
		Existing 2-S cascaded LMS adaptive filter	$3.70E-05$	49.8859	49.9992	43.8492	0.9962	0.0018
		Existing 3-S cascaded LMS adaptive filter	$3.01E-05$	51.9602	52.0741	45.4376	0.9974	0.0016
		Proposed VS Cascaded SELMS Adaptive Filter (FSS)	$3.91E-05$	48.0708	48.1802	43.4126	0.9958	0.0019
		Proposed VS Cascaded SELMS Adaptive Filter (VSS)	$2.03E-05$	55.8844	55.9548	47.7843	0.9985	$9.74E-04$
Pink	+4 dB	Conventional SELMS adaptive filter	$1.72E-04$	34.5489	34.8672	37.6559	0.9845	0.0096
		Existing 2-S cascaded LMS adaptive filter	$1.63E-04$	35.0507	35.3253	37.8738	0.9852	0.0094
		Existing 3-S cascaded LMS adaptive filter	$1.58E-04$	35.4005	35.6751	38.0257	0.9857	0.0093
		Proposed VS Cascaded SELMS Adaptive Filter (FSS)	$1.47E-04$	36.1219	36.3434	38.339	0.9867	0.009
		Proposed VS Cascaded SELMS Adaptive Filter (VSS)	$1.36E-04$	37.0542	37.0618	38.657	0.9876	0.0087
Pink	−4 dB	Conventional SELMS adaptive filter	$2.98E-04$	29.0166	29.5294	35.2532	0.9731	0.0124
		Existing 2-S cascaded LMS adaptive filter	$2.64E-04$	30.2438	30.5464	35.7862	0.9761	0.012
		Existing 3-S cascaded LMS adaptive filter	$2.63E-04$	30.2934	30.5959	35.8077	0.9762	0.012
		Proposed VS Cascaded SELMS Adaptive Filter (FSS)	$2.54E-04$	30.6067	30.8777	35.9438	0.9769	0.0117
		Proposed VS Cascaded SELMS Adaptive Filter (VSS)	$2.36E-04$	31.349	31.5948	36.2661	0.9786	0.0114

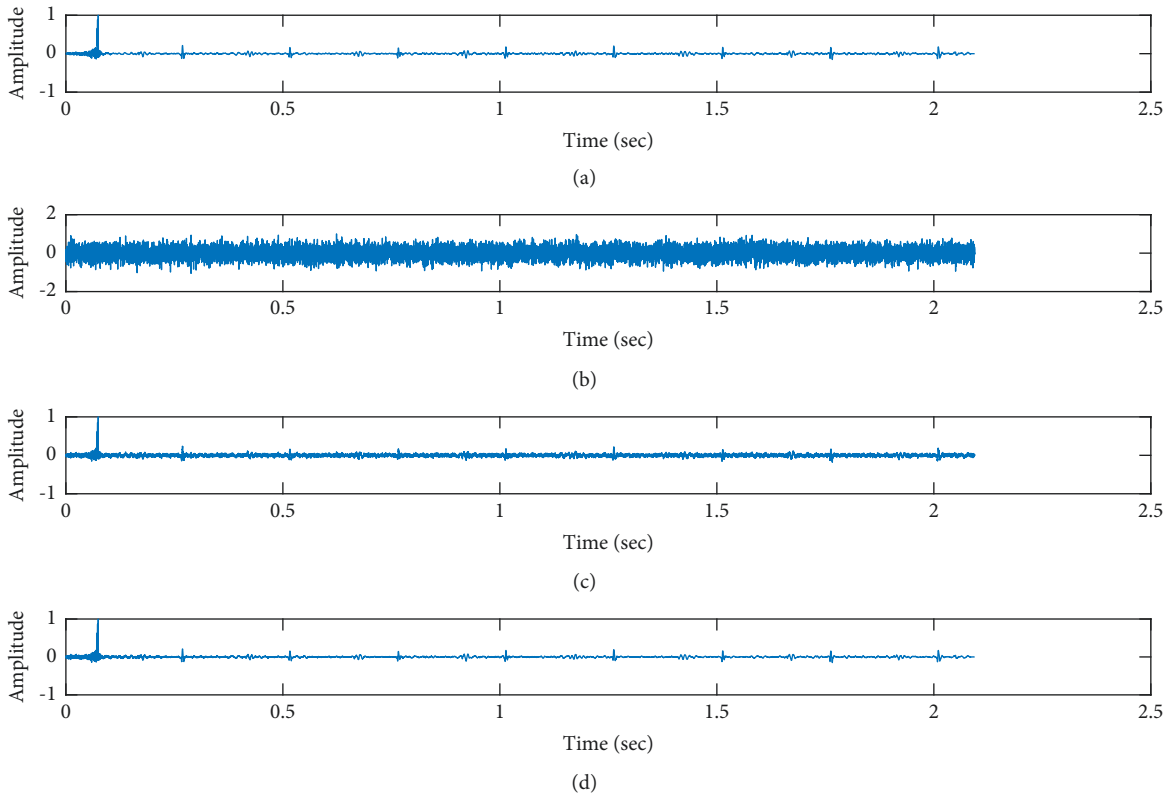

Figure 16: Denoising of pathological PCG signal (a0001) corrupted by Gaussian noise of input SNR = +5 dB using the proposed VS Cascaded SE LMS Adaptive Filter output. (a) Clean signal. (b) Additive Gaussian Noise signal. (c) Noisy signal. (d) Proposed VS Cascaded SE LMS Adaptive Filter output.

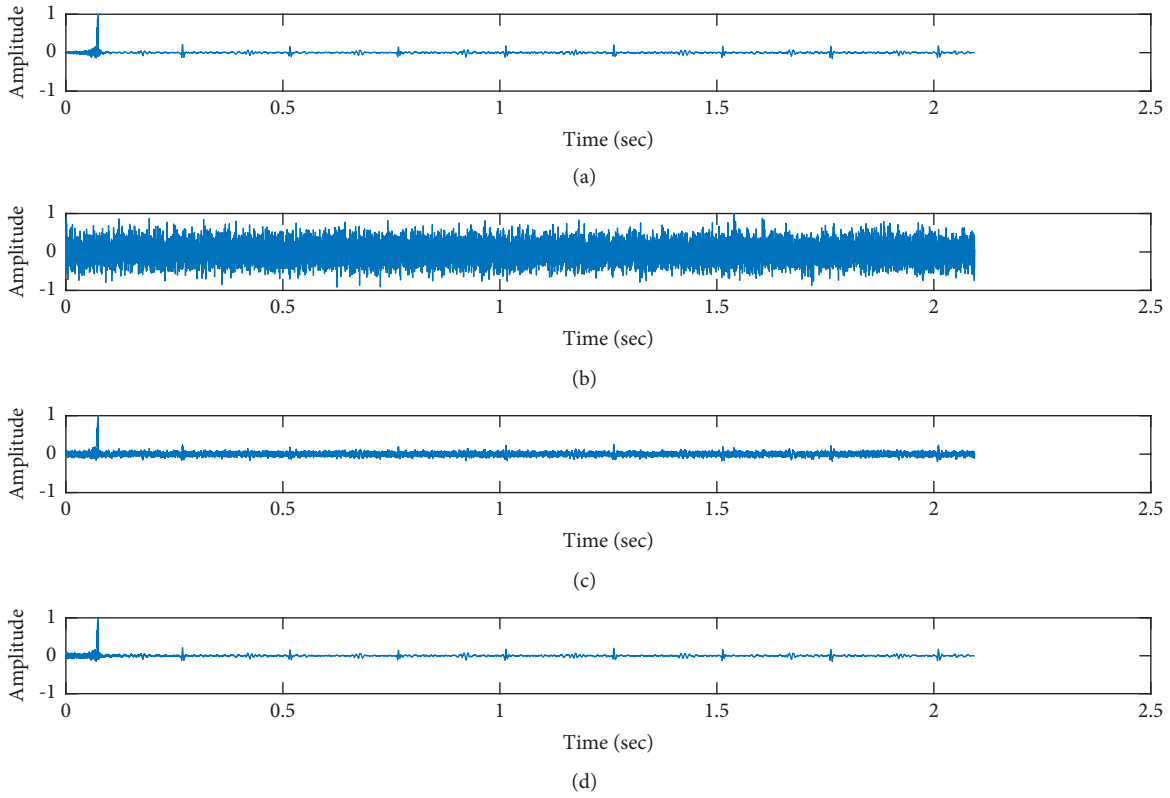

Figure 17: Denoising of pathological PCG signal (a0001) corrupted by Gaussian noise of input SNR = −5 dB using the proposed VS Cascaded SE LMS Adaptive Filter output. (a) Clean signal. (b) Additive Gaussian Noise signal. (c) Noisy signal. (d) Proposed VS Cascaded SE LMS Adaptive Filter output.

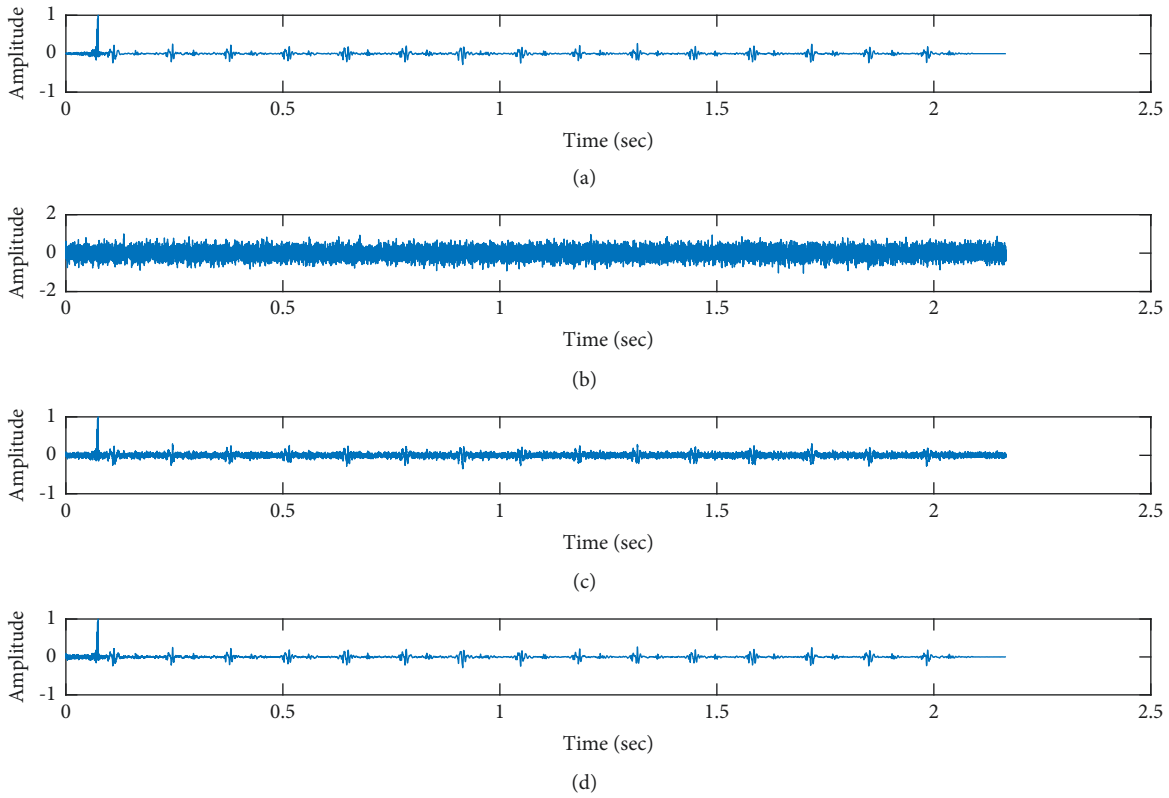

Figure 18: Denoising of pathological PCG signal (a0115) corrupted by Gaussian noise of input SNR = +5 dB using the proposed VS Cascaded SE LMS Adaptive Filter output. (a) Clean signal. (b) Additive Gaussian Noise signal. (c) Noisy signal. (d) Proposed VS Cascaded SE LMS Adaptive Filter output.

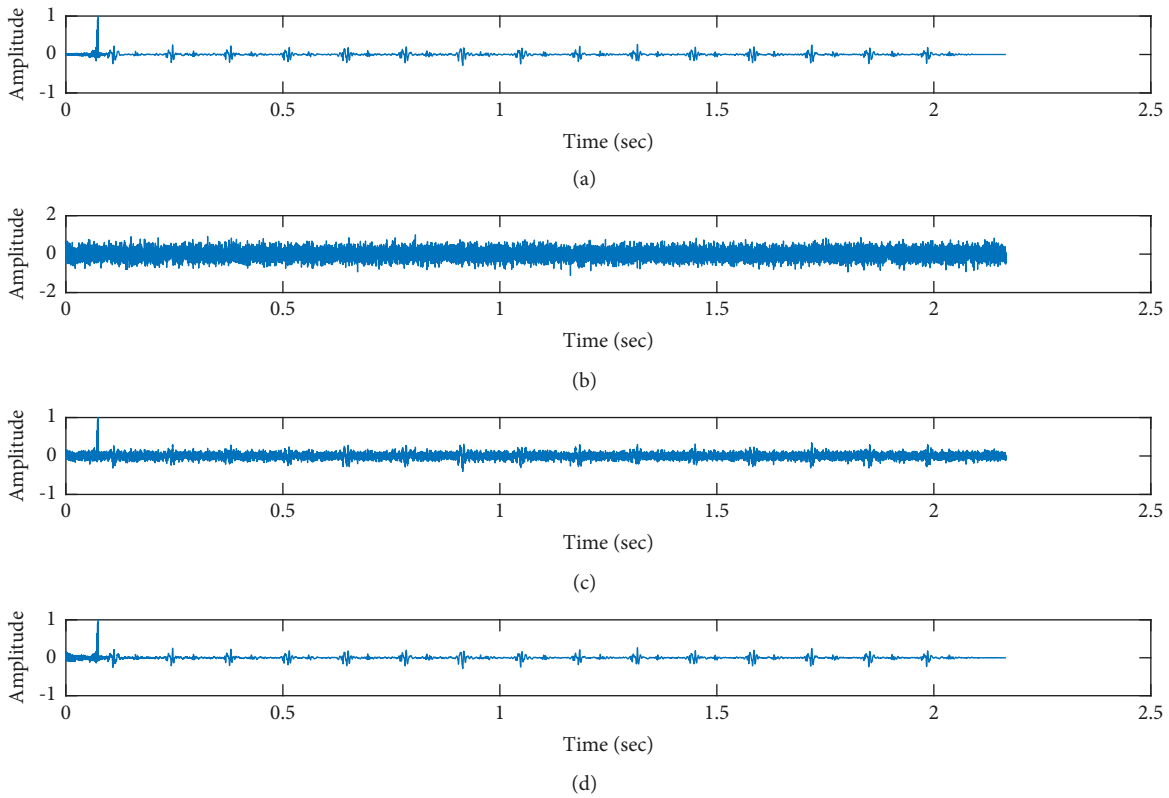

Figure 19: Denoising of pathological PCG signal (a0115) corrupted by Gaussian noise of input SNR = −5 dB using the proposed VS Cascaded SE LMS Adaptive Filter output. (a) Clean signal. (b) Additive Gaussian Noise signal. (c) Noisy signal. (d) Proposed VS Cascaded SE LMS Adaptive Filter output.

Table 3: Comparison of MSE, SNR, ANR, PSNR, MAE, and CC performance of the proposed VS Cascaded SELMS Adaptive Filter with the various existing filter models for pathological PCG signals.

Record	Noise	Input SNR	Filter structure	MSE	SNR (dB)	ANR (dB)	PSNR (dB)	MAE	CC
a0001	Gaussian	+5 dB	Conventional SELMS adaptive filter	$7.59E-05$	21.6266	26.2004	41.1998	0.0052	0.9467
			Existing 2-S cascaded LMS adaptive filter	$9.40E-05$	19.4818	21.3908	40.2684	0.0069	0.9352
			Existing 3-S cascaded LMS adaptive filter	$6.85E-05$	22.651	24.5485	41.6447	0.0051	0.9517
			Proposed VS Cascaded SELMS Adaptive Filter (FSS)	$3.71E-05$	28.7909	29.5316	44.3113	0.0032	0.9731
			Proposed VS Cascaded SELMS Adaptive Filter (VSS)	$1.66E-05$	36.8464	37.4117	47.8097	0.0017	0.9877
a0001	Gaussian	−5 dB	Conventional SELMS adaptive filter	$1.03E-04$	18.5649	28.4198	39.8702	0.0044	0.9308
			Existing 2-S cascaded LMS adaptive filter	$1.07E-04$	18.2324	20.1592	39.7258	0.0056	0.9259
			Existing 3-S cascaded LMS adaptive filter	$6.50E-05$	23.1706	25.2832	41.8704	0.0032	0.9545
			Proposed VS Cascaded SELMS Adaptive Filter (FSS)	$5.34E-05$	25.1399	26.2376	42.7257	0.0027	0.9621
			Proposed VS Cascaded SELMS Adaptive Filter (VSS)	$2.35E-05$	33.3264	33.9951	46.281	0.0015	0.9826
a0115	Gaussian	+5 dB	Conventional SELMS adaptive filter	$1.09E-04$	27.3987	32.2008	39.6225	0.0046	0.9692
			Existing 2-S cascaded LMS adaptive filter	$9.14E-05$	29.1654	30.0147	40.3897	0.0052	0.9741
			Existing 3-S cascaded LMS adaptive filter	$6.12E-05$	33.1816	34.0441	42.1339	0.0031	0.9825
			Proposed VS Cascaded SELMS Adaptive Filter (FSS)	$5.36E-05$	34.5118	34.928	42.7116	0.0029	0.9845
			Proposed VS Cascaded SELMS Adaptive Filter (VSS)	$2.26E-05$	43.1482	43.4444	46.4624	0.0016	0.9934
a0115	Gaussian	−5 dB	Conventional SELMS adaptive filter	$1.66E-04$	23.2246	32.9978	37.8097	0.0043	0.9544
			Existing 2-S cascaded LMS adaptive filter	$9.49E-05$	28.791	29.6225	40.2271	0.0035	0.973
			Existing 3-S cascaded LMS adaptive filter	$6.49E-05$	32.5952	33.4509	41.8793	0.0022	0.9814
			Proposed VS Cascaded SELMS Adaptive Filter (FSS)	$7.83E-05$	30.7113	31.3171	41.0611	0.0027	0.9776
			Proposed VS Cascaded SELMS Adaptive Filter (VSS)	$3.12E-05$	39.9183	40.3421	45.0596	0.0015	0.9909

Table 4: Computational cost of proposed filter model in comparison with the other adaptive filtering algorithms.

Filter structure	'∗'or'/'	'+'or'−'
LMS adaptive algorithm [63]	$2M+2$	$2M$
NLMS adaptive algorithm [64]	$3M+3$	$3M$
FxLMS adaptive algorithm [65]	$3M+1$	$3M-2$
Affine Projection Algorithm [66]	$2P^2+2PM+M$	$2P^2M+PM-P^2$
RLS Algorithm [67]	$3M^2+4M+1$	$3M^2+4M$
Proposed VS Cascaded SE LMS Adaptive Filter	$L(M+1)$	$L(M+1)$

stage reduces the noise more efficiently and at high speeds, as proved in Figure 6(f). Figures 7 and 8 depict the remarkable performance of the proposed filter model in the presence of Gaussian noise of input SNR level −4 dB. We note that, compared to Figures 9(b)–9(e), Figure 9(f) provides better signal denoising, which indicates that the proposed filter with variable step size for each stage is more effective in eliminating the noise signals.

(b) *Pink Noise Environment*. The proposed filter exhibits good denoising properties in nonstationary noise, as noted in Figures 10 and 11 in the presence of pink noise. Figure 12(f) shows that the proposed filter successfully recovers the clean signal with reduced noise. Even if the noise levels are high, the proposed filter model performs efficiently well, as depicted in Figures 13 and 14. It is noted in Figures 15(b)–15(f) that, compared with the existing filters, the proposed filter exhibits better denoising capability. The variable step size for each stage also reduces the noise levels compared to the fixed step size for all the stages. It concludes that the proposed Variable Stage Cascaded SELMS adaptive filter has the best noise reduction capability and proves to be very attractive in biomedical for denoising PCG signals corrupted by Gaussian and colored noises. We also infer from the subjective analysis that the proposed filter model reduces the Gaussian noise more effectively than the colored Pink noise.

6.1.2. Objective Performance Evaluation. The proposed adaptive filter structure has a Variable Stage Cascaded SE LMS adaptive filter configuration with different step sizes for each stage. The number of stages to be cascaded is controlled automatically depending on the correlation between the output error signal of each stage ANC and the reference input noise signal at stage I ANC. As observed from Table 1, the correlation between $e_1(n)$ and $v'(n)$ is higher than the correlation between $e_3(n)$ and $v'(n)$. This means that as we increase the number of cascaded stages, the estimate of a clean signal at the error output of ANC $e_i(n)$ is less related to the noise signal and replicates the clean signal, thus reducing the MSE value. Consider the case of speech signal corrupted by Gaussian noise of input SNR = −4 dB. As it can be observed from Table 1, as the correlation $\rho_{e_3(n)v'}$ drops from 0.0144 at stage II to 0.0123 at stage III, the MSE value also reaches a minimum value of $2.03E-05$ at stage III. Hence, it is concluded that the MSE value keeps reducing if more number of stages are cascaded since $\rho_{e_i(n)v'}$ is lesser as the number of stages i is increased. The value of $\rho_{\text{threshold}}$ is selected depending on the type of noise, input noise level, and output MSE, SNR values desired. The value of $\rho_{\text{threshold}}$ decides the number of filter stages to be cascaded, and this $\rho_{\text{threshold}}$ value can be found by the trial and error method. The adaptive filter at each stage ANC requires a different step size. This is because the reference input signal to the adaptive filter at stage I is a noise signal $v'(n)$ correlated to the additive noise $v(n)$. And the reference input signal to the consecutive stage adaptive filter is the difference between the input and output signal of the previous stage adaptive filter $x_i(n) = x_{i-1}(n) - y_{i-1}(n)$. Thus, the maximum bound on the step size $\mu_{\max}$ changes depending on the input signal. We either multiply or divide the previous stage step-size value by a constant "k" to obtain the next stage's step size. In this case, the fixed step size at stage 1 is assumed to be 0.01, and the value of "k" is selected as 2. The maximum bound on step size increases at each stage. Therefore, we multiplied the step size of the previous stage by a factor of 2 to obtain the step size of the next stage. This provides optimal performance in terms of MSE, as noted in Table 1. Both $\rho_{\text{threshold}}$ and "k" values are determined using the trial and error method, which is the only drawback in the proposed filter model. Table 2 concludes that the proposed filter gives the minimum MSE values for both the noise signals at different input noise levels. At the same time, we also infer that the proposed Variable Stage Cascaded SELMS adaptive filter model gives better performance in Gaussian noise than pink noise environment. The proposed filter outperforms the existing 2-stage and 3-stage cascaded filter models in terms of MSE, SNR, ANR, PSNR, MAE, and CC. The proposed adaptive filter structure gives an output SNR value of at least 10 dB higher than the existing cascaded adaptive filters in a Gaussian noise environment and 2 dB higher output SNR values in the presence of colored noise. In the presence of Gaussian noise, the Peak SNR values are 7 dB higher, and for pink noise, the improvement is 1-2 dB. The average noise reduction is around 10–12 dB improved for Gaussian noise and 1-2 dB higher for pink noise denoising. The proposed filter model reduces Mean Absolute Error values and improves the correlation coefficient between the clean signal and its estimate.

7. Performance of Proposed Variable Stage Cascaded SE LMS Adaptive Filter for the Pathological PCG Signals

7.1. Subjective Performance Evaluation. From Figures 16–19, it is evident that the proposed filter model performs well in the presence of different levels of Gaussian noise and gives excellent denoising of both pathological signals.

7.2. Objective Performance Evaluation. Table 3 infers that the proposed filter model provides an SNR value of 10–15 dB higher than the existing cascaded adaptive filter models for denoising pathological signals. The average noise reduction capability is also 10 dB higher than the existing filter models. The Peak SNR values are improved by 6 dB, and MSE values reduce by 75–80%. There is a reduction of 70–72% in the Mean Absolute Error, and the correlation between the clean signal and its estimate is also high.

7.3. Computational Complexity. We have employed an adaptive filter-based ANC system for fPCG and pathological PCG signal denoising in this work. Adaptive noise cancellers are primarily used to remove noise from speech and audio signals, and we have explored their usage for denoising PCG signals. The main idea is to reduce the computational time and complexity to build cost-effective hardware for recording heart signals without noise. Therefore, we compare the computational complexity of the proposed filter model with other recently proposed filter models for Adaptive Noise Cancellation in various fields. From Table 4, we infer that the conventional SE LMS filter requires a minimum number of computations. The total multiplications and additions for each stage are $M + 1$, where M is the filter order. Therefore, we have employed an SE LMS adaptation algorithm for the filters in all cascaded ANC stages. The total number of computations required for the proposed filter model depends on the number of stages used; the cascaded stages are $L = 3$ for denoising PCG signals in the presence of Gaussian and pink noise. The proposed filter model introduces additional computations to automatically select the number of cascaded stages (based on the correlation coefficient) and different step size for each stage (based on the autocorrelation matrix). We have emphasized that a cascaded filter structure is very efficient for an ANC system. Using other filtering techniques apart from SE LMS in a cascaded filter model will lead to a complex structure. Thus, we can conclude that the proposed Variable Stage (VS) Cascaded SELMS Adaptive Filter model provides a cost-effective and straightforward solution for PCG signal denoising in recording heart signals.

8. Conclusion

A robust signal denoising scheme is presented in this paper based on a novel multistage cascaded LMS adaptive algorithm. The proposed Variable Stage (VS) Cascaded SELMS Adaptive Filter model in ANC systems offers an improved solution to achieve faster convergence speed and a lower MSE by automatically adjusting the number of filter stages cascaded and the step size for each stage. The simulation performed on fetal PCG and pathological PCG signals concludes that the proposed VS Cascaded SELMS Adaptive Filter outperforms the conventional SELMS and the existing 2-stage and 3-stage cascaded LMS adaptive filter structure, thus improving convergence speed. Also, significantly lower MSE is achieved by the proposed filter model than the conventional SELMS, 2-stage, and 3-stage cascaded LMS filter structures. Cost-effective hardware ANC systems can be implemented using the proposed filter model with simple mathematical modeling.

Data Availability

Data were taken from the PhysioNet database. (https://doi.org/10.13026/42eg-8e59).

Conflicts of Interest

The authors declare that they have no conflicts of interest.

Acknowledgments

This work was supported by FRGS, Ministry of Higher Education, Malaysia, and Universiti Malaya under Project FRGS/1/2019/TK04/UM/01/2.

References

[1] A. K. Abbas and R. Bassam, "Phonocardiography signal processing," *Synthesis Lectures on Biomedical Engineering*, vol. 4, no. 1, pp. 1–194, 2009.

[2] A. Leatham, "Auscultation and phonocardiography: a personal view of the past 40 years," *Heart*, vol. 57, no. 5, pp. 397–403, 1987.

[3] H. Kuresan, D. Samiappan, and S. Masunda, "Fusion of WPT and MFCC feature extraction in Parkinson's disease diagnosis," *Technology and Health Care*, vol. 27, no. 4, pp. 363–372, 2019.

[4] S. Latha, D. Samiappan, and R. Kumar, "Carotid artery ultrasound image analysis: a review of the literature," *Proceedings of the Institution of Mechanical Engineers - Part H: Journal of Engineering in Medicine*, vol. 234, no. 5, pp. 417–443, 2020.

[5] D. Kumar, P. Carvalho, M. Antunes, R. P. Paiva, and J. Henriques, "Noise detection during heart sound recording using periodicity signatures," *Physiological Measurement*, vol. 32, no. 5, pp. 599–618, 2011.

[6] A. Abdullrahim and R. De Coster, "A Framework of E-Health Systems Adoption and Telemedicine Readiness in Developing Countries," in *Proceedings of the 2016 International Conference on Information Society (i-Society)*, pp. 105–108, IEEE, Dublin, Ireland, October 2016.

[7] A. H. Salman, N. Ahmadi, R. Mengko, A. Z. Langi, and T. L. Mengko, "Performance comparison of denoising methods for heart sound signal," in *Proceedings of the 2015 International Symposium on Intelligent Signal Processing and Communication Systems (ISPACS)*, pp. 435–440, IEEE, Nusa Dua Bali, Indonesia, November 2015.

[8] S. K. Ghosh, P. R. Nagarajan, and R. K. Tripathy, "Heart sound data acquisition and preprocessing techniques," in *Handbook of Research on Advancements of Artificial Intelligence in Healthcare Engineering*, pp. 244–264, IGI Global, Pennsylvania, PA, USA, 2020.

[9] M. N. Ali, E.-S. A. El-Dahshan, and A. H. Yahia, "Denoising of heart sound signals using Discrete Wavelet Transform," *Circuits, Systems, and Signal Processing*, vol. 36, no. 11, pp. 4482–4497, 2017.

[10] A. Gavrovska, M. Slavković, I. Reljin, and B. Reljin, "Application of wavelet and EMD-based denoising to phonocardiograms," in *Proceedings of the International Symposium on*

Signals, Circuits and Systems ISSCS2013, vol. 2012, pp. 1–10, Lasi, Romania, July 2013.

[11] H. Sun, W. Chen, and J. Gong, "An Improved Empirical Mode Decomposition-Wavelet Algorithm for Phonocardiogram Signal Denoising and its Application in the First and Second Heart Sound Extraction," in *Proceedings of the 6th International Conference on Biomedical Engineering and Informatics*, pp. 187–191, Hangzhou, China, December 2013.

[12] V. Sujadevi, K. Soman, S. S. Kumar, N. Mohan, and A. Arunjith, "Denoising of phonocardiogram signals using variational Mode decomposition," in *Proceedings of the 2017 International Conference on Advances in Computing, Communications and Informatics (ICACCI)*, pp. 1443–1446, IEEE, Udupi, India, September 2017.

[13] M. B. Figueiredo, A. de Almeida, and B. Ribeiro, "Wavelet decomposition and singular spectrum analysis for electrical signal denoising," in *Proceedings of the 2011 IEEE International Conference on Systems, Man, and Cybernetics*, pp. 3329–3334, IEEE, Anchorage, AK, USA, October 2011.

[14] S. Patidar and R. B. Pachori, "Tunable-Q Wavelet Transform Based Optimal Compression of Cardiac Sound signals," in *Proceedings of the 2016 IEEE Region 10 Conference (TENCON)*, pp. 2193–2197, Singapore, November 2016.

[15] S. K. Ghosh, R. K. Tripathy, and R. N. Ponnalagu, "Evaluation of Performance Metrics and Denoising of PCG Signal Using Wavelet Based Decomposition," in *Proceedings of the 2020 IEEE 17th India Council International Conference (INDICON)*, pp. 1–6, New Delhi, India, December 2020.

[16] R. Manohar Potdar, M. R. Meshram, and R. Kumar, "Optimal parameter selection for DWT based PCG denoising," *Turkish Journal of Computer and Mathematics Education*, vol. 12, no. 9, pp. 3207–3219, 2021.

[17] S. G. Sankaran and A. A. Beex, "Acoustic echo and Noise Canceler Improvements for Hands Free Telephones," in *Proceedings of the IEEE Southeastcon'97, Engineering the new Century*, pp. 148–150, Blacksburg, VA, USA, April 1997.

[18] S. Hannah Pauline, D. Samiappan, R. Kumar, A. Ankita Anand, and A. Kar, "Variable Tap Length Non-parametric Variable Step-Size NLMS Adaptive Filtering Algorithm for Acoustic Echo Cancellation," *Applied Acoustics*, vol. 159, pp. 1–9, 2020.

[19] M. Sambur, "Adaptive noise canceling for speech signals," *IEEE Transactions on Acoustics, Speech, & Signal Processing*, vol. 26, no. 5, pp. 419–423, 1978.

[20] M. Kalamani, S. Valarmathy, and M. Krishnamoorthi, "Adaptive noise reduction algorithm for speech enhancement," *World Acad. Sci. Eng. Technol. Int. J. Electr. Comput. Energ. Electron. Commun. Eng.*, vol. 8, no. 6, pp. 1007–1014, 2014.

[21] S. Li, S. Wu, Y. Wang, W. Guo, and Y. Zhou, "An Improved NLMS Algorithm Based on Speech Enhancement," in *Proceedings of the IEEE Advanced Information Technology,Electronic and Automation Control Conference*, pp. 896–899, Chongqing, China, December 2015.

[22] J. D. Krupa Abel, D. Samiappan, R. Kumar, and S. P. Kumar, "Multiple sub-filter adaptive noise canceller for fetal ECG extraction," *Procedia Computer Science*, vol. 165, pp. 182–188, 2019.

[23] N. G. Prelcic, F. P. González, M. Elena, and E. D. Jimenez, "Wavelet packet-based subband adaptive equalization," *Signal Processing*, vol. 81, no. 8, pp. 16–41, 2001.

[24] B. Farhang-Boroujeny, "An IIR adaptive line enhancer with controlled bandwidth," *IEEE Transactions on Signal Processing*, vol. 45, no. 2, pp. 477–481, 1997.

[25] S. Haykin and B. Widrow, *Least-Mean-Square Adaptive Filters*, Wiley, Newyork, NY, USA, First edition, 2003.

[26] A. D. Poularikas, *Adaptive Filtering: Fundamentals of Least Mean Squares with MATLAB®*, CRC Press,Taylor and Francis Group, Boca Rotan, FL, USA, First edition, 2014.

[27] N. Ahmed, D. Hush, G. Elliott, and R. Fogler, "Detection of multiple sinusoids using an adaptive cascaded structure," in *Proceedings of the IEEE International Conference on Acoustics, Speech, and Signal Processing*, pp. 199–202, San Diego, CA, USA, March 1984.

[28] P. Prandoni and M. Vetterli, "An FIR cascade structure for adaptive linear prediction," *IEEE Transactions on Signal Processing*, vol. 46, no. 9, pp. 2566–2571, 1998.

[29] M. Paez and T. Glisson, "Minimum mean-squared-error quantization in speech PCM and DPCM systems," *IEEE Transactions on Communications*, vol. 20, no. 2, pp. 225–230, 1972.

[30] M. Hans and R. W. Schafer, "Lossless compression of digital audio," *IEEE Signal Processing Magazine*, vol. 18, no. 4, pp. 21–32, 2001.

[31] J. Rissanen, "A universal data compression system," *IEEE Transactions on Information Theory*, vol. 29, no. 5, pp. 656–664, 1983.

[32] T. Liebchen, M. Purat, and P. Noll, *Lossless Transform Coding of Audio Signal*, Proc. 102nd AES Conv, Munich, Germany, 1997.

[33] S. Haykin, *Adaptive Filter Theory*, Prentice-Hall, Englewood Cliffs, NJ, USA, 3rd edition, 1996.

[34] K. D. Hyun, K. Tamagawa, and Y. Sakamoto, "Lossless compression applying linear predictive coding based on the directionality of interference patterns of a hologram," *Applied Optics*, vol. 58, no. 18, pp. 5018–5028, 2019.

[35] R. Yu and C. C. Ko, "Lossless compression of digital audio using cascaded RLS-LMS prediction," *IEEE Transactions on Speech and Audio Processing*, vol. 11, no. 6, pp. 532–537, 2003.

[36] H. Haibin Huang, P. Franti, S. Dongyan Huang, and S. Rahardja, "Cascaded RLS-LMS prediction in MPEG-4 lossless audio coding," *IEEE Transactions on Audio Speech and Language Processing*, vol. 16, no. 3, pp. 554–562, 2008.

[37] D. R. Morgan, "An analysis of multiple correlation cancellation loops with a filter in the auxiliary path," *IEEE Transactions on Acoustics, Speech, & Signal Processing*, vol. 28, no. 8, pp. 454–467, 1980.

[38] X. Sun and S. M. Kuo, "Active narrowband noise control systems using cascading adaptive filters," *IEEE Transactions on Audio Speech and Language Processing*, vol. 15, no. 2, pp. 586–592, 2007.

[39] K. Ashok, A. Kalaiselvi, and V. R. Vijaykumar, "Adaptive impulse detection based selective window median filter for removal of random-valued impulse noise in digital images," *COMPEL: The International Journal for Computation & Mathematics in Electrical & Electronic Engineering*, vol. 35, no. 5, pp. 1604–1616, 2016.

[40] K. R. Griffiths, B. J. Hicks, P. S. Keogh, and D. Shires, "Wavelet analysis to decompose a vibration simulation signal to improve pre-distribution testing of packaging," *Mechanical Systems and Signal Processing*, vol. 76-77, no. 3, pp. 780–795, 2016.

[41] F. Miao, R. Zhao, and X. Wang, "A new method of denoising of vibration signal and its application," *Shock and Vibration*, vol. 2020, Article ID 7587840, 2020.

[42] J. Freudenberger and S. Stenzel, *Suppression of Engine Noise Harmonics Using Cascaded LMS Filters*, pp. 1–4, ITG Symposium on Speech Communication, Germany, 2012.

[43] Q. Yang, K. Lee, and B. Kim, "Development of multi-staged adaptive filtering algorithm for periodic structure-based active vibration control system," *Applied Sciences*, vol. 9, 611 pages, 2019.

[44] X. Zhang, N. Feng, Y. Wang, and Y. Shen, "Acoustic emission detection of rail defect based on wavelet transform and Shannon entropy," *Journal of Sound and Vibration*, vol. 339, pp. 419–432, 2015.

[45] X. Zhang, Y. Cui, Y. Wang, M. Sun, and H. Hu, "An improved AE detection method of rail defect based on multi-level ANC with VSS-LMS," *Mechanical Systems and Signal Processing*, vol. 99, pp. 420–433, 2018.

[46] F. C. Robertson, T. S. Douglas, and E. M. Meintjes, "Motion artifact removal for functional near infrared spectroscopy: a comparison of methods," *IEEE Transactions on Biomedical Engineering*, vol. 57, no. 6, pp. 1377–1387, 2010.

[47] H. Kim, S. Kim, N. VanHelleputte et al., "Motion Artifact Removal Using cascade Adaptive Filtering for Ambulatory ECG Monitoring System," in *Proceedings of the IEEE Biomedical Circuits and Systems Conference*, pp. 160–163, Hsinchu, Taiwan, November 2012.

[48] A. Mehmood, M. I. Baig, E.-U. Haq, and L. Aslam, "Artifacts removal from ECG signal using a multistage MNLMS adaptive algorithm," *International Journal of Signal Processing, Image Processing and Pattern Recognition*, vol. 10, no. 11, pp. 13–22, 2017.

[49] S. Dixit and D. Nagaria, "Design and analysis of cascaded LMS adaptive filters for noise cancellation," *Circuits, Systems, and Signal Processing*, vol. 36, no. 2, pp. 1–25, 2017.

[50] A. K. Maurya, "Cascade-cascade least mean Square (LMS) adaptive noise cancellation," *Circuits, Systems, and Signal Processing*, vol. 37, no. 9, pp. 3785–3826, 2018.

[51] M. Liu, M.-J. Wang, and B.-Y. Song, "An Efficient Architecture of the Sign-Error LMS Adaptive Filter," in *Proceedings of the 2016 13th IEEE International Conference on Solid-State and Integrated Circuit Technology (ICSICT)*, pp. 753–755, Hangzhou, October 2016.

[52] D. Bismor, "Extension of LMS stability condition over a wide set of signals," *International Journal of Adaptive Control and Signal Processing*, vol. 29, no. 5, pp. 653–670, 2015.

[53] R. Sameni and M. Samieinasab, "Shiraz university fetal heart Sounds database" (version 1.0.1)," *PhysioNet*, 2021.

[54] M. Samieinasab and R. Sameni, "Fetal Phonocardiogram Extraction Using Single Channel Blind Source Separation," in *Proceedings of the 2015 23rd Iranian Conference on Electrical Engineering*, pp. 78–83, Tehran, Iran, May 2015.

[55] C. Liu, D. Springer, Q. Li et al., "An open access database for the evaluation of heart sound algorithms," *Physiological Measurement*, vol. 37, no. 12, pp. 2181–2213, 2016.

[56] A. Goldberger, "PhysioBank, PhysioToolkit, and PhysioNet: components of a new research resource for complex physiologic signals," *Circulation [Online]*, vol. 101, no. 23, pp. 215–220, 2020.

[57] K. B. Khan, A. A. Khaliq, M. Shahid, and J. A. Shah, "A new approach of weighted gradient filter for denoising of medical images in the presence of Poisson Noise," *Tehnički Vjesnik*, vol. 23, no. 6, pp. 1755–1762, 2016.

[58] K. B. Khan, A. A. Khaliq, M. Shahid, and H. Ullah, "Poisson noise reduction in scintigraphic images using Gradient Adaptive Trimmed Mean filter," in *Proceedings of the 2016 International Conference on Intelligent Systems Engineering (ICISE)*, pp. 301–305, IEEE, Islamabad, Pakistan, January 2016.

[59] H. Ullah, M. Amir, I. Ul Haq, S. U. Khan, M. K. A. Rahim, and K. B. Khan, "Wavelet based de-noising using logarithmic shrinkage function," *Wireless Personal Communications*, vol. 98, no. 1, pp. 1473–1488, 2018.

[60] K. B. Khan, M. Shahid, H. Ullah, E. Rehman, and M. M. Khan, "Adaptive trimmed mean autoregressive model for reduction of Poisson noise in scintigraphic images," *IIUM Engineering Journal*, vol. 19, no. 2, pp. 68–79, 2018.

[61] D. Samiappan and V. Chakrapani, "Classification of carotid artery abnormalities in ultrasound images using an artificial neural classifier," *The International Arab Journal of Information Technology*, vol. 13, no. 6, 2016.

[62] S. Dhanalakshmi and C. Venkatesh, "Classification of ultrasound carotid artery images using texture features," *International Review on Computers and Software (IRECOS)*, vol. 8, no. 4, pp. 933–940, 2013.

[63] Q. Ling, M. A. Ikbal, and P. Kumar, "Optimized LMS algorithm for system identification and noise cancellation," *Journal of Intelligent Systems*, vol. 30, no. 1, pp. 487–498, 2021.

[64] M. Salah, M. Dessouky, and B. Abdelhamid, "Design and Implementation of an Improved Variable Step-Size NLMS-Based Algorithm for Acoustic Noise Cancellation," *Circuits, Systems, and Signal Processing*, vol. 41, pp. 551–578, 2021.

[65] M. W. Munir and W. H. Abdulla, "On FxLMS scheme for active noise control at remote location," *IEEE Access*, vol. 8, pp. 214071–214086, 2020.

[66] G. Li, H. Zhang, and J. Zhao, "Modified Combined-Step-Size Affine Projection Sign Algorithms for Robust Adaptive Filtering in Impulsive Interference Environments," *Symmetry*, vol. 12, 2020.

[67] V. Tejaswi, A. Surendar, and N. Srikanta, "Simulink implementation of RLS algorithm for resilient artefacts removal in ECG signal," *International Journal of Advanced Intelligence Paradigms*, vol. 16, no. 3–4, pp. 324–337, 2020.

Hindawi
Journal of Healthcare Engineering
Volume 2022, Article ID 5998042, 25 pages
https://doi.org/10.1155/2022/5998042

Review Article

Radiological Analysis of COVID-19 Using Computational Intelligence: A Broad Gauge Study

S. Vineth Ligi,[1] **Soumya Snigdha Kundu**,[2] **R. Kumar**,[1] **R. Narayanamoorthi**,[3] **Khin Wee Lai**,[4] **and Samiappan Dhanalakshmi**[1]

[1]*Department of Electronics and Communication Engineering, College of Engineering and Technology, Faculty of Engineering and Technology, SRM Institute of Science and Technology, SRM Nagar, Kattankulathur, Chengalpattu, Chennai, TN, India*
[2]*Department of Computer Science Engineering, College of Engineering and Technology, Faculty of Engineering and Technology, SRM Institute of Science and Technology, SRM Nagar, Kattankulathur, Chengalpattu, Chennai, TN, India*
[3]*Department of Electrical and Electronics Engineering, College of Engineering and Technology, Faculty of Engineering and Technology, SRM Institute of Science and Technology, SRM Nagar, Kattankulathur, Chengalpattu, Chennai, TN, India*
[4]*Department of Biomedical Engineering, Faculty of Engineering, Universiti Malaya, Kuala Lumpur, Malaysia*

Correspondence should be addressed to Khin Wee Lai; lai.khinwee@um.edu.my and Samiappan Dhanalakshmi; dhanalas@srmist.edu.in

Received 13 August 2021; Revised 13 December 2021; Accepted 7 January 2022; Published 23 February 2022

Academic Editor: Cosimo Ieracitano

Pulmonary medical image analysis using image processing and deep learning approaches has made remarkable achievements in the diagnosis, prognosis, and severity check of lung diseases. The epidemic of COVID-19 brought out by the novel coronavirus has triggered a critical need for artificial intelligence assistance in diagnosing and controlling the disease to reduce its effects on people and global economies. This study aimed at identifying the various COVID-19 medical imaging analysis models proposed by different researchers and featured their merits and demerits. It gives a detailed discussion on the existing COVID-19 detection methodologies (diagnosis, prognosis, and severity/risk detection) and the challenges encountered for the same. It also highlights the various preprocessing and post-processing methods involved to enhance the detection mechanism. This work also tries to bring out the different unexplored research areas that are available for medical image analysis and how the vast research done for COVID-19 can advance the field. Despite deep learning methods presenting high levels of efficiency, some limitations have been briefly described in the study. Hence, this review can help understand the utilization and pros and cons of deep learning in analyzing medical images.

1. Introduction

The pandemic brought forth by the coronavirus disease 2019 (COVID-19) not only sustains a devastating response on the well-being and health of the worldwide population but also demands a high rate of monitoring so that it does not extend on its destructive path. A vital aspect of the battle against COVID-19 is the efficient examination of the patients, which can help the infected receive quick treatment and immediate care. As of now, the customary screening process to identify COVID-19 is the reverse transcriptase-polymerase chain reaction (RT-PCR) test method. This test identifies the presence of SARS-CoV-2 ribonucleic acid (RNA) in respiratory specimen samples (obtained via a range of procedures such as the nasopharyngeal or oropharyngeal swabs) [1]. The RT-PCR test method, despite being effective, has a few shortcomings. It is time-consuming, complicated, and involves a lot of manual labor. All these concerns make it difficult to comb through the highly populated regions where millions have to be tested in a rapid norm. It is also

seen that the test's sensitivity aspect is highly variable [2, 3]. Radiographic examination was opted as recourse to surmount the difficulties in RT-PCR testing. Chest radiographs (computed tomography (CT) and chest X-ray (CXR) imaging) are imaged and examined by radiologists (as depicted in Figure 1(a)) to find visible references in tandem to the infection.

Preliminary studies discovered that patients affected by COVID-19 infection have abnormalities in chest radiographic images, with a few proposing that radiographic evaluation could be implemented as the principal method for COVID-19 screening in highly populated epidemic areas [4, 5]. Among radiographs, the CXRs are preferred over CTs [6] as they support rapid triaging in parallel to viral testing while being readily accessible and available. It is also easy to target multiple regions due to its portability. The more outstanding image quality of CT has to be sacrificed to avail these merits. Although the radiographs generated can significantly improve the process, it requires some form of automation. Doctors can hasten the diagnostic procedure, but it still involves scads of manual labor from skilled radiologists, which is not a feasible solution to tackle the large number of COVID-19 patients. To overcome this constraint, there have been constant research attempts utilizing deep learning (DL) methods to find the abnormalities (as seen in Figure 1(b)) in radiographs [7].

Convolutional neural network (CNN) is the primary choice of neural network framework for any DL practitioner working with medical images [8] and radiographs [9] along with vision-based tasks in general such as classification [10], object detection [11], and segmentation [12]. DenseNet, a type of CNN that forms the base to many of the architecture used to recognize COVID-19 from CTs and CXRs, is shown in Figure 2. CNNs stem from the mathematical operation of convolutions (as shown in Figure 3), which expresses the shape modification of functions. The term convolution encompasses the process and its result function. The ability of CNNs to analyze and capture spatial information helps to perform better than most other algorithms present. CNNs generally comprise convolutional layers, pooling layers, and various filters. The architecture usage depends on the demand and size of data available with which it is training. Dropout [13] and transfer learning [14] are commonly used techniques to improve the model's performance. Normalization approaches such as batch normalization [15] and group normalization [16] help improve the model's performance, provide the ability to users in building larger models, and tackle the vanishing gradient problem.

Machine learning (ML) algorithms are generally chosen over DL algorithms to compensate the computational requirements, but in the medical field, time and computational requirements are always traded off for higher standards of precision and hence used in preprocessing [19], feature selection [20], classification [21], and regression [22]. As the COIVD-19 demanded faster results, machine learning avenues have been explored (as shown in Table 1) to account for the global situation constraints. The outline of the application of the COVID-19 detection system in the real world is pictorially represented in Figure 4. In [18], an extensive study comparing K-nearest neighbor (KNN) and support vector machine (SVM) to CNNs was made. The experimentation presented that the DL classifiers trump the machine learning classifiers. Additionally, the DL-based classification methods generate results nearly 5 times faster than the machine learning classifiers. Hence, they are applied in various fields [23–26]. On experimentation with MobileNetV2 [27], the run time and computational power requirements were further reduced. Table 2 lists the history of the networks used.

A simple inference that can be made throughout all the literature is that the DL models (especially CNNs) surmount the ML models due to their capability of capturing spatial information. The spatial correlations are completely absent in general ML methods and hence fail to capture important correlations or key points that are absent while considering the image in a linear aspect. The DL models are ultimately black box models, and the ML methods are easily interpretable. Still, recent explainable methods such as class activation maps [48, 49] help remove that barrier and let the user know how the model is providing an output or how the inference is generally created [50, 51].

1.1. Review Outline. The following contributions are made through this review study:

(i) A detailed discussion is done with respect to the COVID-19 prediction approaches of the preceding reviews. The study analyses their merits and demerits and provides key insights as well regarding the same. It covers the essential aspects of COVID-19 research that the previous studies have missed.

(ii) A systematic comparison is studied encompassing COVID-19 detection techniques about prognosis, diagnosis, and severity/risk detection.

(iii) An extensive discussion on the challenges with regard to fostering high-quality results in detecting COVID-19. Solutions for these challenges are presented alongside as well.

(iv) An in-depth analysis of the pre- and post-processing methods used on the COVID-19 datasets and architectures is provided.

(v) Discussion on the unexplored areas such as meta-learning and self-supervised learning and defining the explorable research avenues regarding the same are presented.

(vi) This work emphasizes how most of the research that takes place for COVID-19 can help propagate research for other diseases and medical image analysis in general.

Moving on to Section 2, the discussion is carried out regarding the premier approaches in COVID-19 detection methodologies on diagnosis, prognosis, and severity/risk detection. The inferences collected from reviewing the papers are also noted. Section 3 discusses the merits and limitations of the past reviews, which have described past attempts on detecting COVID-19 through deep learning

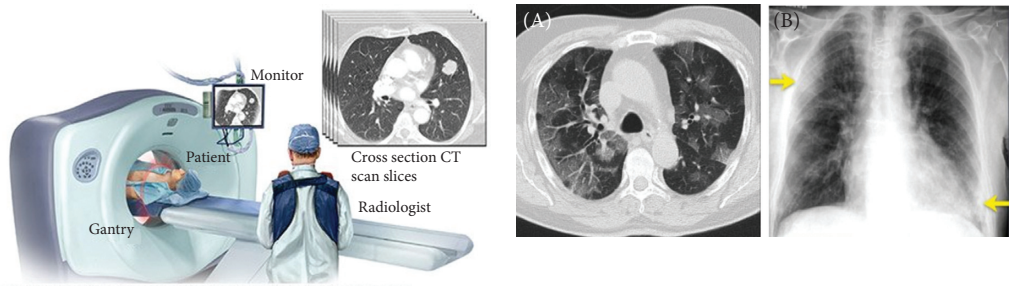

(a) (b)

Figure 1: (a) Radiological image acquisition (courtesy: newsnetwork.mayoclinic.org/discussion/mayo-clinic-radio-lung-cancer-updatehousehold-health-hazardsprediabetes). (b) (A) Axial chest CT image (non-enhanced) of a positive RT-PCR-confirmed 70-year-old man showing ground-glass opacities along with dilated segmental and subsegmental vessels prominent on the right side. (b) (B) CXR showing pulmonary hypertension, mitral insufficiency, and atrial fibrillation along with COVID-19 contagion in an 83-year-old man (arrows indicating ground-glass opacity findings in the upper right lobe and consolidation findings in the lower left lobe of the lungs) (arrows) (courtesy: radiologyassistant.nl).

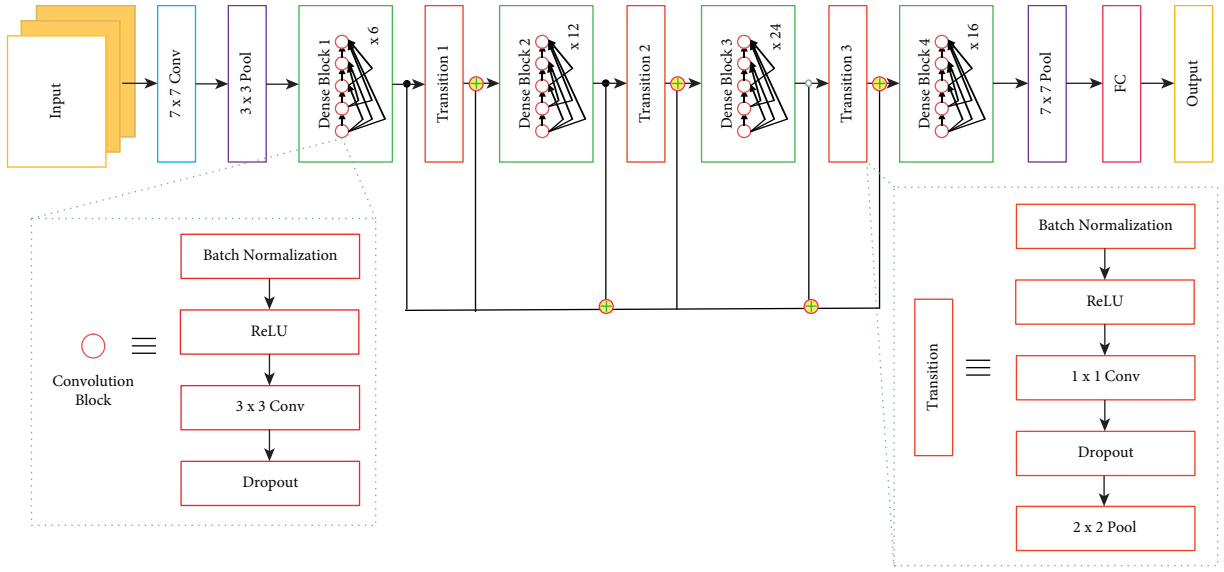

Figure 2: Example of DenseNet architecture.

methods. The section also includes an extension to the solutions provided to the challenges mentioned in Shorten et al. [52] by exploring different paradigms of deep learning. A discussion on the various vision-based pre- and post-processing techniques used to improve deep learning algorithms is given in Section 4. The review continues by identifying more challenges faced while attempting to detect COVID-19 and a brief discourse on the future directions to utilize the vast research done for COVID-19 towards the domain of medical image analysis in general under Section 5 and the conclusion in Section 6.

2. Discussion on COVID-19 Medical Image Analysis

The major COVID-19 medical image analysis tasks are as follows: diagnosis, prognosis, and severity/risk detection. The upsurge of the COVID-19 epidemic has triggered many researchers to contribute their research findings in pulmonary image analysis using DL and other image processing techniques leading to an astonishing breakthrough in COVID-19 diagnosis with stupendous amount of quality works. Discerning COVID-19 from other non-COVID-19 conditions is an important issue to be addressed; hence, the study has been majorly categorized as follows: COVID-19/non-COVID-19 pneumonia (2-class classification) and COVID-19/non-COVID-19 pneumonia/normal (3-class classification). The study also includes a discussion on classifying COVID-19 against normal condition and other lung diseases, the impact of 2-class and 3-class classifications using the same algorithm on the same dataset, and performing the same classification technique on different image modalities (CT and CXR). The aforementioned workflow has been pictorially depicted in Figure 5.

2.1. COVID-19 Diagnosis. COVID-19 diagnostic approach based on medical image analysis utilizes the CXR and CT

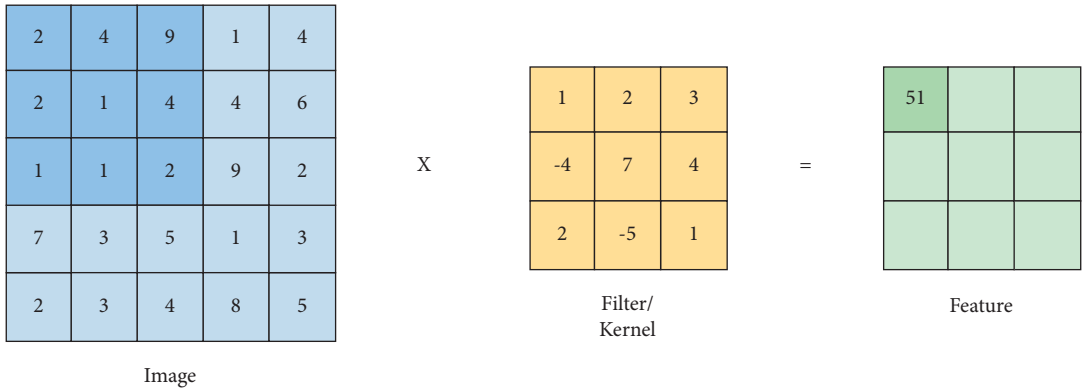

Figure 3: 2D feature extraction by filters and kernels from images through convolution operations.

Table 1: Machine learning techniques tried and true in preceding COVID-19 medical image analysis.

Algorithm	Summary
RF[1] [17]	Utilized quantitative features of CT scans
SVM [18]	Tested SVM (RBF)[1] on raw and modified CT images
KNN [18]	Tested KNN ($N = 21$)[1] on raw and modified CT images

[1]RF indicates random forest algorithm. RBF indicates radial basis function. N indicates the number of neighbors considered. Rest all were set to the general settings.

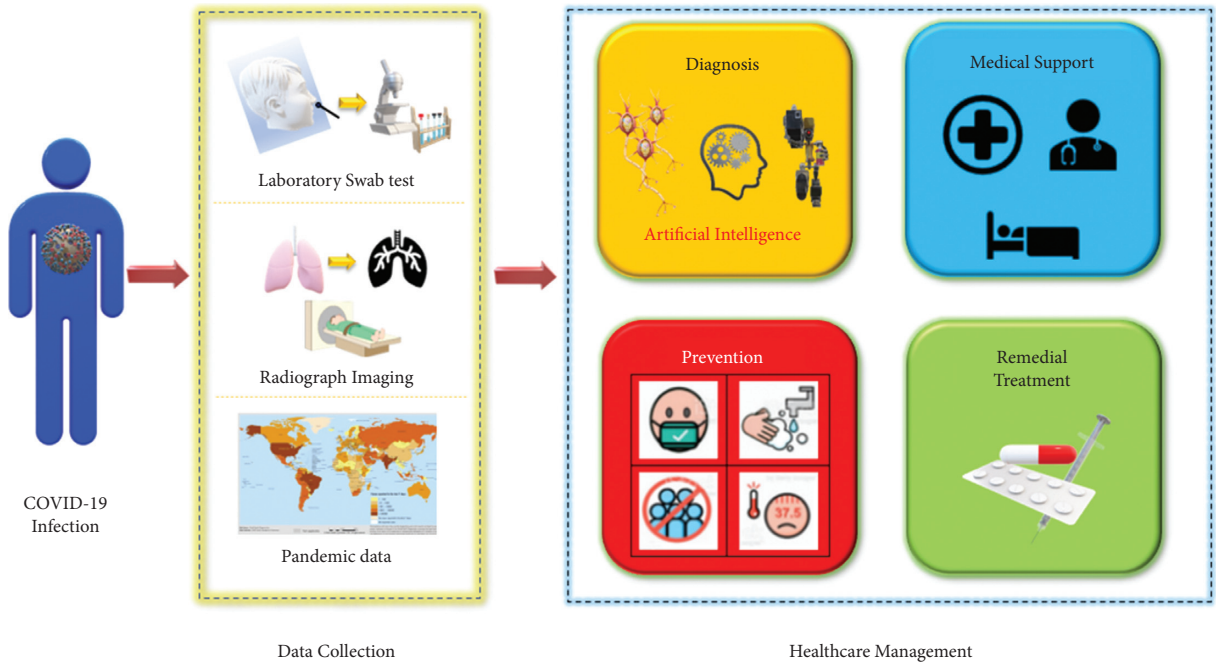

Figure 4: COVID-19 detection system.

images. AI can adequately improve the diagnostic model's efficiency by accurately locating the infections due to the virus in X-ray and CT images, hence facilitating assistance to the radiologists in making clinical decisions for disease diagnosis and triage. [53].

2.1.1. COVID-19/Non-COVID-19 Pneumonia Diagnosis. Harmon et al. [54] proposed an AI-based 3D model using DenseNet-121 to identify COVID-19 from multinational CT data. 2724 scans from 2617 COVID-19 victims were used in this work, among which 1029 scans belonged to 922 RT-PCR-confirmed COVID-19 patients. Initially, the lung region was segmented using Anisotropic Hybrid-Net (AH-Net) architecture. On testing the model using an independent dataset, it achieved accuracy of 90.8%, area under the curve (AUC) of 0.949, sensitivity of 84%, specificity of 93%, positive predictive value (PPV) of 0.794, and negative predictive value (NPV) of 0.984 with sufficient generalization. In 140 non-COVID-19 pneumonia patients, the false-

Table 2: Evolution of CNNs since 1959. The table describes primary points of novelty that motivated new architectures to be produced.

Architecture	Primary focus and novelty	Author and year
Simple and complex cells [28]	Described cells in the human cortex. Proposed its use case in pattern recognition.	Hubel & Wiesel (1959)
Neocognitron [29]	Converted the cell idea from [28] into a computational model. First modern CNN.	Fukushima (1980)
LeNet-5 [30]	Composed of two convolution layers with three fully connected layers. Introduced the MNIST database.	Lecun et al. (1998)
AlexNet [31]	Implemented overlapping pooling and ReLU [32]. Non-saturating neurons are used. Facilities' effective usage of GPU-driven methods.	Krizhevsky et al. (2012)
VGG-16 [33]	Made an exhaustive evaluation on architectures of increasing depth. Used architectures with tiny (3×3) convolution filters.	Simonyan and Zisserman (2014)
Inception [34]	Dimensions of network are increased while keeping the computational budget constant. Utilized the Hebbian principle and multiscale processing.	Szegedy et al. (2015)
Modified VGG-16 [35]	Proposed that if a model is strong enough to fit a large dataset, it can also fit to a small one.	Liu and Deng (2015)
ResNet [36]	Presented a residual learning framework. Allowed building larger models with deeper layers through skip connections. Paved the way for more variants [37, 38].	He et al. (2015)
Xception [39]	Presented a depth-wise separable convolution as an inception module with a maximally large number of towers.	Chollet (2016)
MobileNets [40]	Made for mobile and embedded vision applications. Streamlined architecture using depth-wise separable convolutions.	Howard et al. (2017)
ResNeXt [41]	Presented cardinality (size of the transformation set) as a key factor along with the dimensions of an architecture.	Xie et al. (2017)
DenseNet [42]	Complete intra-layer connections among all singular connections in a feed-forward fashion. Strengthens feature propagation and encourages feature reuse.	Blei et al. (2017)
Squeeze-and-excitation block [43]	Adaptively recalibrates channel-wise feature responses by explicitly modelling interdependencies between channels.	Hu et al. (2018)
Residual inception [44]	Combined residual and inception module.	Zhang et al. (2018)
NASNet search space [45]	Designed a new search space to enable transferability. Presented a new regularization technique—scheduled drop path	Zoph et al. (2018)
EfficientNet [46]	Proposed a novel scaling technique that scales all the dimensions (width/resolution/depth) uniformly using a compound coefficient.	Tan and Le (2019)
Normalizer-free models [47]	Developed an adaptive gradient clipping technique to overcome instability. Designed a significantly improved class.	Brock et al. (2021)

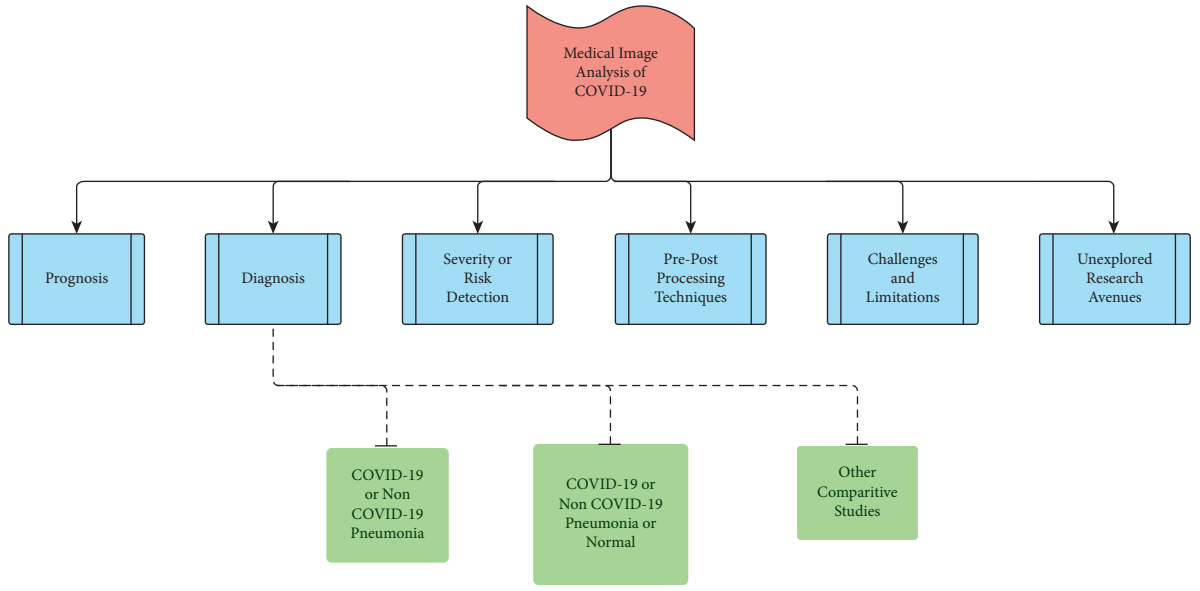

Figure 5: Flow of review on different medical imaging analysis tasks.

positive rate was 10%. This model was able to furnish reasonable performance metrics, thereby enabling it as an unbiased clinical trial tool for assisting the COVID-19 medical image analysis in specific bounded societies during the epidemic outbreak.

A dual-sampling attention network realized by a 3D CNN using ResNet-34 with an online attention refinement and a dual-sampling strategy was proposed by Ouyang et al. [55] to categorize COVID-19 against community-acquired pneumonia (CAP). The model was evaluated on a multicenter CT dataset of 4982 images consisting of 1593 CAP and 3389 COVID-19 images. Dual-sampling strategy (uniform sampling and size-balanced sampling) was used to mitigate the effect of imbalanced learning and the online attention module to target the infected regions, thereby increasing the model explainability and interpretability by showing visual evidence to reveal the critical regions considered by the model for diagnosis. The ability to generalize the proposed model was evaluated using an autonomous test data, which gave an accuracy of 87.5%, AUC value of 0.944, along with sensitivity of 86.9%, specificity of 90.1%, and $F1$ score of 82.0%.

A multiview fusion model using ResNet-50 was developed by Wu et al. [56], which makes use of the axial, sagittal, and coronal views of CT as the three-channel input image to the model. A multicenter dataset consisting of high-resolution CT images of 368 COVID-19-infected patients and 127 patients suffering from other pneumonia (67 viral pneumonia, 47 bacterial pneumonia, 11 mycoplasma pneumonia, and 2 fungal pneumonia) were collected. The multiview model shows better performance than the single-view model with an accuracy of 76%, AUC value of 0.819, sensitivity of 81.1%, specificity of 61.5%, and overcoming the overfitting issue of the single-view model. This model can mitigate the work burden of radiologists and hence improve the diagnostic efficiency.

Ardakani et al. [57] compared ten convolutional neural networks: ResNet-101, ResNet-50, ResNet-18, VGG-16, VGG-19, MobileNetV2, SqueezeNet, AlexNet, GoogLeNet, and Xception to distinguish COVID-19 against non-COVID-19 pneumonia. A dataset consisting of 1020 high-resolution CT scan slices from 108 COIVD-19 victims and 86 victims with non-COVID-19 pneumonia (viral pneumonia and other atypical pneumonia) were collected. ResNet-101 surpassed the other CNNs due to its high sensitivity of 100% and AUC value of 0.994 for the given dataset. It also achieved accuracy of 99.51%, specificity of 99.02%, PPV of 99.03%, and NPV of 100%. This model is claimed to remove the substantial cost and can be used as an ancillary method in CT imaging.

An adaptive feature selection-guided deep forest (AFS-DF) method was proposed by Sun et al. [58] for COVID-19 classification using CT radiographs. The deep forest model was used on four location-specific handcrafted features such as volume, surface area, number of infected lesions, and histogram distribution from the CT images to describe high-level feature representation. The selected features were classified using SVM. A dataset consisting of 2522 de-identified pulmonary CT images from 1027 CAP and 1495 COVID-19-infected patients was used for this study. The proposed AFS-DF variants outperform by achieving 1.38%, 1.15%, and 1.11% enhancement over their obverse methods (logistic regression (LR), SVM, and RF) in most of the evaluation metrics. AFS-DF-SVM outperforms the other models with accuracy of 91.79%, AUC value of 0.9635, sensitivity of 93.05%, and specificity of 89.95%. ASF-DF reduces the repetition of features using the trained forest.

In the study by Narin et al. [59], binary classifications were performed to distinguish COVID-19 against viral and bacterial pneumonia using 341 COVID-19 CXRs and 2800 normal CXRs from the GitHub repository (open source) commonly contributed by Cohen et al. [60] and ChestX-ray8 database [61], respectively. 2772 bacterial pneumonia and 1493 viral pneumonia CXRs were collected from a Kaggle repository called chest X-ray images (pneumonia) [62]. The model performance of five different pre-trained CNN variants (ResNet-152, ResNet-101, ResNet-50, Inception-ResNetV2, and InceptionV3) was compared, among which ResNet-50 model showcased the highest classification performance. This model achieved an accuracy, precision, and specificity of 99.5%, 98.0%, and 99.5%, respectively, for discriminating COVID-19 against other viral pneumonia, whereas for COVID-19/bacterial pneumonia classification, the accuracy, precision, and specificity values were 99.7%, 98.3%, and 99.8%, respectively. This method was implemented directly in an end-to-end manner eliminating manual intervention for feature extraction, feature selection, or classification tasks.

A deep learning model comprising of three major components, a backbone network, a classification head, and an anomaly detection head, was proposed by Zhang et al. [63] to reduce the false-negative rate as much as possible. The model was built using 1431 CXR pneumonia images of 1008 patients from the ChestX-ray14 dataset [61] and 100 images belonging to 70 COVID-19 patients from the GitHub repository [60]. The experiment was conducted for different values of T parameter that controls the compensation between the true-positive rate and the true-negative rate. As the T value decreases from 0.50 to 0.15, the sensitivity increases from 72.00% to 96.00% and the specificity drops from 97.97% to 70.65%, but the AUC value remains the same. Based on the performance metrics (sensitivity—96%, specificity—70.65%, and AUC—95.18), the model performs well for $T = 0.15$ with a reduced false-negative rate of nearly 4%. Despite its good performance, it had its limitations, 4% missing COVID-19 cases and a false-positive rate of almost 30%.

Abraham and Nair [64] used a combination of multi-CNN models (MobileNetV2, SqueezeNet, Xception, DarkNet-53, and ShuffleNet) with correlation-based feature selection (CFS) followed by the BayesNet classifier. The experiment was performed using two datasets: Dataset I: 453 COVID-19 and 107 non-COVID-19 images of either bacterial/viral pneumonia [55] and 390 CXRs of viral and bacterial pneumonia [60, 61, 65, 66] and Dataset II: 71 COVID-19 CXRs and 7 non-COVID-19 CXRs [66]. Only the BayesNet classifier achieved an accuracy of >90%. The

proposed model gave an accuracy of 91.16% and 91.44% for Dataset I and Dataset II, respectively. The multi-CNNs (with 3 or more pre-trained CNNs) comparatively showed better results than the single pre-trained CNNs.

Autee et al. [67] proposed the StackNet-DenVIS to reduce the false-negative rate in classification using a stacked generalization ensemble of four different CNNs. A total of 9953 CXRs consisting of 9085 non-COVID-19 and 868 COVID-19 cases from multiple sources were gathered [60, 65, 68, 69]. The data imbalance problem was handled by generating synthetic images using deep convolutional adversarial generative networks and SMOTE + Tomex links. With an accuracy of 95.07%, this model achieved a low false-negative rate at low cost in comparison with the RT-PCR test.

2.1.2. COVID-19/Non-COVID-19 Pneumonia/Normal or Non-Pneumonia Diagnosis. A 3D deep learning framework, COVNet, realized using ResNet-50 was implemented by Li et al. [70] to distinguish COVID-19 against CAP and non-pneumonia cases. The network was able to extract the 2D local features and the 3D global representative features for better classification. A CT image dataset consisting of 1292 COVID-19 CTs, 1325 CTs with non-COVID-19 pneumonia, and 1735 CTs with CAP infections, totally contributing to 4352 scans, was collected for this study. An AUC value of 0.96, sensitivity of 90%, and specificity of 96% were obtained with 95% confidence interval for an independent test dataset. Due to the shortage of laboratory-confirmed COVID-19 data, the work was unable to present the results for distinguishing COVID-19 from other lung diseases.

Wang et al. [71] have proposed a prior-attention residual model, PA-66-M, using two subnetworks based on 3D ResNets for pneumonia detection and classification of pneumonia type. The two subnetworks were integrated by a late-fusion strategy using a fully connected layer with learning capacity. Lung segmentation was performed using U-Net. The dataset consisting of 936 chest CTs of normal cases, 2406 CT images with interstitial lung disease (only viral pneumonia), and 1315 COVID-19-infected CT images was collected from multiple cooperative hospitals. The proposed model was capable of accurately focusing the lesions with an accuracy, sensitivity, and specificity of 93.3%, 87.6%, and 95.5%, respectively. By applying a constant weighting factor, the prior-attention residual model was able to converge faster than the self-attention strategy. Some of the normal scans were misclassified to pneumonia class by the proposed model, and it also failed to unveil some of the scans with COVID-19 lesions.

Hasan et al. [72] used handcrafted texture features based on Q-deformed entropy along with deep features from CNN. The extracted features were refined by analysis of variance (ANOVA) and then classified to distinguish COVID-19 from other pneumonia types and normal cases. The LSTM neural network classifier outperformed SVM, KNN, and LR with an accuracy of 99.68%. The performance of the combined features was better when compared to using only handcrafted or deep features.

Three-dimensional classification models using two CNNs namely the ResNet-23 and ResNet-18 were used by Butt et al. [73] to classify COVID-19/influenza A viral pneumonia (IAVP)/normal CT image patches. A location attention mechanism was incorporated to identify the corresponding location of the identified patch in the pulmonary CT image. This model was smart enough to accurately distinguish COVID-19, when compared to using a model without location attention mechanism. Hence, an overall accuracy of 86.7% was observed with sensitivity of 98.2%, specificity of 92.2%, and AUC value of 0.996. This work used 618 transverse-section CT samples in which 219 samples were obtained from nearly 110 COVID-19-infected patients, 224 scans from 224 IAVP patients, and 175 from healthy people.

Detailed relation extraction neural network (DRENet) is a pre-trained ResNet-50 with feature pyramid network proposed by Song et al. [74] to derive the top-K-level features and extract the image-level predictions for COVID-19 diagnosis at the patient level. For model development and evaluation, the dataset was collected from different hospitals comprising 777 CT images from 88 COVID-19 victims, 505 CT slices from 100 bacterial pneumonia patients, and 708 CT slices from 86 healthy people. The regions detected by the proposed model contained the most important feature of COVID-19 infection, ground-glass opacity (GGO). DRENet exhibited an efficient performance with an accuracy of 93% and F1 score of 0.93.

A social mimic optimization method was proposed by Toğaçar et al. [75] to select the potential deep features from the combined feature set of MobileNetV2 and SqueezeNet, to categorize COVID-19 from pneumonia and normal conditions. It provides efficient features by stacking the original images with the reconstructed fuzzy color images, which had better quality and reduced noise. It used 76 COVID-19 images from [60] and 295 COVID-19, 98 pneumonia, and 65 normal images from [69]. On classification using SVM, all performance metrics, F score, sensitivity, specificity, precision, and accuracy, were 100% for detecting COVID-19 cases, exhibiting an overall accuracy of 99.27%. The average values of F score, sensitivity, specificity, and precision for all the three classes are 0.9858, 98.33%, 99.69%, and 98.89%, respectively. The model was aimed to produce swift and more authentic results as MobileNetV2 and SqueezeNet used fewer parameters compared with the other networks.

Wang et al. [68] created an open-source network, COVID-Net, and public dataset, COVIDx, consisting of 13,975 CXR images belonging to 13,870 patients obtained by combining data from five different public data repositories [60, 76–79]. COVID-Net architecture used a lightweight residual design pattern called projection-expansion-projection-extension (PEPX) pre-trained on ImageNet dataset.

Compared with VGG-19 and ResNet-50 architectures, COVID-Net has lower complexity in terms of architecture and computations. It showed an accuracy of 93.3% with sensitivity of 91.0%. Qualitative analysis of the network implies that it does not depend on inappropriate information for decision-making.

Nishio et al. [80] have evaluated the performance of conventional neural network architectures with different data augmentation techniques (conventional method, mix up, and random image cropping and patching (RICAP)) to identify COVID-19 pneumonia from pulmonary X-rays. 215 COVID-19-infected, 533 non-COVID-19 pneumonia-infected, and 500 healthy CXR images [60, 80] were used for this work. VGG-16 with the combination of conventional with mix-up data augmentation was found to give better results with an accuracy of 83.7% and a sensitivity value of 90.9% compared with ResNet-50, DenseNet-121, MobileNet, and EfficientNet.

The MH-Net proposed by Canayaz et al. [81] makes use of two meta-heuristic algorithms namely the binary gray wolf optimization (BGWO) and binary particle swarm optimization (BPSO) to select the potential features extracted from VGG-19, ResNet, GoogLeNet, and AlexNet. Finally, an SVM classifier was used. 364 CXR images each of COVID-19, pneumonia, and normal cases ([60, 65, 69]) enhanced by the image contrast enhancement algorithm were used for this work. VGG-19 model with BPSO feature optimization (488 features) on the enhanced data outperforms the other models with an overall accuracy of 99.38%, sensitivity of 99.39%, and specificity of 99.69%. The unbalanced class problem is overcome using equal number of CXRs in each class, and also, it uses fewer parameters compared with other models.

The COVID-19 Inception-ResNet model (CoVIRNet) that uses different inception residual blocks for diagnosing COVID-19 infection from the CXR images was proposed by Almalki et al. [82]. Multiscale feature maps obtained from different depths, which are then concatenated by average pooling, are used to improve the efficiency of the proposed method. The problem of overfitting encountered by small datasets has been overcome using different regularization techniques in the deep learning blocks. The author proposed two approaches: (i) CoVIRNet-Inception-ResNet blocks consisting of a single inception module with extra branches of convolution layer using reduction factorization; (ii) CoVIRNet with RF-multiscale, multilayer features extracted from the proposed Inception-ResNet blocks are classified using a random forest classifier. For this, a multicenter dataset of size of 1251 was used, among which 284 COVID-19 infection images were collected from [79, 83]. 310 normal CXRs, 330 bacterial pneumonia, and 327 viral pneumonia-infected images were collected from [62]. On comparing the performance of CoVIRNet with fine-tuned versions of Xception, ResNet-101, MobileNetV2, and DenseNet-201, the second approach CoVIRNet with RF showed better performance with accuracy of 97.29%, precision of 97.74%, recall of 97.02%, and F score of 0.9732.

Subsection 2.1 gives a brief review on the different COVID-19 diagnostic methods by performing two-class or three-class classifications against other pneumonia/normal cases proposed by various researchers in both CXR and CT imaging modalities. Tables 3 and 4 summarize the studies including the network, dataset, and performance metrics used for the evaluation of COVID-19/non-COVID-19 pneumonia diagnosis and COVID-19/non-COVID-19 pneumonia/normal or non-pneumonia diagnosis, respectively. The performance metrics used for evaluation and their corresponding formulae are tabulated in Table 5.

2.1.3. Other Comparative Studies. Apart from the techniques mentioned in the previous sections, there are also other comparative studies done by some researchers, which explore the performance of a COVID-19 diagnostic algorithm for different image modalities (CT and CXR) or on datasets with binary (COVID-19/non-COVID-19) or multiclass classifications (COVID-19/non-COVID-19/normal/other lung diseases).

(1) Comparison of Binary and Multiclass Classification. Hu et al. [84] performed an automated diagnosis of COIVD-19 based on ShuffleNetV2 on pulmonary CT images. Two classifications are performed on the data collected from multiple sources. 16 different data augmentation operations were performed on the 1042 chest CT images (comprising of 521 COVID-19, 397 healthy, 76 bacterial pneumonia, and 48 SARS) to increase the dataset size for better training of the model. Binary classification of COVID-19 from the healthy cases obtained an accuracy of 91.21% along with sensitivity of 90.52%, specificity of 91.58%, and AUC value of 0.9689. In the case of multiclass classification (COVID-19/bacterial pneumonia/SARS), the accuracy dropped to 85.40% for the same algorithm. The sensitivity, specificity, and AUC values were 85.71%, 84.88%, and 0.9222, respectively.

Chowdhury et al. [69] had compared the performance of different pre-trained CNNs for COVID-19 detection with and without data augmentation using the data collected from multiple public datasets ([60, 83, 85]). Among the various networks analyzed, DenseNet-201 showed comparably better classification results for both COVID-19/normal and COVID-19/normal/pneumonia discrimination with image augmentation. The binary classification shows better performance with an accuracy of 99.7% compared with the multiclass problem with an accuracy of 97.94%. The performance difference was insignificant, and the overall performance of three-class problem was less in comparison with the binary classification problem.

COVID-DenseNet proposed by Sarker et al. [86] is a deep learning architecture realized using DenseNet-121 with transfer learning from CheXNet for the detection of COVID-19 from COVIDx [71] CXR images. The most significant regions in the image that were responsible for the prediction were highlighted by performing an interpretation analysis using Grad-CAM. The overall accuracy for COVID-19/non-COVID-19 classification and COVID-19/pneumonia/normal classification is 0.96 and 0.94, respectively. This work tried to make the model explainable and interpretable to certain extent using the Grad-CAM representation.

DarkCovidNet architecture based on the DarkNet-19 model was designed by Ozturk et al. [87] to identify COVID-19 from X-ray images collected from [60, 61] comprising of 127 COVID-19, 500 pneumonia, and 500 normal images. For COVID-19/no findings/pneumonia classification, the model produced a classification accuracy, sensitivity, and

Table 3: A summary of research reviewed on COVID-19/non-COVID-19 pneumonia diagnosis.

Work	Image modality	Dataset size	Method used	Accuracy (in %)	Sensitivity or recall (in %)	Specificity (in %)	AUC (in %)	Precision (in %)	F1 score
Harmon et al. [54]	CT	(i) 1029 COVID-19 (ii) 1695 non-COVID-19 Pneumonia	DenseNet-121 and AH-Net segmentation	90.8	84	93	94.9	NA	NA
Ouyang et al. [55]	CT	(i) 3389 COVID-19 (ii) 1593 CAP	Dual sampling Attention network with ResNet-34	87.5	86.9	90.1	94.4	NA	0.82
Wu et al. [56]	CT	(i) 331 COVID-19 (ii) 114 other pneumonia	Multiview fusion model using ResNet-50	76	81.1	61.5	81.9	NA	NA
Ardakani et al. [57]	CT	(i) 510 COVID-19 (ii) 510 non-COVID-19	ResNet-101	99.51	**100**	99.02	**99.4**	NA	NA
Sun et al. [58]	CT	(i) 1495 COVID-19 (ii) 1027 CAP	Adaptive feature Selection-guided deep forest—SVM	91.79	93.05	89.95	96.35	NA	NA
Narin et al. [59]	CXR	(i) 341 COVID-19 (ii) 1493 viral pneumonia (iii) 341 COVID-19 (iv) 2772 bacterial pneumonia	ResNet-50	99.5 **99.7**	99.4 98.8	99.5 **99.8**	NA NA	98 98.3	**0.987** 0.985
Zhang et al. [63]	CXR	(i) 100 COVID-19 (ii) 1431 pneumonia	Residual CNN with anomaly detection head	NA	96	70.65	95.18	NA	NA
Abraham and Nair [64]	CXR	(i) 453 COVID-19 (ii) 497 non-COVID-19 Pneumonia (i) 71 COVID-19 (ii) 7 non-COVID-19 Pneumonia	Combination of multi-CNN	91.16 91.44	98.5 98.6	NA NA	96.3 91.1	85.3 **98.6**	0.914 0.986
Autee et al. [67]	CXR	(i) 868 COVID-19 (ii) 9085 non-COVID-19	StackNet-DenVIS	95.07	99.40	94.61	98.40	NA	NA

Bold values represent the best result obtained for each performance metric among all the methodologies compared.

specificity of 87.02%, 85.35%, and 92.18%, respectively. In the case of binary classification COVID-19/no findings, the performance metrics increased to accuracy of 98.08%, sensitivity of 95.13%, and specificity of 95.3%. DarkCovidNet was able to diagnose COVID-19 within seconds.

Mahmud et al. [88] proposed the CovXNet architecture, which is a multi-dilation CNN architecture that makes use of transferable multi-receptive feature optimization technique for COVID-19 detection from CXR images. A balanced dataset consisting of 305 images of different resolutions collected from different medical centers was used for each class: COVID-19, viral pneumonia, bacterial pneumonia, and normal. For distinguishing COVID-19 against normal, bacterial pneumonia, and viral pneumonia, the binary classification resulted in a accuracy of 97.4%, 94.7%, and 87.3%, respectively. While carrying over the same architecture for

Table 4: A summary of research reviewed on COVID-19/non-COVID-19 pneumonia/normal or non-pneumonia diagnosis.

Work	Image modality	Dataset size	Method used	Accuracy (in %)	Sensitivity or recall (in %)	Specificity (in %)	AUC (in %)	Precision (in %)	F1 score
Li et al. [70]	CT	(i) 1292 COVID-19 (ii) 16325 non-COVID-19 pneumonia (iii) 1735 CAP	COVNet	NA	90	96	96	NA	NA
Wang et al. [71]	CT	(i) 1315 COVID-19 (ii) 963 normal (iii) 2406 ILD	Prior-attention Residual model 3D ResNets	93.3	87.6	95.5	NA	NA	NA
Hasan et al. [72]	CT	(i) 118 COVID-19 (ii) 96 pneumonia (iii) 107 normal	LSTM using Q-deformed entropy and deep features	**99.68**	NA	NA	NA	NA	NA
Butt et al. [73]	CT	(i) 219 COVID-19 (ii) 224 IAVP (iii) 175 normal	3D ResNets with location attention mechanism	86.7	98.2	92.2	**99.6**	81.3	0.839
Song et al. [74]	CT	(i) 777 COVID-19 (ii) 505 bacterial pneumonia (iii) 708 normal	DRENet	93	93	NA	NA	93	0.93
Toğaçar et al. [75]	CXR	(i) 371 COVID-19 (ii) 98 pneumonia (iii) 65 normal	SVM—social Mimic optimized deep features	99.27	98.33	99.69	NA	98.89	0.9858
Wang et al. [68]	CXR	(i) 358 COVID-19 (ii) 5538 non-COVID-19 pneumonia (iii) 8066 normal	COVID-Net	93.3	91	NA	NA	NA	NA
Nishio et al. [80]	CXR	(i) 215 COVID-19 (ii) 533 non-COVID-19 pneumonia (iii) 500 normal	VGG-16 with conventional and mix-up augmentation	83.7	90.9	NA	NA	NA	NA
Canayaz [81]	CXR	(i) 364 COVID-19 (ii) 364 pneumonia (iii) 364 normal	MH-Net	99.38	**99.39**	**99.69**	NA	**99.39**	**0.9938**
Almalki et al. [82]	CXR	(i) 284 COVID-19 (ii) 327 viral pneumonia (iii) 330 bacterial pneumonia (iv) 504 normal	CoVIRNet feature extractor with RF	97.29	97.02	NA	NA	97.74	0.9732

Bold values represent the best result obtained for each performance metric among all the methodologies compared.

Table 5: Performance metrics used in COVID-19 detection.

Performance metric	Accuracy	Sensitivity/recall	Specificity	Precision	F1 score
Formula	$(TP + TN)/(TP + FP + TN + FN)$	$TP/(FN + TP)$	$TN/(FP + TN)$	$TP/(FP + TP)$	$(2 * (R * P))/(R + P)$

TP—true positive, TN—true negative, FP—false positive, FN—false negative, R—recall, and P—precision.

multiclass classifications such as COVID-19/viral pneumonia/bacterial pneumonia and COVID-19/normal/viral pneumonia/bacterial pneumonia, the classification accuracies dropped to 89.6% and 90.2%, respectively. Based on the obtained results, distinguishing viral pneumonia from COVID-19 is arduous when compared to other diseases. CovXNet is highly scalable with huge receptive capacity.

(2) Comparison of COVID-19 Diagnostic Performance in CT and CXR Images. COVID-MTNet is a deep learning architecture proposed by Alom et al. [89] to perform multiple tasks such as COVID-19 segmentation and detection from CT and CXR images. A dataset of 3875 samples of COVID-19 pneumonia and 1341samples for normal cases was collected from [60, 62]. The infected regions were segmented using the NABLA-N network, and the detection process was performed using the inception recurrent residual neural network (IRRCNN) model with transfer learning. The segmentation network using pixel-level analysis significantly reduced the possibility of false-positive and false-negative detections. The model produced a segmentation accuracy of 94.52% for CXR images and 99.56% for CT images in the test data. In the detection model, an accuracy of 98.78% and 87.26% was observed in the CT and CXR images, respectively. These results show that the CT imaging modality better discriminates the COVID-19 infection from the normal cases. The detection model can be generalized and made to produce more accurate results by training greater number of samples. Some false-positive detections were observed in the segmentation model for CT images due to the insufficiency of labeled CT data for COVID-19 infection.

Vinod and Prabaharan [90] proposed an artificial intelligence technique for fast COIVD-19 diagnosis using decision tree classifier with deep CNN features. The CXR dataset contains 113 normal images and 306 COVID-19-infected X-rays. The CT dataset contains 350 COVID-19 images and 395 non-COVID-19 images. The test score resulted in 0.82 for CT and 0.87 for CXR. The recall score is high in the case of CT images, i.e., 0.93. The recall score for COVID-19 diagnosis in CXR images is 0.88. The number of false negatives is less for diagnosis in CT image modalities.

In [91] by Perumal et al., Haralick texture features were extracted from the enhanced images. These modified images were then fed into different predefined CNN models such as ResNet-50, VGG-16, and InceptionV3 to find the patterns similar to other pneumonia, so that it can easily detect COVID-19 across other diseases. 14 Haralick features (mean, variance, entropy, etc.) were used for the identification of the relationship between biological features in the data. This method was experimented on data from multiple centers ([60, 65, 92, 93]). VGG-16 using transfer learning achieves better classification with an accuracy of 93%, precision of 91%, and recall of 90%.

Irfan et al. [94] developed a hybrid multimodel deep neural network (HDNN) for COVID-19 detection from multimodal data. It was designed as a mixture of LSTM and CNN to predict the risk of disease onset from both CT and CXRs. 1500 images from healthy patients and 3500 images from infected (COVID-19 and pneumonia) patients were collected from various sources ([60, 77, 78, 95, 96]). Initial preprocessing involves the Kalman discrete-time model-based denoising followed by sampling the 1080×1080 sized images to 256×64 sized time-series data. The hybrid model added efficacy to the work using LSTM to vanish the gradient problem and CNN to extract features automatically. On classifying the data into normal, pneumonia, and COVID-19-infected, an accuracy of 99% and PPV of 98.7% were obtained. This work also concludes that COVID-19 detection from CTs using HDNNs proves to be consistent and fast.

Other approaches that include classification of COVID-19-positive cases against COVID-19-negative cases or healthy cases [97–99] were present and also classification of COVID-19 against other pulmonary diseases as in [100], where a deep neural network with the generative adversarial network (GAN) based on synthetic data augmentation is used to classify 8 different lung pathologies. The collected dataset contains images from Digital Pathology Classification Challenge (Kaggle) and COVID-19 images from [60] comprising of 5789 atelectasis, 1010 cardiomegaly, 6331 effusion, 10317 infiltration, 6046 mass, 1971 nodule, 1062 pneumonia, 2793 pneumothorax, 84312 normal, and 337 COVID-19 images. The proposed model performed better than InceptionV3 and ResNet models with an accuracy of 89.2%. Accurate lung region of interest (ROI) segmentation also takes an indispensable part in better diagnosis of COVID-19 by delineating the lesions and measuring their extent. Most of the works have used U-Net [101] architecture for this purpose ([70, 71, 95, 102]). U-Net is a CNN architecture developed specially for biomedical image segmentation with the ability to give both the localization information and the contextual information, which leads to the better prediction of a segmentation map. Image segmentation can also be applied to quantify the lung-infected region ([101, 103, 104]), which involves visualization of the lesion distribution, prediction of severity, and assessing the progression during follow-up.

2.2. COVID-19 Prognosis. Prognosis refers to predicting the likeliness or expected disease development based on the track of the disease that is diagnosed, the condition of the patient (physical and mental), the available treatments, and other additional factors. Few COVID-19 prognosis methods are explained in this section.

Sverzellati et al. [105] simulated the triage setting of a pandemic environment with large population of COVID-19-infected suspects provided that the clinical decision should be given in the absence of any resource constraints. For this, reconstructed CXR (r-CXR) images were generated from the high-resolution CT (HRCT) images. Mortality prediction was done based on the multivariable (age, sex, duration of symptoms at triage, and a comorbidity score of 0–4) by performing LR analyses to identify the contribution of clinical and radiological variables in the analysis and using a study population of 300 patients. The images were graded as follows: normal, alternative diagnosis (to be specified), indeterminate, or typical for COVID-19 pneumonia by expert radiologists. The study findings put forward that the clinicians can rely on positive CXR for showing the low or high extent of pneumonia, and in the case of the intermediate extent of CXR, it is complemented by CT for optimal stratification of high- and low-risk groups. For indicating the COVID-19 infection, the sensitivity, specificity, PPV, and NPV of HRCT are 95.2%, 32.8%, 82.2%, and 67.9%, respectively, which proves to be better than the corresponding metrics of r-CXR.

Wang et al. [106] proposed the COVID-19Net to identify patients of potentially high risk with poor prognosis using the transfer learning process in two steps. Initially, the network was trained on 4106 non-COVID-19 CT images from epidermal growth factor receptor (EGFR) dataset, which was then transferred to the COVID-19 dataset consisting of CT images from 1266 victims: 924 with COVID-19 (471 patients had follow-up for more than 5 days) and 342 with other pneumonia. For prognostic analysis, 64-dimensional DL features were combined with clinical features (age, sex, and comorbidity) to compose an integrated feature vector. Then, a multivariate Cox proportional hazard model was used to predict the risk of a patient. The Kaplan–Meier analysis and log-rank test implied that the deep features have promising prognostic value for COVID-19 ($p < 0.0001$, $p = 0.013$, and $p = 0.014$ in 3 datasets).

Feng et al. in [107] explored the predictive value of COVID-19 prognosis from chest CT images by comparing the difference in clinical and CT characteristics in the progressive and stable patients by performing multivariate LR and nomogram establishment. Older age, CT severity score on admission, and higher neutrophil-to-lymphocyte ratio (NLR) were identified to be the independent and significant predictive aspects for advancement to severe COVID-19 infection during hospitalization and were supported by an appreciative calibration of the nomogram, a nonsignificant Hosmer–Lemeshow test statistic ($p = 0.791$), and AUC value of 0.898 in the validation cohort. This method was simple with only three easily obtainable variables and was capable of promptly predicting the progression risk (in-hospital) in the moderate stage of COVID-19 patients within 14 days. It was performed on an unbalanced data consisting of only 10% of patients developing severe COVID-19 pneumonia, which seems to be a limitation of this work.

Liang et al. [108] developed and validated a risk prediction method for early diagnosis of COVID-19 infection in patients. For this, different clinical, laboratory, epidemiological, and radiological image variables were screened at the time of admission in medical center/hospital to predict the risk score as low-, moderate-, and high-risk cases. The Least Absolute Shrinkage and Selection Operator (LASSO) was used for screening the variables, and LR was used to formulate the predictive risk score (COVID-GRAM). This method was developed with a cohort of 1590 patients and validated on 710 patients to estimate the risk that they will develop a critical illness. 10 variables including chest radiographic abnormality, age, cancer history, number of comorbidities, and NLR were identified as independent predictive factors among 72 potential factors by the LR model. A mean accuracy of 0.88 was obtained in the validation group. This was designed as a Web-based calculator to assist the clinicians in estimating the possibility of developing critical ailment in individual hospitalized victims. As the development and validation patient group was completely selected from a particular county, there might be limitation in generalizing the work for patients from different regions.

Wu et al. [109] used CT images to develop an easy-to-use and noninvasive prognosis method to predict the clinical risk of COVID-19 patient outcome as death, need for mechanical ventilation, and admission to the intensive care unit. The development cohort consists of 492 patients grouped into the early-phase group and the late-phase group based on their CT scanning performed one week before or after the symptom onset, respectively. A fine-gray competing risk regression model was used to frame the clinical model and CrrScore (the clinic-radiomic signature), and a Least Absolute Shrinkage and Selection Operator (LASSO) was used to construct the RadScore (the radiomic signature). In the late-phase group, the radiomic signature alone proved to be efficient to forecast the poor outcome in patients with an AUC value of 0.976 and C-index of 0.885. In the case of the early-phase group, the clinic-radiomic signature exhibited better efficacy with an AUC value of 0.862 and C-index of 0.850. Therefore, based on the time of CT scanning concerning the symptom onset, appropriate signatures can be used for predicting the prognostic outcome.

Research works on the prognostic analysis of COVID-19 using radiological images are minimal and need to be further explored to keep a check on the severity of the diseases and reduce the mortality rate. For prognosis, the clinical features are combined with the radiological image findings to predict the patient's medical condition for delivering successful triage and lessen the disease spread.

2.3. COVID-19 Severity/Risk Detection. A streamlined severity/risk detection mechanism is highly required for COVID-19 triage to lower the prodigious rate of mortality. Apart from early screening, the severity assessment also plays a vital role in triage and disease management. A review on the related works in the literature is discussed below.

Cohen et al. [110] built a severity prediction model to assist the clinicians in managing the patient care using a regression model to predict two types of scores: extent of

lung involvement (0–8 score) by ground-glass opacity or consolidation and degree of opacity (0–6 score) on the COVID-19-infected CXR images. DenseNet was employed to predict pneumonia from 94 COVID-19 CXR images acquired from [8]. The model was trained with 7 datasets [90, 98, 111–115] with 18 common radiological finding tasks consisting of 88,079 non-COVID-19 CXR images. Just using a single feature (lung opacity) for risk predictions countered to the ground truth value of prediction score, the model was capable of better prediction in both the opacity score and the geographic extent of infection. The Pearson correlation coefficient and R^2 for lung opacity score prediction task are 0.78 ± 0.04 and 0.58 ± 0.09, respectively. Similarly, for the geographic extent prediction the Pearson correlation coefficient of 0.80 ± 0.05 and R^2 value of 0.60 ± 0.09 were obtained. It was capable of predicting the geographic extent score (range 0–8) with 1.14 mean absolute error (MAE) and lung opacity score (range 0–6) with 0.78 MAE generalization that can be improved by performing large-scale evaluations on public datasets from around the world.

Zhu et al. [116] also employed a model similar to [110] for accurate staging of COVID-19 severity on CXRs. A deep CNN model was used to foresee the lung severity scores from 131 CXRs based on the degree of opacity (0–3 score) and geographic extent (0–4 score). A correlation analysis was performed amidst the predicted score and the radiologist scores, which resulted in a higher value of 0.90 and a MAE of 8.5%, making the model yield top results. An average opacity score of 2.52 and average geographic extent score of 3.42 were obtained across three readers.

Tang et al. [17] proposed a severity assessment model to categorize the COVID-19-infected CT images as severe or non-severe. For these, 63 quantitative features of top importance such as volume and ratio of the left/right/whole lung and volume of GGO were extracted from 176 CT images obtained from different hospitals (using different scanners) and trained to the random forest model. An accuracy of 0.85, AUC value of 0.91, true positive rate of 0.933, and true negative rate of 0.745 were obtained for this model. The volume and ratio of GGO were identified to be the feature with most importance to estimate the severity of the disease, and another finding from the study revealed that the quantitative features observed in the right lung were more significantly related to COVID-19 severity than the features of the left lung. The main drawback is that the model is able to label the images as only severe or non-severe instead of multiple classifications such as mild, common, severe, and critical.

The limitation of [17] can be overcome by the COVID-SDNet proposed by Tabik et al. [117], which has better generalization capability. A balanced and homogeneous database, COVIDGR-1.0, was built, which includes different levels of severity such as normal with positive RT-PCR (normal PCR+), mild, moderate, and severe. It consists of 426 COVID-19-positive CXR images and 426 COVID-19-negative images (normal PCR: 76, mild: 100, moderate: 171, and severe: 79). It performs smart data generation using a class-inherent transformation approach motivated by GAN and ResNet-50 loaded with ImageNet weights for classification. Better and more stable results and great balance between specificity and sensitivity were obtained. Comparing the classification accuracies of 4-class classification (normal PCR +: $28.42\% \pm 2.58$, mild: $61.80\% \pm 5.49$, moderate: $86.90\% \pm 3.20$, and severe: $97.72\% \pm 0.95$) and 3-class classification (mild: $46.00\% \pm 7.10$, moderate: $85.38\% \pm 1.85$, and severe: $97.22\% \pm 1.86$), even though normal PCR + seems to be the toughest level to predict, its existence accelerates the accuracy of the minor severity levels, notably mild level. It is also observed that the segmentation of the lung region using U-Net has essentially improved the sensitivity value.

Severity assessment in COVID-19 mostly relies on classifying the pre-identified radiological images or using the clinical data of patients to perform the severity analysis, but pre-identification of radiological images as mild, moderate, or severe infections may be challenging and difficult.

2.4. Inferences. Based on the study described in the previous sections, the review findings and inferences are listed below:

(i) COVID-19 diagnosis can be performed by classification or segmenting the infected region. Classification can be viable and easy to implement in short time as it demands only weak image-level labels and few model specifications for training the classification model.

(ii) Classification of COVID-19 infection against normal cases seems to be much easier with high classification results and performance metrics. In general, binary classification (COVID-19/non-COVID-19, COVID-19/other pneumonia) yields better results than multiclass classification (COVID-19/other pneumonia/normal/other lung diseases).

(iii) Distinguishing COVID-19 from other pneumonia, especially viral pneumonia, is challenging as they show similar characteristics in the radiological images. In such cases, the efficiency of the classifier can be improved by adding more images or other types so that the learning process can be enhanced during training. The performance of distinguishing COVID-19 from normal or bacterial pneumonia can yield better results since there is significant variation in the radiological image features.

(iv) Deep Learning methods are mostly preferred than the machine learning methods for feature extraction as they can extract the inherent deep features specific to each class for a finer classification. The most commonly used deep models for feature extraction and classification that give promising results are DenseNet, ResNet, VGG, and their modified variants. Other networks like Inception, Exception, ShuffleNet, and EfficientNet also have been used in many works. The CNN layer implementation with residual connection is depicted in Figure 6. Diagnosis of COVID-19 employing deep learning techniques have shown

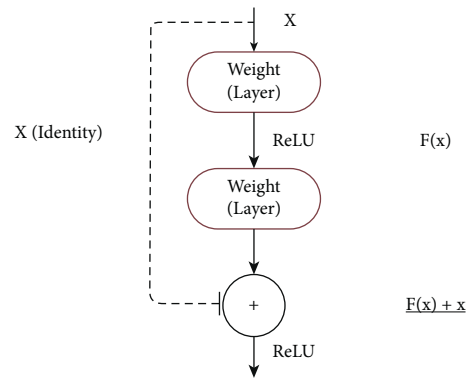

Figure 6: Sample residual connection used in ResNet [40].

better sensitivity and specificity than the radiologist's decision. U-Net is the most widely preferred deep learning architecture for segmentation task, which is depicted in Figure 7.

(v) Deep features can be combined with clinical data such as clinical symptoms, nucleic acid detection results, epidemiology, and laboratory indicators, which can bypass any misdiagnosis and efficaciously improve the clinical triage.

(vi) Prognosis of COVID-19 is of equal importance as that of diagnosis, since it demands medical triage and management of the patient care. Early identification of the disease can aid in the diagnostic ambiguity of radiologists. Works on COVID-19 prognosis are minimal, so this can open up a large research path for many researchers.

(vii) Prediction of COVID-19 infection severity plays a vital role in making clinical decisions so that the medical team can work towards reducing the mortality rate.

(viii) Despite CXRs being cheap and easily obtainable, CTs are highly preferred for COVID-19 analysis as they are capable of early detection of the disease even in victims with negative RT-PCR tests, in asymptotic patients or even ahead symptoms may arise.

Figure 8 illustrates the inferences from the review of different tasks related to medical image analysis of COVID-19.

3. Related Reviews in the Field

There are have been previous reviews [52, 118] that have encompassed most of the research regarding COVID-19 in terms of machine learning, deep learning, and medical imaging along with its analysis and scrutinized them to preference inferences, to promote further research in the field. They also present challenges that future researchers should tackle to incorporate better results and build more efficient models. Table 6 (while there are other reviews present, they were either extremely short, or did not contain valuable information, or were mostly covered in the mentioned reviews.) lists out the most useful reviews, which have taken place till date and their respective merits and limitations. Most reviews covered the architectures used quite broadly and have also made studies in context to their usage (pre-trained or incorporation for custom methods). A general pipeline of the same is shown in Figure 9. Another aspect that was covered in multiple reviews was the use and availability of public datasets, which is paramount to expand the COVID-19 research capabilities.

Model generalization has also been tackled in numerous studies as it is an important aspect to be considered while building deep learning-based models. While the reviews have covered the majority of the research taking place and the challenges accompanied by them, only Shorten et al. [52] accounted for extending work via privacy-preserving methods and mentioned research taking place through other deep learning paradigms such as meta-learning [126] and self-supervised learning [127]. Apart from these, the readmission risk of COVID-19-recovered patients can also be analyzed using a predictive model. Many ML- and DL-based predictive models have been designed to predict the readmission risk of patients discharged from hospitals for various diseases [128, 129]. Increased readmission rates may be liable to high healthcare cost and risk of inpatient hospital mortalities. Several works have been carried out to improve the performance of these predictive models using evaluation metrics [130, 131]. Similarly, many studies have been conducted regarding the COVID-19 case readmission rates and factors [132, 133].

In the field of medicine, data privacy is of utmost importance and is always the leading cause for the shortage of open-source data. Addressing this issue should be the first among the list of challenges concerning COVID-19. One of the main reasons for having such expansive development and testing is because of the large amounts of open-source data present (including open accessing all research), which is generally absent for other diseases. Self-supervised learning approaches have proven to surpass the usual supervised deep learning methods in [134, 135] and should be given more importance and consideration when topics of extension and challenges are brought upon. There is also a major gap in accounting for the research conducted in terms of prognosis for COVID-19. There is no single review that focuses on this aspect. In terms of medical image analysis, few solutions are addressed to the challenges mentioned in [52]. To the best of our knowledge, the previous reviews missed to cover the topics discussed above. Additional information is all part of recent developments, which have taken place post the drafting of those reviews.

3.1. Extension of Discussion on the Limitations of Deep Learning Approaches Discussed in Shorten et al. (2020) [52]

(a) *Explainability*: deep learning models are often called black box models due to their non-interpretive behavior. This highly disregards using deep learning models on sensitive real-world tasks such as medical image analysis and has hence turned into a nontrivial

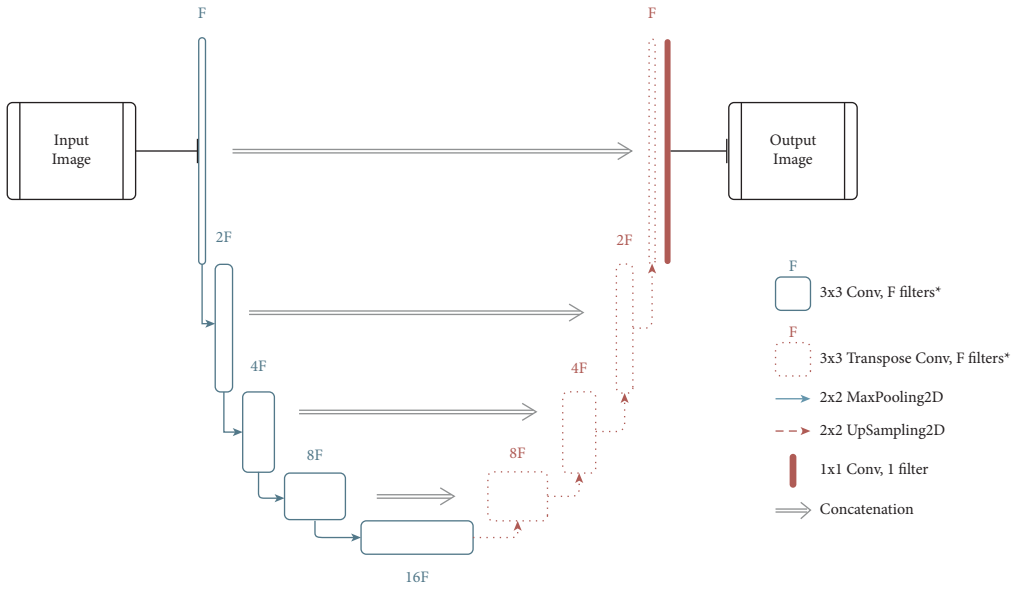

Figure 7: Sample U-Net architecture for medical image segmentation. * in the legend indicates that the filter is followed by a batch normalization layer and a ReLU function.

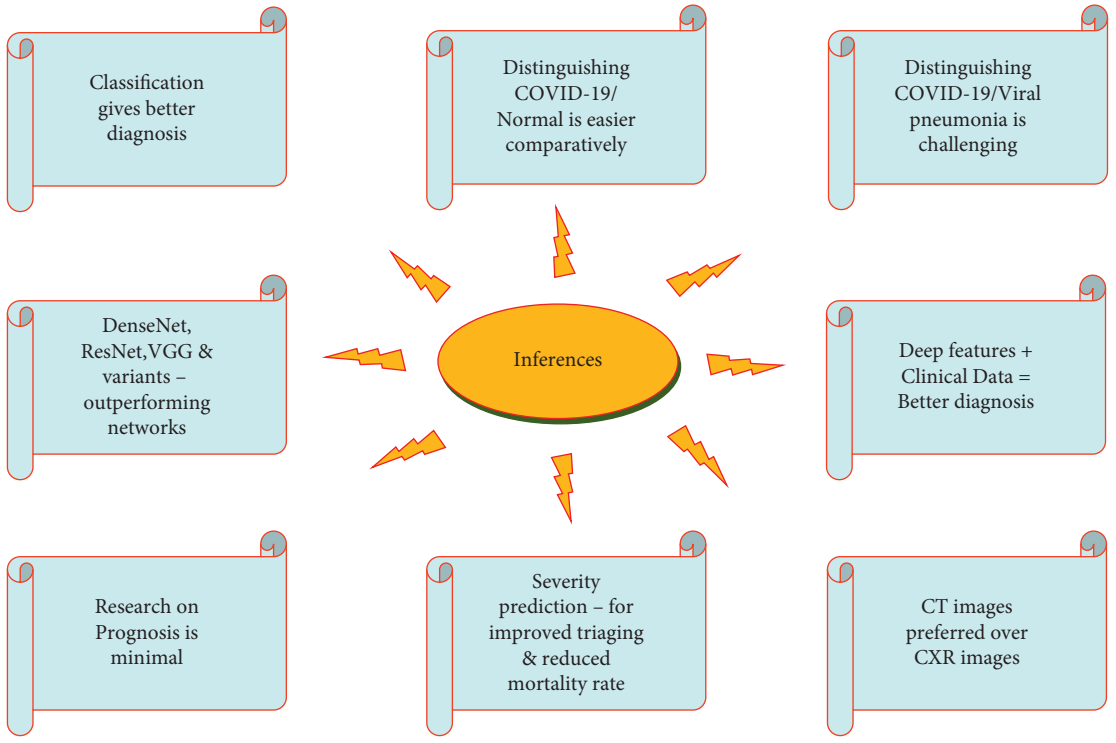

Figure 8: Inferences from the review of COVID-19 medical image analysis.

issue. With the focus here being the same, there are ample explainable techniques that have come up to aid in explaining vision-based deep learning models. Table 7 shows the current state-of-the-art methods used to help interpret vision-based deep learning models. Score-CAM eliminates the dependence on gradients (as seen in Grad-CAM) by securing the weight of individual activation maps, by virtue of its forward passing score on the aimed target class, which results in a linear combination of the activation maps and weights. EVET [135] proposes a heuristic pipeline for strengthening the visual explanations by applying image transformations. Explainability in segmentation tasks (primarily done by U-Nets) is a field that is still being heavily explored. Initial attempts have been done by adapting

Table 6: Merits and limitations of existing review papers exploring the broad depth of COVID-19 research in terms of medical imaging, medical image analysis, machine learning, and deep learning.

Review paper	Merits	Limitations
Ozsahin et al. [119]	Classified different groups of studies. Added a severity constraint.	Only highlights result and techniques without any intuition as to why either are used. Includes segmentation models within classification studies.
Shoeibi et al. [120]	Includes a forecasting study of coronavirus prevalence in multiple countries. Includes pre- and post-processing techniques used in various COVID-19 detection approaches.	Certain figures depict subpar comparisons and include unnecessary comparison samples. The review is more focused on architectures utilized rather than the inference generated from the literature.
Pham [97]	Presents many strong inferences on pre-trained networks. Alleviates the task of data augmentation. Empirically proved DenseNet-201 works best.	Should have considered the use of the Matthews correlation coefficient (MCC) [121] as binary classification was considered.
Shorten et al. [52]	Pinpoints key discussions in regards to deep learning approaches and the challenges faced by same in multiple domains apart from medical imaging. Explores several supporting domains such as federated learning, meta-learning, and self-supervised learning, which is missed in most reviews.	Falsely claims the first paper to review in a deep learning point of view for COVID-19 analysis. Compares paper to other "artificial intelligence"-based methods to their approach.
Alsharif et al. [122]	Attempts to compare deep learning to machine learning approaches.	Fails to dive deep into the problem and hence causes incorrect generalization of methods.
Joy et al. [123]	The review is inclined to help beginners in the field. It poses an extensive study covering various approaches and architectures.	No challenges are mentioned or analyzed.
Alghamdi et al. [124]	Gives in-depth analysis about architectures and the various constraints in tandem to them such as data, explainability, and more.	Does not consider the SOTA methods in explainability terms. Fails to address other possible learning paradigms and privacy-preserving methods. Should be mentioned as the review is architecture-dominated.
Islam et al. [125]	Gives an extensive study on open challenges. Highlights the data partitioning techniques.	Limitations are covered in the paper.

[1]While there are other reviews present, they were either extremely short, or did not contain valuable information, or were mostly covered in the mentioned reviews.

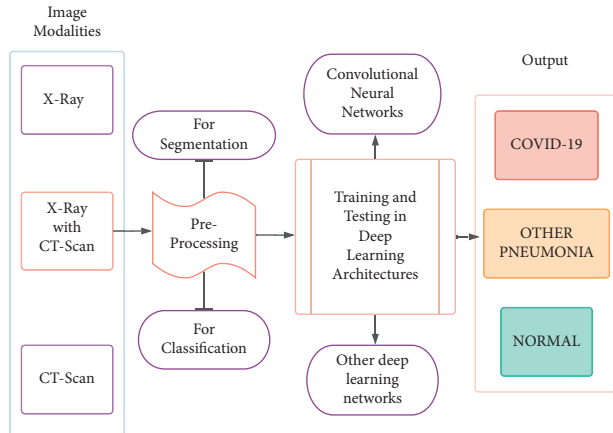

Figure 9: Generalized pipeline of COVID-19 detection from radiological image modalities.

Table 7: State-of-the-art explainable techniques for vision-based deep learning models.

Task	Explainable method
Classification	Grad-CAM [48]
	Score-CAM [49]
	EVET [135]
Segmentation	SEG-GRAD-CAM [136]

Grad-CAM to segmentation in the form of SEG-GRAD-CAM [136]. The origin of the above work comes from [137]. Explainable models can benefit the medical image analysis pipeline in many ways. It helps understand where the model is focusing on the image, increase user confidence, and inspect the model at a deeper level, which in turn helps in debugging the model as well.

(b) *Generalization Metrics*: precision is generally the major metric taken into consideration while accounting for a fair metric for medical image classification methods. While considering segmentation, the authors in [138] give a detailed description regarding which metrics to consider. They also mention the use of precision here as well. A detailed study on generalization concepts and metrics can also be studied in [139].

(c) *Learning From Limited Labeled Datasets or Unlabeled Data:* primary focus on two paradigms of learning is as follows:

(i) Meta-Learning: it follows the approach of learning to learn. It is used to adapt to learn new environments and in a quicker fashion greatly aligns with the demand of COVID-19 research. It also requires lesser data samples. In [118], a trainable n-shot deep meta-learning framework was built to classify COVID-19 cases with limited training CXR images. Another aspect of meta-learning is neural architecture search (NAS) and that has been observed to work better than many baseline models [140].

(ii) Self-Supervised Learning: it is a subgroup of unsupervised learning, which works on the basis of training the deep learning model explicitly with automatically generated labels. As Figure 10 depicts, the process involves learning visual features from pretext task (tasks predesigned for networks to deal with) and acts as a pre-trained model for other downstream tasks (computer vision applications to examine the self-supervised learned feature quality) via fine-tuning. References [133, 134] have rivaled the top-performing models in image tasks, even surpassing the supervised methods. Reference [141] showed that the combination of data augmentation and self-supervised learning has outperformed all previous approaches in severity assessment.

(d) *Data Privacy*: a detailed discussion of data privacy is given in [52]. To extend on the avenues mentioned

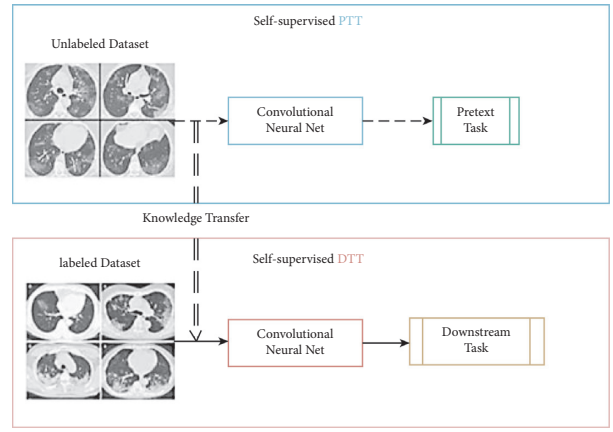

Figure 10: General self-supervised learning pipeline. PTT: pretext task training; DTT: downstream task training.

there, the use of differentially private federated neural architecture search [142] is recommended to preserve data privacy. Through this method, a model can be tested on several subsets of data, which contain varied distributions and distinctions from other datasets and in parallel keep any information about the various data samples completely privatized. Although the method is very computationally demanding, it can help screen through different samples of data and greatly test the robustness of any model. Figure 11 depicts the working of both NAS and federated NAS (FNAS) [143]. An application of federated learning in terms of prognosis can be seen in [144]. A noise implementation algorithm is integrated with a cross-device federated learning, such that the initial symptom prognosis can be achieved during a pandemic like COVID-19.

4. Pre- and Post-Processing Techniques for COVID-19 Medical Image Analysis

4.1. Preprocessing. Preprocessing is a crucial part of vision models' pipeline. The process involves performing operations at the lowest level of abstraction. The objective is to enhance the picture information that suppresses undesired deformities or improves the image features necessary for continued transformations, which is mainly linked with generating higher accuracy in models. Even simple techniques such as resizing or cropping the image can make major difference in deep learning models. For example, cropping out the redundant parts of a scan can help the deep learning model avoid unnecessarily parsing through that spatial information to concentrate on the more essential areas of the scan. Certain models require specific size of input images to fit in. In such situations, rescaling the image is completely unavoidable.

Figure 12 depicts a chest CT scan being put through contrast-limited adaptive histogram equalization (CLAHE) in comparison with an original CT image. A clear depiction of sharper visual features after CLAHE is applied, which makes it easier for the model to develop and correlate these

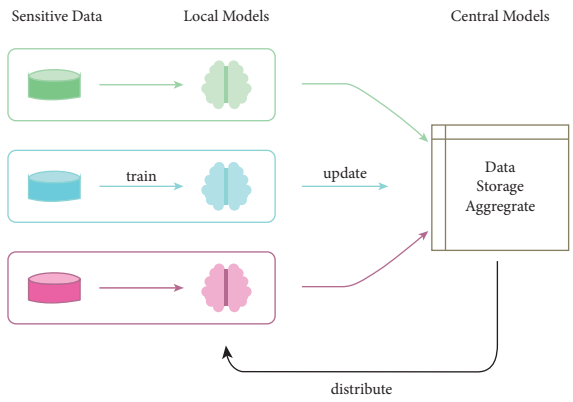

Figure 11: General federated learning pipeline.

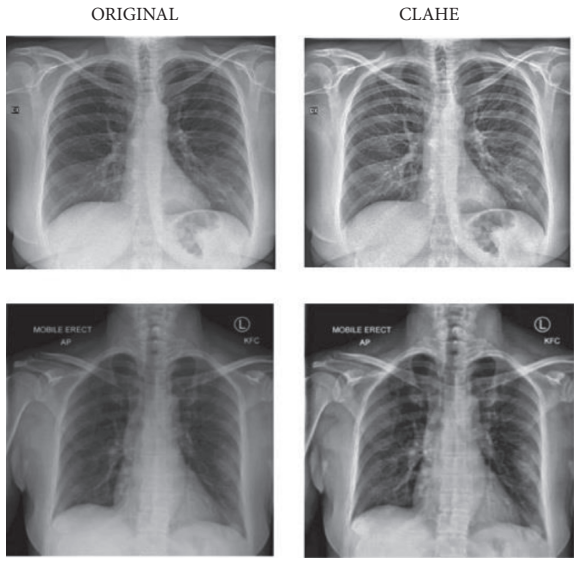

Figure 12: Original CT image versus CLAHE-processed CT image [145].

visual cues. Figure 13 illustrates how the preprocessing step can also help better express the image features through image enlargement. The enlarged points are first targeted (shown as question marks) and then filled through interpolation. A comparative image is also shown with no interpolation done. In addition to the techniques mentioned in Table 8, there are certain methods that can aid in preprocessing. Data augmentation is a widely used method in much literature to help increase the training sample size. GANs have also been applied to increase the sample size [153]. Noise removal techniques without losing the significant edges can also be used to enhance the images [154].

4.2. Post-Processing. Post-processing generally directs to improvement in the images after the model has given an output, but in the case of medical image analysis, it mainly involves generating inferences from the model outputs via explainability measures. The basis of most techniques is class activation maps [137]. These methods are used to pinpoint the focus of the model and understand whether the output generated is on the basis of the detection of the actual disease and not any other factors. The extensions made to [137] are discussed in Section 3.1.1. In [155], a method called the Peekaboo training scheme was used, in which a two-stage patch crop-and-drop strategy promotes the model to furnish activation maps for every target concept.

5. Discussion

In this section, we discuss additional challenges faced while conducting experiments and how the work done with respect to COVID-19 can help the field of medical image analysis in general.

5.1. Challenges Faced. Reviewing of multiple literature samples led to the identification of multiple challenges present in the domain, a few of which are already covered in Section 3.1. In this section, another set of challenges that have been discovered is elucidated.

(i) Interclass analogy and intraclass deviation of pneumonia lesions: COVID-19 pneumonia, which is also caused by viral infection, contains indicative overlay of features and radiological image characteristics with other viral pneumonia leading to the interclass analogical problem. Another problem that arises while dealing with the pulmonary medical images is the intensity in-homogeneity problem caused by the closeness of gray level between the different soft tissues, resulting in segmentation and detection difficulties [156]. Detecting the anomalous features from the medical images becomes challenging due to the noise impedances from the tissues and lesions. The infected region may still contain some non-lesion regions with wide variations in tissues, which further makes it complicated to differentiate.

(ii) Generalization and reproducibility: the COVID-19 detection algorithms proposed by various researchers produce great results for the particular small dataset used in that work. When these trained classifier algorithms are implemented on larger unseen data, they may not be able to generalize their performance. Moreover, problems arise in reproducing the similar performance on other multicenter datasets. One such solution to this problem is the use of vision transformers, which have demonstrated superior performance and greater generalization prowess. These are of paramount importance in the context of a deployment scenario [157].

(iii) Data source learning problem of ML and DL: on applying neural network-based COVID-19 detection protocols to multicenter datasets, most of the detection systems tend to learn the source of dataset, their imaging protocols, mode, and so on, rather than learning the discriminative features among the various classes. Such kind of algorithms may not be

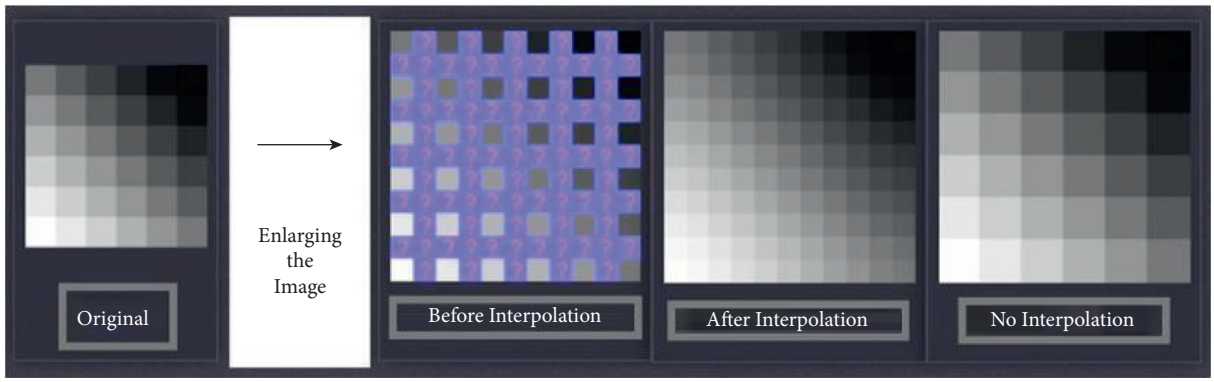

Figure 13: Depiction of a pipeline for enlarging an image through interpolation.

Table 8: List of preprocessing techniques used for analyzing radiological images.

Reference	Technique	Utilization
Pizer et al. [146]	Adaptive histogram equalization	Improves contrasts in images.
Veldhuizen and Jernigan [147]	Wiener filter	Produces an estimate of a desired or target random process.
Lehmann et al. [148]	Interpolation	Best estimation of a pixel's color and intensity in context to the values at neighboring pixels.
Tian et al. [149]	Binarization	Transforms data features of any entity into vectors of binary numbers.
Yadav et al. [145]	CLAHE	Amplifies the contrasts. Works on small regions called tiles.
Prabha and Kumar [150]	Smoothing filter	Utilized in blurring regions.
Kociołek et al. [151]	Normalization	Changes the range of pixel intensity values.
Gungor [152]	Wavelet transform	Reduces noise in images. Decomposes special patterns hidden in mass of data.

fair enough when generalized for different data [158].

(iv) Spread and contamination: contamination of the scanners is also an issue that needs to be considered. There is a great possibility of disease spread during scanning; hence, the radiologists must assure that the scanners are maintained clean after every scanning process.

5.2. Future Scope: Utilizing COVID-19 Medical Image Analysis Research in Other Fields. As seen, enormous amounts of effort take place to furnish new methods through deep learning strategy to tackle the problems of COVID-19 detection. A few potential avenues have been mentioned in this section, which can in general help to extend the field of medical image analysis.

(i) Medical model weights and baseline architectures: utilizing model weights built upon disease-affected scans has shown to improve the efficiency in models [87]. Particular to COVID-19, CheXNet [159] weights utilized in models instead of the usual ImageNet weights have been shown to increase the model [160], which can be utilized to detect other diseases as well. General vision problems are quite different when compared to dealing with medical images such as MRIs, CTs, and PET scans. Training models that are based on the weights gained from training on such images should furnish more accurate models. Apart from COVID-19, there are many other diseases that can be detected from radiographs. As DenseNet is seen to do well for COVID-19 (both from pre-training and for customized models), it should be fair enough for other diseases as well and can act as a good starting point for future researchers to expand existing works.

(ii) Expanding the community and model testing: there are many introductory materials focused on COVID-19 and medical image analysis. This can help build the community further and attract novices to the field. Testing models on scarce datasets make it quite difficult to generate inference about the model's performance. With the massive open-source data available, it also allows potential researchers to realistically test their models and architectures. The variety of data present also helps in testing the model for generalizability, which is one of the biggest obstacles to surmount while utilizing deep learning-based methodologies.

6. Conclusion

A comprehensive description on the various COVID-19 detection techniques using medical image analysis has been

described in this study. The cause, effect, challenges, limitations, and other retrospective discussions on COVID-19 medical image analysis have been discussed through this study to best feature the importance of carrying out more research on this area to reduce the increased mortality count faced by the world. DL can improve the disease diagnosis efficiency by precisely locating the infections in the medical images in a faster and accurate manner. The preceding COVID-19 analysis methodologies proposed by various researchers can be used only as a reinforcement technique to assist the medical teams in highly populated areas and in situations requiring quicker diagnosis. The problems such as unavailability of enough and accurate labeled data, generalization and reproducibility of preceding algorithms for multicenter large datasets, and difficulty to isolate COVID-19 against other pneumonia cases due to the closeness of gray level of the soft lung tissues have been highly challenging to design a diagnostic system with high reliability and accuracy. An intelligent and accurate computer-assisted COVID-19 diagnostic system employing adaptive deep learning models with active/incremental learning is the need of the hour to combat the evolving coronavirus.

Data Availability

The data supporting this systematic review are from previously reported studies and datasets, which have been cited.

Conflicts of Interest

The authors declare that they have no conflicts of interest.

Acknowledgments

This work was supported by the 2020 EBC-C (Extra-Budgetary Contributions from China) Project on Promoting the Use of ICT for Achievement of Sustainable Development Goals and University Malaya under Grant IF015-2021.

References

[1] W. Wang, Y. Xu, R. Gao et al., "Detection of SARS-CoV-2 in different types of clinical specimens," *JAMA*, vol. 323, pp. 1843-1844, 2020.

[2] T. C. Kwee and R. M. Kwee, "Chest CT in COVID-19: what the radiologist needs to know," *RadioGraphics*, vol. 40, no. 7, pp. 1848–1865, 2020.

[3] C. P. West, V. M. Montori, and P. Sampathkumar, "COVID-19 testing," *Mayo Clinic Proceedings*, vol. 95, no. 6, pp. 1127–1129, 2020.

[4] M. Y. Ng, E. Y. P. Lee, J. Yang et al., "Imaging profile of the COVID-19 infection: radiologic findings and literature review," *Radiology. Cardiothoracic imaging*, vol. 2, no. 1, p. e200034, Article ID e200034, 2020.

[5] C. Huang, Y. Wang, X. Li et al., "Clinical features of patients infected with 2019 novel coronavirus in Wuhan, China," *The Lancet*, vol. 395, no. 10223, pp. 497–506, 2020.

[6] M. Durrani, I. U Haq, U. Kalsoom, and A Yousaf, "Chest X-rays findings in COVID-19 patients at a University Teaching Hospital - a descriptive study," *Pakistan journal of medical sciences*, vol. 36, p. S22, 2020.

[7] M. Emmanuel, C. Milena, C. C. Alexandre et al., "Deep learning workflow in radiology: a primer," *Insights Imaging*, vol. 11, 2020.

[8] D. R. Sarvamangala and R. V. Kulkarni, "Convolutional neural networks in medical image understanding: a survey," *Evolutionary intelligence*, pp. 1–22, 2021.

[9] S. Soffer, A. Ben-Cohen, O. Shimon, M. M. Amitai, H. Greenspan, and E. Klang, "Convolutional neural networks for radiologic images: a radiologist's guide," *Radiology*, vol. 290, no. 3, pp. 590–606, 2019.

[10] N. Sharma, V. Jain, and A. Mishra, "An analysis of convolutional neural networks for image classification," *Procedia Computer Science*, vol. 132, pp. 377–384, 2018.

[11] H.-C. Shin, H. R. Roth, M. Gao et al., "Deep convolutional neural networks for computer-aided detection: CNN architectures, dataset characteristics and transfer learning," *IEEE Transactions on Medical Imaging*, vol. 35, no. 5, pp. 1285–1298, 2016.

[12] S. Minaee, Y. Y. Boykov, F. Porikli, A. J. Plaza, N. Kehtarnavaz, and D. Terzopoulos, "Image segmentation using deep learning: a survey," *IEEE Transactions on Pattern Analysis and Machine Intelligence*, 2021.

[13] N. Srivastava, G. Hinton, A. Krizhevsky, I. Sutskever, and R. Salakhutdinov, "Dropout: a simple way to prevent neural networks from overfitting," *Journal of Machine Learning Research*, vol. 15, pp. 1929–1958, 2014.

[14] S. J. Pan and Q. Yang, "A survey on transfer learning," *IEEE Transactions on Knowledge and Data Engineering*, vol. 22, pp. 1345–1359, 2009.

[15] S. Ioffe and C. Szegedy, *Batch Normalization: Accelerating Deep Network Training by Reducing Internal Covariate Shift*, pp. 448–456, PMLR, New York City, NY, USA, 2015.

[16] Y. Wu and K. He, "Group normalization," *Computer Vision - ECCV 2018*, pp. 3–19, 2018.

[17] Z. Tang, W. Zhao, X. Xie et al., "Severity assessment of coronavirus disease 2019 (COVID-19) using quantitative features from chest CT images," 2020, https://arxiv.org/abs/2003.11988.

[18] H. Yasar and M. Ceylan, "A novel comparative study for detection of COVID-19 on CT lung images using texture analysis, machine learning, and deep learning methods," *Multimedia Tools and Applications*, vol. 80, no. 4, pp. 5423–5447, 2021.

[19] S. Latha and D. Samiappan, "Despeckling of carotid artery ultrasound images with a calculus approach," *Current Medical Imaging Formerly Current Medical Imaging Reviews*, vol. 15, no. 4, pp. 414–426, 2019.

[20] K. Selvakuberan, D. Kayathiri, B. Harini, and M. I. Devi, "An efficient feature selection method for classification in health care systems using machine learning techniques,"vol. 4, pp. 223–226, in *Proceedings of the IEEE 2011 3rd International Conference on Electronics Computer Technology*, vol. 4, IEEE, Kanyakumari, India, 8 April 2011.

[21] N. Emanet, H. R. Öz, N. Bayram, and D. Delen, "A comparative analysis of machine learning methods for classification type decision problems in healthcare," *Decision Analytics*, vol. 1, no. 1, pp. 1–20, 2014 Dec.

[22] E. Gambhir, R. Jain, A. Gupta, and U. Tomer, "Regression analysis of COVID-19 using machine learning algorithms," in *Proceedings of the IEEE 2020 International conference on smart electronics and communication (ICOSEC)*, pp. 65–71, IEEE, Trichy, India, 10 September 2020.

[23] P. S. Yeoh, K. W. Lai, S. L. Goh et al., "Emergence of deep learning in knee osteoarthritis diagnosis," *Computational*

Intelligence and Neuroscience, vol. 2021, Article ID 4931437, 20 pages, 2021.

[24] S. Arivazhagan and S. V. Ligi, "Mango leaf diseases identification using convolutional neural network," *International Journal of Pure and Applied Mathematics*, vol. 120, no. 6, pp. 11067–11079, 2018.

[25] V. Yemelyanov, S. Chernyi, N. Yemelyanova, and V. Varadarajan, "Application of neural networks to forecast changes in the technical condition of critical production facilities," *Computers & Electrical Engineering*, vol. 93, Article ID 107225, 2021.

[26] D. Samiappan and V. Chakrapani, "Classification of carotid artery abnormalities in ultrasound images using an artificial neural classifier," *The International Arab Journal of Information Technology*, vol. 13, no. 6A, pp. 756–762, 2016.

[27] M. Sandler, A. Howard, M. Zhu, A. Zhmoginov, and L. C. Chen, "Mobilenetv2: inverted residuals and linear bottlenecks," in *Proceedings of the Proc IEEE Conf Comput Vis Pattern Recognit*, pp. 4510–4520, IEEE, Salt Lake City, UT, USA, 18 June 2018.

[28] D. H. Hubel and T. N. Wiesel, "Receptive fields of single neurones in the cat's striate cortex," *The Journal of Physiology*, vol. 148, no. 3, pp. 574–591, 1959.

[29] K. Fukushima, "Neocognitron: a self-organizing neural network model for a mechanism of pattern recognition unaffected by shift in position," *Biological Cybernetics*, vol. 36, no. 4, pp. 193–202, 1980.

[30] Y. LeCun, "The MNIST database of handwritten digits," 1998, http://yann. lecun. com/exdb/mnist/.

[31] A. Krizhevsky, I. Sutskever, and G. E. Hinton, "Imagenet classification with deep convolutional neural networks," *Advances in Neural Information Processing Systems*, vol. 25, pp. 1097–1105, 2012.

[32] V. Nair and G. E. Hinton, "Rectified linear units improve restricted Boltzmann machines," *InIcml*, 2010.

[33] K. Simonyan and A. Zisserman, "Very deep convolutional networks for large-scale image recognition," 2014, https://arxiv.org/abs/1409.1556.

[34] C. Szegedy, W. Liu, Y. Jia et al., "Going deeper with convolutions," in *Proceedings of the Proc IEEE Conf Comput Vis Pattern Recognit*, pp. 1–9, IEEE, Boston, MA, 7 June 2015.

[35] S. Liu and W. Deng, "Very deep convolutional neural network based image classification using small training sample size," in *Proceedings of the 2015 3rd IAPR (ACPR)*, pp. 730–734, IEEE, Kuala Lumpur, Malaysia, 3 November 2015.

[36] K. He, X. Zhang, S. Ren, and J. Sun, "Deep residual learning for image recognition," in *Proceedings of the Proc IEEE Conf Comput Vis Pattern Recognit*, pp. 770–778, IEEE, Las Vegas, NV, USA, 27 June 2016.

[37] S. Zagoruyko and N. Komodakis, "Wide residual networks," 2016, https://arxiv.org/abs/1605.07146.

[38] K. He, X. Zhang, S. Ren, and J. Sun, "Identity mappings in deep residual networks," *Computer Vision - ECCV 2016*, Springer, vol. 9908, pp. 630–645, Cham, 2016.

[39] F. Chollet, "Xception: deep learning with depthwise separable convolutions," in *Proceedings of the Proc IEEE Conf Comput Vis Pattern Recognit*, pp. 1251–1258, IEEE, Honolulu, HI, USA, 21 June 2017.

[40] A. G. Howard, M. Zhu, B. Chen et al., "Mobilenets: efficient convolutional neural networks for mobile vision applications," 2017, https://arxiv.org/abs/1704.04861.

[41] S. Xie, R. Girshick, P. Dollár, Z. Tu, and K. He, "Aggregated residual transformations for deep neural networks," in *Proceedings of the Proc IEEE Conf Comput Vis Pattern Recognit*, pp. 1492–1500, IEEE, Honolulu, HI, USA, 21 July 2017.

[42] D. M. Blei, A. Y. Ng, and M. I. Jordan, "Latent dirichlet allocation," *Journal of Machine Learning Research*, vol. 3, pp. 993–1022, 2003.

[43] J. Hu, L. Shen, and G. Sun, "Squeeze-and-excitation networks," in *Proceedings of the Proc IEEE Conf Comput Vis Pattern Recognit*, pp. 7132–7141, Salt Lake City, UT, USA, 18 June 2018.

[44] X. Zhang, S. Huang, X. Zhang, W. Wang, Q. Wang, and D. Yang, "Residual inception: a new module combining modified residual with inception to improve network performance," in *Proceedings of the 2018 25th IEEE (ICIP)*, pp. 3039–3043, IEEE, Athens, Greece, 7 October 2018.

[45] B. Zoph, V. Vasudevan, J. Shlens, and Q. V. Le, "Learning transferable architectures for scalable image recognition," in *Proceedings of the Proc IEEE Conf Comput Vis Pattern Recognit*, pp. 8697–8710, IEEE, Salt Lake City, UT, USA, 18 June 2018.

[46] M. Tan and Q. Le, "Efficientnet: rethinking model scaling for convolutional neural networks," *Mach Learn Based Proced*, PMLR, vol. 97, pp. 6105–6114, 2019.

[47] A. Brock, S. De, S. L. Smith, and K. Simonyan, "High-performance large-scale image recognition without normalization," https://arxiv.org/abs/2102.06171 2021.

[48] R. R. Selvaraju, M. Cogswell, A. Das, R. Vedantam, D. Parikh, and D. Batra, "Grad-cam: visual explanations from deep networks via gradient-based localization," in *Proceedings of the IEEE Int Conf Comput Vis*, pp. 618–626, IEEE, Venice, Italy, 22 October 2017.

[49] H. Wang, R. Naidu, J. Michael, and S. S. Kundu, "SS-CAM: smoothed Score-CAM for sharper visual feature localization," 2020, https://arxiv.org/abs/2006.14255.

[50] H. Alshazly, C. Linse, E. Barth, and T. Martinetz, "Explainable COVID-19 detection using chest CT scans and deep learning," *Sensors*, vol. 21, no. 2, p. 455, 2021.

[51] R. K. Singh, R. Pandey, and R. N. Babu, "COVIDScreen: explainable deep learning framework for differential diagnosis of COVID-19 using chest X-Rays," *Neural Computing & Applications*, vol. 8, pp. 1–22, 2021.

[52] C. Shorten, T. M. Khoshgoftaar, and B. Furht, "Deep learning applications for COVID-19," *J Big Data*, vol. 8, pp. 1–54, 2021.

[53] F. Shi, J. Wang, J. Shi et al., "Review of artificial intelligence techniques in imaging data acquisition, segmentation and diagnosis for COVID-19," *IEEE Rev Biomed Eng*, vol. 14, 2020.

[54] S. A. Harmon, T. H. Sanford, S. Xu et al., "Artificial intelligence for the detection of COVID-19 pneumonia on chest CT using multinational datasets," *Nature Communications*, vol. 11, pp. 4080–4087, 2020.

[55] X. Ouyang, J. Huo, L. Xia et al., "Dual-sampling attention network for diagnosis of COVID-19 from community acquired pneumonia," *IEEE Transactions on Medical Imaging*, vol. 39, no. 8, pp. 2595–2605, 2020.

[56] X. Wu, H. Hui, M. Niu et al., "Deep learning-based multiview fusion model for screening 2019 novel coronavirus pneumonia: a multicentre study," *European Journal of Radiology*, vol. 128, Article ID 109041, 2020.

[57] A. A. Ardakani, A. R. Kanafi, U. R. Acharya, N. Khadem, and A. Mohammadi, "Application of deep learning technique to manage COVID-19 in routine clinical practice using CT

images: results of 10 convolutional neural networks," *Computers in Biology and Medicine*, vol. 121, p. 103795, 2020.

[58] L. Sun, Z. Mo, F. Yan et al., "Adaptive feature selection guided deep forest for COVID-19 classification with chest ct," *IEEE Journal of Biomedical and Health Informatics*, vol. 24, no. 10, pp. 2798–2805, 2020.

[59] A. Narin, C. Kaya, and Z. Pamuk, "Automatic detection of coronavirus disease (COVID-19) using x-ray images and deep convolutional neural networks," *Pattern Analysis and Applications : PAA*, vol. 24, no. 3, pp. 1–14, 2021.

[60] J. P. Cohen, P. Morrison, L. Dao, K. Roth, T. Q. Duong, and M. Ghassemi, "COVID-19 image data collection: prospective predictions are the future," 2020, https://github.com/ieee8023/covid-chestxray-dataset.

[61] X. Wang, Y. Peng, L. Lu, Z. Lu, M. Bagheri, and R. M. Summers, "Chestx-ray8: hospital-scale chest x-ray database and benchmarks on weakly-supervised classification and localization of common thorax diseases," in *Proceedings of the Proc IEEE Conf Comput Vis Pattern Recognit*, pp. 2097–2106, IEEE, Honolulu, HI, USA, 21 July 2017.

[62] P. Mooney, "Chest x-ray images (pneumonia)," 2018, https://www.kaggle.com/paultimothymooney/chest-xray-pneumonia.

[63] J. Zhang, Y. Xie, Y. Li, C. Shen, and Y. Xia, "COVID-19 screening on chest x-ray images using deep learning based anomaly detection," p. 27, 2020, https://arxiv.org/abs/2003.12338.

[64] B. Abraham and M. S. Nair, "Computer-aided detection of COVID-19 from X-ray images using multi-CNN and Bayesnet classifier," *Biocybernetics and Biomedical Engineering*, vol. 40, no. 4, pp. 1436–1445, 2020.

[65] D. S. Kermany, M. Goldbaum, W. Cai et al., "Identifying medical diagnoses and treatable diseases by image-based deep learning," *Cell*, vol. 172, no. 5, pp. 1122–1131, 2018.

[66] A. M. Dadario, "COVID-19 X rays," 2020, https://www.kaggle. com/andrewmvd/convid19-X-rays.

[67] P. Autee, S. Bagwe, V. Shah, and K. Srivastava, "StackNet-DenVIS: a multi-layer perceptron stacked ensembling approach for COVID-19 detection using X-ray images," *Physical and Engineering Sciences in Medicine*, vol. 43, no. 4, pp. 1399–1414, 2020.

[68] L. Wang, Z. Q. Lin, and A. Wong, "Covid-net: a tailored deep convolutional neural network design for detection of COVID-19 cases from chest x-ray images," *Scientific Reports*, vol. 10, pp. 1–12, 2020.

[69] M. E. H. Chowdhury, T. Rahman, A. Khandakar et al., "Can AI help in screening viral and COVID-19 pneumonia?" *IEEE Access*, vol. 8, pp. 132665–132676, 2020.

[70] L. Li, L. Qin, Z. Xu et al., "Artificial intelligence distinguishes COVID-19 from community acquired pneumonia on chest CT," *Radiology*, 2020.

[71] J. Wang, Y. Bao, Y. Wen et al., "Prior-attention residual learning for more discriminative COVID-19 screening in CT images," *IEEE Transactions on Medical Imaging*, vol. 39, no. 8, pp. 2572–2583, 2020.

[72] A. M. Hasan, M. M. Al-Jawad, H. A. Jalab, H. Shaiba, R. W. Ibrahim, and A. a. R. AL-Shamasneh, "Classification of COVID-19 coronavirus, pneumonia and healthy lungs in ct scans using q-deformed entropy and deep learning features," *Entropy*, vol. 22, no. 5, p. 517, 2020.

[73] C. Butt, J. Gill, D. Chun, and B. A. Babu, "Deep learning system to screen coronavirus disease 2019 pneumonia," *Applied Intelligence*, vol. 6, pp. 1–7, 2020.

[74] Y. Song, S. Zheng, L. Li et al., "Deep learning enables accurate diagnosis of novel coronavirus (COVID-19) with CT images," *IEEE/ACM Transactions on Computational Biology and Bioinformatics*, vol. 18, no. 6, 2021.

[75] M. Toğaçar, B. Ergen, and Z. Cömert, "COVID-19 detection using deep learning models to exploit Social Mimic Optimization and structured chest X-ray images using fuzzy color and stacking approaches," *Computers in Biology and Medicine*, vol. 121, Article ID 103805, 2020.

[76] A. Chung, "Figure 1 COVID-19 chest x-ray data initiative," 2020, https://github.com/agchung/Figure1-COVID-chestxray-dataset.

[77] A. Chung, "Actualmed COVID-19 chest x-ray data initiative," 2020, https://github.com/agchung/Actualmed-COVID-chestxray-dataset.

[78] RS, "COVID-19 radiography database," 2020, https://www.kaggle.com/tawsifurrahman/covid19-radiography-%20database.

[79] RS, "RSNA pneumonia detection challenge," https://www.kaggle.com/c/rsna-pneumonia-detection-challenge/data.

[80] M. Nishio, S. Noguchi, H. Matsuo, and T. Murakami, "Automatic classification between COVID-19 pneumonia, non-COVID-19 pneumonia, and the healthy on chest X-ray image: combination of data augmentation methods," *Scientific Reports*, vol. 10, pp. 17532–17536, 2020.

[81] M. Canayaz, "MH-COVIDNet: diagnosis of COVID-19 using deep neural networks and meta-heuristic-based feature selection on X-ray images," *Biomedical Signal Processing and Control*, vol. 64, Article ID 102257, 2021.

[82] Y. E. Almalki, A. Qayyum, M. Irfan et al., "A novel method for COVID-19 diagnosis using artificial intelligence in chest X-ray images," *Healthcare*, vol. 9, no. 5, p. 522, 2021.

[83] [dataset], "Radiopaedia," 2020, https://radiopaedia.org/search?lang=uspage=4q=covid+19scope=allutf8=%e2%9c%93.

[84] R. Hu, G. Ruan, S. Xiang, M. Huang, Q. Liang, and J. Li, *Automated Diagnosis of COVID-19 Using Deep Learning and Data Augmentation on Chest Ct*, medRxiv, 2020.

[85] [dataset], "COVID-19 database," 2020, https://www.sirm.org/category/senzacategoria/COVID-19/.

[86] L. Sarker, M. M. Islam, T. Hannan, and Z. Ahmed, "Covid-densenet: a deep learning architecture to detect COVID-19 from chest radiology images," *Preprints*, 2020.

[87] T. Ozturk, M. Talo, E. A. Yildirim, U. B. Baloglu, O. Yildirim, and U. Rajendra Acharya, "Automated detection of COVID-19 cases using deep neural networks with X-ray images," *Computers in Biology and Medicine*, vol. 121, Article ID 103792, 2020.

[88] T. Mahmud, M. A. Rahman, and S. A. Fattah, "CovXNet: a multi-dilation convolutional neural network for automatic COVID-19 and other pneumonia detection from chest X-ray images with transferable multi-receptive feature optimization," *Computers in Biology and Medicine*, vol. 122, Article ID 103869, 2020.

[89] M. Z. Alom, M. M. Rahman, M. S. Nasrin, T. M. Taha, and V. K. Asari, "Covid_mtnet: COVID-19 detection with multi-task deep learning approaches," 2020, https://arxiv.org/abs/2004.03747.

[90] D. N. Vinod and S. R. S. Prabaharan, "Data science and the role of Artificial Intelligence in achieving the fast diagnosis of COVID-19," *Chaos, Solitons & Fractals*, vol. 140, p. 110182, 2020.

[91] V. Perumal, V. Narayanan, and S. J. S. Rajasekar, "Detection of COVID-19 using CXR and CT images using Transfer

Learning and Haralick features," *Applied Intelligence*, vol. 51, no. 1, pp. 341–358, 2021.

[92] D. Singh, V. Kumar, M. Vaishali, and M. Kaur, "Classification of COVID-19 patients from chest CT images using multi-objective differential evolution-based convolutional neural networks," *European Journal of Clinical Microbiology & Infectious Diseases*, vol. 39, no. 7, pp. 1379–1389, 2020.

[93] Z. Xue, D. You, S. Candemir et al., "Chest x-ray image view classification," in *Proceedings of the 2015 IEEE 28th International Symposium on Computer-Based Medical Systems*, pp. 66–71, IEEE, Sao Carlos, Brazil, 22 June 2015.

[94] M. Irfan, M. A. Iftikhar, S. Yasin et al., "Role of hybrid deep neural networks (HDNNs), computed tomography, and chest X-rays for the detection of COVID-19," *International Journal of Environmental Research and Public Health*, vol. 18, no. 6, p. 3056, 2021.

[95] J. Chen, L. Wu, J. Zhang et al., "Deep learning-based model for detecting 2019 novel coronavirus pneumonia on high-resolution computed tomography," *Scientific Reports*, vol. 10, no. 1, pp. 1–11, 2020.

[96] D. Demner-Fushman, M. D. Kohli, M. B. Rosenman et al., "Preparing a collection of radiology examinations for distribution and retrieval," *Journal of the American Medical Informatics Association*, vol. 23, no. 2, pp. 304–310, 2016.

[97] T. D. Pham, "A comprehensive study on classification of COVID-19 on computed tomography with pretrained convolutional neural networks," *Scientific Reports*, vol. 10, pp. 16942–16948, 2020.

[98] H. Panwar, P. K. Gupta, M. K. Siddiqui, R. Morales-Menendez, and V. Singh, "Application of deep learning for fast detection of COVID-19 in X-Rays using nCOVnet," *Chaos, Solitons & Fractals*, vol. 138, Article ID 109944, 2020.

[99] M. Rahimzadeh, A. Attar, and S. M. Sakhaei, "A fully automated deep learning-based network for detecting COVID-19 from a new and large lung ct scan dataset," *Biomedical Signal Processing and Control*, vol. 68, Article ID 102588, 2021.

[100] S. Albahli, "Efficient GAN-based Chest Radiographs (CXR) augmentation to diagnose coronavirus disease pneumonia," *International Journal of Medical Sciences*, vol. 17, no. 10, pp. 1439–1448, 2020.

[101] Y. Cao, Z. Xu, J. Feng et al., "Longitudinal assessment of COVID-19 using a deep learning-based quantitative CT pipeline: illustration of two cases," *Radiology: Cardiothoracic Imaging*, vol. 2, no. 2, Article ID e200082, 2020.

[102] B. Wang, S. Jin, Q. Yan et al., "AI-assisted CT imaging analysis for COVID-19 screening: building and deploying a medical AI system," *Applied Soft Computing*, vol. 98, Article ID 106897, 2021.

[103] L. Huang, R. Han, T. Ai et al., "Serial quantitative chest CT assessment of COVID-19: a deep learning approach," *Radiology: Cardiothoracic Imaging*, vol. 2, no. 2, Article ID e200075, 2020.

[104] F. Shan, Y. Gao, J. Wang et al., "Lung infection quantification of COVID-19 in CT images with deep learning," 2020, https://arxiv.org/abs/2003.04655.

[105] N. Sverzellati, C. J. Ryerson, G. Milanese et al., "Chest x-ray or CT for COVID-19 pneumonia? Comparative study in a simulated triage setting," *European Respiratory Journal*, vol. 58, 2021.

[106] S. Wang, Y. Zha, W. Li et al., "A fully automatic deep learning system for COVID-19 diagnostic and prognostic analysis," *European Respiratory Journal*, vol. 56, 2020.

[107] Z. Feng, Q. Yu, S. Yao et al., "Early prediction of disease progression in COVID-19 pneumonia patients with chest CT and clinical characteristics," *Nature Communications*, vol. 11, pp. 4968-4969, 2020.

[108] W. Liang, H. Liang, L. Ou et al., "Development and validation of a clinical risk score to predict the occurrence of critical illness in hospitalized patients with COVID-19," *JAMA Internal Medicine*, vol. 180, no. 8, pp. 1081–1089, 2020.

[109] Q. Wu, S. Wang, L. Li et al., "Radiomics Analysis of Computed Tomography helps predict poor prognostic outcome in COVID-19," *Theranostics*, vol. 10, no. 16, pp. 7231–7244, 2020.

[110] J. P. Cohen, L. Dao, K. Roth et al., "Predicting COVID-19 pneumonia severity on chest x-ray with deep learning," *Cureus*, vol. 12, p. e9448, 2020.

[111] G. Shih, C. C. Wu, S. S. Halabi et al., "Augmenting the national institutes of health chest radiograph dataset with expert annotations of possible pneumonia," *Radiology: Artificial Intelligence*, vol. 1, no. 1, Article ID e180041, 2019.

[112] J. Irvin, P. Rajpurkar, M. Ko et al., "Chexpert: a large chest radiograph dataset with uncertainty labels and expert comparison," *Proceedings of the AAAI Conference on Artificial Intelligence*, vol. 33, pp. 590–597, 2019.

[113] A. Majkowska, S. Mittal, D. F. Steiner et al., "Chest radiograph interpretation with deep learning models: assessment with radiologist-adjudicated reference standards and population-adjusted evaluation," *Radiology*, vol. 294, no. 2, pp. 421–431, 2020.

[114] A. E. Johnson, T. J. Pollard, N. R. Greenbaum et al., "MIMIC-CXR-JPG, a large publicly available database of labeled chest radiographs," 2019, https://arxiv.org/abs/1901.07042.

[115] A. Bustos, A. Pertusa, J.-M. Salinas, and M. de la Iglesia-Vayá, "Padchest: a large chest x-ray image dataset with multi-label annotated reports," *Medical Image Analysis*, vol. 66, Article ID 101797, 2020.

[116] J. Zhu, B. Shen, A. Abbasi, M. Hoshmand-Kochi, H. Li, and T. Q. Duong, "Deep transfer learning artificial intelligence accurately stages COVID-19 lung disease severity on portable chest radiographs," *PLoS One*, vol. 15, no. 7, Article ID e0236621, 2020.

[117] S. Tabik, A. Gomez-Rios, J. L. Martin-Rodriguez et al., "COVIDGR dataset and COVID-SDNet methodology for predicting COVID-19 based on Chest X-Ray images," *IEEE Journal of Biomedical and Health Informatics*, vol. 24, no. 12, pp. 3595–3605, 2020.

[118] M. Shorfuzzaman and M. S. Hossain, "MetaCOVID: a Siamese neural network framework with contrastive loss for n-shot diagnosis of COVID-19 patients," *Pattern Recognition*, vol. 113, Article ID 107700, 2021.

[119] I. Ozsahin, B. Sekeroglu, M. S. Musa, M. T. Mustapha, and D. Uzun Ozsahin, "Review on diagnosis of COVID-19 from chest CT images using artificial intelligence," *Comput Math Methods Med*, vol. 2020, Article ID 9756518, 10 pages, 2020.

[120] A. Shoeibi, M. Khodatars, R. Alizadehsani et al., "Automated detection and forecasting of COVID-19 using deep learning techniques: a review," 2020, https://arxiv.org/abs/2007.10785.

[121] D. Chicco and G. Jurman, "The advantages of the Matthews correlation coefficient (MCC) over F1 score and accuracy in binary classification evaluation," *BMC Genomics*, vol. 21, pp. 6–3, 2020.

[122] M. H. Alsharif, Y. H. Alsharif, K. Yahya, O. A. Alomari, M. A. Albreem, and A. Jahid, "Deep learning applications to combat the dissemination of COVID-19 disease: a review,"

European Review for Medical and Pharmacological Sciences, vol. 24, pp. 11455–11460, 2020.

[123] S. K. Joy, F. Ahmed, M. Humaira et al., "A comprehensive survey of COVID-19 detection using medical images," *SN Comput Sci.*vol. 2, 2020.

[124] H. Alghamdi, G. Amoudi, S. Elhag, K. Saeedi, and J. Nasser, "Deep learning approaches for detecting COVID-19 from chest X-ray images: a survey," *IEEE Access*, vol. 9, 2021.

[125] M. M. Islam, F. Karray, R. Alhajj, and J. Zeng, "A review on deep learning techniques for the diagnosis of novel coronavirus (COVID-19)," *IEEE Access*, vol. 9, pp. 30551–30572, 2021.

[126] A. Sriram, M. Muckley, K. Sinha et al., "COVID-19 deterioration prediction via self-supervised representation learning and multi-image prediction," 2021, https://arxiv.org/abs/2101.04909.

[127] A. Artetxe, A. Beristain, and M. Graña, "Predictive models for hospital readmission risk: a systematic review of methods," *Computer Methods and Programs in Biomedicine*, vol. 164, pp. 49–64, 2018.

[128] X. Min, B. Yu, and F. Wang, "Predictive modeling of the hospital readmission risk from patients' claims data using machine learning: a case study on COPD," *Scientific Reports*, vol. 9, no. 1, pp. 1–0, 2019.

[129] K. Teo, C. W. Yong, F. Muhamad et al., "The promise for reducing healthcare cost with predictive model: an analysis with quantized evaluation metric on readmission," *J Healthcare Eng*, vol. 2021, Article ID 9208138, 10 pages, 2021.

[130] J. Donzé, D. Aujesky, D. Williams, and J. L. Schnipper, "Potentially avoidable 30-day hospital readmissions in medical patients: derivation and validation of a prediction model," *JAMA Internal Medicine*, vol. 173, no. 8, pp. 632–638, 2013.

[131] O. A. UyaroĞlu, N. Ç BaŞaran, L. ÖziŞik et al., "Thirty-day readmission rate of COVID-19 patients discharged from a tertiary care university hospital in Turkey: an observational, single-center study," *International Journal for Quality in Health Care : Journal of the International Society for Quality in Health Care*, vol. 33, no. 1, p. 144, 2021.

[132] S. Sotoodeh Ghorbani, N. Taherpour, S. Bayat, H. Ghajari, P. Mohseni, and S. S. Hashemi Nazari, "Epidemiologic characteristics of cases with reinfection, recurrence, and hospital readmission due to COVID-19: a systematic review and meta-analysis," *Journal of Medical Virology*, vol. 94, no. 1, pp. 44–53, 2021.

[133] P. Goyal, M. Caron, B. Lefaudeux et al., "Self-supervised pretraining of visual features in the wild," 2021, https://arxiv.org/abs/2103.01988.

[134] H. Pham, Z. Dai, Q. Xie, M. T. Luong, and Q. V. Le, "Meta pseudo labels," 2020, https://arxiv.org/abs/2003.10580.

[135] Y. Oh, H. Jung, J. Park, and M. S. Kim, "EVET: enhancing visual explanations of deep neural networks using image transformations," in *Proceedings of the IEEE Winter Conf Appl Comput Vis*, pp. 3579–3587, IEEE, Waikoloa, HI, USA, 3 January 2021.

[136] K. Vinogradova, A. Dibrov, and G. Myers, "Towards interpretable semantic segmentation via gradient-weighted class activation mapping," 2020, https://arxiv.org/abs/2002.11434.

[137] B. Zhou, A. Khosla, A. Lapedriza, A. Oliva, and A. Torralba, "Learning deep features for discriminative localization," *Proc IEEE Conf Comput Vis Pattern Recognit*, pp. 2921–2929, 2016.

[138] A. A. Taha and A. Hanbury, "Metrics for evaluating 3D medical image segmentation: analysis, selection, and tool," *BMC Medical Imaging*, vol. 15, pp. 29–28, 2015.

[139] R. Roelofs, *Measuring Generalization and Overfitting in Machine Learning*, Doctoral dissertation, UC Berkeley), 2019.

[140] X. He, S. Wang, G. Ying, J. Zhang, and X. Chu, "Efficient multi-objective evolutionary 3D neural architecture search for COVID-19 detection with chest CT scans.," 2021, https://arxiv.org/abs/2101.10667.

[141] Z. Li, W. Zhao, F. Shi et al., "A novel multiple instance learning framework for COVID-19 severity assessment via data augmentation and self-supervised learning," *Medical Image Analysis*, vol. 69, Article ID 101978, 2021.

[142] I. Singh, H. Zhou, K. Yang, M. Ding, B. Lin, and P. Xie, "Differentially-private federated neural architecture search," 2020, https://arxiv.org/abs/2006.10559.

[143] M. Xu, Y. Zhao, K. Bian, G. Huang, Q. Mei, and X. Liu, "Eural architecture search over decentralized data," in *N*, https://arxiv.org/abs/2002.06352, 2020.

[144] A. Priyanshu and R. Naidu, "FedPandemic: a cross-device federated learning approach towards elementary prognosis of diseases during a pandemic," 2021, https://arxiv.org/abs/2104.01864.

[145] G. Yadav, S. Maheshwari, and A. Agarwal, "Contrast limited adaptive histogram equalization based enhancement for real time video system," in *Proceedings of the 2014 International Conference on Advances in Computing, Communications and Informatics*, pp. 2392–2397, IEEE, Delhi, India, 24 September 2014.

[146] S. M. Pizer, E. P. Amburn, J. D. Austin et al., "Adaptive histogram equalization and its variations," *Computer Vision, Graphics, and Image Processing*, vol. 39, no. 3, pp. 355–368, 1987.

[147] T. L. Veldhuizen and M. E. Jernigan, "Grid filters for local nonlinear image restoration,"vol. 5, pp. 2885–2888, in *Proceedings of the 1998 IEEE International Conference on Acoustics, Speech and Signal Processing, (Cat. No. 98CH36181)*, vol. 5, pp. 2885–2888, IEEE, Seattle, WA, USA, 15 May 1998.

[148] T. M. Lehmann, C. Gonner, and K. Spitzer, "Survey: interpolation methods in medical image processing," *IEEE Transactions on Medical Imaging*, vol. 18, no. 11, pp. 1049–1075, 1999.

[149] J. Tian, Y. Wang, X. Dai, and X. Zhang, "Medical image processing and analysis," in *Mol Imaging*, pp. 415–469, Springer, Berlin, Heidelberg, 2013.

[150] D. S. Prabha and J. S. Kumar, "Performance analysis of image smoothing methods for low level of distortion," in *Proceedings of the 2016 IEEE International Conference on Advances in Computer Applications*, pp. 372–376, IEEE, Coimbatore, India, 24 October 2016.

[151] M. Kociołek, M. Strzelecki, and R. Obuchowicz, "Does image normalization and intensity resolution impact texture classification?" *Computerized Medical Imaging and Graphics*, vol. 81, Article ID 101716, 2020.

[152] M. A. Gungor, "A comparative study on wavelet denoising for high noisy CT images of COVID-19 disease," *Optik*, vol. 235, Article ID 166652, 2021.

[153] A. Waheed, M. Goyal, D. Gupta, A. Khanna, F. Al-Turjman, and P. R. Pinheiro, "Covidgan: data augmentation using auxiliary classifier gan for improved COVID-19 detection," *IEEE Access*, vol. 8, pp. 91916–91923, 2020.

[154] D. Samiappan, S. Latha, T. R. Rao, D. Verma, and C. Sriharsha, "Enhancing machine learning aptitude using significant cluster identification for augmented image refining," *International Journal of Pattern Recognition and Artificial Intelligence*, vol. 34, no. 09, Article ID 2051009, 2020.

[155] A. Mobiny, P. A. Cicalese, S. Zare et al., "Radiologist-level COVID-19 detection using ct scans with detail-oriented capsule networks," 2004, https://arxiv.org/abs/2004.07407.

[156] A. Oulefki, S. Agaian, T. Trongtirakul, and A. Kassah Laouar, "Automatic COVID-19 lung infected region segmentation and measurement using CT-scans images," *Pattern Recognition*, vol. 114, Article ID 107747, 2021.

[157] S. Park, G. Kim, Y. Oh et al., "Vision transformer for COVID-19 CXR diagnosis using chest X-ray feature corpus," 2021, https://arxiv.org/abs/2103.07055.

[158] G. Maguolo and L. Nanni, "A critic evaluation of methods for COVID-19 automatic detection from x-ray images," *Information Fusion*, vol. 76, 2021.

[159] P. Rajpurkar, J. Irvin, K. Zhu et al., "Chexnet: radiologist-level pneumonia detection on chest x-rays with deep learning," 2017, https://arxiv.org/abs/1711.05225.

[160] A. S. Al-Waisy, S. Al-Fahdawi, M. A. Mohammed et al., "COVID-CheXNet: hybrid deep learning framework for identifying COVID-19 virus in chest X-rays images," *Soft Comput*, pp. 1–6, 2020.

Hindawi
Journal of Healthcare Engineering
Volume 2022, Article ID 1872412, 10 pages
https://doi.org/10.1155/2022/1872412

Research Article

Construction of a Diagnostic Model for Lymph Node Metastasis of the Papillary Thyroid Carcinoma Using Preoperative Ultrasound Features and Imaging Omics

Chao Zhang[1], **Lihua Cheng**[1], **Weiwen Zhu**[1], **Jian Zhuang**[1], **Tong Zhao**[2], **Xiaoqin Li**[1], **and Wenfeng Wang**[3]

[1]*Department of Ultrasound, The Affiliated Changzhou No. 2 People's Hospital with Nanjing Medical University, Changzhou 213004, China*
[2]*Graduate School, Dalian Medical University, Dalian 116000, China*
[3]*School of Science, Shanghai Institute of Technology, Shanghai 201418, China*

Correspondence should be addressed to Xiaoqin Li; xiaoqinl_cz@outlook.com

Received 23 August 2021; Revised 14 December 2021; Accepted 7 January 2022; Published 8 February 2022

Academic Editor: yan chai hum

In this paper, we mainly adopted 337 patients who had undergone the surgery on lymph node metastasis of papillary thyroid carcinoma (PTC) as the sample population. In order to provide clinical reference for the intelligent decision-making in treatment plan and improvement of prognosis, we utilized ultrasound features and imaging features to construct five early diagnosis models for patients based on the ultrasound features, imaging features, and combined features. The model integrated with broad learning system (BLS) showed the best performance, with the area under the curve (AUC) of 0.857 (95% confidence interval (CI): 0.811–0.902)) and the accuracy of 0.805 (95% CI: 0.759–0.850). For demographic and clinical features, the prediction effect was also good, with the AUC more than 0.700.

1. Introduction

Papillary thyroid carcinoma (PTC) is one of the most common pathologic types of thyroid cancer [1]. The current clinical problem is to find regions where lymph node metastasis is prone to occur [2]. This problem is usually solved by utilizing the ultrasound technology, which is also the first choice for thyroid cancer examination. Ultrasound technology can determine whether the patient has cervical lymph node metastasis before surgery, which is of great significance for the selection of surgical methods, radiotherapy and chemotherapy, and the judgment of prognosis [3]. The major advantage of machine learning is that the learning model can improve treatment decisions for cancers and provide clinical references to improve the prognosis [4]. Deep learning models have been used in previous studies, but it takes a lot of time in training stage [5–7].

As an effective and efficient incremental learning system, broad learning system (BLS) can provide value for prediction model, which largely reduced the time cost of model training [5]. If combined with imaging omics, broad learning features can then be utilized in establishing the lymph node metastasis model [6–8]. Imaging omics is mainly based on the extraction and analysis of images features from CT, MRI, PET, and other medical images to quantitatively evaluate diseases such as thyroid papillary carcinoma and lymph nodes [9]. It can be used to diagnose diseases, predict prognosis, and analyze biological behavior of diseases [10]. Imaging omics was proved to be objective in image extraction of lymph node features in PTC and had important implications for prediction of clinical outcome [11–15]. Since imaging omics has been successfully applied to the diagnosis of thyroid cancer, lung cancer, liver cancer, breast cancer, and other diseases [16–22], it will also be employed in the present study.

Table 1: Sensitivity analysis before and after gap-filling.

Variables	Missing number	Before filling ($n = 428$)	After filling ($n = 428$)	Statistics	P
Carcinoembryonic antigen, M(Q_1,Q_3)	17 (3.97%)	1.42 (0.88, 2.10)	1.42 (0.89, 2.07)	$Z = -0.066$	0.948
Free triiodothyroxine, mean ± SD	8 (1.87%)	5.15 ± 1.31	5.16 ± 1.32	$t = -0.06$	0.949
Free thyroxine, mean ± SD	8 (1.87%)	18.29 ± 4.76	17.96 ± 3.70	$t = 1.12$	0.261
Thyroid stimulating hormone, M(Q_1,Q_3)	8 (1.87%)	1.93 (1.12, 3.17)	1.96 (1.15, 3.19)	$Z = 0.368$	0.713
Thyroid globulin antibody, M(Q_1,Q_3)	8 (1.87%)	19.04 (12.98, 66.89)	18.66 (12.97, 57.48)	$Z = -0.397$	0.691
Maximum diameter of nodule, M(Q_1,Q_3)	1 (0.23%)	0.80 (0.50, 1.20)	0.80 (0.50, 1.20)	$Z = -0.055$	0.956

To combine imaging omics with broad learning features, random forest is employed to develop the basic analytic models, which is a combination of decision trees [23]. Each decision tree is trained by randomly generating a new data set from the original data set. The result of random forest is the decision of most decision trees [24–28]. But a single model classification method is often prone to overfitting problem. Many scholars often improve the prediction accuracy through the combination of multiple single models, which is called classifier combination method. Random forest is an algorithm that proposed to solve the overfitting problem of a single decision tree model [29]. Random forest uses the bootstrap resampling method to extract multiple samples from the original samples and then conducts decision tree modeling for each bootstrap sample, and then synthesizes multiple decision trees for prediction, and obtains the final prediction result through voting [30, 31].

The organization of this article is as follows. We will use preoperative ultrasound features and image analyses to construct an early diagnosis model for lymph node metastasis in PTC in Section 2. These models will be performed, evaluated, and then integrated with BLS in Section 3.

2. Materials and Methods

2.1. Study Design and Population. This study was a cross-sectional study which was approved by the Institutional Review Board of The Affiliated Changzhou No. 2 People's Hospital with Nanjing Medical University (approval number: [2021]KY021-01). The sample population was 337 patients who had undergone PTC surgery in Changzhou Second People's Hospital after inclusion and exclusion.

The inclusion criteria were as follows: (1) patients aged ≥18 years old; (2) PTC patients who received fine needle biopsy before operation and were confirmed; (3) patients without benign lesions or single malignant lesions; (4) patients who underwent extensive neck lymph node dissection; (5) patients with complete clinical data.

The exclusion criteria were as follows: (1) patients who received anticancer treatment such as radiotherapy and chemotherapy before operation; (2) patients without undergoing ultrasound examination before operation.

2.2. Missing Data Assessment. There were 428 nodules in 337 patients. Noting that each nodule had two or more ultrasound images from different angles, there were a total of 973 ultrasound images for 428 nodules in 337 patients. Alternatively, a total of 428 data and 973 representative ultrasound images were collected. Missing values in the data were filled by random interpolation. Sensitivity analysis before and after gap-filling is shown in Table 1.

2.3. Image Preprocessing and Classification. In the present study, Lasso regression filtering is used for image processing [32, 33]. The processes were to sample n original sample data with the sample size of N and each observation object had an equal probability of being selected, which was 1/N. The sample was regarded as the whole, and the subsamples sampled were regarded as samples from the sample. Such subsample was called the bootstrap sample. The sampling process can be formulated as follows. Let H(x) represent the random forest classification result, $h_i(x)$ represent the classification result of a single decision tree, Y represent the classification target, $I(\cdot)$ represent indicative function, and the random forest classification model adopt a simple voting strategy to complete the final classification.

(1) Each decision tree was generated by training sample X with sample size K and random vector θ_k

(2) Random vector sequence $\{\theta_k, \quad 1, \ldots, K\}$ was independently and identically distributed

(3) Random forest was the set of all decision trees $\{h(X, \theta_k), \quad k = 1, 2, \ldots, K\}$

Among these processes, each decision tree model $h(X, \theta_k)$ had one vote to select the classification result of input variable X: $H(x) = \max_Y \sum_{i=1}^{k} I(h_i(x) = Y)$.

The remaining variable of image feature was gray-level size zone matrix (GLSZM) entropy. The remaining three variables were gender, age, and carcinoembryonic antigen in the demographic information and clinical data, and the remaining four features were the maximum diameter of nodule in ultrasound features, aspect ratio, calcification, and relative capsule position. BLS was established for image classification through learning the variables in the model to obtain the output variables. In the process of image classification, broad learning mapped the input data, constructed the mapping features, and then activated the mapping features to enhance the features, and output the two parts together. We screened out the new features by using the loss function of the 1-norm in Lasso regression, and the new features were merged into the random forest as follows:

$$J(w, b) = \frac{1}{2m} \arg\min_{w,b} \sum_{i=1}^{m} (\hat{y}_i - y_i)^2 + \alpha \sum_{i=1}^{n} \|w_i\|. \quad (1)$$

2.4. Establishment of the Diagnostic Models. For each nodule, the ROI was delineated according to the gray image

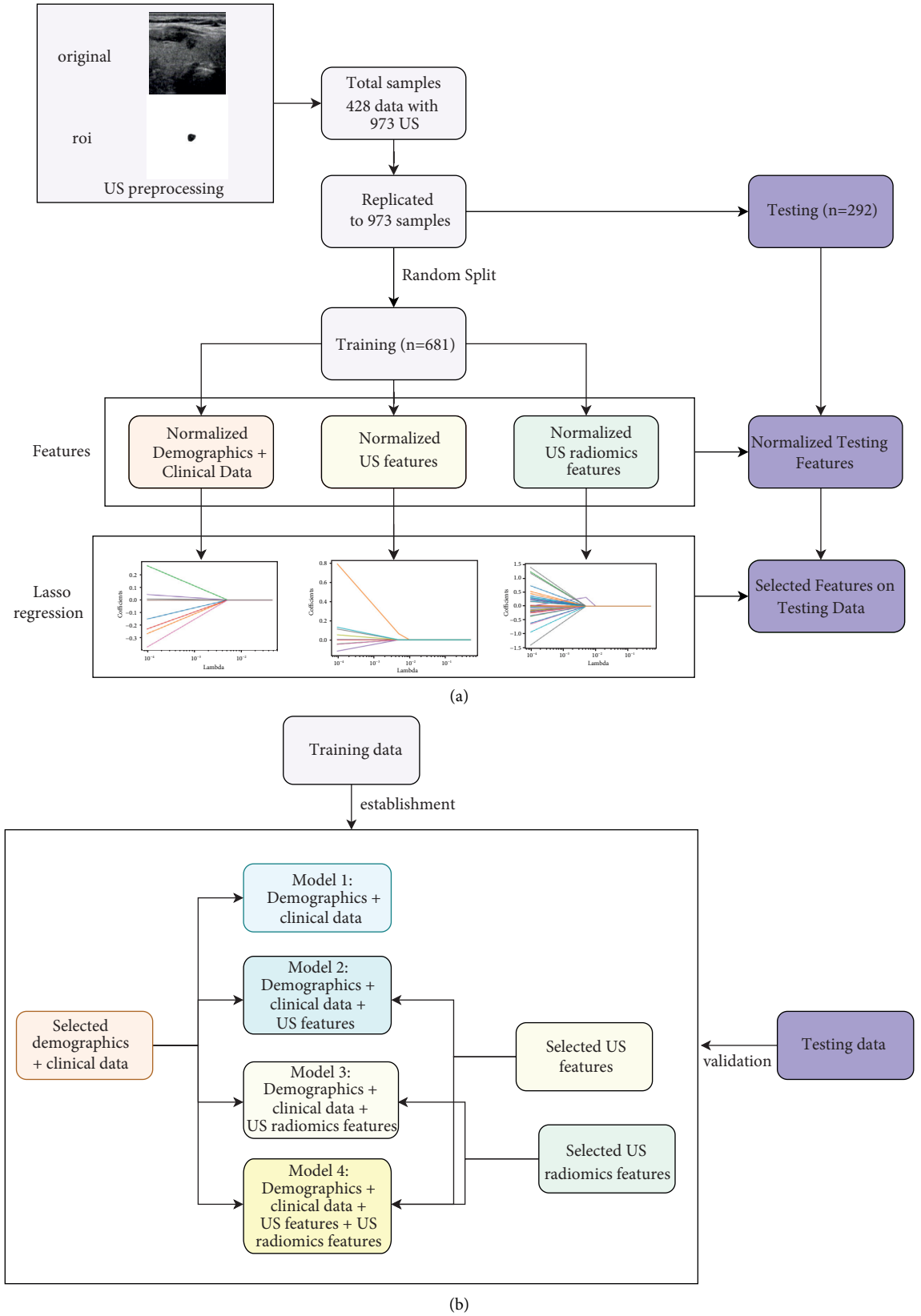

Figure 1: (a) Flow chart for the model development and validation. (b) Characteristics of the diagnostic models.

Table 2: Characteristics comparison for the training and testing sets.

Variables	Total ($n = 973$)	Training set ($n = 681$)	Testing set ($n = 292$)	Statistics	P
Gender, n (%)					
Male	207 (21.27)	143 (21.00)	64 (21.92)	$\chi^2 = 0.103$	0.748
Female	766 (78.73)	538 (79.00)	228 (78.08)		
Age, mean ± SD	44.74 ± 11.25	44.66 ± 11.05	44.91 ± 11.70	$t = -0.32$	0.752
BMI, mean ± SD	23.87 ± 3.39	23.90 ± 3.43	23.82 ± 3.29	$t = 0.30$	0.763
Carcinoembryonic antigen, M(Q_1, Q_3)	1.34 (0.86, 2.02)	1.34 (0.84, 2.02)	1.33 (0.89, 2.05)	$Z = 0.067$	0.947
The free triiodide, M(Q_1, Q_3)	5.10 (4.60, 5.50)	5.10 (4.60, 5.50)	5.00 (4.60, 5.50)	$Z = -0.201$	0.841
Free thyroxine, mean ± SD	18.61 ± 5.03	18.58 ± 4.80	18.67 ± 5.55	$t = -0.24$	0.812
T stimulating hormone, M(Q_1, Q_3)	1.91 (1.11, 3.19)	1.94 (1.15, 3.25)	1.78 (1.06, 2.99)	$Z = -1.374$	0.169
T globulin antibody, M(Q_1, Q_3)	20.92 (12.98, 78.98)	20.92 (13.04, 83.68)	19.11(12.27, 73.34)	$Z = -0.982$	0.326
Part, n (%)					
Ru	105 (10.79)	73 (10.72)	32 (10.96)	$\chi^2 = 6.065$	0.416
Right middle school	266 (27.34)	199 (29.22)	67 (22.95)		
Lower right	148 (15.21)	101 (14.83)	47 (16.10)		
Left	73 (7.50)	47 (6.90)	26 (8.90)		
Left middle school	237 (24.36)	167 (24.52)	70 (23.97)		
The lower left	100 (10.28)	64 (9.40)	36 (12.33)		
Isthmus	44 (4.52)	30 (4.41)	14 (4.79)		
Max diameter of nodule, M(Q_1, Q_3)	0.80 (0.54, 1.20)	0.80(0.53, 1.20)	0.80(0.57, 1.31)	$Z = 0.867$	0.386
Form, n (%)					
Rules	95 (9.76)	64 (9.40)	31 (10.62)	$\chi^2 = 1.327$	0.515
Under-rule	318 (32.68)	217 (31.86)	101 (34.59)		
Irregular	560 (57.55)	400 (58.74)	160 (54.79)		
Boundary, n (%)					
Clear	170 (17.47)	113 (16.59)	57 (19.52)	$\chi^2 = 1.226$	0.542
Lack of clarity	368 (37.82)	261 (38.33)	107 (36.64)		
Unclear or vague	435 (44.71)	307 (45.08)	128 (43.84)		
Aspect ratio, n (%)					
≤1	415 (42.65)	282 (41.41)	133 (45.55)	$\chi^2 = 1.431$	0.232
>1	558 (57.35)	399 (58.59)	159 (54.45)		
Composition, n (%)					
Cystic or almost totally cystic	1 (0.10)	1 (0.15)	0 (0.00)	Fisher	1.000
Capsule solidity	19 (1.95)	13 (1.91)	6 (2.05)		
Real or almost all real	953 (97.94)	667 (97.94)	286 (97.95)		
Echo, n (%)					
Isoechoic or hyperechoic	5 (0.51)	3 (0.44)	2 (0.68)	Fisher	0.898
Low echo	926 (95.17)	649 (95.30)	277 (94.86)		
Extremely low echo	21 (2.16)	14 (2.06)	7 (2.40)		
Mixed echo	21 (2.16)	15 (2.20)	6 (2.05)		
Calcification, n (%)					
No calcification	362 (37.20)	262 (38.47)	100 (34.25)	Fisher	0.293
Coarse calcification	62 (6.37)	47 (6.90)	15 (5.14)		
Eggshell calcification	6 (0.62)	5 (0.73)	1 (0.34)		
Microcalcification	543 (55.81)	367 (53.89)	176 (60.27)		
Relative coating position, n (%)					
Stay away from	398 (40.90)	286 (42.00)	112 (38.36)	$\chi^2 = 1.123$	0.570
Cling	485 (49.85)	333 (48.90)	152 (52.05)		
Breakthrough	90 (9.25)	62 (9.10)	28 (9.59)		
TI_DS classification, *n* (%)				$\chi^2 = 0.812$	0.937
LNM transfer, n (%)					
No	576 (59.20)	410 (60.21)	166 (56.85)	$\chi^2 = 0.953$	0.329
Yes	397 (40.80)	271 (39.79)	126 (43.15)		

T: thyroid; TI_DS: ultrasonic thyroid imaging and data system; LNM: lymph node metastases.

selected in the largest long axis cross section. The early diagnosis model of lymph node metastases (LNM) was constructed by combining the preoperative ultrasound features and ultrasound image features, as shown in Figures 1(a) and 1(b). The focus area of PTC was framed by the clinician, and then the imaging features of the focus area were extracted by the pyradiomics algorithm.

Table 3: The predictive performance of these models in the training and testing sets.

Models	Cut-off	Sensitivity (95% CI)	Specificity (95% CI)	PPV (95% CI)	NPV (95% CI)	AUC (95% CI)	Accuracy (95% CI)
Model 1[a]	0.348	0.849 (0.806–0.891)	0.851 (0.817–0.886)	0.790 (0.744–0.837)	0.895 (0.864–0.925)	0.913 (0.893–0.934)	0.850 (0.823–0.877)
Model 1[b]	0.348	0.738 (0.661–0.815)	0.771 (0.707–0.835)	0.710 (0.632–0.788)	0.795 (0.733–0.857)	0.813 (0.762–0.863)	0.757 (0.708–0.806)
Model 2[a]	0.437	0.808 (0.761–0.855)	0.868 (0.836–0.901)	0.802 (0.755–0.849)	0.873 (0.840–0.905)	0.913 (0.892–0.934)	0.844 (0.817–0.872)
Model 2[b]	0.437	0.730 (0.653–0.808)	0.789 (0.727–0.851)	0.724 (0.647–0.802)	0.794 (0.732–0.856)	0.818 (0.769–0.868)	0.764 (0.715–0.812)
Model 3[a]	0.360	0.886 (0.848–0.924)	0.827 (0.790–0.863)	0.772 (0.725–0.818)	0.916 (0.888–0.944)	0.941 (0.925–0.957)	0.850 (0.823–0.877)
Model 3[b]	0.360	0.762 (0.688–0.836)	0.723 (0.655–0.791)	0.676 (0.599–0.753)	0.800 (0.736–0.864)	0.821 (0.772–0.871)	0.740 (0.689–0.790)
Model 4[a]	0.500	0.823 (0.777–0.868)	0.966 (0.948–0.983)	0.941 (0.911–0.971)	0.892 (0.863–0.921)	0.984 (0.977–0.990)	0.909 (0.887–0.931)
Model 4[b]	0.500	0.667 (0.584–0.749)	0.910 (0.866–0.953)	0.848 (0.778–0.919)	0.782 (0.724–0.841)	0.857 (0.811–0.902)	0.805 (0.759–0.850)

[a]Using the training set; [b]using the testing set. PPV: positive predictive value; NPV: predictive value; AUC: area under the curve; CI: confidence internal.

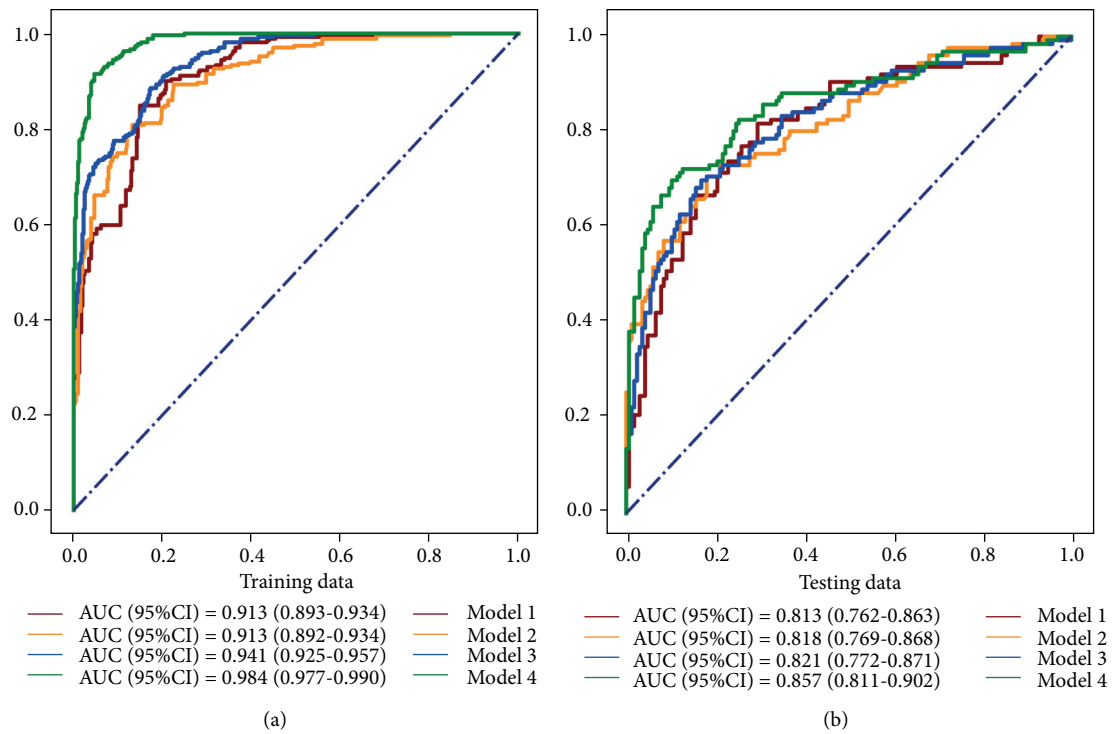

Figure 2: ROC curves of the four models in training and testing sets.

Table 4: The predictive performance of lymph node metastasis by BLS feature learning.

Models	Cut-off	Sensitivity (95% CI)	Specificity (95% CI)	PPV (95% CI)	NPV (95% CI)	AUC (95% CI)	Accuracy (95% CI)
Model 4[a]	0.500	0.823 (0.777–0.868)	0.966 (0.948–0.983)	0.941 (0.911–0.971)	0.892 (0.863–0.921)	0.984 (0.977–0.990)	0.909 (0.887–0.931)
Model 4[b]	0.500	0.667 (0.584–0.749)	0.910 (0.866–0.953)	0.848 (0.778–0.919)	0.782 (0.724–0.841)	0.857 (0.811–0.902)	0.805 (0.759–0.850)
Model 5[a]	0.465	0.959 (0.936–0.983)	0.973 (0.958–0.989)	0.959 (0.936–0.983)	0.973 (0.958–0.989)	0.995 (0.992–0.998)	0.968 (0.954–0.981)
Model 5[b]	0.465	0.778 (0.705–0.850)	0.843 (0.788–0.899)	0.790 (0.719–0.862)	0.833 (0.777–0.890)	0.853 (0.806–0.901)	0.815 (0.771–0.860)

[a]Using the training set; [b]using the testing set. PPV: positive predictive value; NPV: predictive value; AUC: area under the curve; CI: confidence internal.

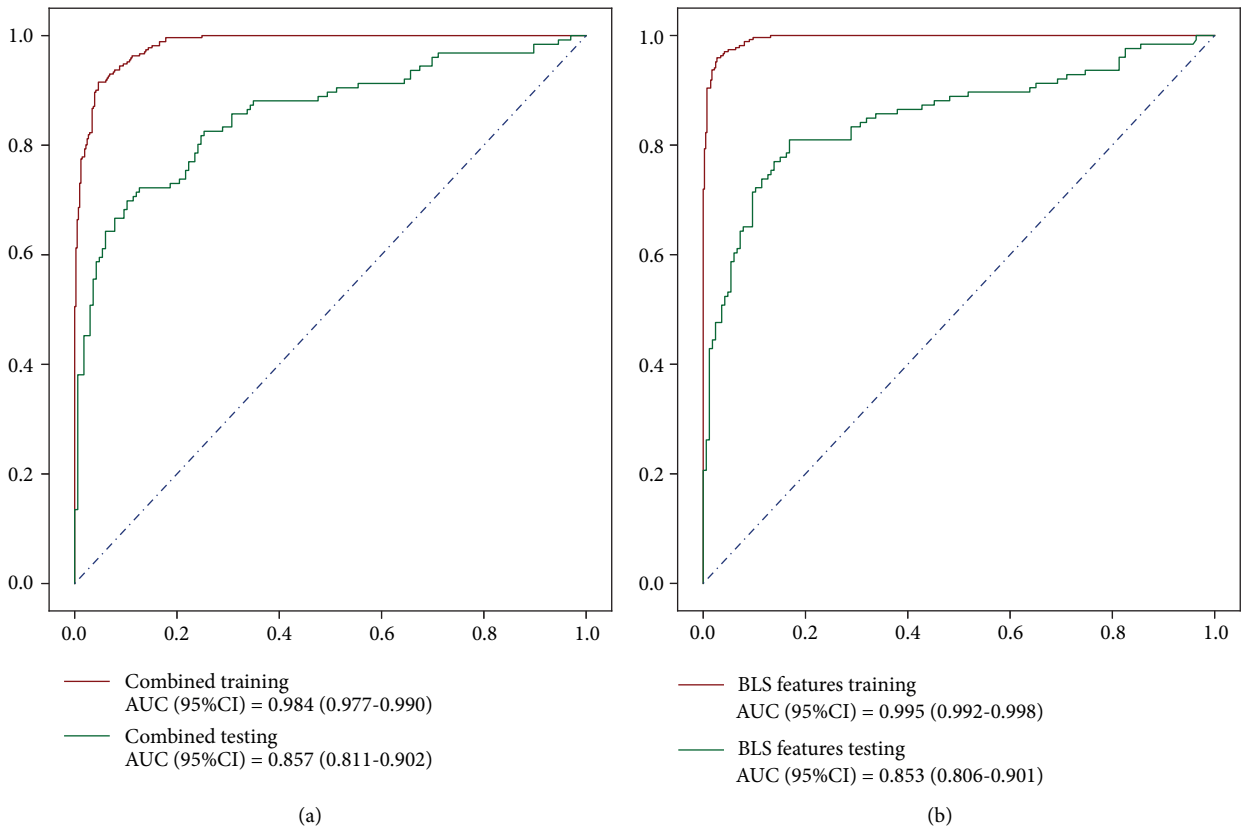

Figure 3: The ROC curve of Model 4 and Model 5 in training and testing sets.

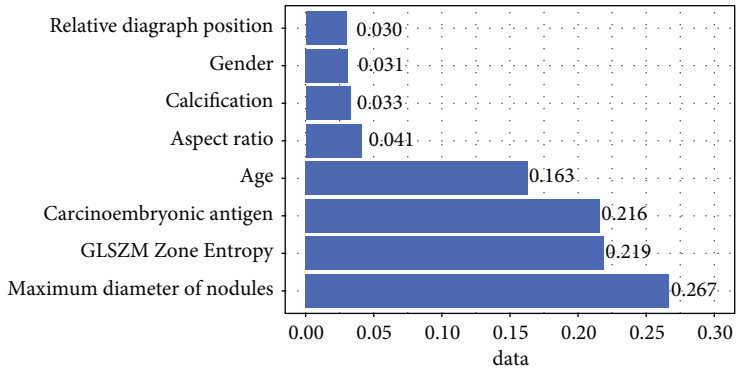

Figure 4: Features importance map.

The strategy in construction of the five diagnostic models was different. In Model 1, only demographic information and clinical data were used. In Model 2, we combined demographic information, clinical data, and ultrasound features. Model 3 combined demographic information, clinical data, and imaging features. Model 4 combined the demographic information, clinical data, ultrasound features, and imaging features. Broad learning was used to learn the variables in Model 4, and new variables were obtained, which were incorporated into the random forest model to obtain Model 5.

The data set was randomly divided into 7 : 3 training set and testing set, which were then normalized, respectively. Lasso regression was used to filter features in the training set, and then the prediction model was constructed.

The area under the curve (AUC), accuracy, sensitivity, and specificity were used to evaluate the model. Then, the importance of features was expressed by using the feature importance map.

3. Results and Discussion

3.1. Diagnostic Performance of the Five Models. As shown in Table 2, because the data were randomly divided into training sets and testing sets, the ultrasonic features were compared in balance. Because their P values were all >0.05,

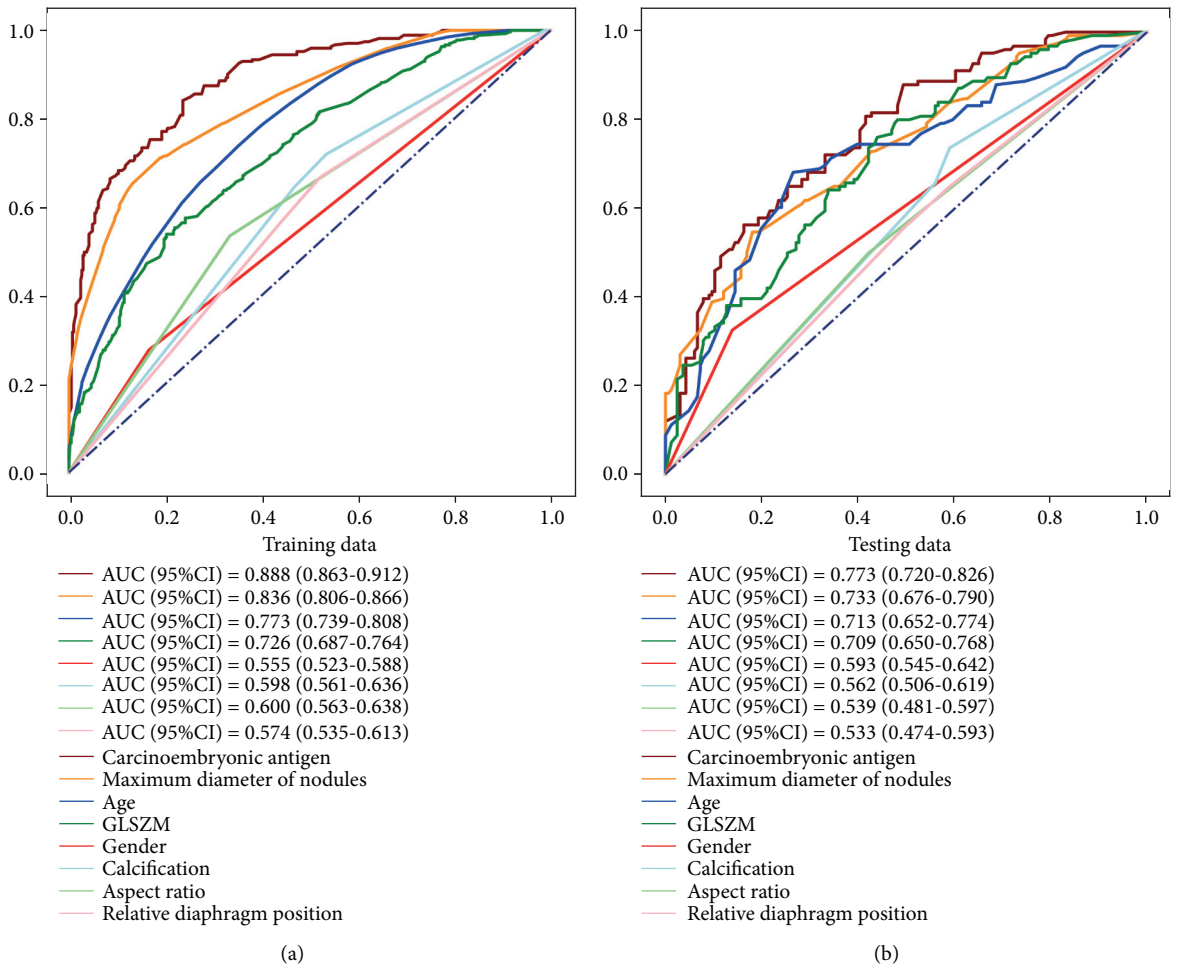

Figure 5: Ultrasonic features AUC: testing set on the left and training set on the right (carcinoembryonic antigen, maximum diameter of nodule, age, GLSZM zone entropy, sex, calcification, aspect ratio, and relative capsule position in turn, which are modified according to translation.

the difference between training sets and testing sets was not statistically significant. This confirmed that the performances between training sets and testing sets were comparable.

As shown in Table 3, it can be found from the prediction results that Model 4 performed best in the testing set, which combined ultrasound features and imaging features in our data set, with the AUC of 0.857 (95% confidence internal (CI): 0.811–0.902) and the accuracy of 0.805 (95%CI: 0.759–0.850). The receiver operator characteristic (ROC) curves of the four models are shown in Figure 2.

3.2. Prediction Results after Integrated with Broad Learning. Eight features in Model 4 were included in BLS model to get 106 features, and then 5 features were screened out by Lasso using $\alpha = 0.004$. Five features put into the stochastic forest prediction model to predict whether lymph node metastasis occurred are shown in Table 4. Figure 3 shows the ROC curve of Model 4 and Model 5 in training and testing sets.

3.3. Discussion on the Importance of Model Features. Since the prediction results of Model 4 and Model 5 were relatively close, and the difference was not statistically significant, we finally chose Model 4 because of its high interpretability. From the map of feature importance (Figure 4), it can be found that the most important variable was the maximum diameter of nodules, followed by GLSZM zone entropy in imaging features, and the third was carcinoembryonic antigen.

Overall, carcinoembryonic antigen and age were the best predictors of demographic and clinical features. Among ultrasonic features, the maximum diameter of the nodule was the best predictor. Imaging features also predict well, as seen in Figure 5.

As the most common thyroid malignancy, the papillary thyroid cancer is associated with cervical lymph node metastases in 30% to 90% of patients [34]. The lymph node dissection (LND) is the mainstay treatment for clinically evident cervical lymph node metastases [35]. So far, surgical treatment options in the literature include the traditional radical LND, the modified radical LND, the selective LND, and a "berry picking" resection in which only the grossly abnormal lymph nodes are excised [36–42]. The selective LND represents a compartment-based resection based on documented lymph node metastases [43, 44]. This study constructed diagnostic models through an integration of the

random forest and BLS, which was demonstrated to be a successful attempt to break the related bottlenecks in the future.

Before constructing the diagnostic models for lymph node metastasis, we considered using the ultrasound features of lymph nodes as input. But cervical lymph nodes are widely distributed (mainly in 6 regions) and there are some limitations in the feature recognition of cervical lymph nodes by ultrasound, especially the lymph nodes in the central area, as well as the special anatomical structures such as posterior trachea, posterior esophagus, retropharyngeal area, and mediastinum, which cannot be displayed well by ultrasound [45]. Meanwhile, researches in modeling, diagnosis, and treatment have confirmed that some ultrasonic features of primary lesions are related to lymph node metastasis [46, 47]. Our experiment also demonstrated that we can better identify lymph node metastasis in different regions through imaging features of primary lesions. This was the reason why no lymph node features were used as input in the present study.

Unlike the analysis of normal cancer [48, 49], lymph node metastasis is detected through postoperative pathology (gold standard) [50]. The inclusion criteria of this study were those who underwent extensive neck lymph node dissection to ensure the accurate diagnosis of LNM. The potential risk of lymph node metastasis has led to many PTC patients receiving total thyroidectomy, lymph node dissection, and other treatments, resulting in widespread overtreatment. Therefore, we hope to build a diagnostic model of preoperative LNM to help realize accurate identification of high-risk patients with LNM in this population to reduce overtreatment.

We constructed five early diagnosis models of LNM by combining the preoperative ultrasound features and ultrasound image features. These models were chosen for the convenience to extract the imaging features of the focus area of PTC. The strategy in construction of the five diagnostic models was different, and finally, we founded that the top three parameters are more important than the others. These results present further evidence for a systematic review and meta-analysis in previous studies, which indicated that patient gender is a factor associated with lymph node metastasis in T1 colorectal cancer [51]. The clinical significance lies in helping the clinicians in early diagnosis, which not only reduces the workload of clinicians but also cut off the suffering of patients [52–54]. The previous studies utilized deep learning algorithms for detection of lymph node metastases, while broad learning algorithms were rarely utilized [54]. Deep learning models spend too much time in the training stage and BLS can greatly reduce the time cost in training the model [53, 54]. This was also the major innovation of our study.

4. Conclusion

In this paper, five early diagnostic models were developed from random forest and integrated with the BLS to obtain experimental results with population informatics, clinical data, and ultrasonic characteristics. There was no significant difference between the combining of BLS and random forest and random forest was chosen to make predictions for the model. The most important feature map statistics show the maximum diameter of the nodule. It was the most important variable, followed by the GLSZM zone entropy and hence should be employed in subsequent studies [55–60].

Data Availability

All the data to support the experiments and findings in this study are available from the corresponding authors upon request.

Conflicts of Interest

The authors declare that they have no conflicts of interest.

Acknowledgments

This research was supported by the Shanghai High-Level Base-Building Project for Industrial Technology Innovation (1021GN204005-A06).

References

[1] N. Tohnosu, S. Onoda, and K. Isono, "Ultrasonographic evaluation of cervical lymph node metastases in esophageal cancer with special reference to the relationship between the short to long axis ratio (S/L) and the cancer content," *Journal of Clinical Ultrasound*, vol. 17, no. 2, pp. 101–106, 2010.

[2] S. Natsugoe, H. Yoshinaka, T. Morinaga et al., "Ultrasonographic detection of lymph-node metastases in superficial carcinoma of the esophagus," *Endoscopy*, vol. 28, no. 8, pp. 674–679, 1996.

[3] Y. Liu, J. W. Zhang, and Q. M. Wang, "Diagnostic efficacy of ultrasonographic characteristics of thyroid carcinomain predicting cervical lymph node metastasis," *Ultrasound in Medicine and Biology*, vol. 42, no. 1, pp. 68–74, 2016.

[4] J. M. Fitzpatrick, C. N. Sternberg, F. Saad et al., "Treatment decisions for advanced genitourinary cancers: from symptoms to risk assessment," *European Urology Supplements*, vol. 8, no. 9, pp. 738–746, 2009.

[5] C. L. Philip Chen and Z. L. Liu, "Broad learning system: an effective and efficient incremental learning system without the need for deep architecture," *IEEE Transactions on Neural Networks and Learning Systems*, vol. 29, no. 99, pp. 10–24, 2018.

[6] P. Oehr, "Omics"-based imaging in cancer detection and therapy," *Personalized Medicine*, vol. 3, no. 1, pp. 19–32, 2006.

[7] S. M. Han, H. J. Lee, and J. Y. Choi, "Computer-aided prostate cancer detection using texture features and clinical features in ultrasound image," *Journal of Digital Imaging*, vol. 21, no. S1, pp. 121–133, 2008.

[8] J. E. Belizário, B. A. Sangiuliano, M. Perez-Sosa, B. V Santos, and G Machado-Santelli, "Advances in the integration of optical and mass spectrometry molecular imaging technologies: from omics data to molecular signature discovery," *Discovery Medicine*, vol. 20, no. 112, pp. 393–401, 2015.

[9] K. Zetzmann, I. Ludolph, R. E. Horch, and A. M. Boss, "Imaging for treatment planning in lipo-and lymphedema," *Phlebologie*, vol. 49, no. 2, pp. 72–78, 2020.

[10] A. Holzinger, B. Haibe-Kains, and I. Jurisica, "Why imaging data alone is not enough: AI-based integration of imaging,

omics, and clinical data," *European Journal of Nuclear Medicine and Molecular Imaging*, vol. 46, no. 9, pp. 2722–2730, 2019.

[11] D. De Groot, F. Kuper, M. Radonjic et al., "Imaging and "omics" in rats demonstrate impact of juvenile versus developmental exposure to TBTO," *Reproductive Toxicology*, vol. 32, no. 2, pp. 165-166, 2011.

[12] J.-K. Hériché, S. Alexander, and J. Ellenberg, "Integrating imaging and omics: computational methods and challenges," *Annual Review of Biomedical Data Science*, vol. 2, no. 1, pp. 175–197, 2019.

[13] D. De Groot, D. De Groot, F. Kuper et al., "Imaging and omics in developing and juvenile rats after exposure to TBTO," *Toxicology Letters*, vol. 211, no. supp-S, p. S155, 2012.

[14] A. J. Benjamin, M. M. Buschmann, A. Schneider et al., "Can comprehensive imaging analysis with analytic morphomics and geriatric assessment predict serious complications in patients undergoing pancreatic surgery?" *Journal of Gastrointestinal Surgery*, vol. 21, no. 6, pp. 1009–1016, 2017.

[15] J. A. Disselhorst, M. A. Krueger, S. M. M. Ud-Dean et al., "Linking imaging to omics utilizing image-guided tissue extraction," *Proceedings of the National Academy of Sciences*, vol. 115, no. 13, pp. E2980–E2987, 2018.

[16] D. Viola, G. Materazzi, L. Valerio et al., "Prophylactic central compartment lymph node dissection in papillary thyroid carcinoma: clinical implications derived from the first prospective randomized controlled single institution study," *Journal of Clinical Endocrinology & Metabolism*, vol. 100, no. 4, pp. 1316–1324, 2015.

[17] H. Y. Chai, L. K. Wee, T. T. Swee, ShH Salleh, and L. Y Chea, "An artifacts removal post-processing for epiphyseal region-of-interest (EROI) localization in automated bone age assessment (BAA)," *BioMedical Engineering Online*, vol. 10, no. 1, pp. 87–22, 2011.

[18] A. Faisal, S.-C. Ng, S.-L. Goh, and K. W. Lai, "Knee cartilage segmentation and thickness computation from ultrasound images," *Medical, & Biological Engineering & Computing*, vol. 56, no. 4, pp. 657–669, 2018.

[19] S. M. Lewis, M. L. Asselin-Labat, N. Quan et al., "Spatial omics and multiplexed imaging to explore cancer biology," *Nature Methods*, pp. 1–16, 2021.

[20] T. Smets, T. De Keyser, T. Tousseyn, E. Waelkens, and B. De Moor, "Correspondence-aware manifold learning for microscopic and spatial omics imaging: a novel data fusion method bringing mass spectrometry imaging to a cellular resolution," *Analytical Chemistry*, vol. 93, no. 7, pp. 3452–3460, 2021.

[21] V. Kumar, Y. Gu, S. Basu et al., "Radiomics: the process and the challenges," *Magnetic Resonance Imaging*, vol. 30, no. 9, pp. 1234–1248, 2012.

[22] R. Miotto, F. Wang, S. Wang, X. Jiang, and J. T. Dudley, "Deep learning for healthcare: review, opportunities and challenges," *Briefings in Bioinformatics*, vol. 19, no. 6, pp. 1236–1246, 2017.

[23] P. Jiang, H. Wu, W. Wang, W. Ma, X. Sun, and Z. Lu, "MiPred: classification of real and pseudo microRNA precursors using random forest prediction model with combined features," *Nucleic Acids Research*, vol. 35, pp. W339–W344, 2007.

[24] V. F. Rodriguez-Galiano, B. Ghimire, J. Rogan, M. Chica-Olmo, and J. P. Rigol-Sanchez, "An assessment of the effectiveness of a random forest classifier for land-cover classification," *ISPRS Journal of Photogrammetry and Remote Sensing*, vol. 67, pp. 93–104, 2012.

[25] R. L. Lawrence, S. D. Wood, and R. L. Sheley, "Mapping invasive plants using hyperspectral imagery and Breiman Cutler classifications (randomForest)," *Remote Sensing of Environment*, vol. 100, no. 3, pp. 356–362, 2006.

[26] H. Bart, B. Stefan, V. R. Frans, and D. B. Pieter, "A flexible integrative approach based on random forest improves prediction of transcription factor binding sites," *Nucleic Acids Research*, vol. 40, no. 14, p. e106, 2012.

[27] Y. Qi, J. Klein-Seetharaman, and Z. Bar-Joseph, "Random forest similarity for protein-protein interaction prediction from multiple sources," *Pacific Symposium on Biocomputing Pacific Symposium on Biocomputing*, vol. 10, pp. 531–542, 2005.

[28] W. G. Touw, J. R. Bayjanov, L. Overmars et al., "Data mining in the Life Sciences with Random Forest: a walk in the park or lost in the jungle?" *Briefings in Bioinformatics*, vol. 14, no. 3, pp. 315–326, 2013.

[29] T. Shi, D. Seligson, A. S. Belldegrun, A. Palotie, and S. Horvath, "Tumor classification by tissue microarray profiling: random forest clustering applied to renal cell carcinoma," *Modern Pathology*, vol. 18, no. 4, pp. 547–557, 2005.

[30] J. Butaye, H. Jacquemyn, and M. Hermy, "Differential colonization causing non-random forest plant community structure in a fragmented agricultural landscape," *Ecography*, vol. 24, no. 4, pp. 369–380, 2001.

[31] J. C.-W. Chan and D. Paelinckx, "Evaluation of random forest and adaboost tree-based ensemble classification and spectral band selection for ecotope mapping using airborne hyperspectral imagery," *Remote Sensing of Environment*, vol. 112, no. 6, pp. 2999–3011, 2008.

[32] D. W. Hosmer, T. Hosmer, C. S. Le, and S. Lemesshow, "A comparison of goodness-of-fit tests for the logistic regression model," *Statistics in Medicine*, vol. 16, no. 9, pp. 965–980, 2015.

[33] B. Foa and B. Ga, "Fitting logistic regression models to assess vitamin D deficiency with clinical parameters in chronic hepatitis B patients," *Infectious Disease Modelling*, vol. 6, pp. 612–617, 2021.

[34] N. R. Caron and O. H. Clark, "Papillary thyroid cancer: surgical management of lymph node metastases," *Current Treatment Options in Oncology*, vol. 6, no. 4, pp. 311–322, 2005.

[35] T. P. J. Hennessy, "Lymph node dissection," *World Journal of Surgery*, vol. 18, no. 3, pp. 367–372, 1994.

[36] R. Groningen, "Extended lymph node dissection for gastric cancer: who may benefit? Final results of the randomized Dutch gastric cancer group trial," *Journal of Clinical Oncology*, vol. 23, no. 23, pp. 5404-5405, 2005.

[37] G. J. Jager, R. A. Heesakkers, and J. A. Witjes, "The importance of the extent of pelvic-lymph-node dissection in the diagnosis of lymph-node metastases in prostate cancer-Reply," *The Lancet Oncology*, vol. 9, no. 10, pp. 915–917, 2008.

[38] N. Martini, "Mediastinal lymph node dissection for lung cancer. The Memorial experience," *Chest Surgery Clinics of North America*, vol. 5, no. 2, pp. 189–203, 1995.

[39] M. Noguchi, "Benefits of D_2 lymph node dissection for patients with gastric cancer and pN0 and pN1 lymph node metastases," *British Journal of Surgery*, vol. 83, no. 7, pp. 1144–1147, 2010.

[40] P. Shen, J. M. Guenther, L. A. Wanek, and D. L. Morton, "Can elective lymph node dissection decrease the frequency and mortality rate of late melanoma recurrences?" *Annals of Surgical Oncology*, vol. 7, no. 2, pp. 114–119, 2000.

[41] S. M. Keller, S. Adak, H. Wagner, and D. H. Johnson, "Mediastinal lymph node dissection improves survival in patients with stages II and IIIa non-small cell lung cancer," *The Annals of Thoracic Surgery*, vol. 70, no. 2, pp. 358–365, 2000.

[42] B. H. Bochner, H. W. Herr, and V. E. Reuter, "Impact of separate versus en bloc pelvic lymph node dissection on the number of lymph nodes retrieved in cystectomy specimens," *The Journal of Urology*, vol. 166, no. 6, pp. 2295-2296, 2001.

[43] D. E. Elder, D. Guerry, M. Vanhorn et al., "The role of lymph node dissection for clinical stage I malignant melanoma of intermediate thickness (1.51-3.99 mm)," *Cancer*, vol. 56, no. 2, pp. 413–418, 2015.

[44] M. E. Allaf, G. S. Palapattu, B. J. Trock, H. B. Carter, and P. C. Walsh, "Anatomical extent of lymph node dissection: impact on men with clinically localized prostate cancer," *The Journal of Urology*, vol. 172, no. 5, pp. 1840–1844, 2004.

[45] H. K. Su, L. L. Dos Reis, M. A. Lupo et al., "Striving toward standardization of reporting of ultrasound features of thyroid nodules and lymph nodes: a multidisciplinary consensus statement," *Thyroid*, vol. 24, no. 9, pp. 1341–1349, 2014.

[46] M. Yoshimasa, Y. Masahiro, H. Shotaro, M. Takata, and W. Nishio, "Chemosensitivity of lung cancer: differences between the primary lesion and lymph node metastasis," *Oncology Letters*, vol. 1, no. 2, p. 345, 2010.

[47] H. A. Weinberger and D. Stetten, "Extensive secondary axillary lymph node carcinoma without clinical evidence of primary breast lesion," *Surgery*, vol. 29, no. 2, pp. 217–222, 1951.

[48] Z. Jahanzad, Y. M. Liew, M. Bilgen et al., "Regional assessment of LV wall in infarcted heart using tagged MRI and cardiac modelling," *Physics in Medicine and Biology*, vol. 60, no. 10, pp. 4015–4031, 2015.

[49] K. Azira, S. C. Ng, M. L. Yih, and K. W. Lai, "An overview on image registration techniques for cardiac diagnosis and treatment," *Cardiology Research and Practice*, vol. 2018, Article ID 1437125, 15 pages, 2018.

[50] R. Narinder, "Epidural technique for postoperative pain: gold standard no more?" *Regional Anesthesia and Pain Medicine*, vol. 37, no. 3, pp. 310–317, 2012.

[51] K. Ichimasa, S.-E. Kudo, H. Miyachi et al., "Patient gender as a factor associated with lymph node metastasis in T1 colorectal cancer: a systematic review and meta-analysis," *Molecular and Clinical Oncology*, vol. 6, no. 4, pp. 517–524, 2017.

[52] J. A. Golden, "Deep learning algorithms for detection of lymph node metastases from breast cancer: helping artificial intelligence Be seen," *JAMA*, vol. 318, no. 22, pp. 2184–2186, 2017.

[53] K. G. Andersen, E. K. Aasvang, N. Kroman, and N. Kehlet, "Intercostobrachial nerve handling and pain after axillary lymph node dissection for breast cancer," *Acta Anaesthesiologica Scandinavica*, vol. 58, no. 10, pp. 1240–1248, 2015.

[54] H. H. N. Pham, M. Futakuchi, A. Bychkov, T. Furukawa, K. Kuroda, and J. Fukuoka, "Detection of lung cancer lymph node metastases from whole-slide histopathologic images using a two-step deep learning approach," *American Journal Of Pathology*, vol. 189, no. 12, pp. 2428–2439, 2019.

[55] A. Briganti, M. L. Blute, J. H. Eastham et al., "Pelvic lymph node dissection in prostate cancer," *European Urology*, vol. 55, no. 6, pp. 1251–1265, 2009.

[56] R. Essner, A. Conforti, M. C. Kelley et al., "Efficacy of lymphatic mapping, sentinel lymphadenectomy, and selective complete lymph node dissection as a therapeutic procedure for early-stage melanoma," *Annals of Surgical Oncology*, vol. 6, no. 5, pp. 442–449, 1999.

[57] H. Shimada, I. Endo, S. Togo, A. Nakano, T. Izumi, and G. Nakagawara, "The role of lymph node dissection in the treatment of gallbladder carcinoma," *Cancer*, vol. 79, no. 5, pp. 892–899, 2015.

[58] J. H. M. Blom, H. van Poppel, J. M. Maréchal et al., "Radical nephrectomy with and without lymph-node dissection: final results of European organization for research and treatment of cancer (EORTC) randomized phase 3 trial 30881," *European Urology*, vol. 55, no. 1, pp. 28–34, 2009.

[59] N. Altorki, M. Kent, C. Ferrara, and J. Port, "Three-field lymph node dissection for squamous cell and adenocarcinoma of the esophagus," *Annals of Surgery*, vol. 236, no. 2, pp. 177–183, 2002.

[60] H. Hayashi, T. Ochiai, H. Shimada, and Y. Gunji, "Prospective randomized study of open versus laparoscopy-assisted distal gastrectomy with extraperigastric lymph node dissection for early gastric cancer," *Surgical Endoscopy*, vol. 19, no. 9, pp. 1172–1176, 2005.

Hindawi
Journal of Healthcare Engineering
Volume 2021, Article ID 8106467, 13 pages
https://doi.org/10.1155/2021/8106467

Review Article

Cloud-Based Fault Prediction Using IoT in Office Automation for Improvisation of Health of Employees

Mudita Uppal,[1] **Deepali Gupta**,[1] **Sapna Juneja**,[2] **Gaurav Dhiman**,[3] **and Sandeep Kautish**[4]

[1]*Chitkara University Institute of Engineering and Technology, Chitkara University, Punjab, India*
[2]*IMS Engineering College, Ghaziabad, India*
[3]*Government Bikram College of Commerce, Patiala, India*
[4]*LBEF Campus, Kathmandu, Nepal*

Correspondence should be addressed to Sandeep Kautish; dr.skautish@gmail.com

Received 8 September 2021; Accepted 18 October 2021; Published 3 November 2021

Academic Editor: Yan Chai Hum

The novel paradigm of Internet of Things (IoT) is gaining recognition in the numerous scenarios promoting the pervasive presence of smart things around us through its application in various areas of society, which includes transportation, healthcare, industries, and agriculture. One more such application is in the smart office to monitor the health of devices via machine learning (ML) that makes the equipment more efficient by allowing real-time monitoring of their health. It guarantees indoor comfort as per the user's satisfaction as it emphasizes on fault prediction in real-life devices. Early identification of various types of faults in IoT devices is the key requirement in smart offices. IoT devices are becoming ubiquitous and provide an assistant to supervise an office that is regulated by ML and data received from sensors is stored in cloud. A recommender system facilitates the selection of an appropriate solution for faults in IoT-enabled devices to mitigate faults. The architecture proposed in this paper is used to monitor each and every office appliance connected via IoT technology using ML technique, and recommender system is used to recommend solutions for fault patterns without much human intervention. The ultrasonic motion sensor is used to fetch the information of employee availability in cubicles and data is sent to the cloud through the WiFi module. ATmega8 is used to control electrical appliances in the office environment. The significance of this work is to forecast the faults in IoT appliances which will have an impact on life and reliability of IoT appliances. The main objective is to design a prototype of a smart office using IoT that can control and automate workplace devices and forecast whether the device needs repairing or replacing, thus reducing the overall burden on the employee and helping out in increasing physical as well as mental health of the person.

1. Introduction

The 21st century is witnessing a fast-paced digital revolution. Internet of Things (IoT) is a recent concept in which real-world physical entities can be remotely controlled with the help of the Internet. IoT architecture contains a physical object network that is integrated with sensors, electronic devices, and software which allow them to gather and transfer data through an IoT network. These entities are also called smart objects because they can sense the environment and can be remotely controlled through existing IoT network architecture by integrating with the physical environment. IoT has a positive impact on daily lives as it provides new solutions to every aspect of society. Therefore, IoT is a phenomenon that results in an event between the sensor, real-time network, and the data centres [1].

In an IoT application, the perception layer consists of smart objects embedded with sensors that collect and process real-time information of the physical and digital worlds. These sensors help in the measurement of the physical resources and monitor the changes in the physical environment [2]. Figure 1 represents the architecture of an IoT application [7].

There is a need for memory in the gateway to receive the sensor data that the sensors send to the gateways. Sometimes, these sensors generate a large amount of data that

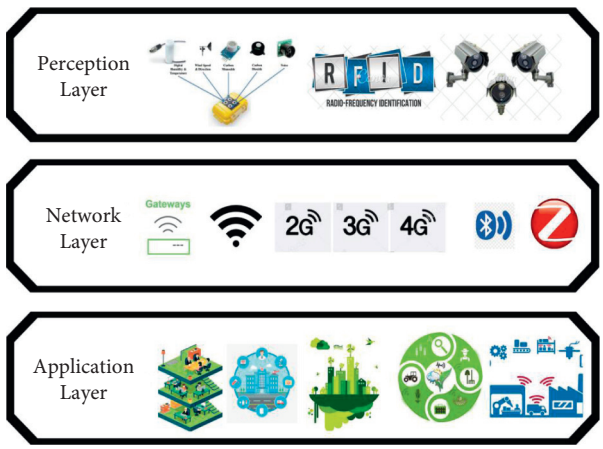

Figure 1: Architecture of an IoT application [3–6].

need a robust and high-performance WSN that transports these data to the destination gateway on time. Several protocols and technologies are needed in the heterogeneous configuration of an IoT application [8]. Also, a broad range of IoT services or applications like speed transactions, compatibility, or context-aware applications are demanded.

IoT is gaining popularity worldwide in different situations of the advanced wireless communications network while supporting the presence of smart things around us. IoT is capable of changing the world [9]. There has been an abundance of information and this advanced technology has opened many paths to access this information. Every part of our lives is getting changed by the development of IoT [10]. IoT frameworks are intensely used in many applications as demonstrated below. Figure 2 outlines some of the fundamental areas and applications of IoT which includes smart traffic system, smart environment, smart healthcare, smart home, smart agriculture, smart office, and supply chains logistics IoT [14–16].

Smart office automation is the latest and upcoming technology in the market that is easier to control and makes life simpler. A smart office is a place where one would find desktop computers and printers connected to a router via cable for Internet access. Also, appliances like laptops, printers, smart heaters, smart window blinds, coffee machines, etc., are all connected to the Internet.

There are many advantages of IoT, but still there are some issues that must be addressed to advance its growth [17]. The applicability of IoT devices is a complex mixture of various technologies that provide solutions based on the integration of various heterogeneous technologies. In many cases, IoT applications heavily depend on a network of connected components embedded in physical objects, such as appliances or devices [18]. The functionality and operation of these physical objects are important in communication and connectivity. The complexity of these devices and technology leads to the challenge of creating a dependable IoT application [19].

Cloud computing uses central remote servers to manage data and applications via the Internet. It allows users to run applications without installing them or directly accessing their files at any time on any machine having Internet access. It provides on-demand computing services such as applications, storage, and processing power. Cloud gives several services to the client like Platform as a Service (PaaS), Software as a Service (SaaS), and Infrastructure as a Service (IaaS) [20]. The integration of cloud and IoT leads to the expansion of available technologies in cloud environments. The information and applications used by the IoT technology can be stored on cloud storage. The integration of cloud and IoT technology is represented in Figure 3. Cloud allows users to access all the information needed for IoT connectivity [24].

Energy is an important technological challenge in IoT and in-depth research is required to develop systems that can save energy during the operational environment [25, 26]. IoT needs ways to minimize the energy spent on communication and computing. Also, it requires techniques to harvest energy that will assist IoT devices to relieve from the restrictions foisted by battery operations, scarce energy, and limited resources that need to be tackled in IoT applications. Therefore, there is a need to devise solutions that will optimize energy usage in IoT devices [27]. Also, early fault prediction can extend equipment life, increase safety, and reduce manufacturing costs [28]. Fault prediction is a crucial aspect to be evaluated because it helps in determining the fault proneness of IoT devices. The elimination of faults enhances the quality and improves the effectiveness of the whole process. Machine Learning (ML) acts as a key factor in fault prediction and helps in getting more accurate results. ML has many techniques and algorithms, such as Artificial Neural Networks, Multilayer Perceptron, Naive Bayes, Genetic Algorithms, and many more that can be used in fault prediction and save time [29]. ML can automatically examine heterogeneous data by applying smart algorithms and models to achieve better results. The techniques and algorithms used in ML are different from one another in terms of their working, hypotheses, properties, precision, advantages, disadvantages, and solving category. The actions required to find the faulty devices are planned earlier in case of any problem. The consequences can be catastrophic if faults are not tackled beforehand and they may also disrupt the actual result [30, 31].

IoT is a booming shift in the IT epoch. IoT developments are accelerating innovation-driven information and technological applications in several areas such as production processes, agricultural fields and home or office automation. The increased demand for digital terminals configured with a robust variety of sensors enables a greater process of data acquisition module for industrial IoT. Prediction of faults is a big security challenge in IoT devices but still, it is one of the safe methods of fault prevention [32]. Smart automation has a significant impact on the customer's experience by giving fault-free solutions. Early prediction of faults plays a very important role in terms of quality measurement. ML-based approaches have been considered the most promising technique due to the learning mechanism of classifiers. To predict a fault before its occurrence reduces the overall cost and time and cost of the projects. Also, the need for a reliable and refined technique is a point of concern. IoT is a convergence of many technologies, real-time analytics, and ML.

Figure 2: IoT and its application areas [11–13].

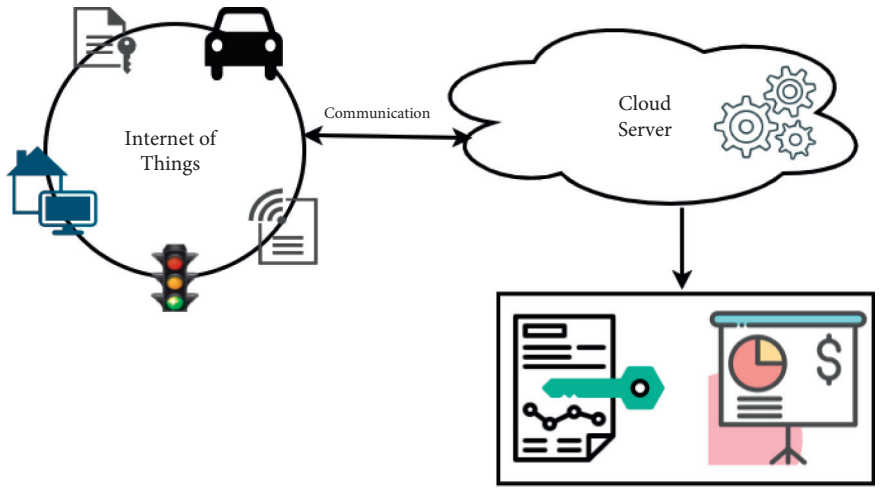

Figure 3: Integration of IoT with cloud [21–23].

It gave birth to many customer demands like office automation, prior fault prediction of devices, and remote monitoring of applications. ML techniques open the potential for IoT applications by feeding information gathered by sensors into ML models, thereby applying results to enhance the business services [33]. Recommender system helps in fault prediction in smart office to predict faults at an early stage.

1.1. Motivation of Work. In this era, many people spend most of their time in offices or companies. The efficiency of employees is influenced by the environment of their workplace. To increase productivity, comfort is required in the office. So, the concept of the smart office is rapidly evolving and becoming the need of the hour. Smart office is a place where technology enables people to work properly, smartly, and speedily. It is a platform that enhances the capability of employees via different progressive technologies and tools. A smart office guarantees the active exploitation of IT resources and physical infrastructure. There is a need for predicting the faults in IoT-enabled devices to prevent devices from damaging. Thus, office automation allows the systems to become more transparent, which helps in achieving a decision that will result in the excellent functioning of an office. So, a smart office should be constructed to predict a fault early in any appliance [34].

1.2. Problem Statement. The study originates from the problem to automatically predict the fault in the office buildings. For offices that are big in size, it often becomes

difficult to search for any faulty appliance in the whole office and to see if it needs replacement or not. The recommendation system is used to predict the fault in the office and the problems faced with the currently installed system are semiautonomous, no Internet connection, high cost, and the limited size of memory that stores user credentials. The problems mentioned above clearly depict that most of the recommendation systems are not user friendly and are not convenient to use for most of the users. A novel smart and autonomous recommendation system must be designed using machine learning techniques to provide an optimal solution.

1.3. Existing IoT Solutions in Smart Office. To enhance the performance of devices in a smart office, some existing solutions are suggested below [35]:

(i) *Business Assistants*. These virtual assistants synchronize with smart devices in the office to create an effective IoT environment. They have features of text-to-speech conversion, weather reports, meeting tracking, and many more.

(ii) *IoT Tagging*. It is used for tracking the devices (i.e., monitor the current location or position of the device). These assets can be found out with the help of IoT tags.

(iii) *Smart Thermostats*. They help in dynamically adjusting the temperature of the office, which makes the working environment more comfortable and cuts down the costs spent on inefficient control systems. They can be remotely controlled by voice assistance. They are used in buildings' HVAC to control different temperature zones.

(iv) *Environment Monitoring Tools*. Some tools are required to monitor the devices in an office (i.e., whether they are working well or not).

(v) *Intelligent Lightning*. Smart bulbs can be used in offices that use the concept of motion sensors and adjust brightness and color balance throughout the day as per the user's requirement. It will also lead to less electricity bills.

(vi) *Smart Printing*. A printer having an Internet connection monitors the paper as well as the ink of the printer and warns the person if it is getting low. It can also be connected to inventory systems to make orders for more actions without human involvement. Self-diagnostics in these smart printers are performed to notify the resource person about the quick fix or serious repair is required.

(vii) *Smart Locks*. To keep offices safe and make entrance procedures easier for the employees, smart locks can be installed. These can be connected to attendance system to keep record of employee that when he is entering or leaving the office. Also, smart locks minimize the risk of break-ins.

(viii) *Smart Meeting Room*. IoT is used to maintain a track of occupied meeting rooms as it is a must for every busy office.

(ix) *Smart Vacuums*. Custodial staff is required to maintain cleanliness or pick up the slack, but they may cause a disruption to a security hole. An office can save from this by using a robotic vacuum and even they warn when they need to be emptied.

(x) *Smart Coffee Machines*. Coffee keeps up the productivity level of the employees. These machines keep the machine material in stock and keep a track of caffeine intake.

In this paper, a prototype of a smart office using IoT, cloud, and ML is designed that can control and automate devices at the workplace. The proposed architecture helps to forecast whether the device needs repairing or replacing when a fault a predicted. The major contributions of the paper are as follows:

(1) The concept of fault prediction in IoT devices is elaborated where the role of ML in fault prediction to get accurate results is explained.

(2) Furthermore, the use of the recommender system for fault prediction in the smart offices is discussed.

(3) Also, the existing IoT solutions are described that enhance the performance of devices in the smart office.

(4) An in-depth systematic literature survey is done to discuss the role of ML techniques in IoT devices.

(5) An architecture is proposed that connects all office devices via IoT technology and uses a machine learning algorithm for fault prediction in IoT-enabled devices. Experimental setup, device specifications, and methodology of a new automated environment which is the integration of cloud, IoT, and ML are defined.

The rest of the paper is organized as follows. In Section 2, a related literature survey of the recent studies is carried out and based on that some conclusions have been derived. Section 3 presents the proposed architecture of the work with its hardware specifications and experimental setup. Section 4 highlights the methodology used to implement the proposed work. Section 5 describes the workflow for fault prediction in office automation. Section 6 concludes this study.

2. Literature Survey

In the present work, a comprehensive literature study has been carried out for fault prediction based on different ML techniques in IoT applications. Liu et al. [32] presented a framework of self-learning sensor fault detection that represented the sensor value, relationship, and status transformation. The group-based fault detection (GbFD) algorithm detected the fault in the sensor for validation in data of an oil field. The results showed that this method successfully detected 95% of total faults in the simulation data that carries around 752 million samples out of 5800 sensors. In addition to this, Vibhute and Gundale [36] presented a sensor failure prediction model. The sensor

failure prediction involves the collection of sensor output data and the implementation of algorithms to anticipate impending failure. The algorithm represents the behavior of the system by identifying the factors contributing to sensor failure and then a predictive model is defined. This modeling is followed by the test data to check the reliability of the predictive model. With this implementation, the sensor failure with 98-99% accuracy was predicted as this prediction is applicable for all nonlinear systems. The proposed system has grown in accuracy and sensor maintenance can be done to fulfill reliability requirements. Early fault detection can minimize plant downtime, extended equipment life, increase safety and reduction in manufacturing costs.

For the very first time, Cicirelli et al. [37] proposed a meta-model of the smart environment. It exploits the concepts that are specific to the smart office application. A case study was presented by following the guidelines regarding its design and implementation. It helped in optimizing the architectural design. Then, Furdik et al. [38] presented a prototype of a smart office system which was developed as an application of the ELLIOT project. The described solution was based on the LinkSmart semantic middleware which is an open-source technology used for the development of IoT applications. They discussed principles of the system architecture and demonstrated on this prototype by using user experience monitoring approach and continuous evaluation was done on social and business parameters.

Xu et al. [39] systematically summarized the recent state-of-the-art industrial IoT. The paper reviewed the current researches of IoT in industries. The service-oriented architecture models of IoT were introduced and then basic technologies used in IoT were also discussed. Also, the essential applicability of IoT in industries was introduced. After that, the upcoming trends and research challenges linked with IoT were investigated. This paper focuses on the applications of IoT in industries and highlights the difficulties and potential possibilities for industrial researchers in the future. In addition to the previous, Mundada et al. [40] emphasize on the software fault prediction technique which is based on an artificial neural network with a back-propagation learning algorithm. Artificial Neural Network is adopted to locate the erroneous module and predict them. The results concluded that artificial neural network trained by utilizing resilient back-propagation produces better results rather than the algorithm of conventional back-propagation. Also, Barbosa et al. [41] presented a recommendation service named RS4IoT for smart devices. It provided an API that performs recommendation tasks for multiattribute sensors as informed by client applications which contain the features of sensors to be recommended. Also, RS4IoT helps users to evaluate some sensors and actuators after interacting in their social networks and gauges their importance in the recommendation.

Bakker et al. [42] studied the occupancy-based lighting control in an office affected by the potential of energy savings under different sizes of control zones. This strategy helps in optimizing the lighting control at room level as it can provide the first qualitative and quantitative advantages. The results concluded that it was beneficial to implement occupancy-based lighting in an office at each desk level. However, Rao et al. [43] focused on energy management in office cubicles and employee login information. A grid-based user interface is implemented to observe the occupancy of the employee in the office cubicle. A load cell and ultrasonic sensor are used to fetch the information of employee availability at designated cubicles. The fetched data is sent to the secured office cloud database through ESP8266 Node MCU for further control of the electrical appliances in office. The administrator can switch ON or OFF the required office electrical appliances.

With the advancement, Bhavana et al. [44] suggested a model that involves monitoring each home device through the Internet and detection of faults without human interference. The paper primarily emphasizes fault prediction in real-life devices. It uses the calculation of Naive Bayes for checking the abnormal condition in the devices. Hence, the proposed system helps in fault detection and saves time. Cloud computing, IoT, and mobile app are used in the implementation of this proposed solution; that is why it is called a multitechnology environment as many technologies are used in the system. Arun et al. [45] presented a smart office system based upon the IoT application. The smart office contains the biometric for opening the door locks, temperature and humidity sensor, smoke detection sensor for fire indication, and automatic lighting system. The fingerprint biometric sensor was used for security purposes so that other people cannot arrive at the office area. When any unauthorized person enters the office area, the buzzer will ring in control room and an e-mail will be forwarded to security guards. In this system, there were two working modes: one is automatic mode, and another is manual mode.

In 2018, Gouthaman and Suresh [46] emphasized on risk analysis and management of the development of agile software using IoT and cloud computing. The authors proposed a framework that includes a design of IoT-Fog-based agile software risk management as well as an assessment system. They focused on different types of risk in the IoT-Fog-based frameworks that could end up being more effective. The fundamental goal was to address the significance of the agile approach and the importance of risk management towards cutting edge frameworks such as cloud, Fog, and IoT utilizing relevant tools. Whereas, in 2020, Bak et al. [47] proposed an approach that visualizes applications of IoT as a collection of IoT services. They proposed an event-flow-based visualization technique where an IoT service is viewed as a flow from event to action. A tool named SmartVisual was implemented by the authors that perform a static investigation on SmartApps to create an event flow diagram. This tool assesses the inputs, actions, events, and event flows of 64 samples of SmartApps which are rendered by SmartThings. Each SmartApp had 2 input devices, 2 output devices, and 4 event flows. In 2019, Xenakis et al. [48] presented an IoT and cloud-based framework for fault prediction and machine condition monitoring for Industrial IoT. This study provided real-time cloud-oriented maintenance using the tool MATLAB. To minimize the cost, the authors founded a cross-layer optimization problem for

adequate energy consumption using a method of multipliers algorithms.

Bhatnagar et al. [29] summarized different ML techniques that proved to give better results and improve speed for prediction and classification. These technique improves the various performance parameters of the system like the reduction of noise, recovered lost data, increase prediction rate (using device location and state) to achieve better and faster results. The error reduction rate is approx 1% using clustering algorithms, neural networks, and Bayesian network. Other techniques like decision trees, regression analysis, Principal Component Analysis, *k*-nearest neighbors algorithm, random forests, genetic algorithms, and support vector machines also give great results. The ML algorithms predict the changes themselves due to their learning properties. ML algorithms tend to decide to achieve a goal. Thus, it is clear from the above that the ML algorithms decrease the error rate in IoT. Also, Souri et al. [49] presented a prediction model with particle swarm optimization and multilayer perceptron for formal verification and behavioral modeling using ML. Also, the defect metrics were detected for the verification of the fault prediction behavior in IoT applications. It is observed from the result that the verification method has very little operating time and memory usage as compared to other methods. However, Lo et al. [50] summarized the various approaches that are used to diagnose the industrial complex system using artificial intelligence. The articles published from 2002 to 2018 were covered for fault diagnosis using ML tools in industrial systems. In addition to this, Pathak et al. [51] developed an IoT-based system that is used to monitor the patient's position without a hidden activity. The basic target of this system is to monitor the patients' subtleties. The system was built to enhance speed and accuracy rate. Data is analyzed based on age, time, obesity, month, heartbeat, and temperature and humidity using *R* and implemented the use of linear regression and decision tree for analyzing the accuracy. The authors discussed about the IoT-based recommendation technologies that will recommend future IoT solutions. [52].

Meena et al. [53] proposed a system that localizes a person and controls the devices. An indoor localization technique was applied to localize a person. This technique obtains the location of an individual inside a room using RFID tags and PIR sensors by identifying their patterns. After the implementation of the system, the authors prove that energy consumption was comparatively less. Also, Jia et al. [54] investigated the recent projects and technologies of IoT used for smart building development in academia and industry contexts. Afterward, they selected some latest IoT building applications to build smart buildings. They also discussed some challenges and future research questions on IoT integration in smart buildings. They concluded that there is a need for more work from researchers in this field.

Nan [55] introduces a process that designs and implements a network monitoring system using VC++ platform to monitor network traffic and detect suspicious data while accessing database records to achieve network security. Whereas Wang et al. [56] propose a collaborative office automation system that improves the work efficiency of team. This system has feature of continuous and stable operation that saves resources.

After reviewing the above discussed literature survey and 1651 papers from the Scopus database, the following conclusions have been derived:

(i) In the last 10 years from 2012 to 2021, the number of papers published is increasing year by year as shown in Figure 4. The maximum number of papers is published in 2019 and the annual growth rate is 5.5%.

(ii) 3-Field plot applies clustering technique that correlates different parameters like keyword, country, and year. Figure 5 shows in which year, how the different countries use multiple keywords. In the year 2015, this work gained an increase and USA, China, and India are the leading countries.

(iii) In Figure 6, the top five sources in which maximum papers published are shown. This figure represents the documents published in specific sources year-wise. The maximum papers, i.e., 31, are published in ACM International Conference Proceeding Series followed by Advances in Intelligent Systems and Computing having 22 papers. Constant growth is seen in the IEEE Internet of Things Journal.

(iv) Figure 7 shows the trending topics as per the author keywords year-wise. Each keyword has a minimum frequency of 15 and the anomaly detection, sensors, deep learning are the latest keywords.

3. Proposed Framework for Office Automation

IoT-based appliances enhance the performance of the system and reduce human intervention. The proposed architecture performs all the tasks automatically while interacting securely with appliances. The main focus of this proposed architecture is to connect all office appliances using the Internet with the help of IoT technology. The novelty of this work is to develop a smart and autonomous recommendation system for prediction of faults using a machine learning technique. Figure 8 is the proposed fault prediction system using an ML algorithm. It contains electrical office appliances, sensors, and a database server. It has a live monitoring feature on the cloud that can be accessed by users and an ML-based fault prediction algorithm that predicts faults in the appliances. Cloud has features of nonvolatile memory and excess space, so the data can be retrieved from it on regular basis. When office appliances are ON, then this system starts checking the health of appliances and in case of any abnormal values, the fault prediction mechanism starts. A primary unit of the proposed architecture is the ML algorithm. The ML algorithm predicts the inevitable faults based on the analysis of the existing dataset and also, divides or clusters the obtained data based on similarity. This collected data is stored on the cloud so that this data can be used for fault prediction in IoT-enabled appliances in the future. Also, this algorithm finds the

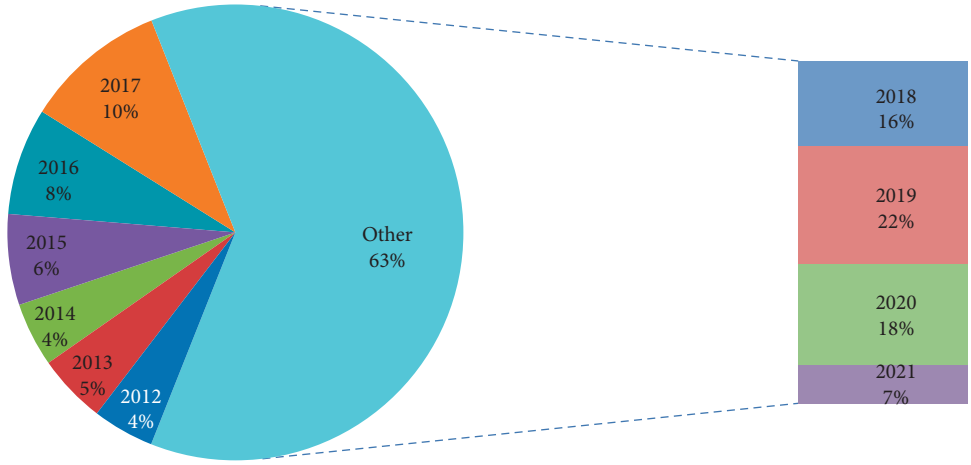

Figure 4: Number of documents published year-wise.

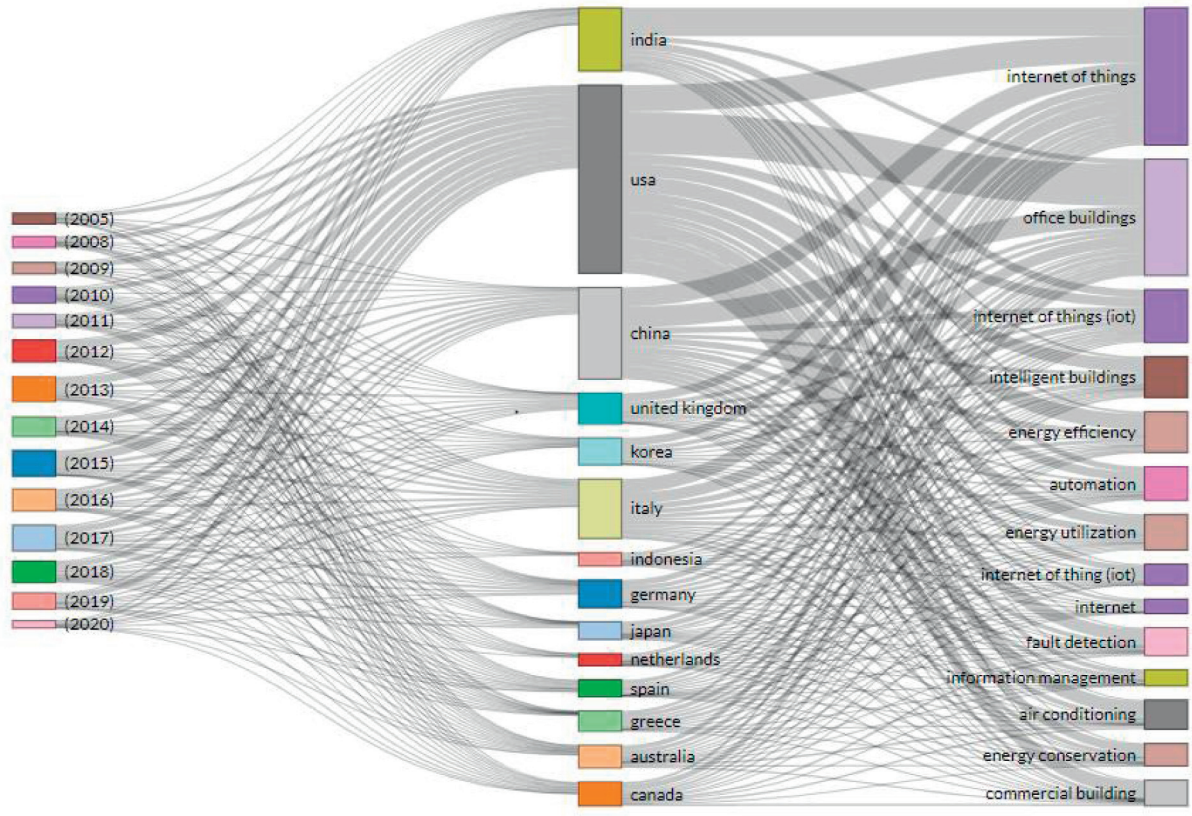

Figure 5: 3-Field plot classification of published papers by year, country, and keyword.

similarity among different datasets based on prior data available with the algorithm. This work is implemented in the IoT-enabled office to predict both healthy and unhealthy appliances.

A software application keeps the track of live monitoring of cloud data received from appliances. Hence, if any appliance does not work in normal conditions, then the fault can be predicted and matched with the existing fault by ML algorithm and a relevant solution will be recommended. Also, an alert message will be delivered on the concerned person's smartphone when any abnormal functioning of the appliance is predicted. The data fetched is utilized by the ML algorithm to determine faults that are going to happen or had already occurred. This is the pivotal functionality of the proposed architecture. The end-user can monitor the power consumption of each and every office appliance and determine the future prediction of any fault. Any change in observed values sends an alert message to the end-user. Hence, the proposed architecture will predict the fault at an early stage and prevents the damage of the appliance.

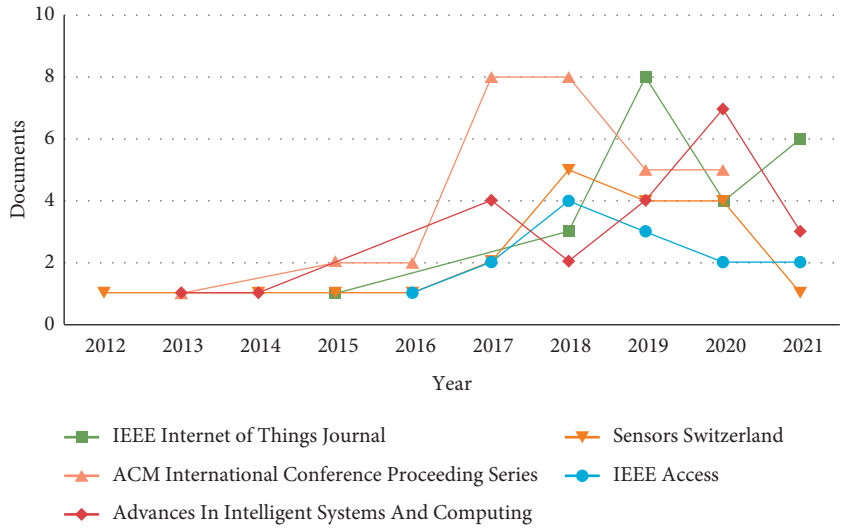

Figure 6: Number of documents per year per source.

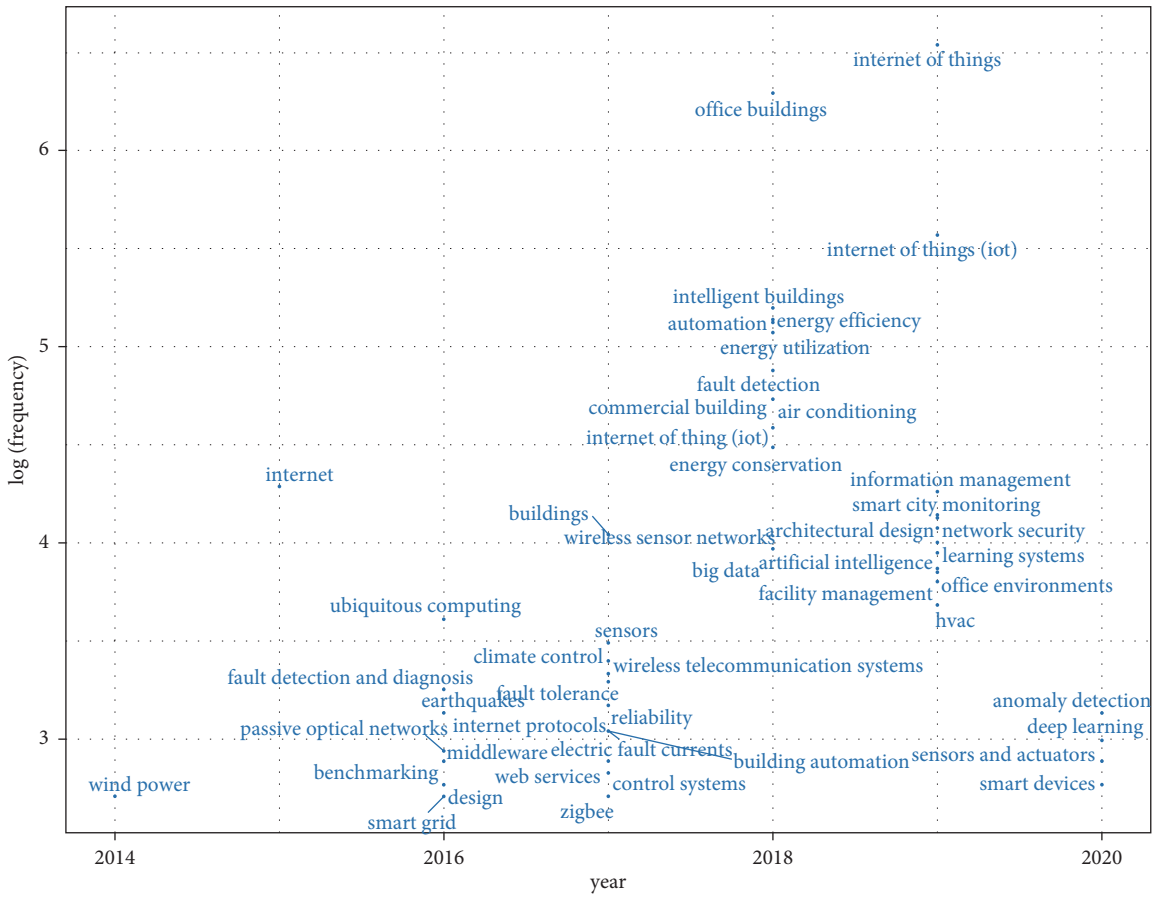

Figure 7: Trending topics as per the author keywords.

3.1. Experimental Setup. The proposed architecture consists of an ATmega8 microcontroller that works as the fundamental controller. This framework deals with continuous real-time monitoring of the electrical appliances through current sensors that can be remotely controlled. The inputs from different sensors are checked against the constant gadget working. A gas sensor is used to detect toxic gases or identify any gas leakage whereas the temperature and humidity sensor is used to control air conditions. An ultrasonic sensor is used to detect object proximity. Figure 9 presents the block diagram of smart office.

Figure 10 shows the prototype of the smart office which controls the appliances in office by the occupancy and movement of office staff. This paper represents the

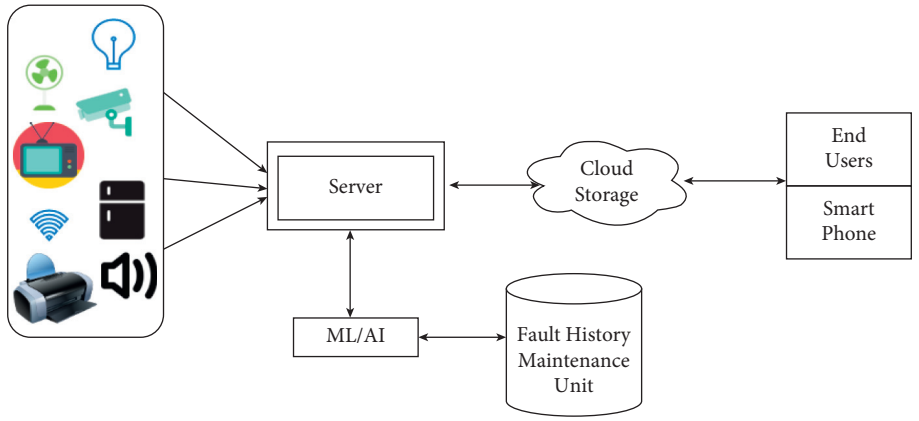

Figure 8: Framework for office automation.

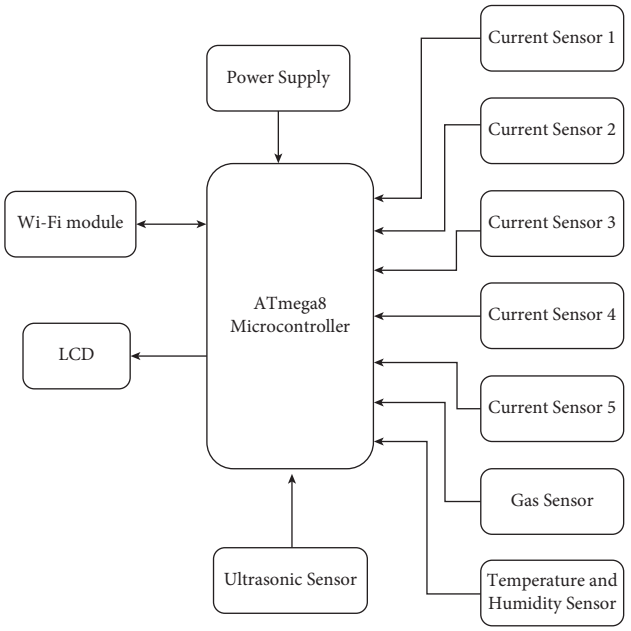

Figure 9: Block diagram of smart office.

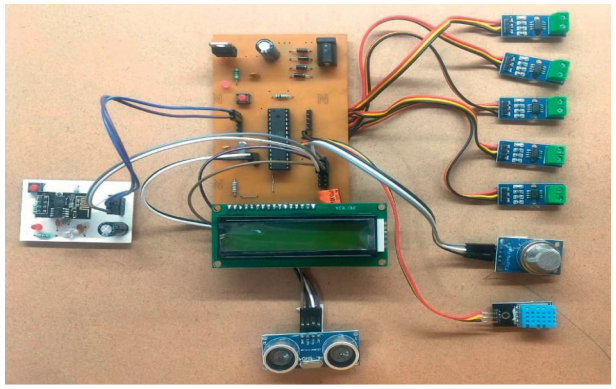

Figure 10: Prototype of the smart office.

implementation of a new system for office employees to control electric appliances automatically and save energy. This framework is better than other existing frameworks because of the following:

(i) The office is monitored unit-wise rather than exercising the whole office space

(ii) It is economical and cost-efficient as an ATmega8 microcontroller is deployed

(iii) A 16×2 LCD is used to check the status of appliances as well as the security of the office

(iv) The WiFi module is used to send an alert message to the end-user

3.2. Hardware Components

(a) *ATmega8 Microcontroller*. ATmega8 microcontroller is the cheapest microcontroller and provides many features in lesser pins. It consists of 1 kilobyte of SRAM and 512 bytes of EEPROM. The ATmega8 application is very versatile because of the program memory of 8 kilobytes. Due to its compact size, it can be placed on many small boards.

(b) *WiFi Module*. ESP8266 WiFi module is used for endpoint IoT developments. It has an integrated TCP/IP protocol stack and can be controlled from a local WiFi network. ESP8266 has low cost and high functionality, which makes it an ideal module for IoT. It fetches data from the Internet using API's and accesses any information available on Internet, thus making it smarter.

(c) *Current Sensors*. ACS712 current sensor is applied to measure the current flowing within a wire. It uses the concept of the magnetic field to sense the current and produce a proportional output. It is used with both AC and DC. It determines energy usage and keeps the cost down to increase efficiency. They help in predicting faults in a device and prevent damaging of equipment.

(d) *Gas Sensor*. MQ-135 gas sensor is applied in air quality control equipment to measure common air quality gases such as CO_2, smoke, NH_3, NO_x, alcohol, and benzene. The detection range of this sensor is 10~1000 ppm. It detects different types of toxic gases and is known as a low-cost sensor for

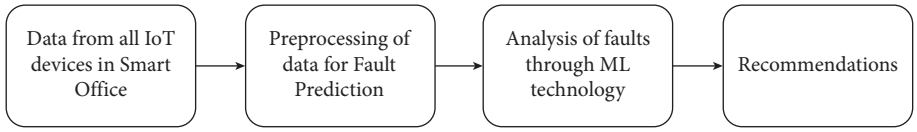

Figure 11: Analysis of fault flow diagram.

such kinds of applications. It is ideally used in offices with a monitoring circuit.

(e) *Temperature and Humidity Sensor*. DHT11 sensor calculates humidity from 20 to 90% and temperature from 0°C to 50°C with an accuracy of ±1% and ±1°C, respectively. It is an economic digital sensor that employs a thermistor and capacitive humidity sensor to estimate the surrounding air. It can be easily interfaced with the ATmega8 microcontroller.

(f) *Ultrasonic Sensor*. SR04 ultrasonic motion detection sensor is applied to detect the motion of moving objects. It is used in automatic door opening devices and contact-less-speed measurement equipment. They are also able to measure an approaching or receding object.

(g) *Power Supply*. Any IoT device will need electricity to work whether it comes from a power outlet or a battery. A certain amount of voltage and current is always required.

(h) *16 × 2 LCD Screen*. In this, 16 × 2 indicates two lines per column and each line has 16 columns, so a total of 32 characters. To display custom text, numbers, and special characters, it is programmed using a microcontroller board with the liquid crystal library.

4. Proposed Methodology

This section defines a methodology of a new automated environment which is the integration of cloud, IoT, and ML. In the literature survey section, many researchers separately research in one domain taking into consideration their unique properties, features, attributes, advantages, and disadvantages. But the proposed architecture features all these concepts and finds a new way to integrate them into a new concept by analyzing their common features. Faults are predicted in IoT appliances to enhance their performance and reliability. The existing fault dataset and device's current status are maintained to observe changes in values which could lead to a fault that can be prevented at an early stage. The proposed architecture fetches data from office appliances to enhance the performance of each appliance. The data being collected by IoT is sent to the ML algorithm for future fault prediction. This data stored in database is connected to a cloud server. The prediction and classification process of faults is done via an ML algorithm. Then, this information is shared with the end-user as well as the solutions will be recommended using a mobile application. The mobile application with the end-user comprises software that keeps track of all devices and alerts the user on deviation or abnormal functioning of any appliance.

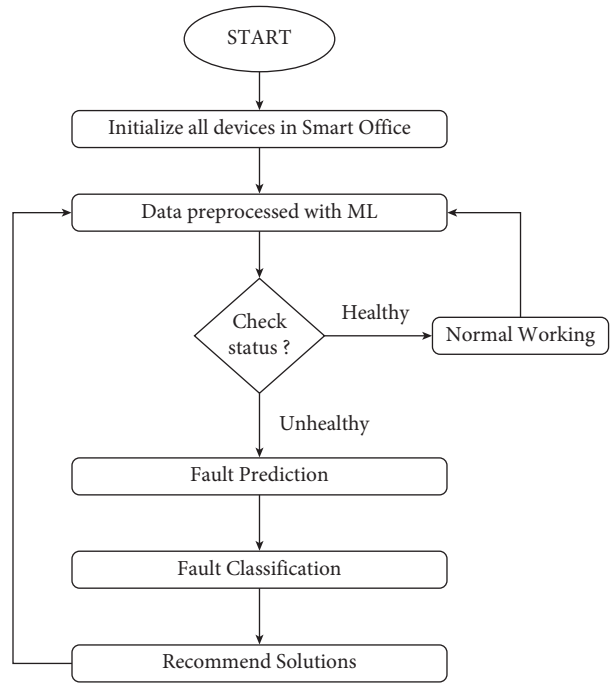

Figure 12: Flowchart of the proposed architecture.

5. Workflow for Fault Prediction in Office Automation

Figure 11 shows the analysis of the flow of the faults. Initially, data from all IoT appliances in a smart office like electrical appliances or sensors is gathered. This gathered data is saved on a server that is responsible for controlling all the IoT devices. Then, this data is being preprocessed for fault identification and prediction. Once the faults are identified, then they are analyzed through ML. Also for excess data, the smart office server transfers data to the cloud and users can remotely access all data via a software application interface on their smartphone. The solutions will be recommended for identified faults. An Internet connection allows the user to communicate with the smart office to get all the details and remotely handle devices if that person is not in the office.

A complete flowchart of our proposed architecture is shown in Figure 12. The working model of our proposed architecture firstly requires initializing all devices and sensors in the smart office. Then, the data fetched from all devices is preprocessed using ML. Then, the status of each and every device is checked. Every device will have 2 states, either healthy or unhealthy. If the device is in a healthy state, then normal working will take place. If the device is in an unhealthy state, then the fault prediction and classification process will take place. The solutions will be recommended

whether the device needs repairing or replacing, and a notification will be sent to the concerned person's smartphone and an e-mail will be sent to the guard who will repair the fault or replace the device.

6. Conclusion

Machine learning is a growing technology that plays a vital role in the advancement of the IT sector. The proposed architecture presents a prototype of a smart office that uses IoT, cloud, and ML technology for office people so that their efficiency can be increased. It has a multitechnology environment as many technologies are involved in this. Live monitoring of office appliances helps in the early fault prediction without any intervention of human effort and also saves the maximum power of office appliances. This proposed architecture identifies and classifies the faults before their occurrence and hence, recommends the most suitable solution that can be used for fixing these faults in a smart office. ATmega8 microcontroller is used to automatically control the devices present in the smart office. The current sensors, temperature and humidity sensors, detection sensors, and gas sensors are being premeditated in this system to make the work more relaxed. Whenever the values are not normal, a notification will be flashed on the end-user smartphone and an e-mail will be forwarded to the concerned security person. The smart office system is prolonged to the whole smart building. The fault prediction capabilities can be expanded to include fault diagnosis, identification, and prognosis. This paper proposed a solution to manage and monitor the office cubicles easily. This proposed system provides many advantages like security, improved comfort, and saves energy and cost. Thus, it helps to build an autonomous environment in a smart office. In the future, new technologies and techniques could be investigated to enhance the performance and reliability of IoT appliances.

Data Availability

The data used to support the findings of this study are available from the corresponding author upon request (gdhiman0001@gmail.com).

Conflicts of Interest

The authors declare that they have no conflicts of interest regarding the publication of this study.

References

[1] L. Stogner, "An introduction to the internet of things from the perspective of the IEEE internet of things initiative," in *Proceedings of the Internationfal Conference on Collaboration Technologies and Systems (CTS)*, June 2015.

[2] F. Xia, L. T. Yang, L. Wang, and A. Vinel, "Internet of things," *International Journal of Communication Systems*, vol. 25, no. 9, pp. 1101-1102, 2012.

[3] C. Adam, "Architectures in the IoT civilization," 2021.

[4] C. R. Storck and F. D. Figueiredo, "A survey of 5G technology evolution, standards, and infrastructure associated with vehicle-to-everything communications by internet of vehicles," *IEEE Access*, vol. 8, Article ID 117593, 2020.

[5] L. Antao, R. Pinto, J. Reis, and G. Gil, "Requirements for testing and validating the industrial internet of things," in *Proceedings of the IEEE International Conference on Software Testing, Verification and Validation Workshops (ICSTW)*, pp. 110–115, IEEE, Sweden, April 2018.

[6] "IoT system model," 2021, https://cryptiot.de/iot/security/security-in-iot/.

[7] S. Talari, M. S. Khah, P. Siano, V. Loia, A. Tommasetti, and J. Catalão, "A review of smart cities based on the internet of things concept," *Energies*, vol. 10, no. 4, 2017.

[8] K. K. Patel and S. M. Patel, "Internet of things-IOT: definition, characteristics, architecture, enabling technologies, application & future challenges," *International journal of engineering science and computing*, vol. 6, no. 5, 2016.

[9] J. C. Zhao, J. F. Zhang, F. Yu, and J. Guo, "The study and application of the IOT technology in agriculture," in *Proceedings of the 3rd International Conference on Computer Science and Information Technology*, pp. 462–465, IEEE, Chengdu, China, July 2010.

[10] P. P. Ray, "A survey of IoT cloud platforms," *Future Computing and Informatics Journal*, vol. 1, no. 1-2, pp. 35–46, 2016.

[11] "IoT and its role in a smart office," 2021, https://agatelevelup.id/iot-role-in-smart-office/.

[12] S. Sholla, R. Naaz, and M. A. Chishti, "Incorporating ethics in Internet of Things (IoT) enabled connected smart healthcare," in *Proceedings of the 2017 IEEE/ACM International Conference on Connected Health: Applications, Systems and Engineering Technologies (CHASE)*, pp. 262-263, IEEE, Philadelphia, PA, USA, July 2017.

[13] "IoT in smart home and smart city application," 2021, https://www.javatpoint.com/iot-smart-home-and-smart-city.

[14] S. P. Gochhayat, C. Lal, L. Sharma et al., "Reliable and secure data transfer in iot networks," *Wireless Networks*, vol. 26, pp. 1–14, 2019.

[15] M. H. Miraz, P. S. E. A. Maaruf, and P. Rich, "A review on internet of things (IoT), internet of everything (IoE) and internet of nano things (IoNT," in *Proceedings of the 2015 Internet Technologies and Applications (ITA)*, pp. 219–224, IEEE, Wrexham, UK, September 2015.

[16] J. Gubbi, R. Buyya, S. Marusic, and M. Palaniswami, "Internet of Things (IoT): a vision, architectural elements, and future directions," *Future Generation Computer Systems*, vol. 29, no. 7, pp. 1645–1660, 2013.

[17] O. Vermesan, *Internet of Things-From Research and Innovation to Market Deployment*, P. Friess, Ed., River publishers, Aalborg, Denmark, 2014.

[18] L. Silva, R. Leandro, D. Macedo, and L. A. Guedes, "A dependability evaluation tool for the Internet of Things," *Computers & Electrical Engineering*, vol. 39, no. 7, pp. 2005–2018, 2013.

[19] H. D. Ma, "Internet of things: objectives and scientific challenges," *Journal Of Computer Science and Technology*, vol. 26, no. 6, pp. 919–924, 2011.

[20] A. Fox, R. Griffith, A. Joseph et al., *Above The Clouds: A Berkeley View Of Cloud Computing*, Report. UCB/EECS 28, Dept. Electrical Eng. and Comput. Sciences, University of California, Berkeley, CA, USA, 2009.

[21] C. Stergiou, K. E. Psannis, B.-G. Kim, and B. Gupta, "Secure integration of IoT and cloud computing," *Future Generation Computer Systems*, vol. 78, pp. 964–975, 2018.

[22] G. Peralta, R. G. C. Fuentes, J. Bilbao, and P. M. Crespo, "Homomorphic encryption and network coding in iot

architectures: advantages and future challenges," *Electronics*, vol. 8, no. 8, p. 827, 2019.

[23] "Benefits of a cloud platform in the IoT," 2021, https://www.avsystem.com/blog/iot-cloud-platform/.

[24] M. Aazam, I. Khan, and E. N. Huh, "Cloud of things: integrating internet of things and cloud computing and the issues involved," in *Proceedings of the 2014 11th International Bhurban Conference on Applied Sciences & Technology (IBCAST)*, pp. 414–419, IEEE, Islamabad, Pakistan, January, 2014.

[25] B. Shakerighadi, A. A. Moghaddam, J. Vasquez, and J. Guerrero, "Internet of things for modern energy systems: state-of-the-art, challenges, and open issues," *Energies*, vol. 11, no. 5, 2018.

[26] S. Kumar, N. Lal, and V. K. Chaurasiya, "An energy efficient IPv6 packet delivery scheme for industrial IoT over G.9959 protocol based Wireless Sensor Network (WSN)," *Computer Networks*, vol. 154, pp. 79–87, 2019.

[27] Z. Sheng, S. Yang, Y. Yu, A. Vasilakos, J. Mccann, and K. Leung, "A survey on the ietf protocol suite for the internet of things: standards, challenges, and opportunities," *IEEE Wireless Communications*, vol. 20, no. 6, pp. 91–98, 2013.

[28] S. Jain and K. Chandrasekaran, "Industrial automation using internet of things," *Security and Privacy Issues in Sensor Networks and IoT*, IGI Global, PA, USA, pp. 28–64, 2020.

[29] A. Bhatnagar, S. Shukla, and N. Majumdar, "Machine learning techniques to reduce error in the internet of things," in *Proceedings of the 2019 9th International Conference on Cloud Computing, Data Science & Engineering (Confluence)*, pp. 403–408, IEEE, Uttar Pradesh, India, January 2019.

[30] A. Arora, S. Aditya, and L. Ramanathan, "A systematic literature review on software fault prediction and fault tolerance in software engineering," *International Research Journal of Engineering and Technology (IRJET)*, vol. 4, no. 4, 2017.

[31] Mudita and D. Gupta, "The aspects of artificial intelligence in software engineering," *Journal of Computational and Theoretical Nanoscience*, vol. 17, no. 9-10, pp. 4635–4642, 2020.

[32] Y. Liu, Y. Yang, X. Lv, and L. Wang, "A self-learning sensor fault detection framework for industry monitoring IoT," *Mathematical Problems in Engineering*, vol. 2013, Article ID 712028, 8 pages, 2013.

[33] B. Qian, J. Su, Z. Wen et al., "Orchestrating the development lifecycle of machine learning-based IoT applications," *ACM Computing Surveys*, vol. 53, no. 4, pp. 1–47, 2020.

[34] L. M. Gladence, V. M. Anu, R. Rathna, and E. Brumancia, "Recommender system for home automation using IoT and artificial intelligence," *Journal of Ambient Intelligence and Humanized Computing*, pp. 1–9, 2020.

[35] M. A. Chaqfeh and N. Mohamed, "Challenges in middleware solutions for the internet of things," in *Proceedings of the 2012 international conference on collaboration technologies and systems (CTS)*, pp. 21–26, IEEE, Denver, CO, USA, May 2012.

[36] D. S. Vibhute and A. S. Gundale, "Early detection of sensors failure using IoT," *International Research Journal of Engineering and Technology (IRJET)*, vol. 6, no. 5, 2019.

[37] F. Cicirelli, G. Fortino, A. Guerrieri, G. Spezzano, and A. Vinci, "Metamodeling of smart environments: from design to implementation," *Advanced Engineering Informatics*, vol. 33, pp. 274–284, 2017.

[38] K. Furdik, L. Gabriel, T. Sabol, and P. Kostelnik, "The network architecture designed for an adaptable IoT-based smart office solution," *International Journal of Computer Networks and Communications Security*, vol. 1, no. 6, pp. 216–224, 2013.

[39] L. D. Xu, W. He, and S. Li, "Internet of things in industries: a survey," *IEEE Transactions on industrial informatics*, vol. 10, no. 4, pp. 2233–2243, 2014.

[40] D. Mundada, A. Murade, O. Vaidya, and J. N. Swathi, "Software fault prediction using artificial neural network and Resilient Back Propagation," *International Journal on Computer Science and Engineering*, vol. 503 pages, 2016.

[41] C. M. Barbosa, R. L. Gomes, J. G. F. Pereira, J. L. M. Rebelo, J. P. F. Gonçalves, and J. R. M. Luiz, "RS4IoT: a recommender system for IoT," *Enterprise Interoperability: Smart Services and Business Impact of Enterprise Interoperability*, Wiley, NJ, USA, pp. 225–231, 2018.

[42] D. Bakker, T. V. D. V. Christel, and R. Alexander, "The energy saving potential of occupancy-based lighting control strategies in open-plan offices: the influence of occupancy patterns," *Energies*, vol. 11, no. 1, pp. 1–18, 2017.

[43] M. V. Rao, T. V. R. Krishna, R. Ganduri, and A. Roohi, "An effective energy management system for smart office cubicles using IoT," *Journal Of Advanced Research In Dynamical And Control Systems*, vol. 10, no. 2, pp. 338–347, 2018.

[44] K. Bhavana, V. Nekkanti, and N. Jayapandian, "Internet of things enabled device fault prediction system using machine learning," in *Proceedings of the International Conference on Inventive Computation Technologies*, pp. 920–927, Springer, Coimbatore, India, August 2019.

[45] S. Arun, L. R. Anjaneya, K. Dharshan, and N. Srinivasa, "Smart office monitoring system using IoT," *International Research Journal of Engineering and Technology*, vol. 6, no. 4, pp. 4560–4564, 2019.

[46] P. Gouthaman and S. Suresh, "Agile software risk management architecture for IoT-fog based systems," in *Proceedings of the International Conference on Smart Systems and Inventive Technology (ICSSIT)*, pp. 48–51, IEEE, Tirunelveli India, December 2018.

[47] N. Y. Bak, B. M. Chang, and K. Choi, *SmartVisual: A Visualisation Tool for SmartThings IoT Apps Using Static Analysis*, IET Software, Stevenage, England, 2020.

[48] A. Xenakis, A. Karageorgos, E. Lallas, A. E. Chis, and H. V. González, "Towards distributed IoT/cloud based fault detection and maintenance in industrial automation," *Procedia Computer Science*, vol. 151, pp. 683–690, 2019.

[49] A. Souri, A. S. Mohammed, M. P. Yousif, M. H. Malik, F. Safara, and M. Hosseinzadeh, "Formal verification of a hybrid machine learning-based fault prediction model in Internet of Things applications," *IEEE Access*, vol. 8, Article ID 23863, 2020.

[50] N. G. Lo, J. M. Flaus, and A. Olivier, "Review of machine learning approaches in fault diagnosis applied to IoT systems," in *Proceedings of the 2019 International Conference on Control, Automation and Diagnosis (ICCAD)*, pp. 1–6, IEEE.

[51] D. Pathak, K. Kotecha, S. Pandya, and R. Desai, "IoT based intelligent health surveillance & alert system with fault prediction using machine learning," *International Journal of Advanced Science and Technology*, vol. 28, no. 18, pp. 660–76, 2019.

[52] Mudita and D. Gupta, "A comprehensive study of recommender systems for the internet of things," *Journal of Physics: Conference Series*, IOP Publishing, vol. 1969, no. 1, 2021.

[53] B. S. Meena, R. U. Laskar, and K. Hemachandran, "Indoor localization-based office automation system using IOT devices," in *Intelligent Computing in Engineering*, pp. 199–212, Springer, Singapore, 2020.

[54] M. Jia, A. Komeily, Y. Wang, and R. S. Srinivasan, "Adopting Internet of Things for the development of smart buildings: a

review of enabling technologies and applications," *Automation in Construction*, vol. 101, pp. 111–126, 2019.

[55] T. Nan, "Design and Implementation of office automation network security system," in *Journal of Physics: Conference Series*vol. 1802, no. 3, IOP Publishing, Article ID 032108, 2021.

[56] C. Wang, S. Feng, P. Liu, and X. Liu, "Design and development of collaborative office automation system based on hierarchical structure," in *Proceedings of the E3S Web of Conferences, EDP Sciences*, Dali, China, February 2021.

Hindawi
Journal of Healthcare Engineering
Volume 2021, Article ID 3361755, 9 pages
https://doi.org/10.1155/2021/3361755

Research Article

Management and Plan of Undergraduates' Mental Health Based on Keyword Extraction

Weifeng Zhang

Xinxiang University, Xinxiang, Henan 453003, China

Correspondence should be addressed to Weifeng Zhang; zhangweifeng02@xxu.edu.cn

Received 23 September 2021; Revised 6 October 2021; Accepted 11 October 2021; Published 28 October 2021

Academic Editor: yan chai hum

Mental health issues are alarmingly on the rise among undergraduates, which have gradually become the focus of social attention. With the emergence of some abnormal events such as more and more undergraduates' suspension, and even suicide due to mental health issues, the social attention to undergraduates' mental health has reached a climax. According to the questionnaire of undergraduates' mental health issues, this paper uses keyword extraction to analyze the management and plan of undergraduates' mental health. Based on the classical TextRank algorithm, this paper proposes an improved TextRank algorithm based on upper approximation rough data-deduction. The experimental results show that the accurate rate, recall rate, and $F1$ of proposed algorithm have been significantly improved, and the experimental results also demonstrate that the proposed algorithm has good performance in running time and physical memory occupation.

1. Introduction

The mental health and wellbeing of undergraduates have deteriorated over the last decade. Before the COVID-19 pandemic, higher education was facing a "mental health crisis" [1, 2]. The rapid onset of the COVID-19 pandemic has introduced countless additional stressors, and faculty concern over student wellbeing has increased. Over the past ten or twenty years, the depression has increased from about 25% of undergraduates in 2010 to almost 30% of undergraduates in 2020, and the anxiety of undergraduates has increased from 22% in 2014 to 31% in 2020. Suicidal ideation of undergraduates has increased from 6% in 2010 to 11% in 2020 [3]. The frequency of mental health management organization in undergraduates varies from university to university. Definitely influence of the pandemic on mental health concerns within undergraduates is a big concern. The pandemic has affected the economic development of many countries, and the cooperation of relevant countries on the pandemic has also led to conflicts. The widespread public reports on the Internet and the media have made simple and inexperienced undergraduates unable to distinguish. So, the management and plan of undergraduates' mental health are important under COVID-19 pandemic [4, 5].

Keywords are words that express the central content of a document. Keywords from a document can accurately describe the document's content and facilitate fast information processing. There are two main types of keyword extraction algorithms, which are unsupervised keyword extraction method and supervised keyword extraction method [6–8]. Unsupervised keyword extraction method does not need manually labeled corpus, but it uses some methods to find important words in the text as keywords for keyword extraction. In unsupervised keyword extraction method, candidate words are firstly extracted, and then each candidate word is scored, so top-K candidate words with the highest score are output as keywords. According to different ranking strategies, there are different algorithms such as term frequency-inverse document frequency (TF-IDF), TextRank, and latent Dirichlet allocation (LDA). The supervised keyword extraction method regards the keyword extraction process as a binary classification problem. At first, the candidate words are extracted, and then each candidate word is labeled, so the keyword extraction classifier is

trained. When a new document is coming, all candidate words are extracted, and then the trained keyword extraction classifier is used to classify each candidate word. Finally, the candidate words labeled as keywords are used as keywords [9, 10].

Accordingly, the main contributions of this paper are summarized as follows. (i) I study the TextRank keyword extraction algorithm. (ii) An improved TextRank algorithm based on upper approximation rough data-deduction is proposed.

The rest of this paper is structured as follows. Section 2 reviews the related work. In Section 3, I propose an improved TextRank algorithm based on upper approximation rough data-deduction. The experimental results are shown in Section 4. Section 5 concludes this paper.

2. Related Work

Many strategies of management and plan for undergraduates' mental health have been proposed. In [11], the authors studied to examine student perspectives about college mental health including the primary mental health issues affecting students, common college student stressors, student awareness of campus mental health resources, and mental health topics students wanted more information about. Little research existed into the trends associated with on-campus service utilization for mental health concerns of college students. Rates of broad service utilization existed, but no published study had examined the direct relationship between a range of common mental health symptoms and on-campus service utilization. In [12], the authors studied to explore which common mental health concerns were associated with specific on-campus service utilization in undergraduate students and whether endorsement of more mental health concerns would predict a higher number of services utilized. In [13], the study investigated the moderating role of perceived social support in the relationship between academic demands (measured as perceived academic stress) and mental health of undergraduate students in full-time employment. A growing number of developing countries had experienced worsening air pollution, which had been shown to cause significant health problems. However, few studies had explored the impact of air pollution on the mental health of university students, particularly in the Chinese context. In order to address this gap, in [14], through a large-scale cross-sectional survey, the study aimed to examine the effects of air pollution on final-year Chinese university undergraduates' mental health by employing multivariable logistic regression.

The TextRank algorithm plays an important role in keyword extraction. In [15], the author presented an automatic keyword extraction algorithm based primarily on a weighted TextRank model. In the model, word embedding vectors were used to compute a similarity measure as an edge weight. As a typical keyword extraction technology, TextRank had been used in a wide variety of commercial applications, including text classification, information retrieval, and clustering. In these applications, the parameters of TextRank, including the cooccurrence window size, iteration number, and decay factor, were set roughly. In [16], the authors conducted an empirical study on TextRank, towards finding optimal parameter settings for keyword extraction. The keyword weight propagation in TextRank focused only on word frequency. To improve the performance of the algorithm, in [17], the authors proposed semantic clustering TextRank, a semantic clustering news keyword extraction algorithm based on TextRank. In [18], the authors introduced a new human-annotated Chinese patent dataset and proposed a sentence-ranking-based term frequency-inverse document frequency algorithm for patent keyword extraction, motivated by the thought of "the keywords were in the key sentences." In the algorithm, a sentence-ranking model was constructed to filter top-K-s percent sentences from each patent based on a sentence semantic graph and heuristic rules. In [19], the authors introduced a word network whose nodes represented words in a document and defined that any keyword extraction method based on a word network was called as a Word-net method. Then, the authors proposed a new network model which considered the influence of sentences and a new word-sentence method based on the new model. In [20], the authors proposed an ontology and enhanced word embedding-based methodology for automatic keyphrase extraction from geoscience documents.

There are also some other methods for keyword extraction. In [21], an enhancement of the term weighting was proposed particularly in the form of a series of modified term frequency-inverse document frequencies, for improving keyword extraction. In [22], the authors proposed an improved rapid automatic keyword extraction method, which used the word string matching feature in the dictionary method to correspond to the relevant execution action function. In [23], a novel text mining approach based on keyword extraction and topic modeling was introduced to identify key concerns and their dynamics of on-site issues for better decision-making process.

3. Improved Algorithm Based on Rough Data-Deduction

TextRank keyword extraction algorithm is a graph-based ranking algorithm, which is derived from Google's PageRank algorithm [24]. TextRank firstly divides the target text into several meaningful words and constructs the candidate word graph and then uses the voting mechanism to rank the candidate words to achieve keyword extraction. The task of keyword extraction is to extract several important words from the target text. TextRank algorithm uses the local correlation between words (i.e., cooccurrence sliding window) to determine the correlation between candidate words and then performs iterative calculation and ranking of candidate keywords. Rough set theory is originally used for text classification to speed up classification and improve accuracy. Rough data-deduction is based on rough set theory, which integrates approximate information from upper approximation concept into data reasoning process. This paper introduces upper approximation-based rough data-deduction to TextRank keyword extraction algorithm,

and the extracted keywords are used in undergraduates' mental health management and plan.

In TextRank keyword extraction algorithm, the candidate keywords in the text are the graph model constructed by the cooccurrence correlation, and then the weights of each node are calculated by the average transition probability matrix for many times until convergence. After convergence, words are ranked in descending order according to their weights, and the first N words are selected as the extracted keywords. This method is more concise and effective, but it has certain limitations. In [25], the convergent operation utilizes a clustering strategy to group the population into multiple clusters. The use of cooccurrence window only considers the correlation between local words, so some words closely related to a certain keyword may be ignored, but keywords from a document are not just limited to the keywords around the words. When doing text keyword extraction, I should fully consider the words in the text as well as some potentially related words. Words with potential correlation will have an important impact on the whole iterative ranking process, and the potential relation can be discovered by the theory of rough data-deduction. Therefore, this paper proposes an improved TextRank algorithm based on upper approximation rough data-deduction.

Based on the word sense similarity of mental health words, the candidate keywords are divided. As there may be a group of words with similar word sense in a document, the weight of this group of words should be increased to improve the accuracy of extraction results when describing the same important content. TextRank algorithm only considers the word sense themselves and ignores the contribution of words with similar word sense. Therefore, the improved algorithm takes the word sense into account and divides the candidate words by word sense, which can extract keywords more effectively.

The rough data-deduction space $M = (U, N, D)$ is introduced to describe the keyword extraction of undergraduates' mental health issue structurally. U is the universe of discourse (UOD) and the dataset composed of candidate keywords of undergraduates' mental health. N is a set of equivalence relation, and $E \in N$. If and only if p is similar to q, then $p, q \in U$ and $<p, q> \in E$. $D \subseteq U \times U$ is defined as $D = \{<p, q> | p, q \in U$ and there is a relation between p and $q\}$.

Assuming that deduction correlation is defined as equation (1) by using rough data-deduction,

$$D = \{\langle cw_1, cw_4\rangle, \langle cw_2, cw_6\rangle, \langle cw_3, cw_6\rangle, \langle cw_6, cw_5\rangle\}, \tag{1}$$

where cw_1–cw_6 are the candidate keywords from the text through word segmentation and filtering, and the deduction correlation is determined by the degree of the association rules, that is, pointwise mutual information (PMI).

At the same time, for equivalence relation $E \in N$,

$$\frac{U}{E} = \{\{cw_1, cw_2, cw_3\}, \{cw_4, cw_6\}, \{cw_5, cw_7\}\}, \tag{2}$$

where the equivalence division is based on the similarity between the candidate words.

In rough data-deduction, for candidate word cw_1, the algorithm obtains cw_2 and cw_3 based on similarity rule and then divides cw_1, cw_2, and cw_3 into one dataset, and cw_4–cw_7 can be similarly divided. Then, cw_4 can be obtained from cw_1 based on the degree of the association rules of PMI, as well as cw_5, cw_6, and cw_7. According to rough data-deduction, for cw_1, $[cw_1]_E = \{cw_1, cw_2, cw_3\}$, and $[cw_1 - E] = \{cw_4, cw_6\}$. $E^*([cw_1 - E]) = \{cw_4, cw_6\}$, so $cw_1 \Rightarrow_E cw_6$. For candidate word cw_6, $[cw_6]_E = \{cw_4, cw_6\}$, and $[cw_6\text{-}E] = \{cw_5\}$. $E^*([cw_6 - E]) = \{cw_5, cw_7\}$, so $cw_6 \Rightarrow_E cw_7$. $Cw_1 =_E cw_7$ can be obtained from $cw_1 \Rightarrow_E cw_6$ and $cw_6 \Rightarrow_E cw_7$. As described, there is also a potential correlation between cw_1 and cw_7, which can provide a certain contribution rate for calculation. The association between candidate keywords is established by the above rules, and the association weight can be added to the iterative calculation process as contribution rate to improve the accuracy of keyword extraction.

The upper approximation-based rough data-deduction to TextRank keyword extraction algorithm is summarized as follows.

Step 1. Based on TextRank algorithm, the text related to undergraduates' mental health is preprocessed, which includes clause, word segmentation, and part of speech (POS) tagging, and candidate keywords are obtained.

Step 2. The candidate keywords are divided into different equivalence classes according to their similarities. This paper is divided based on WordNet and Wikitext. For any two candidate words cw_1 and cw_2, the division rule is defined as follows:

$$s = \omega_1 s_1 + \omega_2 s_2, \tag{3}$$

where s_1 and s_2 are the similarities calculated by WordNet and Wikitext, respectively. ω_1 and ω_2 are the two weights assigned to s_1 and s_2, and $\omega_1 + \omega_2 = 1$.

Assuming that candidate word cw_1 is distributed in WordNet WN, and cw_2 is distributed in Wikitext WT, the intersection of WN and WT is WW. The value strategy of ω_1 and ω_2 is summarized as follows:

(i) When $cw_1 \in WW$ and $cw_2 \in WW$, the similarity to cw_1 and cw_2 is calculated based on WN and WT, respectively, which are denoted as s_1 and s_2. In this paper, $\omega_1 = \omega_2 = 0.5$.

(ii) When $cw_1 \in WN$ and $cw_2 \in WN$, or $cw_1 \in WT$ and $cw_2 \in WT$, cw_1 and cw_2 are calculated as s_1 or s_2 based on WN and WT, where one of the ω_1 and ω_2 is 1, and the other one is 0.

(iii) When $cw_1 \in WN$ and $cw_2 \in WT$, the synonym set of cw_2 is searched based on WT, and then the similarity with cw_1 is calculated based on WN, and the maximum value is denoted as s_1. If cw_2 has no synonym in WT, then $s_1 = 0.2$, $\omega_1 = 1$, and $\omega_2 = 0$.

(iv) When $cw_1 \in WN$ and $cw_2 \in WW$, the similarity to cw_1 and cw_2 is calculated based on WN and denoted as s_1. Then, the synonym set of cw_2 is searched in WT, and then the similarity to cw_1 is calculated based on

WN, and the maximum value is denoted as s_2. If cw_2 has no synonym in *WT*, then $s_2 = s_1$, and $\omega_1 > \omega_2$. In this paper, $\omega_1 = 0.6$, and $\omega_2 = 0.4$.

(v) When $cw_1 \in WT$ and $cw_2 \in WW$, the similarity to cw_1 and cw_2 is calculated based on *WT* and denoted as s_2. Then, the synonym set of cw_1 is searched in *WT*, and then the similarity to cw_2 is calculated based on *WN*, and the maximum value is denoted as s_1. If cw_1 has no synonym in *WT*, then $s_1 = s_2$, and $\omega_2 > \omega_1$. In this paper, $\omega_1 = 0.4$, and $\omega_2 = 0.6$.

Here, the calculation of word similarity based on WordNet is defined as follows:

$$s(WW_1, WW) = \sum_{m=1}^{3} \ln \delta_m \prod_{n=1}^{m} s_n(WW_1, WW_2), \quad (4)$$

$$s(cw_1, cw_2) = \max_{m=1\ldots i, n=1\ldots j} s(WW_{1m}, WW_{2n}). \quad (5)$$

In equation (4), $s_1(WW_1, WW_2)$ is the similarity calculated by the set of independent minimum semantic units. $s_2(WW_1, WW_2)$ is the similarity of feature structure of minimal semantic unit of correlation. $s_3(WW_1, WW_2)$ is the similarity of the characteristic structure of the relational sign. The parameter δ_m $(1 \le m \le 3)$ is adjustable and meets the requirement of $\delta_1 + \delta_2 + \delta_3 = 1$. In this paper, δ_1, δ_2, and δ_3 are set as 0.6, 0.25, and 0.15, respectively. Equation (5) can obtain the sense similarity. When there are multiple senses in a word, equation (5) is used to calculate the maximum similarity among all combinations of senses, that is, the similarity to two words, where i is the sense number of the word cw_1, and j is the sense number of the word cw_2.

The calculation of word similarity based on *WT* is defined as follows:

$$s(WW_1, WW_2) = (1 - 0.5\mathrm{d}t(WW_1, WW_2))\sqrt{e^{-\mathrm{d}i/2j}}, \quad (6)$$

where $dt(WW_1, WW_2)$ is the distance function of word codes WW_1 and WW_2 in the tree structure. j is the total number of nodes in the branch layer, which indicates the number of direct child nodes of the nearest common parent node of two words. di represents the distance between branches where two words are located in the nearest public parent node.

Step 3. The correlation of association rules in rough data-deduction is defined as follows:

$$\mathrm{PMI}(cw_1, cw_2) = \frac{p(CW_1, CW_2)}{p(CW_1)p(CW_2)}, \quad (7)$$

where cw_1 and cw_2 are two candidate keywords in the text. $p(cw_1, cw_2)$ is the probability of cw_1 and cw_2 appearing in the same sentence. $p(cw_1)$ is the probability of occurrence of cw_1, and $p(cw_2)$ is the probability of occurrence of cw_2.

According to the correlation, the candidate keywords with direct correlation are determined, when $PMI(cw_1, cw_2) \neq 0$, there is a direct correlation between cw_1 and cw_2, and cw_1, cw_2 and their correlation degrees are stored in the correlation set. Meanwhile, the rough data-deduction relation *D* can be established according to the correlation degree.

Then, by using the rules of rough data-deduction, I get the correlation between the other candidate keywords in all the different equivalence classes, and these words and their correlation degrees are stored into the correlation set.

Step 4. According to the correlation set obtained in Step 3, candidate keyword graphs with weights are constructed. Then, according to the equation of TextRank algorithm, the weight of each candidate keyword is calculated iteratively until convergence.

4. Experiment and Results Analysis

4.1. Experimental Data and Evaluation Criteria. The experiment selects 26300 questionnaires of mental health management of undergraduates from Xinxiang University with 23 schools and 60 majors, which consist of psychological distress, depression, suicidal tendency, and self-evaluation related to mental health within 300 to 1000 words. In particular, these undergraduates are distributed for different grades uniformly. The 19000 valid questionnaires are obtained by excluding questionnaires with self-evaluation less than 300 words to test the effect of proposed method in this paper. The questionnaires use silver ink with a metal oxide [26]. 10 keywords of each questionnaire are extracted and ranked by the importance. In this paper, ω_1 and ω_2 are set 0.5.

In addition, for comparison purposes, TextRank, a keyword extraction using supervised cumulative TextRank (KESCT) [27], scientific research project TF-IDF (SRP-TF-IDF) [28], and high representation tags LDA (HRT-LDA) [29] are selected. Three evaluation indexes commonly used in classification are used to compare and evaluate the quality of experimental results, which include precision (*P*), recall rate (*R*), and *F*1 (*F*). *P* is the accuracy of extraction results. *R* is the coverage degree of the extraction results to the correct keywords. *F* is a comprehensive evaluation index of harmonic average of *P* and *R*.

4.2. Experimental Results. It is found in the experiment that the two important parameters can affect the keyword extraction result of TextRank algorithm, which are the cooccurrence window size and the number of keywords, while the implementation of TF-IDF algorithm based on statistical feature and the algorithm proposed in this paper are not affected by the cooccurrence window size. I set the number of extracted keywords as 10, and the value of the comparison window is within [4, 10]. The *F*1 under different cooccurrence window sizes is shown in Figure 1.

It can be seen from Figure 1 that TextRank algorithm has different extraction effects under different cooccurrence window sizes. In the same test set, this paper compares the effect of different cooccurrence window sizes, and when the cooccurrence window size is 5, the original TextRank algorithm has the best extraction effect with high *F* value.

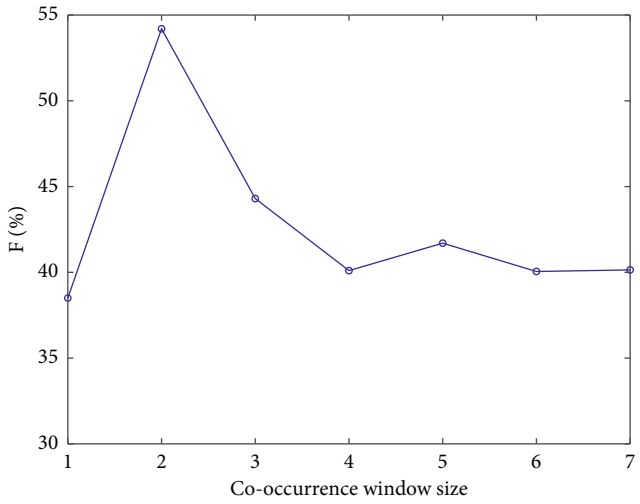

Figure 1: F value under different cooccurrence window sizes.

Therefore, in order to ensure the effectiveness of the proposed algorithm, the cooccurrence window size is set to 5.

The initial window value is set to 5, and P, R, and F are calculated with the number of keywords within [3, 10]. The calculation results are shown in Table 1.

At the same time, in order to observe the experimental results of five algorithms conveniently, the P, R, and F of the algorithm are plotted, as shown in Figures 2–4.

Figure 2 describes the variation trend of the accuracy of the five algorithms when extracting different numbers of mental health keywords. As can be seen from Figure 2, with the increasing number of mental health keywords extracted, the accuracy of each algorithm decreases, but the accuracy of the algorithm proposed in this paper is always higher than other four baselines. The TextRank algorithm based on rough data-deduction proposed in this paper will integrate upper approximation information into the process of data-deduction so that the mutual deduction between data presents the characteristics of approximate entailment or imprecise association, and the potential association between candidate keywords can be mined. If the potential association is added to the iterative calculation of the weight of each candidate keyword, more accurate extraction results can be obtained. Therefore, the accuracy of the algorithm proposed in this paper is theoretically higher, and its accuracy P value is higher than other four baselines.

Figure 3 describes the change of recall rate of five algorithms when extracting different numbers of mental health keywords. In Figure 3, the recall rate of the algorithm proposed in this paper is higher than that of other four baselines, and the recall rate increases with the increasing number of mental health keywords. The SRP-TF-IDF algorithm relies too heavily on word frequency and does not use correlation between words at all. KESCT algorithm adopts the cooccurrence window principle. Although the relation between words is considered, the algorithm is more inclined to put forward frequent words due to its limitations, which may ignore important words with low word frequency that can describe the topics. However, the rough data-deduction used in this paper can expand the correlation range and enhance the coverage of the keywords of the correct correlation in order to improve the recall rate of the algorithm. The influence of word frequency decreases with the increasing number of keywords, and the advantages of the algorithm proposed in this paper will be more obvious.

Figure 4 describes the F values of five algorithms when extracting different numbers of mental health keywords. When evaluating the experimental results, it is expected that both P and R should be as high as possible. However, in most cases, the two values are contradictory. Therefore, F value should be used to comprehensively consider the two values, which can reflect the effectiveness of the whole algorithm. Keyword extraction based on rough data-deduction can mine the potential association between candidate keywords theoretically, which increases the candidate words and range of the association. The keyword extraction based on rough data-deduction adds the potential association to the iterative

Table. 1: The comparison of experimental results of five algorithms.

The number of keywords	Algorithm	P (%)	R (%)	F (%)
	TextRank	52.32	15.50	23.79
	KESCT	55.03	22.35	30.08
3	SRP-TF-IDF	64.10	23.00	33.59
	HRT-LDA	70.54	24.56	34.16
	This paper	80.67	29.30	36.51
	TextRank	49.06	19.71	28.01
	KESCT	54.76	24.33	33.08
4	SRP-TF-IDF	62.15	26.94	34.15
	HRT-LDA	69.87	29.41	35.09
	This paper	79.06	31.08	43.66
	TextRank	48.51	25.16	32.18
	KESCT	52.61	27.66	36.07
5	SRP-TF-IDF	60.48	28.54	37.22
	HRT-LDA	66.92	30.69	39.05
	This paper	78.35	32.17	47.65
	TextRank	42.67	27.65	32.01
	KESCT	49.62	30.25	36.95
6	SRP-TF-IDF	55.40	32.49	34.12
	HRT-LDA	60.73	34.16	40.08
	This paper	77.70	39.58	51.89
	TextRank	41.19	29.90	33.77
	KESCT	45.12	34.15	33.99
7	SRP-TF-IDF	50.08	36.58	40.06
	HRT-LDA	55.64	38.04	45.37
	This paper	74.39	45.89	54.68
	TextRank	39.66	31.57	34.55
	KESCT	40.51	35.26	32.89
8	SRP-TF-IDF	45.99	38.16	39.98
	HRT-LDA	49.30	42.53	44.38
	This paper	70.88	50.07	55.81
	TextRank	36.78	32.36	33.99
	KESCT	37.41	36.45	34.01
9	SRP-TF-IDF	44.01	40.19	40.71
	HRT-LDA	40.09	45.20	46.39
	This paper	65.72	55.06	56.09
	TextRank	35.87	35.64	33.87
	KESCT	33.02	40.16	33.66
10	SRP-TF-IDF	38.28	42.26	38.74
	HRT-LDA	39.16	49.39	43.91
	This paper	60.10	59.03	55.99

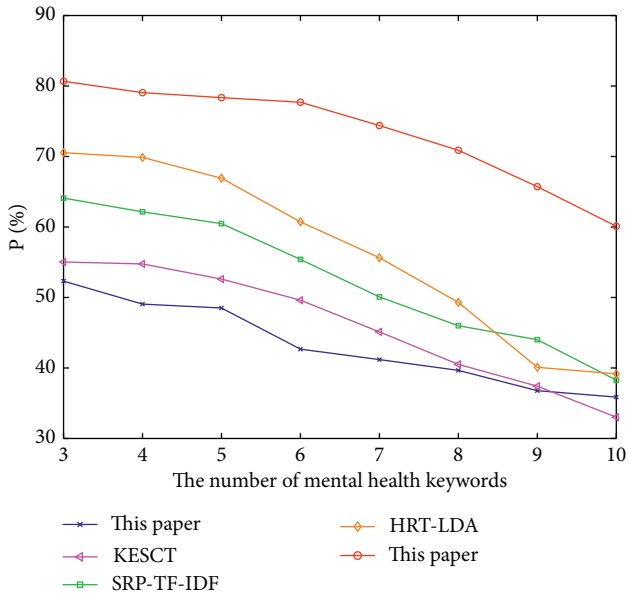

Figure 2: The comparison of P of the five algorithms.

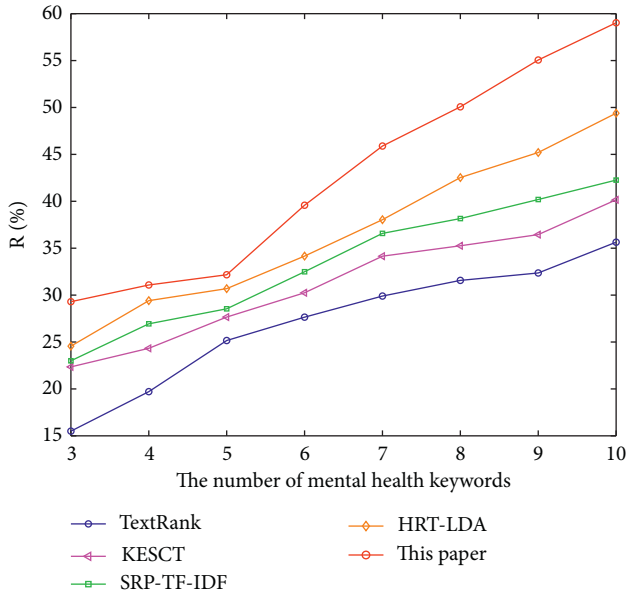

Figure 3: The comparison of R of the five algorithms.

calculation of the weight of each candidate keyword, so the extraction results will be more accurate, that is, the algorithm is also more effective.

According to the experimental results, the proposed algorithm has higher P and R than the other four baselines. The F will be higher with the higher P and R, and the higher F can indicate the effectiveness of the algorithm. In conclusion, the accuracy rate, recall rate, and comprehensive evaluation index $F1$ of the proposed algorithm are higher than those of the four baselines, which indicates that the improved TextRank algorithm based on upper approximation rough data-deduction is more effective in mental health keyword extraction.

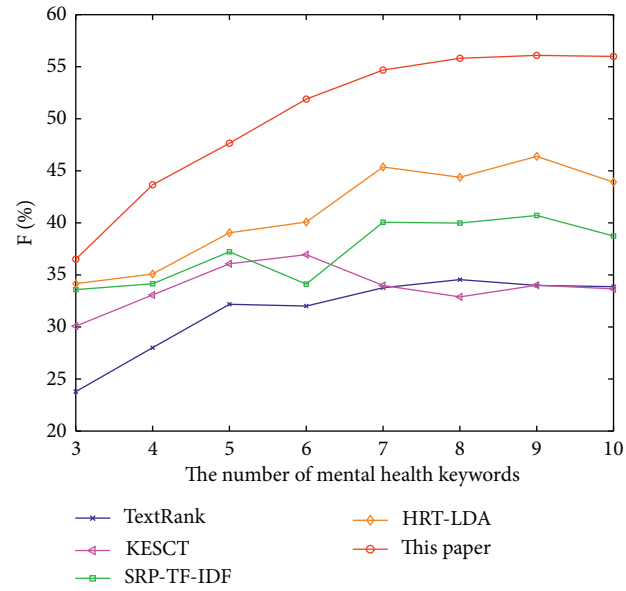

Figure 4: The comparison of F of the five algorithms.

The test set of this paper uses the self-evaluation in the questionnaire of undergraduates' mental health. The text length is generally less than 500 words, which is mainly concentrated in 300–500 words. This paper divides the test set by the number of self-evaluation words. Each test set randomly selects 30 texts of corresponding text words to compare the running time and physical memory occupation of the five algorithms.

As can be seen from Figure 5, when the number of words in the text is 300–400, the number of deduction and semantic calculation is small, and the running time of the algorithm is also short. The number of deduction and semantic calculations increases with the increasing number of words. Compared with TextRank, the running time of the proposed method is still shorter than that of the other three baselines, which is similar to TextRank's efficiency.

It can be seen from Figure 6 that the physical memory occupation of the proposed method is small with good efficiency. When the number of words in the text is 600–800 or 800–1000, the physical memory occupation of SRP-TF-IDF and KESCT is nearly the same.

This paper manages the undergraduates' mental health through the keyword extraction. The results show that academic problem, emotional problem, interpersonal problem, anxiety problem, sexual problem, and adaptation to college life are the universal mental health issues of undergraduates. Currently, how to deal with mental crisis is an urgent problem that colleges cannot avoid. The proposed bounded area elimination algorithm in [30] analyzes the feature extraction, and the idea of feature extraction is similar to the TextRank keyword extraction algorithm proposed in this paper . Timely plan of mental health crisis is to provide supports and help to those who have experienced personal crisis so that they can restore their mental balance and have full confidence in life.

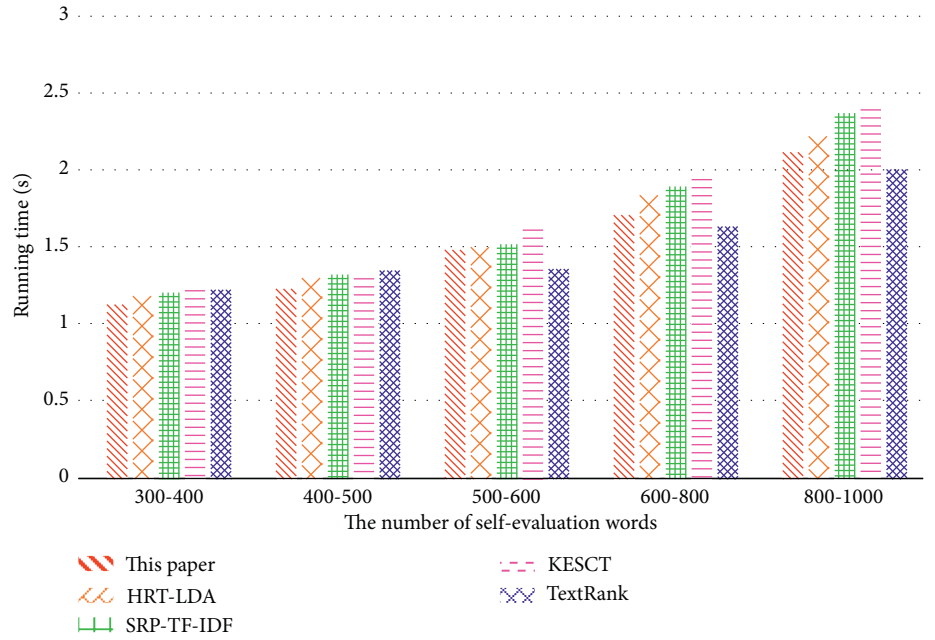

Figure 5: The comparison of running time of keyword extraction algorithms.

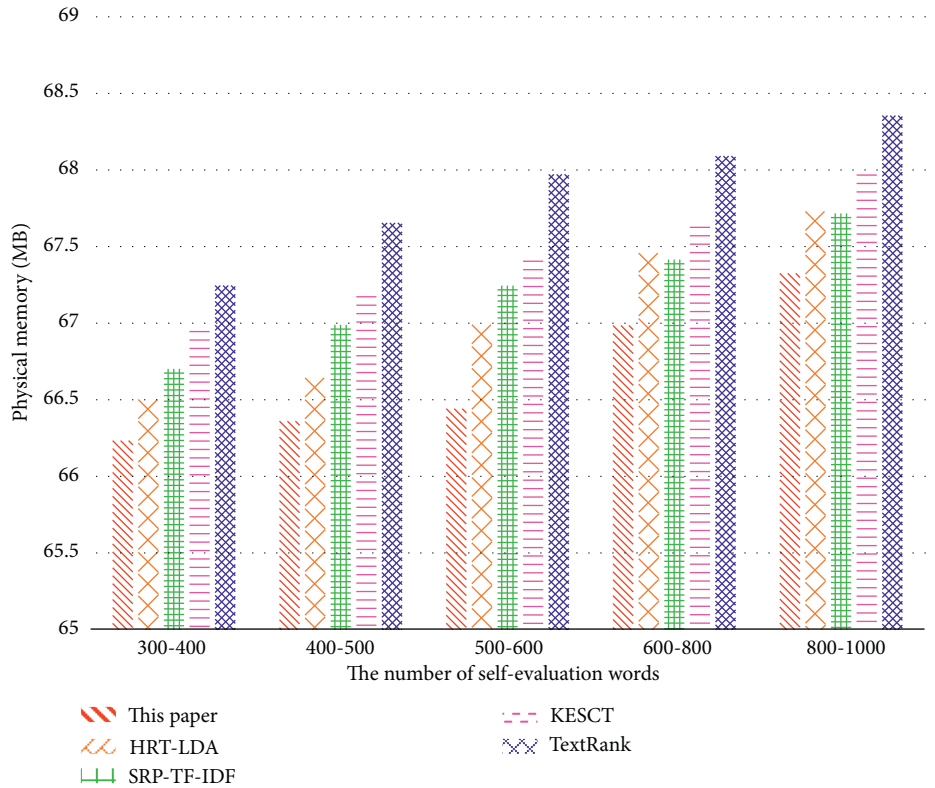

Figure 6: The comparison of physical memory occupation of keyword extraction algorithms.

5. Conclusions

In a fast-paced society, there is more competition among undergraduates, that is, they are facing the dual pressure of enrollment and employment, and mental health is very important for them. Mental health is the necessary condition and foundation for everyone's all-round development in today's society, which is also a necessary psychological quality for undergraduates. This paper introduces upper approximation-based rough data-deduction to TextRank

keyword extraction algorithm, and the extracted keywords are used in undergraduates' mental health management and plan. The comparison experiments reveal that the proposed algorithm outperforms four baselines in terms of accuracy rate, recall rate, $F1$, running time, and physical memory occupation.

The future works are stated as follows. (i) The deduction rules of rough data will be further refined and improved, so as to get better extraction effect. (ii) The words related to mental health may be incomplete in WordNet and Wikitext, which results in unsatisfactory keyword extraction. The following research will consider using a corpus of mental health related to achieve keyword extraction.

Data Availability

All data used to support the findings of the study are included within the article.

Conflicts of Interest

The author declares no conflicts of interest.

References

[1] S. Rosenberg, J. Mendoza, H. Tabatabaei-Jafari, and L. Salvador-Carulla, "International experiences of the active period of COVID-19 - mental health care," *Health Policy and Technology*, vol. 9, no. 4, pp. 503–509, 2020.

[2] S. Johnson, C. Dalton-Locke, N. Vera San Juan et al., "Impact on mental health care and on mental health service users of the COVID-19 pandemic: a mixed methods survey of UK mental health care staff," *Social Psychiatry and Psychiatric Epidemiology*, vol. 56, no. 1, pp. 25–37, 2021.

[3] J. D. Buckner, E. M. Lewis, and R. P. Tucker, "Mental health problems and suicide risk: the impact of acute suicidal affective disturbance," *Archives of Suicide Research*, vol. 24, no. sup1, pp. 303–313, 2020.

[4] M. M. Kibbey, E. J. Fedorenko, and S. G. Farris, "Anxiety, depression, and health anxiety in undergraduate students living in initial US outbreak "hotspot" during COVID-19 pandemic," *Cognitive Behaviour Therapy*, vol. 50, no. 5, pp. 409–421, 2021.

[5] A. Saha, A. Dutta, and R. I. Sifat, "The mental impact of digital divide due to COVID-19 pandemic induced emergency online learning at undergraduate level: evidence from undergraduate students from Dhaka City," *Journal of Affective Disorders*, vol. 294, pp. 170–179, 2021.

[6] N. Firoozeh, A. Nazarenko, F. Alizon, and B Daille, "Keyword extraction: issues and methods," *Natural Language Engineering*, vol. 26, no. 3, pp. 259–291, 2020.

[7] R. Campos, V. Mangaravite, A. Pasquali, A. Jorge, C. Nunes, and A. Jatowt, "Yake! keyword extraction from single documents using multiple local features," *Information Sciences*, vol. 509, pp. 257–289, 2020.

[8] S. Duari and V. Bhatnagar, "sCAKE: semantic connectivity aware keyword extraction," *Information Sciences*, vol. 477, pp. 100–117, 2019.

[9] X. Mao, S. Huang, R. Li, and L. Shen, "Automatic keywords extraction based on co-occurrence and semantic relationships between words," *IEEE Access*, vol. 8, pp. 117528–117538, 2020.

[10] A. K. Bhunia, P. P. Roy, A. Sain, and U. Pal, "Zone-based keyword spotting in Bangla and Devanagari documents," *Multimedia Tools and Applications*, vol. 79, no. 37-38, pp. 27365–27389, 2020.

[11] S. Gibbons, T. Trette-McLean, A. Crandall, J. L. Bingham, C. L. Garn, and J. C. Cox, "Undergraduate students survey their peers on mental health: perspectives and strategies for improving college counseling center outreach," *Journal of American College Health*, vol. 67, no. 6, pp. 580–591, 2019.

[12] J. L. Bourdon, A. A. Moore, E. C. Long, K. S. Kendler, and D. M. Dick, "The relationship between on-campus service utilization and common mental health concerns in undergraduate college students," *Psychological Services*, vol. 17, no. 1, pp. 118–126, 2020.

[13] C. U. Onuoha and E. S. Idemudia, "Academic demands and mental health among undergraduate students in full-time employment: the moderating role of perceived social support," *Journal of Psychology in Africa*, vol. 30, no. 2, pp. 89–95, 2020.

[14] D. Zu, K. Zhai, Y. Qiu, P. Pei, X. Zhu, and D. Han, "The impacts of air pollution on mental health: evidence from the Chinese university students," *International Journal of Environmental Research and Public Health*, vol. 17, no. 18, 2020.

[15] P. Wongchaisuwat, "Automatic keyword extraction using textrank," in *Proceedings of the IEEE 6TH International Conference on Industrial Engineering and Applications (ICIEA)*, pp. 377–381, Tokyo Japan, April 2019.

[16] M. Zhang, X. Li, S. Yue, and L. Yang, "An empirical study of TextRank for keyword extraction," *IEEE Access*, vol. 8, pp. 178849–178858, 2020.

[17] A. Xiong, D. Liu, H. Tian, Z. Liu, P. Yu, and M. Kadoch, "News keyword extraction algorithm based on semantic clustering and word graph model," *Tsinghua Science and Technology*, vol. 26, no. 6, pp. 886–893, 2021.

[18] Z. Wang and Y. Guo, "Sentence-ranking-enhanced keywords extraction from Chinese patents," *Journal of Information Science and Engineering*, vol. 35, no. 3, pp. 651–674, 2019.

[19] L. Yang, K. Li, and H. Huang, "A new network model for extracting text keywords," *Scientometrics*, vol. 116, no. 1, pp. 339–361, 2018.

[20] Q. Qiu, Z. Xie, L. Wu, and W Li, "Geoscience keyphrase extraction algorithm using enhanced word embedding," *Expert Systems with Applications*, vol. 125, pp. 157–169, 2019.

[21] B. Chiraratanasopha, S. Boonbrahm, and T. Theeramunkong, "Effect of term weighting on keyword extraction in hierarchical category structure," *Computing and Informatics*, vol. 40, no. 1, pp. 57–82, 2021.

[22] C.-H. Shih, C.-J. Lin, and S.-Y. Jeng, "Improved rapid automatic keyword extraction for voice-based mechanical arm control," *Sensors and Materials*, vol. 33, no. 8, pp. 2897–2909, 2021.

[23] J.-R. Lin, Z.-Z. Hu, J.-L. Li, and L-M Chen, "Understanding on-site inspection of construction projects based on keyword extraction and topic modeling," *IEEE Access*, vol. 8, pp. 198503–198517, 2020.

[24] P. Carmona and J. L. Castro, "fuzzyfeaturerank. bringing order into fuzzy classifiers through fuzzy expressions," *Fuzzy Sets and Systems*, vol. 401, pp. 78–90, 2020.

[25] L. Ma, S. Cheng, and Y. Shi, "Enhancing learning efficiency of brain storm optimization via orthogonal learning design," *IEEE Transactions on Systems, Man, and Cybernetics: Systems*, vol. 51, no. 11, pp. 6723–6742, 2021.

[26] L. Yung, C. Fei, J. Mandeep, H. Abdullah, and L. Wee, "Synthesis of a nano-silver metal ink for use in thick conductive film fabrication applied on a semiconductor package," *PLoS One*, vol. 9, no. 5, 2014.

[27] M. Bordoloi, P. C. Chatterjee, S. K. Biswas, and B Purkayastha, "Keyword extraction using supervised cumulative textrank," *Multimedia Tools and Applications*, vol. 79, no. 41-42, pp. 31467–31496, 2020.

[28] Z. Wang, D. Wang, and Q. Li, "Keyword extraction from scientific research projects based on SRP-TF-IDF," *Chinese Journal of Electronics*, vol. 30, no. 4, pp. 652–657, 2021.

[29] Y. Zhao, Y. Qiao, and K. He, "A novel tagging augmented LDA model for clustering," *International Journal of Web Services Research*, vol. 16, no. 3, pp. 59–77, 2019.

[30] H. Y. Chai, L. K. Wee, T. T. Swee, S. H. Salleh, and L. Y. Chea, "An artifacts removal post-processing for epiphyseal region-of-interest (EROI) localization in automated bone age assessment (BAA)," *BioMedical Engineering Online*, vol. 10, p. 87, 2011.

Hindawi
Journal of Healthcare Engineering
Volume 2023, Article ID 9875341, 1 page
https://doi.org/10.1155/2023/9875341

Retraction

Retracted: Application of Intelligent Nursing Information System in Emergency Nursing Management

Journal of Healthcare Engineering

Received 17 October 2023; Accepted 17 October 2023; Published 18 October 2023

This article has been retracted by Hindawi following an investigation undertaken by the publisher [1]. This investigation has uncovered evidence of one or more of the following indicators of systematic manipulation of the publication process:

(1) Discrepancies in scope
(2) Discrepancies in the description of the research reported
(3) Discrepancies between the availability of data and the research described
(4) Inappropriate citations
(5) Incoherent, meaningless and/or irrelevant content included in the article
(6) Peer-review manipulation

The presence of these indicators undermines our confidence in the integrity of the article's content and we cannot, therefore, vouch for its reliability. Please note that this notice is intended solely to alert readers that the content of this article is unreliable. We have not investigated whether authors were aware of or involved in the systematic manipulation of the publication process.

In addition, our investigation has also shown that one or more of the following human-subject reporting requirements has not been met in this article: ethical approval by an Institutional Review Board (IRB) committee or equivalent, patient/participant consent to participate, and/or agreement to publish patient/participant details (where relevant).

Wiley and Hindawi regrets that the usual quality checks did not identify these issues before publication and have since put additional measures in place to safeguard research integrity.

We wish to credit our own Research Integrity and Research Publishing teams and anonymous and named external researchers and research integrity experts for contributing to this investigation.

The corresponding author, as the representative of all authors, has been given the opportunity to register their agreement or disagreement to this retraction. We have kept a record of any response received.

References

[1] Q. Li and Y. Chen, "Application of Intelligent Nursing Information System in Emergency Nursing Management," *Journal of Healthcare Engineering*, vol. 2021, Article ID 3998830, 13 pages, 2021.

Hindawi
Journal of Healthcare Engineering
Volume 2021, Article ID 3998830, 13 pages
https://doi.org/10.1155/2021/3998830

Research Article

Application of Intelligent Nursing Information System in Emergency Nursing Management

Qing Li and Yujie Chen

Shengjing Hospital of China Medical University, Shenyang, Liaoning 110022, China

Correspondence should be addressed to Yujie Chen; chenyujie@sj-hospital.org

Received 18 May 2021; Revised 28 June 2021; Accepted 24 July 2021; Published 5 August 2021

Academic Editor: Khin wee Lai

This paper is combined with the intelligent nursing information system to build the emergency nursing platform architecture, from the system emergency procedures, system functionality, network environment deployment, and database design aspects of the discussion. Based on hospital information security, the nursing monitoring system of the intelligent nursing information system is constructed to realize network communication, which is clear and intuitive. The intelligent information system is applied to safety control, medical order information, condition information, and information inquiry, which can save working time and complete the rapid transmission and accurate execution of medical order, making the network communication of medical care more quick and convenient and maximizing the overall efficiency. Based on the disordered phenomenon of registration triage, the Relief algorithm is used to classify the aetiology and triage, and the combination of medical advice, information query, and IT technology is optimized, so as to eliminate the phenomenon of round diagnosis, insert number, and improve the medical environment of waiting for diagnosis, taking medicine, examination, and testing. Finally, through the testing of system information security, information traceability, and rapid information query, the problems in nursing management have been basically solved.

1. Introduction

The rapid development of computer information technology makes nursing management develop into intelligence gradually. Foreign researchers use Internet technology to connect nursing management to the hospital information network so that medical staff can obtain patients' physical signs data remotely. The nursing management system uses information technology to set various parameters in advance. The system can set various parameters in advance, the system can remind the patient to take medicine on time according to the parameters set, and the collection of the patient's signs' data through the Internet can be sent to the terminal, for doctors and family members to view. The social medical service system in China is not perfect. Most patients go to tertiary hospitals regardless of the severity of their illness, which makes the emergency departments of tertiary hospitals overcrowded. When emergency medical resources are inevitably dispersed to noncritical patients, the ability of the entire emergency medical system to treat critically ill patients will decrease. With the increasing workload of emergency departments, manual statistical data and information will be lost to varying degrees, and the preservation, collection, and analysis of emergency medical data lack norms and efficiency. The lack and lag of emergency information management lead to difficulties in the evaluation, monitoring, and analysis of emergency service process, medical quality, workload, and content. Medical information or medical services of digital, network, and information inaction is referred to by computer science and the modern network communication technology and database technology, for each hospital between patients and hospitals between their respective departments to provide information and management information collection, storage, processing, extraction, and data exchange and satisfy the functional requirements of all authorized users. With the

development of wireless information technology, mobile communication technology, and Internet of Things technology, it is possible to effectively preserve and standardize the clinical data of emergency patients through the establishment of an integrated information system before and within the hospital. It has become an urgent problem for the development of the emergency department to strengthen the information construction and the application of nursing management data.

Ang et al. aimed to better apply the nursing information system to nursing management, so as to promote the change of hospital nursing management mode [1]. Jiang proposed the application effect of emergency triage safety management in emergency nursing, effectively improving nursing satisfaction, reducing the incidence of safety accidents, and enhancing the quality of nursing [2]. Al-Fattah et al. proposed to implement the integration of information system platform, prehospital emergency, hospital emergency department, and other emergency procedures seamless; the sharing of medical information of all patients makes the communication between medical care more accurate and timely, optimizes the emergency work process, significantly shortens the rescue time of patients, and saves lives for patients [3]. Yu et al. proposed an intelligent clinical nursing management information system, which can systematically manage the basic work of nurses, monitor the quality of nursing work in real time, record the work of nursing, evaluate the performance of nursing, and so on, meeting the requirements of nursing management normalization [4]. Li et al. introduced an information zed nursing information system in the outpatient department to reduce the treatment congestion in the outpatient and emergency infusion room, improve patients' satisfaction in the clinical nursing process, and reduce the drug depletion rate and the incidence of nursing complaints and errors [5].

The application and development of nursing information system in the process of clinical medicine practice, the comprehensive development path and development needs of modern clinical nursing work in China show the characteristics of close correlation that cannot be ignored, and the prosperity and development of modern clinical nursing practice create and provide support and guarantee conditions that cannot be ignored [6]. Sharing the communication data information module with the primary hospital nursing information system can provide active support for the construction and development of the remote nursing expert system [7]. Nursing theoretical knowledge and practical experience can be shared in different regions and different hospitals, and remote nursing practice assistance guidance can be carried out. This is the sharing of advanced nursing practice experience across the country, enabling the comprehensive skills of daily nursing practice work organization at all levels of primary hospitals to continuously improve, thereby providing solid and sufficient experience and supporting conditions for construction and promotion.

2. Intelligent Emergency Care System

2.1. Intelligent Emergency Procedure. The system software consists of two aspects of database and application software, system database through HIS database related tables, to establish patients primary index, application area table, and orders table, to establish relevant views, and to make nursing system tables associated with HIS data table and data table field be extended, so as to improve the efficiency of the system maintenance and access [8]. The system is developed by using 3-layer B/S architecture. The database is connected by Oracle DBC driver to realize the mutual connection of data. The hospital Intranet enables access to fixed workstations and mobile nursing workstations via the wireless network in the hospital. For other clients such as handheld nursing record terminals, nurse workstations, and mobile ward rounds, the system can be accessed through all compatible browsers except for PDA terminals. The PDA terminal is developed with the template of the Smart Device Cab Project, which can work online or offline. The specific software process is shown in Figure 1.

2.2. Basic Architecture of Intelligent Emergency Care. The intelligent emergency centre applies intelligent information technology to the emergency environment with strict real-time requirements. As the intersection of modern information technology and medicine, the intelligent emergency centre has broad development space and practical value. According to the current situation of the low emergency degree in emergency centres and combined with the urgent and hectic characteristics of emergency medical work, an information project was designed and implemented [9]. Based on the hospital network platform, the layout structure, business process, service management, and quality control of outpatient and emergency departments are optimized in an all-round way, so as to alleviate the pain of patients. In this whole process link to develop the corresponding information system, intelligently building this platform, with platform "all-in-one-card" as the core, it runs through the whole process of prehospital appointment, in-hospital reception and treatment, posttreatment inquiry, and evaluation: making an appointment, self-help leading examining, self-help do card, prepaid phone, registering, clinic queuing howl, outpatient doctor workstation, taking medicine denominated in a queue, auxiliary diagnosis department charge confirmation, blood line up your turn, check the line up your turn, inspection result message booking, inspection report self-service printing, mobile infusion, EICU intensive care, patients self-help query, hospital self-help evaluation system, restructuring the medical treatment process with the implementation point deduction mode, changing the traditional medical treatment mode of outpatient department, realizing the complete sharing of business data, the maximum optimization of the medical treatment process, and the quality supervision of the whole process.

According to the work unit of the emergency centre, the digital system designed eight subsystems, including registration workstation, triage workstation, consulting workstation, emergency room workstation, ICU workstation, doctor workstation in observation ward, nurse workstation in observation ward, infusion room workstation. Registration workstation is to complete the patient's basic

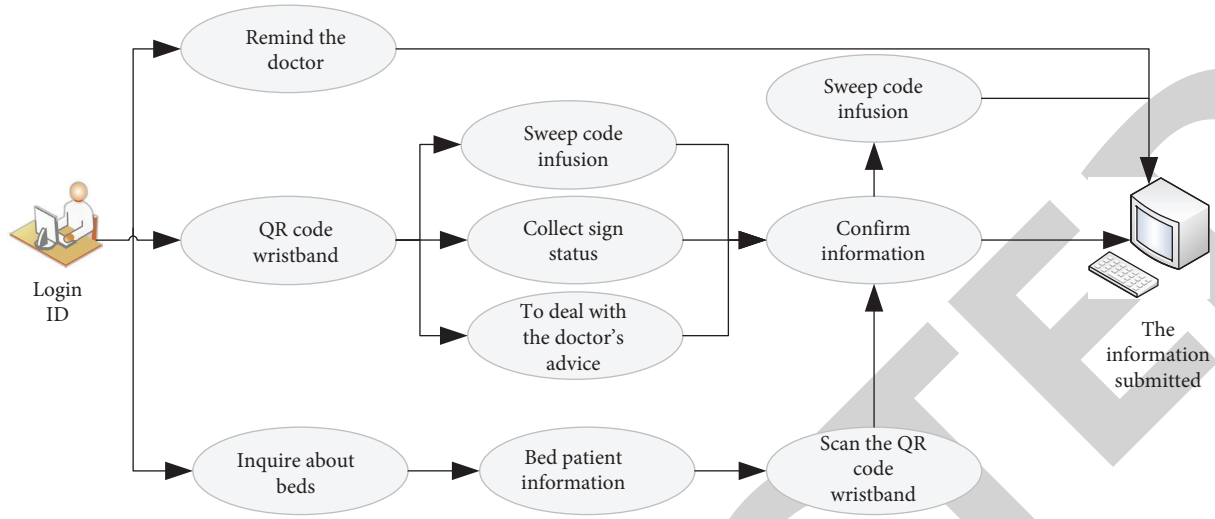

Figure 1: Intelligent emergency procedure.

information entry and registration. The triage workstation will guide the patient to the corresponding consultation room according to the condition. The clinical workstation completes the treatment of very urgent and critically ill patients. According to the particularity of the work of the emergency room, the functions of the emergency room workstation include the management of access to the department, the treatment of medical orders, the documentation of the course of the disease, and the management of expenses, realizing the automatic valuation of medical orders and the automatic generation of various disposal orders. The ICU workstation system is equipped with a nurse station and doctor station, automatically generating special nursing record sheets, physical sign observation sheets, and other nursing medical documents and automatically completing fluid balance calculation, critical score, and other services. According to the patient's postoperative recovery, the best treatment plan was developed. The system also supports research statistics, providing first-hand information for the development of evidence-based medicine and critical care medicine. Under observation ward medical and nursing workstation system based on computer of HIS ward management pattern, design features, setting up beds, patient access management, orders issued, copying and filling in the inspection sheet, checklists, writing electronic medical records, medicine and nursing information of the input, pricing, cost management, nursing information management, information query, and so forth, realize the automatic valuation of medical orders, automatic generation of all kinds of disposal lists, reduce the number of manual duplicate copies of medical orders, reduce the workload of medical staff, and realize bedside record of patients' condition information. Set up patient emergency treatment information, vital signs' information, and other files. Complete relevant information input and inquiry processing of patients in emergency operating room workstation. According to the work requirements of the infusion room, the system is equipped with infusion sheet management and patient call response management to complete the call, input, query, and processing of the patient infusion sheet; generate infusion bottle label and respond to the patient's call and other functions. The basic mechanism diagram is shown in Figure 2.

2.3. Intelligent Nursing Monitoring System Framework. Client application: an intelligent terminal used by medical staff to edit and consult business data through this application, which is the user's actual operation interface. It is mainly composed of two parts: Android terminal and iPad. Application server: sandwiched between the database server and the client application, it plays the role of data exchange, is responsible for the implementation of the business logic of the whole system, can carry on the security authentication and the system upgrade to the client, has the role of connecting the preceding and the following, and is the core key of the whole system. Part of the application server is made up of mature and functional Microsoft IIS. Database server: the lowest level of the system, mainly composed of the existing information system of the hospital, which provides data and updates. His, LIS, and EMR are its main components. The monitoring framework is shown in Figure 3.

2.4. Intelligent Nursing Function. The intelligent nursing system is that nurses use mobile intelligent terminals to scan the barcode of patients' wristbands, accurately identify the identity of patients, input vital signs beside the patient's bed, and write the condition observation, so as to reduce paper transcribing, reduce workload, and improve the accuracy and timeliness of nursing work [10]. Nurses scan the barcode of medicines and check patients' wristbands through handheld smart terminals to avoid medical errors. At the same time, the closed-loop implementation of the doctor's order is achieved, and the traceability problem of the infusion and drug is realized. The mobile nursing subsystem not only ensures the safety of patient diagnosis and treatment but also evaluates the performance of nursing work, guarantees the safety of patients' clinical nursing, improves

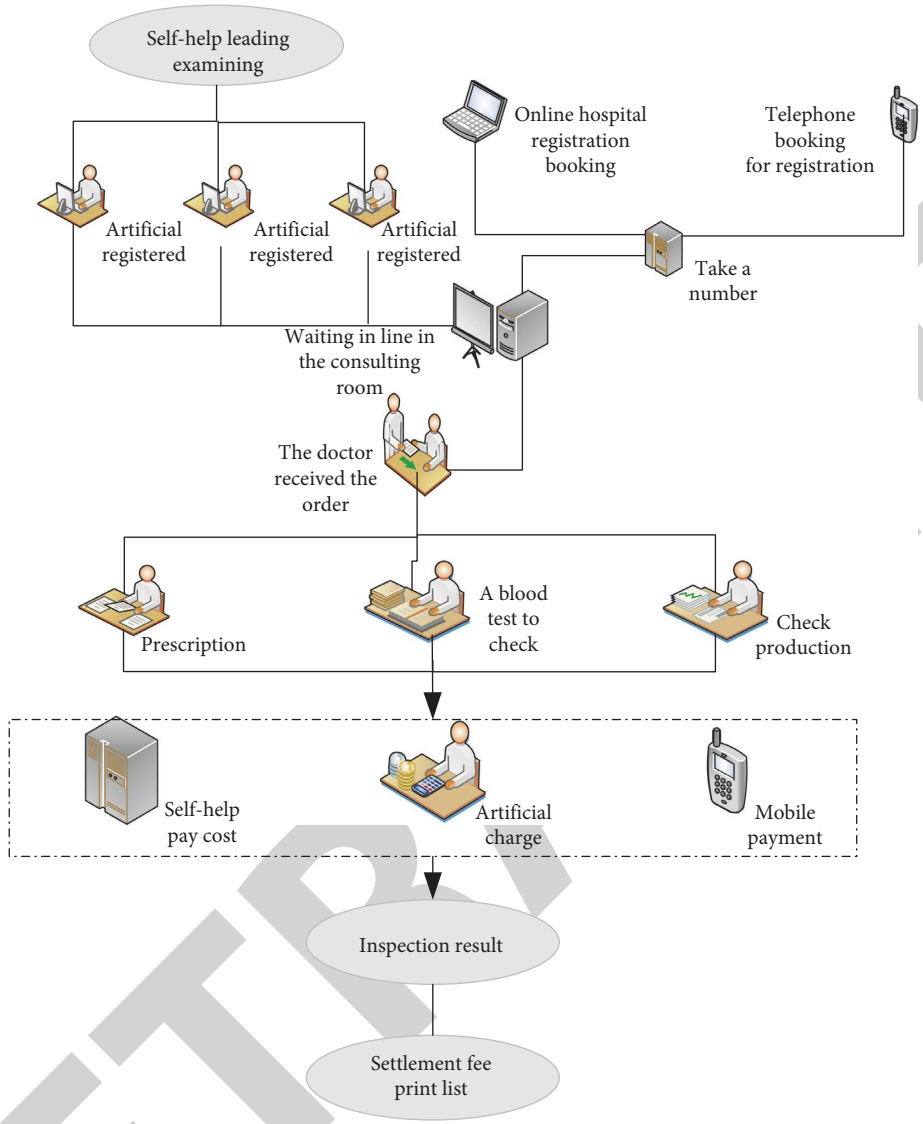

Figure 2: Basic architecture of intelligent emergency care.

the nursing level, and normalizes nursing behaviour [11]. The functional requirements of the intelligent nursing system are shown in Figure 4.

Bulletin board: this interface displays the basic information of the ward of the hospital, such as the number of patients in the ward, the grade of nursing, and the information of critical patients. The key point records at work should be viewed and edited by all nurses in the ward, and the head nurse needs to manage; the ward nurses work in some requirements of the record.

Execution of medical orders: the mobile nursing subsystem is mainly to execute the clinical medical orders and complete the closed-loop operation of medical orders. Entering the doctor's order execution window and scanning the barcode on the patient's wristband, you can view the doctor's order items that the patient has executed and the doctor's order items to be executed. The patient's infusion bottle sticker, drug package barcode, and test tube barcode can be scanned again to complete the closed-loop execution of infusion and medication and test doctor's orders. The barcode of patients' wristbands, drugs, infusion, and test specimens can be matched one-to-one, which not only realizes the traceability of medical orders but also effectively fills the last ten meters of medical workstations and patients' beds.

Nursing evaluation: within 24 hours of admission, nurses need to conduct admission nursing evaluation, fall bed evaluation, and pressure sores nursing evaluation on patients through mobile handheld terminals, so as to understand the basic situation of patients, determine the nursing level of patients, reduce a large number of nurses to copy labour, and improve nursing efficiency.

Nursing records: all nursing services received by patients should be recorded through intelligent terminals, nursing data should be saved, patient nursing data

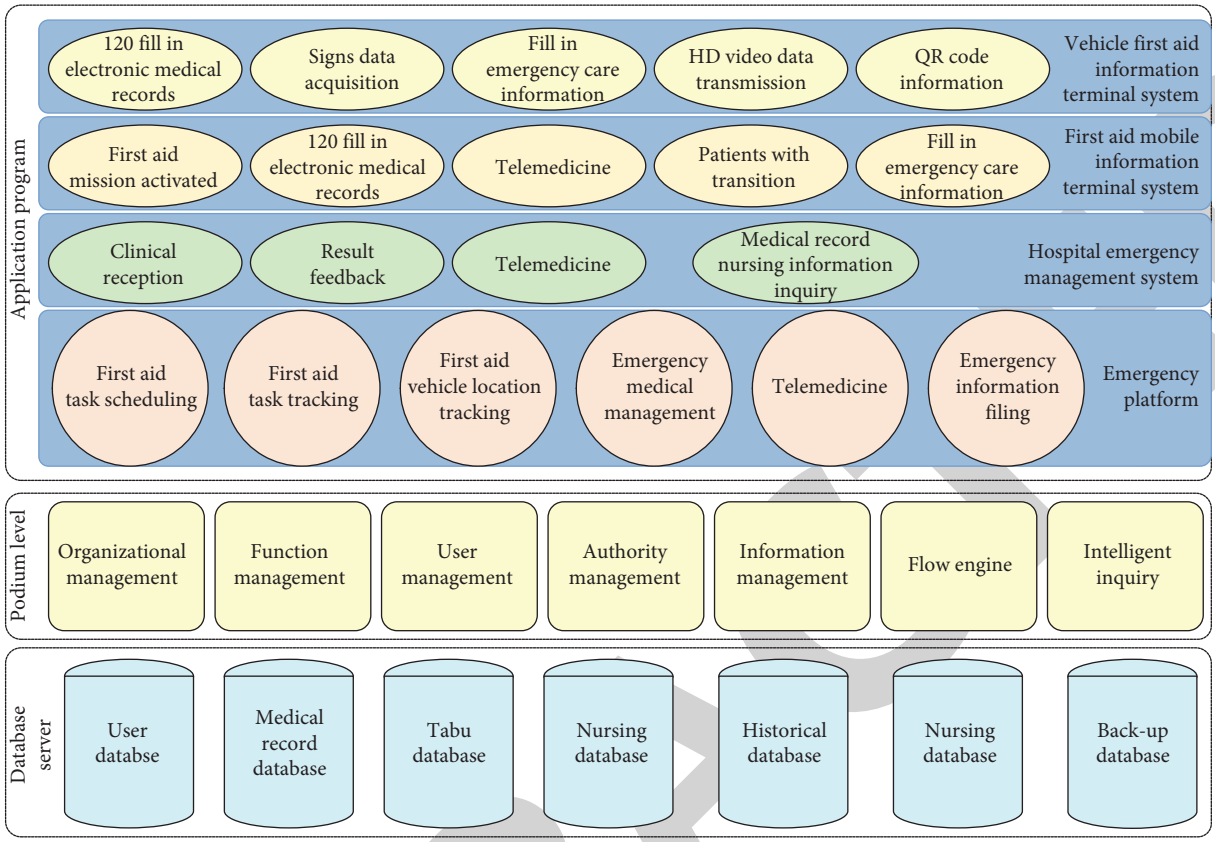

Figure 3: Basic architecture of intelligent nursing monitoring.

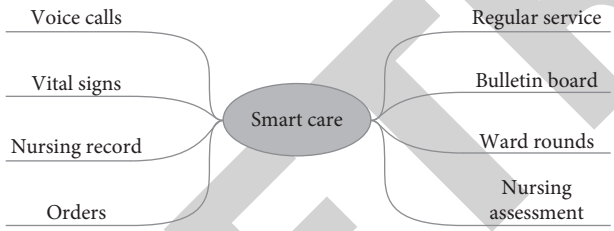

Figure 4: Intelligent nursing function.

should be summarized, effective management of nurse nursing services can be realized, service quality can be improved, and patient satisfaction can be promoted.

Vital signs: the nurse can connect the internal network of the hospital through the intelligent handheld terminal and record the patient's temperature, pulse, respiratory frequency, frequency of urine, and faces beside the patient's bed, which will be synchronized to the hospital database server and sent to the doctor in time to provide a medical diagnosis. At the same time, the system can carry out the batch entry of vital signs and accurate and efficient entry of patients' nursing indicators.

Voice call: when the infusion is about to end in the ward, the patient's family members or patients themselves need to go to the nurse station to remind the nurse that the infusion is about to run out, and the needle can be pulled out or the bottle can be changed. In practice, the information that "infusion is about to end" cannot be conveyed to the treating nurse due to various conditions of the patient. It not only affects the treatment of patients but also has life-threatening risks, and the timeliness of artificial oral replacement cannot be guaranteed. Through the intelligent nursing system, a direct voice call can be made to the current treatment nurse in the ward, informing the responsible nurse in the first time, so that patients can run fewer errands and much information.

Thermometer distribution: at this stage, the patient's temperature is mainly measured through a mercury thermometer, and then the nurse takes back the thermometer and records it. Due to the large number of rooms and patients in the ward, it is often not possible to clearly record the distribution of thermometers. The intelligent nursing system has the function of thermometer management, which records the distribution of the thermometer and reminds the nurse to recover the thermometer after the end of the measurement time, so as to achieve accurate management.

Ward patrol: according to the time required by the standard of graded nursing, the nurse needs to patrol the ward according to the condition and needs of special patients. The mobile nursing system adopts a ward inspection interface, which is convenient for nurses to scan patients' wristbands, conduct ward inspections, record inspection data, and collect them at

the end of the month, so as to realize the assessment of nursing quality.

2.5. Multisystem Integration. Integration is to integrate several small systems with different functions into a large system with multiple functions by using systems engineering theory, so as to give full play to the comprehensive efficiency of the large system [12]. Intelligent emergency centre is an intelligent system with a complex structure that integrates HIS, LIS, PACS, critical care information system, emergency information system, and other functions related to emergency treatment. The system will be doctors and nurses operation process; inspection, application for inspection, and return of results; handling of charge accounting; and department management and other links into the computer management system, to replace the flow of people with information flow, to realize the emergency centre of the flow of people, logistics, capital flow, and other information implementation of decentralized collection, unified management, centralized use, and all the automated mode of sharing, to provide a fast navigation device or interface for medical staff. It is the emphases and difficulties of the research to enable doctors to switch quickly among various systems and apply various information synthetically. System integration is shown in Figure 5.

2.6. System Network Design. In the construction of the mobile medical system, the wireless network is the top priority. Only a scientific overall structure of the wireless network can achieve stable and high-speed data transmission. The ward in the hospital is different from the general conference venue. There are many rooms in the hospital. The room area is large, the walls are thick, the corridor of the department is long and narrow, and there are various cables such as oxygen, circuit, and communication above the ceiling, and the environment is complex. In view of the above special environment and the actual situation of the hospital, wireless controller, wireless switch, and wireless access point are adopted to build the hospital wireless network [13]. The topology of the wireless network is shown in Figure 6.

3. Application of the Intelligent Nursing Information System

3.1. Application and Management of the Intelligent Protest and Triage System. The automatic classification of quantified triage indicators and region-oriented intelligent triage system are based on the quantifiable triage standard system of emergency reexamination and triage, and the intelligent software of emergency reexamination and triage is developed by using computer technology to realize computer-aided reexamination and triage [14]. The intelligent triage system for patients' disease classification mainly takes the symptoms of body parts as the evaluation guide; inputs the patient's name, age, vital signs parameters, pain score, adjustment parameters, and so on the computer; and automatically generates the patient's condition grade. At the same time, a printer is connected to print out the patient's information and grade on red, yellow, and green printed paper and affixed to the patient's medical record. The principle of disease classification and treatment time in our hospital is as follows: red refers to Grade 1 resuscitation or endangered patients, and patients are directly sent to the emergency room in the red zone. The first-grade critically ill patients were rescued immediately and treated within 15 minutes in the red zone or the yellow zone. Level 2 emergency patients: according to the condition, emergency arrangement of priority diagnosis and treatment is generally done within 30 minutes of emergency treatment in the yellow area. Level 3 nonemergency patients are treated sequentially in the green area and treated within 2 hours.

The triage desk is equipped with an auxiliary triage system connected to command platform, which releases the general information of the next emergency patient on the LED display terminal in advance, including gender, age, main illness, departure place, and approximate arrival time; makes full preparations for supplies; and informs the doctor in advance of the layout and equipment of 1 division. At the time of developing the intelligent triage system, the environment of the emergency room was modified to match its function. Three colours of red, yellow, and green represent the three areas in the transformed emergency department, and the background decoration and medical signs in each area are corresponding colours. The red area is the emergency room, the yellow area is the emergency treatment area, adjacent to the emergency room, and the green area is the general treatment area. In addition, red, yellow, and green landmarks are adopted in the emergency area, and the arrow guiding function is clear at a distance. The emergency hall provides TV and wireless network and other services to improve details and humanized services, which to some extent reduces the anxious state of patients waiting for treatment.

Division nursing human resources allocation and management personnel management is mainly for the yellow area, the green area, and the prediagnosis table. Since the general diagnosis and treatment is divided into yellow area and green area, one more itinerant nurse is added to carry out treatment and health education and other services for emergency patients in the yellow area. The other nurse is mainly responsible for the order of the rooms in the yellow area and the green area and the coordination of patient diversion. Due to the use of the new intelligent system, the workload of prediagnosis increased. Two nurses were assigned to the post and the admission system of prediagnosis nurses was established. Only those with certain working experience, clear thinking, and qualified training of the new system could take the post. The prediagnosis nurse makes the correct disease classification, communicates with the itinerant nurse in time, and plays a guiding role in the patient's regional consultation.

3.2. Intelligent Nursing Safety Control Application. Patient safety control is primarily concerned with problematic areas of health care, particularly the identification of patients during the administration of drugs, transfusions, or blood

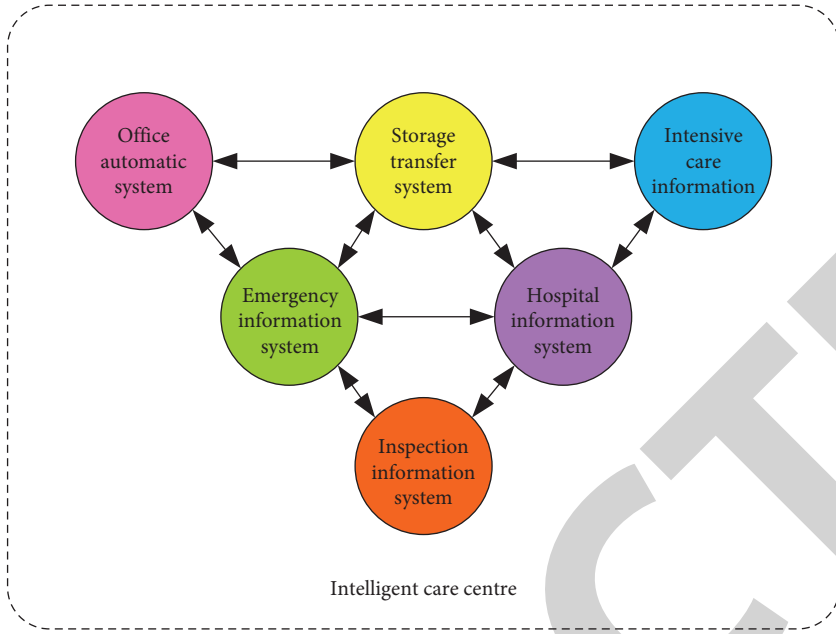

Figure 5: System integration diagram.

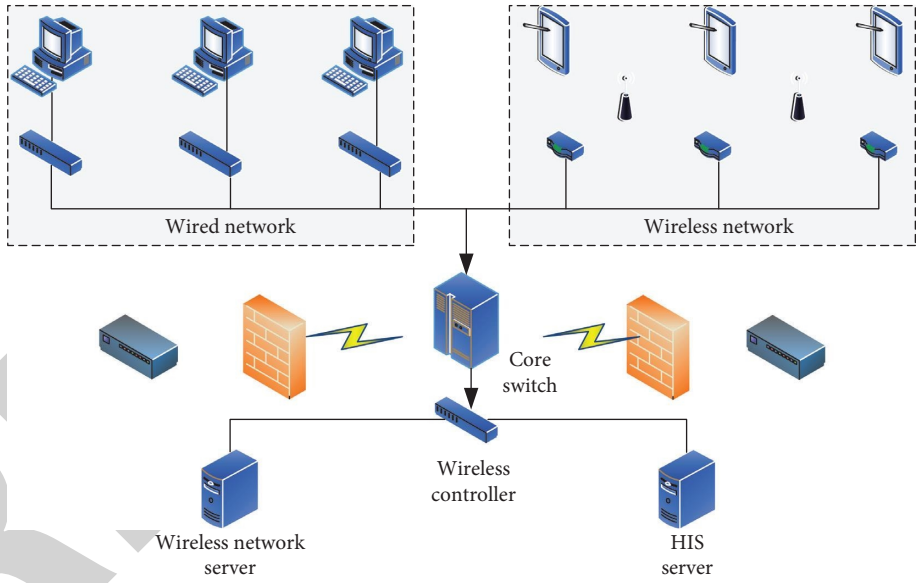

Figure 6: Wireless network topology.

products; the drawing of blood or the testing of other clinical specimens; or the delivery of treatment or procedures. The hospital's compliance with patient safety objectives is regarded as an independent decision item in the review and decision-making process, and the one-vote veto system is implemented. It can be seen that patient safety plays a very important role in the quality of hospital medical service.

At present, barcode technology has been widely used in the system, outpatient and emergency mobile infusion management system, prescription dispensing subsystem, etc., providing a simple and convenient management approach for the safety control of outpatient and emergency patients. A barcode is a mark that expresses a group of information by arranging multiple black bars and blanks with different widths according to certain coding rules [15]. The bar is the part that is less reflective of light, and the empty is the part that is more reflective of light. Barcode technology is born along with the development and application of computer and information technology. It can be converted into binary or decimal information which can be recognized by the computer. It is a new technology integrating coding, printing, identification, and data acquisition and processing. In the process of medical service, the barcode can be used as the identification information and

scanned by the scanning gun to realize the rapid extraction of the corresponding patient information from the database of the computer system. The hospital tests equipment to achieve all online.

The whole inspection process includes barcode label printing, barcode specimen identification processing, report feedback transmission, and self-service query and printing of clinical departments and outpatient and emergency patients. Barcode technology plays an important role in the diagnosis and treatment of outpatient and emergency infusion. In the past, the outpatient and emergency infusion is manually checked by the nurse, the liquid, and the filling of drugs. The nurse checks again and again, which is inefficient and risky. The outpatient mobile infusion management system automatically generates the patient's barcode information by computer and automatically prints two sets of infusion cards with identical information, including the patient's name, gender, age, drug dose, concentration, drip count, time of treatment, and other information. One is given to the patient for scanning at the time of injection, and the other is affixed to the pouch. Before the injection, the nurse uses a handheld computer to scan the barcode of the infusion card on the soft infusion bag. An electronic voice system automatically calls the number, and the patient hears the call and arrives at the puncture table. If the patient's line does not match the barcode of the fluid, the computer will send an alarm to remind the patient not to inject. After the infusion, the palm computer scanning, the patient's total bag of infusion, each bag of drug type, specific time, and infusion process can be clear at a distance, before pulling out the needle to understand the patient's treatment effect, after the confirmation of the end of treatment and then pulling out the needle. The use of barcode can effectively identify the identity of patients and drugs in both directions, which adds a safe defence line for outpatient and emergency infusion management. While optimizing the traditional workflow, it reduces the labour intensity of nurses and improves their work efficiency. The infusion card and bottle label are automatically printed to avoid the hidden danger caused by unclear handwriting by hand, check the infusion drugs with patients, and implement the system of three checks and eight pairs into the monitoring state to ensure the safety of patients' medication and treatment.

3.3. Intelligent Nursing Medical Advice Information Application. After the nurse scans the barcode of the patient's wristband through the intelligent terminal, the patient is identified and the detailed information of the patient is displayed, as well as the content of the doctor's order. According to the type of the doctor's order, the label is divided into infusion book, treatment book, medication book, doctor's order book, new start, and new stop. The nurse can directly click the execute button on the doctor's order information to execute or confirm the execution by scanning the outer package of the drug, the infusion bottle sticker, and the barcode on the test tube. Meanwhile, the system automatically records the executor and the execution time [16]. The diagram of the medical order processing module is shown in Figure 7.

3.4. Intelligent Nursing Letter Observation Application. By observing the patient's mental state, consciousness, and mobility, the nurse writes the nursing assessment sheet, the risk assessment sheet of falling on the bed, and the admission assessment sheet [17]. At the same time, nurses can record nursing and nursing measures in the intelligent terminal and can also save the written content as a template and view the historical nursing data. The module diagram of disease observation is shown in Figure 8.

3.5. Integrated Query Information Module Application. After the nurse logs in the system, the patient is displayed in the form of a label, which contains the patient's name, gender, age, bed number and other basic information. After clicking the label, the detailed information of the patient can be viewed, including diagnostic information, nursing level, allergy drugs, attending physician, and other information. The nurse can also click on the patient's label to see the patient's medical record and examination report, as well as the patient's expense information: advance payment, expense details, and account balance. The comprehensive query module is shown in Figure 9.

4. Debugging and Testing of the Intelligent Nursing System

4.1. Information System Selection Method. Relief algorithm was first proposed by Kara, aiming at two classification problems, and its theoretical basis is as follows: a good feature should make the similar sample of the nearest neighbour characteristic values between the same or similar, and the nearest neighbour value differences between the different classes of samples or difference are very big, therefore giving each feature corresponding weights for sorting; the greater the weight of characteristic, the stronger the feature classification ability; on the contrary, the feature classification ability is weak. By setting the feature weight threshold or the number of feature subsets, the corresponding feature selection can be carried out, and the feature can be evaluated according to the feature's ability to distinguish the close samples. The main idea behind Relief's algorithm is that good features should keep samples of the same class close and samples of different classes away. Assume that the interval is defined as the maximum distance that the decision surface can move without changing the sample classification, which can be expressed as

$$\phi = 11 \times \left(\left|x - y_x\right| - \left|x - h_x\right|\right), \tag{1}$$

where Y_x means similar to x and h_x with x means nonhomogeneous nearest neighbour.

The weight of the update attribute P of sample X can be expressed as

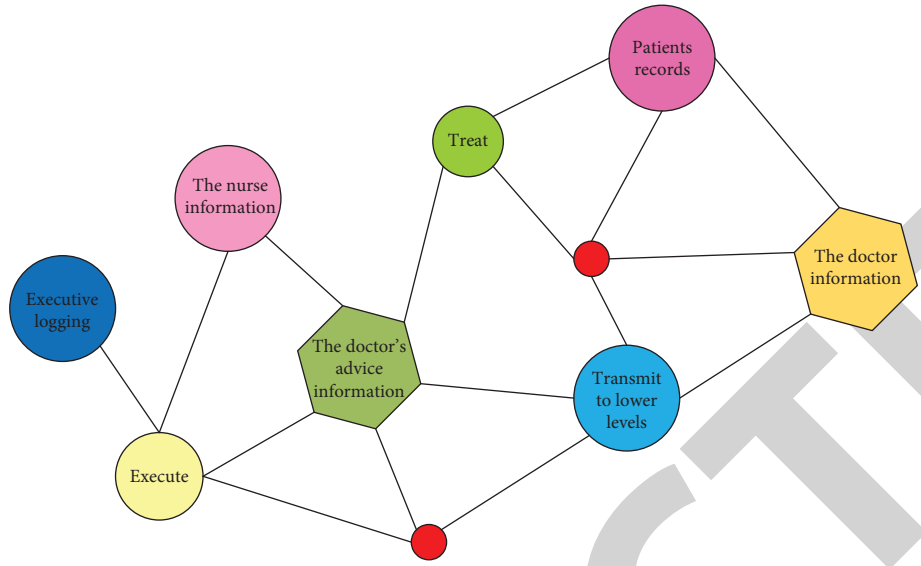

Figure 7: Medical order processing module diagram.

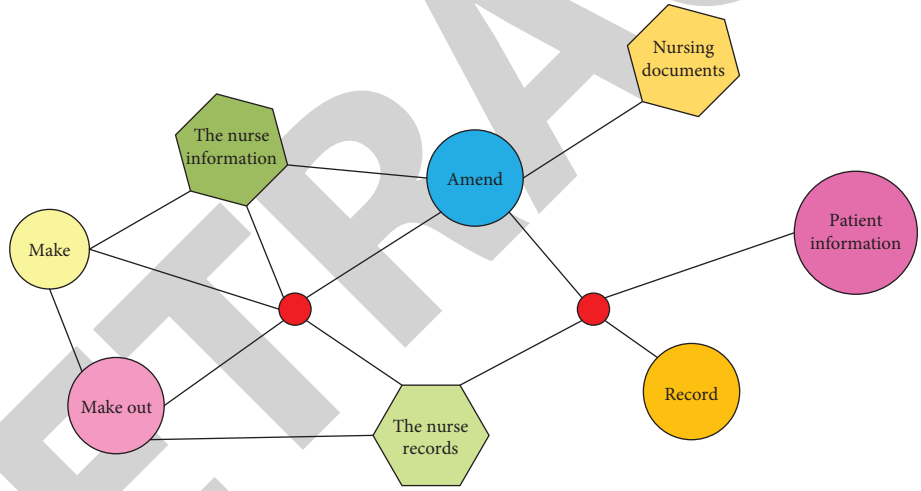

Figure 8: Module diagram of disease observation.

$$W_p^{i+1} = W_p^i - f\{p, x, H_j(x)\} + \frac{P(x)}{1 - P(x)} \times f\{p, x, H_j(x)\} + m. \quad (2)$$

Koromiko extended the Relief algorithm to get the Relief algorithm, which can be applied to multiple sample cases. When dealing with multiclass problems, the Relief algorithm does not uniformly select the nearest neighbour samples from all sample sets of different classes but selects the nearest neighbour samples from each sample set of different classes and selects k nearest neighbour samples. The weight update formula is

$$W_p^{i+1} = W_p^i - \sum_{j=1}^{k} f\{p, x, H_j(x)\} + \sum \frac{P(x)}{1 - P(x)} \cdot \sum_{j=1}^{k} f\{p, x, H_j(x)\} + m \times k. \quad (3)$$

Artificial Fish Swarms Algorithm is a swarm intelligence optimization algorithm based on fish swarm behaviour proposed by domestic scholars Ian Jixi and Li Xiao lei et al. According to the bionic characteristics of fish swarm, it simulates foraging, clustering, and tailgating behaviours of fish swarm by constructing artificial fish [18], so as to realize

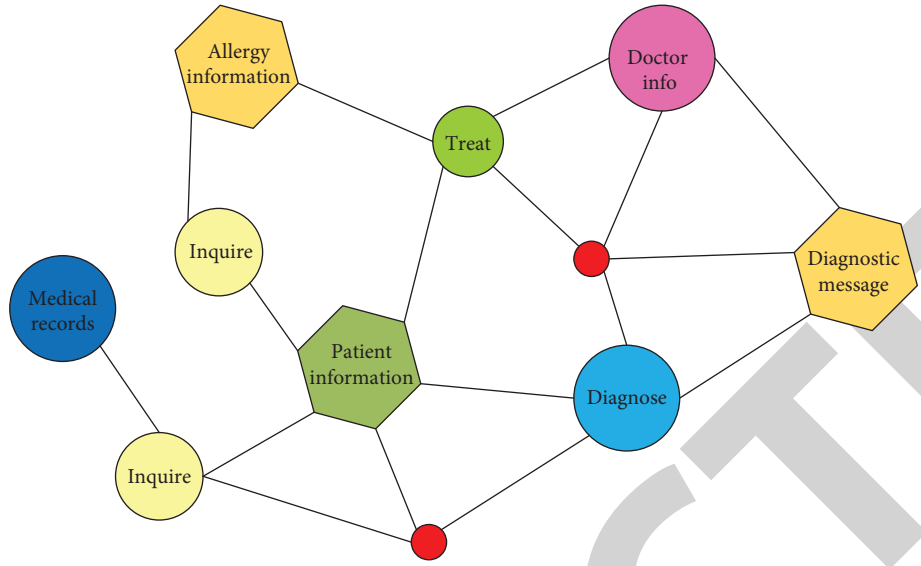

Figure 9: Comprehensive query module diagram.

optimization. Artificial fish include the following behaviours. Foraging behaviour: assume that the current state of the artificial fish is Xi, and select a state x within its field of vision at random. If $Yi < I$, it will move further in this direction; otherwise, it will move one step at random. If the constraint is not satisfied, cut it out:

$$\begin{pmatrix} x_j & \cdots & y_j \\ \vdots & \ddots & \vdots \\ y_{\mathrm{jn}} & \cdots & x_{\mathrm{jn}} \end{pmatrix}. \tag{4}$$

4.2. Intelligent Triage Disease Grading Factors. Patients with acute and critical illness are mainly aged, and by referring to the previous data of researchers, three levels of proportions are summarized, among which patients with grade over 60 years old account for 58.45% of the total number of patients, and patients with grade A only account for 41.55%. It can be seen that the elderly population is typical potential acute patients, and the elderly patients with grade A are the focus group in the dynamic triage process.

The correlation of blood pressure indexes in patients with II grade critical illness was gradually enhanced with the increase of blood pressure, suggesting that blood pressure was of great significance in the recognition of the disease in patients with the normal grade, while there was no significant correlation in patients with the mild or moderate grade. The possible reasons for the correlation were as follows: III grade acute patients with more acute symptoms, but the vital signs are stable, although there is a risk of deterioration, but there is no risk of life-threatening or disability, so the abnormal blood pressure exposure is not obvious; IV grade nonemergency patients mostly have no acute symptoms, and almost no exposure to abnormal blood pressure, or after brief exposure, it can be relieved and disappear after rest.

Breathing and blood oxygen saturation index reaction is a more sensitive index for the human body, breathing >20 times/min, the total number of I~III levels accounted for 89%, and 60.98% were III level; therefore the postoperative respiratory management of critically ill patients directly affects the survival and quality of patients, which is acute and potentially dangerous. Paying close attention to changes in breathing is important for early recognition and correct treatment.

On the basis of preliminary construction of emergency patients nursing difficulty evaluation index system, the results summed up four categories of influencing factors: patient factor, nurse factor, organizational factor, and nursing equipment condition factor. Among the patient factors, 7 factors were extracted, including age, severity of disease, self-care ability, mental and psychological status, social support system, compliance, and expectation [19].

Patient expectation refers to the degree to which patients place their expectations and wishes on medical institutions before treatment, which is mainly reflected in treatment effect, treatment cost, medical service quality, length of hospital stay, and pain in the process of diagnosis and treatment. The influencing factors include individual needs of patients, commitment of medical institutions, medical experience of patients, and severity of diseases [20]. The first-level indicators are broken down as follows: the general condition of patients covers the age and complications of patients. Severity of disease in emergency patients, self-care ability: according to the industry recommended standard published by the National Health and Family Planning Commission Barthes Index Evaluation Table, the evaluation can be divided into four grades, which are, respectively, heavy dependence, moderate dependence, mild dependence, and complete self-care. Mental health status: the Hospital Anxiety and Depression Scale is a self-rating scale [21], including 2 subscales of anxiety and depression, respectively, for 7 questions of anxiety (A) and depression (D). 0–7 are

Table 1: The basic operation tests.

Test project	The test operation	Test result
Inquire	Scan the patient's wristband	Display basic patient information
Signs of entry	Enter the signs and click save	Save record results
Dispense medicines	Click on the dispensing	Prepare medicine as prescribed
Nuclear medicine	Scan the barcode of the infusion	The barcode is the same as the patient
Walk around	Inspect patient information after matching	Record client information after tour
Nursing record	Click on basic care	Display basic care information

asymptomatic; 8–10 are suspicious. 11~21 categories definitely have anxiety. Social and economic status: social and economic status is mainly evaluated by three indicators: social support, economic income, and education level. Compliance: observe the patient's compliance to treatment, nursing, and examination and comprehensively evaluate the patient's overall compliance by asking the patient's doctor in charge and the responsible nurse, which can be divided into five grades: very cooperative, cooperative, basic cooperative, noncooperative, and very noncooperative.

4.3. Test Process and Results. In the completion of the design and coding of intelligent nursing information system, in order to ensure that the software shows fatal functional errors, improve the reliability and efficiency of the implementation of the software. Software validation is required according to software functional requirements. When testing the software, make sure you can deploy the appropriate operating system to the business server and install the basic operation profile and execution file.

In this paper, 20 emergency patients were randomly selected and 5 outstanding nursing staff were selected to complete the basic operation, statistical function, and operational function tests of the software functional modules, and the test results of the functional modules were collected and recorded. The basic operation tests are shown in Table 1.

Ten emergency patients were selected for the test, and the basic operation tests of inquiry, physical sign entry, drug dispensing, nuclear drug, patrol, and nursing records were recorded, respectively. The test results are shown in Figure 10.

In order to verify the reliability of the statistical function of the intelligent emergency information system, the beds, workload, execution status, and reminder of the emergency department of a simulated hospital for one week were tested and entered into the system. The test results are shown in Figure 11.

The sensitivity of the intelligent nursing system to the screening of patients in the emergency was tested, and 20 emergency patients were randomly selected to enter the sign information. The sensitivity is shown in Figure 12.

The basic operation test in this paper mainly includes inquiry, physical sign entry, drug dispensing, nuclear drug, patrol, and nursing record test. The passing rate of basic operation test and system function test of the intelligent nursing system is more than 94%. Simulating the intelligent nursing system and summarizing the test data, the sensitivity of emergency patient screening was 82.22%, and the

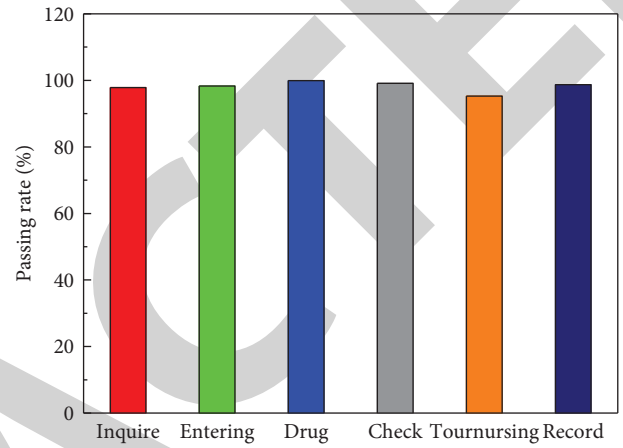

Figure 10: Statistical chart of nurses' basic operation test.

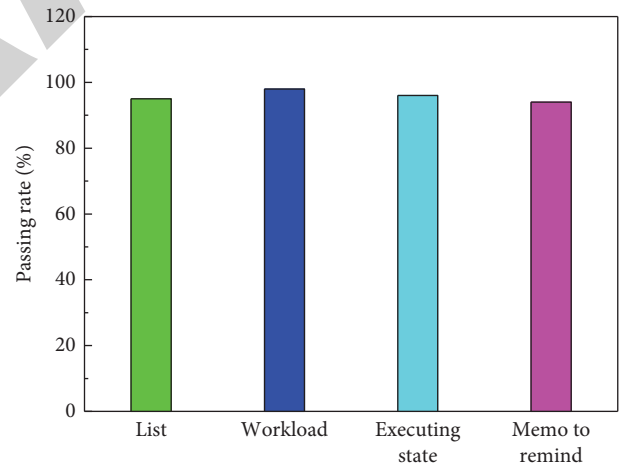

Figure 11: Statistical functional test diagrams.

predictive index was 85.82%, but 90% are not ideal; it may be related to the small sample size in this study; I and II patients only accounted for 25% of the total; the emergency cancer accounts for about 75% therefore, the specific degree as an important evaluation index system, namely, the identification capability of the emergency patients. Calculating system specificity through artificial fish swarm algorithm, the specificity was 94.67%, and the prediction index for nonemergency patients was 91.03%, indicating that the system had a good effect on objective and quantitative identification of nonemergency patients. In the case of limited time and emergency resources, potential risk patients could be found,

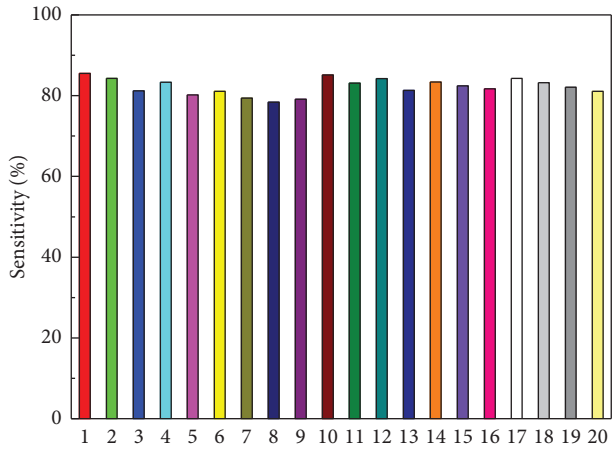

Figure 12: Intelligent recognition level sensitivity map.

so as to ensure the safety of emergency patients and assist triage nurses in making decisions on a reasonable allocation of emergency resources.

5. Conclusion

In this paper, an intelligent information zed nursing system is constructed to realize the information sharing in the whole domain, and intelligent auxiliary diagnosis and treatment information is provided to facilitate nursing inquiries of diagnosis and treatment information, which is of great help to patients' follow-up medical activities such as condition analysis, medical history grasp and supplement, and disease diagnosis. The data information stored completely through barcode intelligent information makes it more convenient for medical staff to collect cases and carry out nursing management. At the same time, nursing management online and bar code information collection, without manual transcription and triage, make nursing management faster, more accurate, and more reliable. This shortens the time for emergency nurses to complete the special care record form and effectively reduces the workload of medical staff. It maximizes the integration and utilization of quality-related information through emergency care terminal services.

Data Availability

Relevant data are available upon request to all authors.

Conflicts of Interest

The authors declare that there are no conflicts of interest.

References

[1] B. Y. Ang, S. W. S. Lam, Y. Pasupathy, and M. E. H. Ong, "Nurse workforce scheduling in the emergency department: a sequential decision support system considering multiple objectives," *Journal of Nursing Management*, vol. 26, no. 4, pp. 432–441, 2018.

[2] G. Y. Jiang, "Application of optimized nursing group management mode in emergency nursing management," *China's health industry*, vol. 16, no. 13, pp. 14-15, 2019.

[3] M. Al-Fattah, "Assessments of the application of nursing process in surgical wards," *Mosul Journal of Nursing*, vol. 7, no. 1, pp. 50–59, 2019.

[4] Y.-F. Li, M. Chao, and C.-T. Shih, "Nurses' intention to resign and avoidance of emergency department violence: a moderated mediation model," *International Emergency Nursing*, vol. 39, pp. 55–61, 2018.

[5] L. Ding and S. K. Hospital, "Application of PDCA management mode in psychiatric emergency nursing management," *China Medicine and Pharmacy*, 2019.

[6] K. Lyell, L. Cone, J. Daniels et al., "The changing epidemiology of autism spectrum disorders," *Annul Rubric Health*, vol. 38, no. 10, pp. 81–102, 2017.

[7] F. Wang, L. Lu, S.-B. Wang et al., "The prevalence of autism spectrum disorders in China: a comprehensive meta-analysis," *International Journal of Biological Sciences*, vol. 14, no. 7, pp. 717–725, 2018.

[8] M. Jung, Y. Too, C. A. Lang et al., "Decreased structural connectivity and resting-stage brain activity in the lateral occipital cortex is associated with social communication deficits in boys with autism spectrum disorder," *NeuroImage*, vol. 19, no. 1, pp. 205–212, 2017.

[9] Y. Saito and Y. Kobayashi, "Percutaneous coronary intervention strategies in patients with acute myocardial infarction and multivessel disease: completeness, timing, lesion assessment, and patient status," *Journal of Cardiology*, vol. 74, no. 2, pp. 95–101, 2019.

[10] G. Kusumoto, K. Shigematsu, K. Iwashita, K. Tominaga, T. Totoki, and K. Yamaura, "Association between preoperative cardiac left ventricular dysfunction and perioperative intraaortic balloon pump in patients undergoing off-pump coronary artery bypass surgery," *The Heart Surgery Forum*, vol. 20, no. 4, pp. 147-148, 2017.

[11] Y. Han, "A treatment strategy for acute myocardial infarction and personal protection for medical staff during the COVID-19 epidemic: the Chinese experience," *European Heart Journal*, vol. 41, no. 23, pp. 2148-2149, 2020.

[12] J. Sensmeier, "Harnessing the power of artificial intelligence," *Nursing Management*, vol. 48, no. 11, pp. 14–19, 2017.

[13] C. K. Lo, H. C. Chen, P. Y. Lee, M. Ku, L. Ogiela, and C. Chuang, "Smart dynamic resource allocation model for patient-driven mobile medical information system using C4. 5 algorithm," *Journal of Electronic Science and Technology*, vol. 17, no. 3, pp. 231–241, 2019.

[14] T. Risling and C. Low, "Advocating for safe, quality and just care: what nursing leaders need to know about artificial intelligence in healthcare delivery," *Canadian Journal of Nursing Leadership*, vol. 32, no. 2, pp. 31–45, 2019.

[15] S. Kang, H. Baek, E. Jung, H. Hwang, and S. Yoo, "Survey on the demand for adoption of Internet of Things (IOT)-based services in hospitals: investigation of nurses' perception in a tertiary university hospital," *Applied Nursing Research*, vol. 47, pp. 18–23, 2019.

[16] F. Cui, L. Ma, G. Hou, Z. Pang, Y. Hou, and L. Li, "Development of smart nursing homes using systems engineering methodologies in industry 4.0," *Enterprise Information Systems*, vol. 14, no. 4, pp. 463–479, 2020.

[17] A. R. Coladonato and M. L. Manning, "Nurse leader emotional intelligence," *Nursing Management*, vol. 48, no. 9, pp. 26–32, 2017.

Hindawi
Journal of Healthcare Engineering
Volume 2021, Article ID 5598077, 12 pages
https://doi.org/10.1155/2021/5598077

Research Article

5G Edge Computing Enabled Directional Data Collection for Medical Community Electronic Health Records

Xiaoqiang Yan [1] **and Xiaogang Ren** [1,2]

[1]*The Affiliated Changshu Hospital of Soochow University (Changshu No. 1 People's Hospital), Jiangsu, 215500 Changshu, Suzhou, China*
[2]*China University of Mining Technology, Jiangsu, 221116 Xuzhou, China*

Correspondence should be addressed to Xiaogang Ren; lb20060005@cumt.edu.cn

Received 2 March 2021; Revised 13 May 2021; Accepted 9 July 2021; Published 23 July 2021

Academic Editor: Khin wee Lai

It is important to promote the development and application of hospital information system, community health service system, etc. However, it is difficult to realize the intercommunication between various information systems because it is not enough to realize the in-depth management of health information. To address these issues, we design the 5G edge computing-assisted architecture for medical community. Then, we formulate the directional data collection (DDC) problem to gather the EMR/HER data from the medical community to minimize the service error under the deadline constraint of data collection deadline. Moreover, we design the data direction prediction algorithm (DDPA) to predict the data collection direction and propose the data collection planning algorithm (DCPA) to minimize the data collecting time cost. Through the numerical simulation experiments, we demonstrate that our proposed algorithms can decrease the total time cost by 62.48% and improve the data quality by 36.47% through the designed system, respectively.

1. Introduction

Recently, the core role of smart medicine is the construction of hospital information platform based on electronic medical records and regional health information platform with resident's electronic health records [1]. Electronic health records [2] can improve the phenomenon of information asymmetry between doctors and patients and satisfy the demand-oriented development of medical service reform. The construction of electronic health records is the focus of future smart medicine [3], which can not only satisfy the diversity requirements of medical and health reform but also accelerate and strengthen the development of information technology in medical and health institutions. Recently, the vigorous development of information technology in China's medical and health industry has given birth to the vigorous development and application of hospital information system (HIS), community health service system (CHSS), and other information systems. However, it is difficult to realize the intercommunication between various information systems because it is not enough to realize the in-depth management of health information.

The National Health Commission of the People's Republic of China [4] is committed to promoting the 5G-assisted medical action project. On the basis of medical and health information, it can promote not only the implementation of hierarchical diagnosis and treatment but also the reform of public medical institutions and public health management mode. Then, 5G-assisted medical care aims to improve the efficiency of medical institutions and integrate high-quality medical resources such as electronic health records (EHRs) [5], overcoming the shortcoming of traditional medical services and enabling patients and improving the upgrading of traditional medical service mode.

The scientific and technological application of medical community [6] electronic health records have been attracting the attention of many researchers and enterprises. Reference [7] compared achievement of and improvement

in quality standards for diabetes at practices using EHRs with those at practices using paper records. Reference [7] examined the effects of electronic health records on the safety of patients in medical facilities. Reference [8] analyzed the costs and benefits of EHRs in six community health centers (CHCs) that serve disadvantaged patients.

However, the above researches do not deeply study the requirements and data characteristics of medical community platform for EHR management. In terms of credibility, reliability, and real-time, it is necessary to deeply study the directional collection mechanism of archival data, such as large-scale mobile terminal sensing under 5G, diversified archival data collection, and archival information sharing under the medical community.

So, there are some major challenges as follows:

(i) The diversity and complexity of medical community seriously restrict the classification efficiency and marking accuracy of medical community electronic health records data, which affects the intelligent management efficiency of EHRs.

(ii) The differences of medical level and service objects between different medical institutions in the medical community make the sharing of electronic records, which is an important basis for specialist collaboration, more complex. The low efficient and precision data sharing will seriously restrict the medical community's ability to solve major diseases, and it is difficult to form a complementary development mode.

(iii) How to accurately and timely collect the data of medical community electronic health record management has become a difficult problem because it is difficult to predict which medical structure will produce what type of electronic health record data at what time.

Our key contributions can be summarized as follows:

(i) We design the 5G edge computing-assisted architecture for medical community.

(ii) We formulate the directional data collection (DDC) problem to gather the EMR/HER data from the medical community with minimizing the service error under the deadline constraint of data collection.

(iii) We design the data direction prediction algorithm (DDPA) to predict the data collection direction and propose the data collection planning algorithm (DCPA) to minimize the data collecting time cost.

(iv) We conduct extensive simulations for the designed system and proposed algorithms. The results show that our proposed algorithms can decrease the total time cost by 62.48% and improve the data quality by 69.95% through the designed system, respectively.

The rest of the paper is organized as follows. We review the state-of-the-art research in Section 2. We design the 5G-assisted edge computing system in Section 3. We present the system model and formulate the DDC problem in Section 4. We design the intelligent data collection scheme with the assistance of random forest for solving the DDC problem in Section 5. We conduct the simulations in Section 6. We conclude this work in Section 7.

2. Related Work

The current situation of medical archives management in the medical community is discussed as follows. Reference [9] found the significant deficiencies in the practice of warfarin management and suggestive evidence that anticoagulation services can partially ameliorate these deficiencies. Reference [10] described a randomized trial of a program to identify and treat depression among high utilizers of general medical care. Reference [11] designed an intelligent archive management system by integrating 5G network and Internet of Things for smart hospitals. Reference [12] used the exome sequencing for infants in intensive care units to determine the diagnostic yield and use of clinical exome sequencing in critically ill infants. Reference [13] proposed a novel drug supply chain management using hyper ledger fabric based on block-chain technology to handle secure drug supply chain records.

About the status of data collection, reference [14] extracted security data that plays an important role in detecting security anomaly toward security measurement. Reference [15] provided a theoretical model of privacy in which data collection requires the consent of consumers who are fully aware of the consequences of consent. Reference [16] considered a scenario where an unmanned aerial vehicle collects data from a set of sensors on a straight line. Reference [17] proposed a low redundancy data collection scheme to reduce the delay as well as energy consumption for monitoring network by using matrix completion technique. Reference [18] proposed a practical framework called *Privacy Protector*, patient privacy-protected data collection, with the objective of preventing these types of attacks.

3. 5G-Assisted Edge Computing System

First of all, according to the requirements of medical community e-health records management, based on the complex environment of regional medical institutions information platform, we design the mathematical model of e-health records management and its 5G application system framework. Secondly, by deploying multiple mobile terminal nodes, we design the medical community electronic health records management 5G architecture, to provide real-time and reliable communication guarantee for large-scale medical community electronic health records data application business. Then, in order to ensure the real-time and reliability of data sharing of medical community electronic health records, a massive data collection mechanism based on edge computing is established. Finally, based on the above requirements, we combine the large-scale mobile communication of 5G with the massive data real-time collection technology of edge computing to study the ap-

plication mechanism of data directional collection, so as to provide the reliability, credibility, and feasibility guarantee for the data update and sharing application of medical community electronic health records management.

According to the requirements of regional medical institutions information platform construction, we analyze the information interconnection and regional differences between community health service centers and municipal hospitals. Then, we introduce edge computing into 5G through the organic allocation and deep integration between the mobile terminals and cloud computing server. The edge computing reasonably allocates the storage, computing, and network services resources between the computing center and the mobile terminals, so as to achieve the local optimal division of labor and cooperation before the network service quality and user experience quality. Therefore, the introduction of edge computing into 5G can satisfy the computing and communication needs of mobile terminals with distributed and random characteristics. Hence, edge computing can well solve the geographical deployment characteristics of 5G nodes scattered between community health service centers and municipal hospitals. Moreover, the edge computing architecture with 5G is shown in Figure 1. Here, the 5G platform is the center, i.e., the municipal hospital, and several subnets of edge community service center are deployed. The network control ability of these center subnets is the same as that of the servers in the platform, where the architecture can effectively reduce the calculation delay and improve the storage efficiency of medical community electronic health record data.

The 5G architecture shown in Figure 1 can provide convenient services, health management services, traditional Chinese medicine (TCM) health care services, and other services. This architecture can give full play to its advantages in data sharing and family doctor follow-up, continuously improve the accessibility and effectiveness of services, comprehensively improve service level and satisfaction, and provide medical services and health management services to the majority of residents conveniently and quickly. At the same time, the medical community platform can solve the following problem, lack of medical resources shortage, difficulty to see a doctor, and realize the integration of health resources and then improve the level of primary health care through the establishment of complete electronic health records for residents. Then, we integrate the sharing of medical records and test results, medical images, medication records, and patients' basic health information between secondary and tertiary comprehensive medical institutions in the community to realize the sharing of high-quality medical resources in the region.

With the rapid development of 5G edge terminals used to collect electronic health records data, how to reasonably allocate and effectively recover the diversity resources of 5G has become a key problem. In 5G environment, the distribution and recovery of resources and the reconstruction of network topology are dynamic. There is an unknown mapping and interference relationship between 5G real-time resource statistics, computing task resource allocation and task scheduling, and 5G network edge computing terminal trusted resource information. These relationships are real-time and random. It is the main goal of network resource management to make 5G system execution efficiency and resource utilization always in the best state. It is well known that 5G supports a large amount of traffic. The resource request queue is very easy to overflow, which makes the arrival rate and processing efficiency of resource request signaling and computing task control signaling between the network control center and the edge terminal irregular, and the reliability of resource allocation and computing task unbalanced among different services. In order to improve the instantaneous resource management level of 5G and the utilization rate of global resources and make 5G better communication support for medical community electronic health records management, we design the 5G edge computing architecture as shown in Figure 2, where we deployed with multiple edge terminals, multiple autonomous base stations, and multiple autonomous control networks.

In Figure 2, edge computing terminals share EHR information and exchange unified standard data sources through regional platform interfaces of medical institutions. According to the edge computing architecture shown in Figure 2, medical institutions improve the interconnection architecture of regional health information platform and guide the electronic medical record system and electronic health record management system of medical institutions under their jurisdiction. In particular, electronic health records need to achieve unified data interface standards of medical institutions, medical insurance, community, and other related systems, so as to facilitate information sharing.

The common data element established in the 5G control center of medical community can efficiently improve the real-time sharing efficiency of electronic medical record (EMR) and EHR. Therefore, the electronic medical records and electronic health records storage system of medical institutions in medical community must follow the standardized description of national public health data element attributes, describe the extracted data element attributes, conduct business modeling, and realize data sharing. Medical institutions at all levels should use the ID number as the main identification code for the transmission and circulation of information in the diagnosis and treatment of public health services in the business system, so as to ensure the effective collection of archival information. Each edge computing terminal server should ensure the validity and timeliness of data transmission, verification, process tracking, and traceability, so as to ensure that all kinds of information can be uploaded to 5G information platform timely, accurately, and comprehensively.

Therefore, how to collect and improve data from the community and medical institutions at all levels in accordance with the electronic medical record information standards and unified specification of disease coding and other important databases, to ensure the quality of data, has become the key of medical community archives management. The process of data collection should have the following properties:

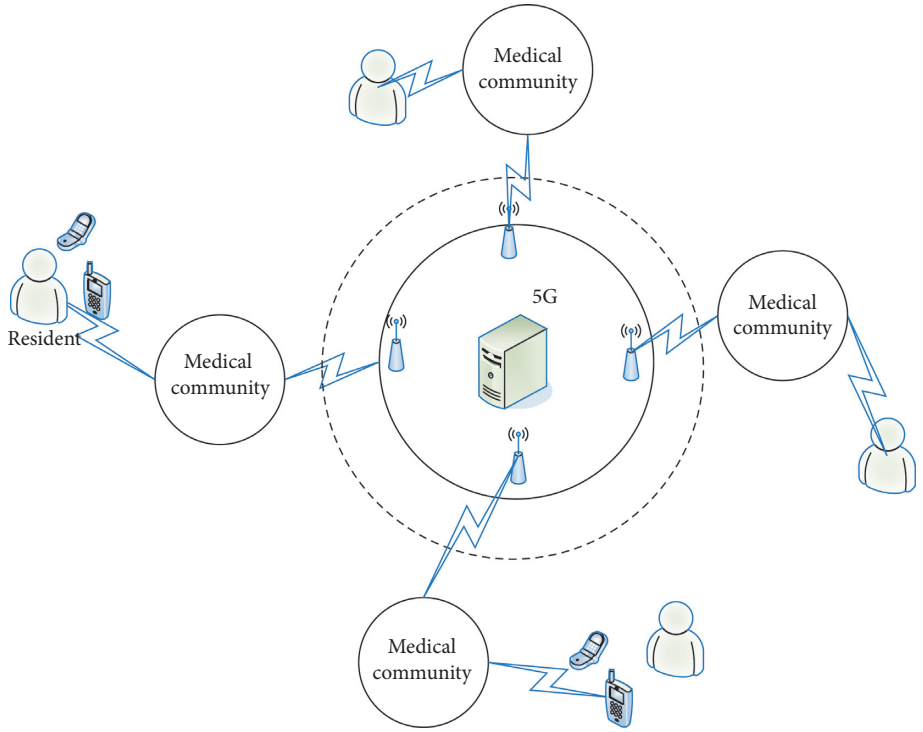

Figure 1: 5G architecture for medical community.

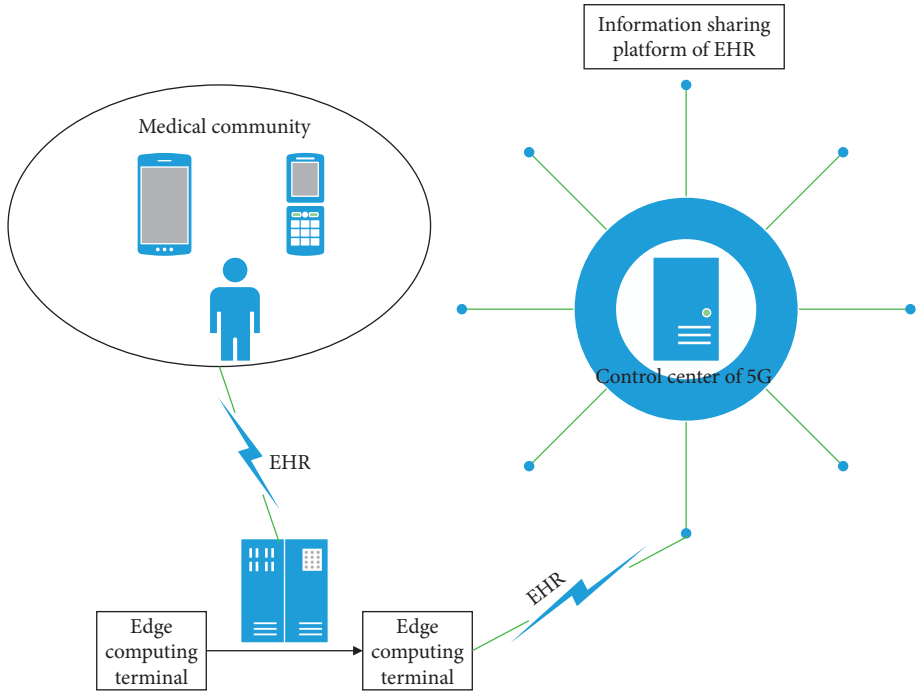

Figure 2: 5G edge computing architecture for medical community.

(i) The process of data collection should be based on the main index of patient identity, correctly associated with the previous diagnosis and treatment data, and form a complete and standardized medical record file, which is convenient for medical staff to use.

(ii) The process of data collection should be carried out according to the interface specification of regional information platform. The diagnosis and treatment information should be uploaded and collected into health records in time.

(iii) The process of data collection should implement the codes of clinical symptoms, diagnosis, surgery, drugs, inspection, and so on released by the state to ensure the standardization and unification of diagnosis and treatment information uploaded to the platform.

Figure 3 gives a toy example for the Directional Data Collection and application of medical community electronic health record with the above characteristics. In this scenario, cloud platform, edge computing terminal, and 5G platform are effectively integrated into the directional data collection of medical community electronic health records, such as community classification, data directional collection, and data storage.

The edge computing procedure is illustrated as follows:

(1) The communities generate their EMR/HER data, which can be collected by a corresponding opportunistically encountered edge computing terminal.

(2) The edge computing terminal analyzes and mines the valid information from collected EMR/HER data, e.g., the location, resident ID, and his/her historical records. Then, the dataset is sent to the cloud servers in real time. The edge computing terminal predicts their medical demand according to the historical records by using the algorithm proposed in Section 4.1 and returns the prediction results to the 5G cloud servers.

(3) The 5G cloud servers periodically compute the data collection route via the algorithms in Section 4.2 for data collection terminal according to the information of communities and residents from edge computing terminals.

(4) The data is collected by the data collection terminal through the route calculated in the above step.

4. Directional Data Collection for Medical Community

4.1. System Model. Suppose that the 5G platform of medical community includes m medical institutions and n communities. According to the scope of service and medical level, the mapping relationship between each community and different medical institutions is established, denoted by $C = \{c_{ij}\}_{i=1,j=1}^{m,n}$. Here, the electronic file data is generated by the medical institutions according to the community it serves, which is used to obtain the medical needs and feedback of residents. Note that each medical institution initiates one data collection task in the time dimension. So, $T = \{t_i\}_{i=1}^{m}$ denotes the task set. For convenience, we define the data collection process as follows.

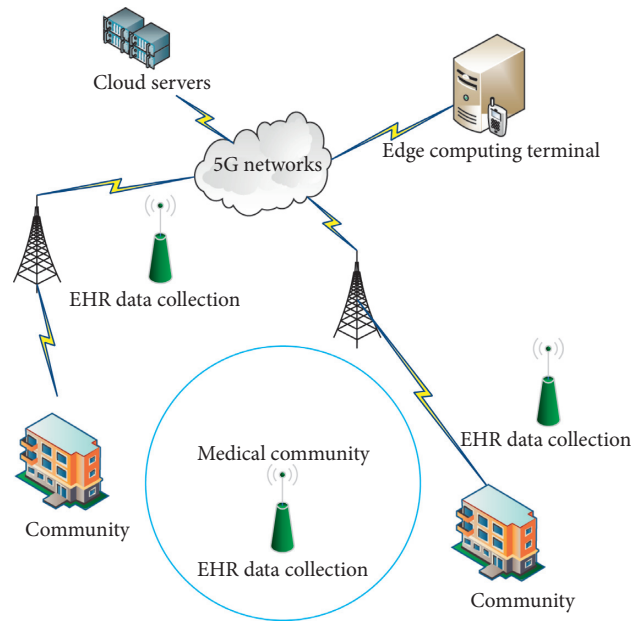

Figure 3: Application of directional data collection with the assistance of 5G and edge computing system.

Definition 1 (data collection task). The process of edge computing terminal completing data collection task is to select the corresponding observation values from a series of candidate data samples corresponding to the community for 5G platform.

For each data collection task t_i, we assume that it has a candidate sample set A_i shown as follows:

$$A_i = \{a_i(1), a_i(2), \ldots, a_i(|A_i|)\}. \quad (1)$$

Then, let $a_i(0)$ denote the optimal data sample corresponding to the task t_i. Therefore, the data error caused by task t_i can be calculated by

$$e_i = \frac{1}{|A_i|}\left(\sum_{k=1}^{|A_i|} a_i(k) - a_i(0)\right). \quad (2)$$

The resident set who provides the EMR/HER dataset from all communities can be represented as follows:

$$B_i = \{b_i^j\}_{j=1}^{n}. \quad (3)$$

Here, b_i^j represents the data in task t_i, which is provided by the j-th community when the i-th task is initiated by i-th medical institution when there is the mapping relationship belonging to C. So, we can calculate the data matrix corresponding to data collection tasks from all communities through the following equation:

$$\begin{aligned} A &= \{a_{ij}\}_{i=1,j=1}^{m,n} \\ &= \prod_{i=1}^{m} (A_i - e_i B_i) \\ &= \prod_{i=1}^{m} \left(\sum_{k=1}^{|A_i|} \int a_i(k)^t \mathrm{d}t - e_i B_i \right) \\ &= \prod_{i=1}^{m} \left(\sum_{k=1}^{|A_i|} \int a_i(k)^t \mathrm{d}t - e_i \sum_{j=1}^{n} b_i^j \right). \end{aligned} \tag{4}$$

Here, we redefine the data sample $a_i(k)$ in A_i as $a_i(k)^t$, which is calculated according to the time dependence of edge computing. Note that we can update the mapping relationship between each community and different medical institutions through the following equation:

$$c_{ij} = \begin{cases} 0, & \text{if } 0 < \dfrac{a_{ij}}{e_i} < \gamma_{ij}, \\ 1, & \text{if } \dfrac{a_{ij}}{e_i} \geq \gamma_{ij}. \end{cases} \tag{5}$$

Here, γ_{ij} is the tolerance threshold of the data collection error, which is a given empirical value.

In order to analyze the direction accuracy of data collection conveniently, we give the following definition of data collection aggregation reliability.

Definition 2 (data collection task). For m data collection tasks and n communities, the direction of data collection is accurate when each task satisfies the following conditions:

(1) The i-th task and j-th community have the mapping relationship, i.e., $c_{ij} = 1$.

(2) A_i and B_i have the same rank for each task t_i.

(3) All the data samples collected by all the medical institutions have consistency; i.e., the following function $f(A)$ is valid:

$$f(A) = \lim_{n \longrightarrow \infty} \frac{\lim_{m \longrightarrow \infty} A}{\sum_{i'=1}^{i} r_i' + \sum_{e \in T_i} t_e}. \tag{6}$$

(4) Let $\Gamma(t_i)$ denote the data collection time cost. The time cost of the i-th task is not larger than the deadline τ_i.

4.2. Problem Formulation. The objective of directional data collection (DDC) problem is to design a data collection scheme based on 5G edge computing system to gather the EMR/HER data from the medical community to minimize the service error under the deadline constraint of data collection. x_{ij} is a binary variable to indicate whether data of task t_i is collected from j-th community. $x_{ij} = 1$ if data of task t_i is collected from j-th community. $x_{ij} = 0$ otherwise.

The DDC problem can be formulated as follows:

$$\begin{aligned} \text{DDC min} \quad & x_{ij} \sum_{i=1}^{m} e_i \\ & \text{(a) } x_{ij} \in \{0,1\}, \qquad \forall t_i \in T; \\ & \text{(b) } r(A_i) = r(B_i), \quad \forall t_i \in T; \\ \text{s.t.} \quad & \text{(c) } \prod_{i=1}^{m} \prod_{j=1}^{n} c_{ij} = 1; \\ & \text{(d) } \Gamma(t_i) \leq \tau_i, \qquad \forall t_i \in T. \end{aligned} \tag{7}$$

Constraint (a) gives the value range of $x_{i,j}$. Constraint (b) ensures that the rank of candidate data sample set is equal to that of data in task t_i on the basis of C. Constraint (c) ensures that each mapping between the task and its corresponding community is valid. Constraint (d) ensures that the time cost of data collection in each task is not larger than its deadline.

We list the frequently used notations in Table 1.

5. Intelligent Data Collection Scheme

In this section, we propose our 5G edge computing enabled directional data collection (5EDDC) algorithm. Then, the detailed description of the proposed algorithm is presented in two phases: data direction prediction and data collection planning.

5.1. Data Direction Prediction Algorithm. Medical behaviors and requirements of residents in different communities actually reflect the regeneration direction of EMR, which contains a lot of medical information, such as common diseases and medical habits. Based on the implementation of a variant of algorithms [19], we design Algorithm 1 for solving the problem of data direction prediction.

First, we predict the medical behavior of residents through the following steps:

Step 1. Feature extraction takes into account the following features for each behavior in community generating along the historical records B_i with the last data collection task t_i and candidate sample set A_i of current medical community: time of day, medical behavior starting time, medical community name and its location, resident ID, and medical treatment time of each location. The above procedure is denoted as function Feature Extraction (dataset).

Step 2. Random forest-based prediction needs the input vector n_t representing the information of a resident, which includes the origin community and destination medical institute, as well as the corresponding extracted features from step 1. Then, the data generating time of any community can be predicted based on temporal

Table 1: Frequently used notations.

Notation	Description
c_{ij}	Mapping relationship between i-th community and j-th different medical institution
C	Set of mappings
t_i	i-th data collection task
T	Set of tasks
A_i	Set of candidate data samples belonging to i-th task
$a_i(k)$	k-th data sample in A_i
$\|A_i\|$	Size of data sample in A_i
$a_i(0)$	Optimal data sample corresponding to task t_i
e_i	Data error caused by task t_i
b_i^j	Data in task t_i provided by the j-th community when the i-th task is initiated by i-th medical institution
B_i	Set of data in task t_i on the basis of C
$a_i(k)^t$	k-th data sample calculated according to the time dependence of edge computing
γ_{ij}	Tolerance threshold of the data collection error between the i-th task and j-th community
$f(A)$	Consistence function
τ_i	Deadline of task t_i

data dependencies and spatial data correlations. The above process is denoted as function Random Forests.

Second, we can predict the data direction of community for collecting data via the Interval-based Historical Average (IHA) [20] as shown in the following equation:

$$\mathrm{IHA}\left(E[t_a], \lambda\right) = \frac{1}{2\lambda + 1} \sum_{p=-\lambda}^{\lambda} \left(\sum_{q=1}^{\mathrm{days}} \left(t_p - E[t_a] - q\right) \right). \quad (8)$$

Here, $E[t_a]$ is the expectation of data generating time of task t_a based on historical EMR/HER data, λ is the mean absolute error of the random forests [21] for data generating time prediction, and days is the days of historical EMR/EHR dataset. t_p is the first data collection starting time after $E[t_a] + q$ in the p-th day of the dataset, where $E[t_a] + q$ is the generating time of EMR/HER data for recording residents in a-th community at the q-th day. Thus, $t_p - E[t_a] - q$ is the historical data collection time on the q-th day. Finally, we calculate the EMR/EHR data generating time of communities and data collection direction of medical community.

In Algorithm 1, the Sink (F, B) function is used to find all the data collection sinks of EMR/EHR at its medical community. In addition, Algorithm 1 updates all the data samples and records between any two communities and computes their collecting time through the following steps:

(1) Find all $\overline{a}_i$, which can satisfy the tolerance

(2) Extract all the features from historical dataset

5.2. Data Collection Planning Algorithm. Based on the direction prediction of data collection, the DDC problem is equivalent to finding a data route to collect the EMR/HER data for all selected medical communities with minimum time cost. The above data collection planning (DCP) problem can be formulated as follows:

$$\mathrm{DCP} \min \sum_{0=1}^{C} \Gamma\left(t_o\right). \quad (9)$$

Moreover, we design the data collection planning algorithm (DCPA) to solve the DCP problem. The basic idea is given as follows (see Algorithm 2):

(1) Transform A_i and integrate into $\widetilde{A}$ (line 5)

(2) Update $\widetilde{B}$ (line 6)

(3) For each element in $\widetilde{B}$, we first divide it into two separate sets P_1 and P_2, and then remove half of elements in $\widetilde{B}$ (lines 8–10), and then find the corresponding subroutes (lines 11–14)

(4) Integrate all the subroutes into the final data collection planning P (lines 15–18) where the symbol $\uplus$ represents the integration of some routes.

6. Numerical Experiments

In this section, we conduct extensive simulations to verify the performance of our proposed algorithms with different number of medical institutions, number of communities, days of month, and number of residents of a community.

6.1. Data Description. The dataset used in our experiments is from the electronic records system of Changshu No. 1 People's Hospital. The dataset shows a kind of representative medical community data. It is generated by the medical community supported by Changshu No. 1 People's Hospital, which covers the period from January 1, 2018, to November 30, 2018. The dataset includes the record data of medical institute and residents, and GPS data of medical institutes. The data record contains various fields, such as time of day, medical behavior starting time, medical community name and its location, resident ID, medical treatment time of each

Input: T, dataset
Output: A, B
(1) **for** $i = 2$ to m **do**
(2) $\quad e_i \longleftarrow (1/|A_i|)(\sum_{k=1}^{|A_i|} a_i(k) - a_i(0))$
(3) $\quad \overline{A}_i \longleftarrow \{\overline{a}_i | \overline{a}_i < e_i\}$;
(4) **for** $j = 1$ to n **do**
(5) $\quad b_i^j \longleftarrow \overline{a}_i(j)$;
(6) **for each** $a \in A$ **do**
(7) $\quad F \longleftarrow$ Feature Extraction (dataset);
(8) $\quad \overline{B} \longleftarrow \text{Sink}(F, B)$;
(9) **for each** $\overline{b} \in \overline{B}$ **do**
(10) $\quad (A, B) \longleftarrow$ Random Forests $(F, \overline{A}, \overline{B})$;

Algorithm 1: Data direction prediction algorithm (DDPA).

Input: A, B
Output: P
(1) count $\longleftarrow 0$; $\widehat{A} \longleftarrow A$; $\widetilde{B} \longleftarrow \varnothing$;
(2) **while** count $\leq \log B - 1$ **do**
(3) $\quad$ **for** $i = 1$ to m **do**
(4) $\quad\quad$ **for** $j = 1$ to n **do**
(5) $\quad\quad\quad \widetilde{A} \longleftarrow \{\widetilde{a}_i(1), \widetilde{a}_i(2), \ldots, \widetilde{a}_i(|A_i|)\}$
(6) $\quad\quad\quad \widetilde{B} \longleftarrow \left\{\widetilde{b}_i^j\right\} \cup \widetilde{B}$;
(7) $\quad$ **for each** $\widetilde{b} \in \widetilde{B}$ **do**
(8) $\quad\quad$ Take $(|\widetilde{B}|/2)$ elements to P_1;
(9) $\quad\quad$ Take another $(|\widetilde{B}|/2)$ elements to P_2;
(10) $\quad\quad$ Remove $(|\widetilde{B}|/2)$ elements from $\widetilde{B}$;
(11) $\quad\quad$ Find subroute p_1^{count} of P_1;
(12) $\quad\quad P_1^{\text{count}} \longleftarrow P_1^{\text{count}} \cup \{p_1^{\text{count}}\}$;
(13) $\quad\quad$ Find subroute p_2^{count} of P_2;
(14) $\quad\quad P_2^{\text{count}} \longleftarrow P_2^{\text{count}} \cup \{p_2^{\text{count}}\}$;
(15) $\quad\quad$ **for each** $p_1 \in P_1$ **do**
(16) $\quad\quad\quad P \longleftarrow P \uplus \{p_1\}$;
(17) $\quad\quad$ **for each** $p_2 \in P_2$ **do**
(18) $\quad\quad\quad P \longleftarrow P \uplus \{p_2\}$;

Algorithm 2: Data Collection Planning Algorithm (DCPA).

location, and the number of patients of the corresponding medical institute, etc. The GPS data contains latitude, longitude, and treatment time of medical institute.

6.2. Simulation Setup and Benchmark. We assume that there are 10 medical institutions to provide medical care for 10 communities, which are supported by Changshu No. 1 People's Hospital. The residents receive medical treatment from the above medical institutions. In our simulation, we evaluate the total time cost of data collection, and data quality calculated by equation (2). All the simulations were run on a cloud server ECS [23] with 12-core Intel Xeon Platinum 8269CY and 48 GB memory. The other parameter settings of our simulations are listed in Table 2.

We develop the data collection algorithm DCA in [22] as the benchmark algorithm for comparison, which can make an efficient tradeoff between the data collection efficiency and energy consumption through the combination of the energy of the emotional device wireless device.

6.3. Performance Evaluation. In this subsection, we evaluate the performance of our algorithms and DCA in the scenario shown in Figure 4. Tables 3 and 4 give the locations of medical institutions and communities in the area, respectively. The above information is calculated based on Google Maps.

Figure 5 shows the prediction errors on two different days, i.e., March 10, 2018, and October 20, 2018. The prediction results demonstrate the effectiveness of our proposed prediction algorithm DDPA. The average prediction error on March 10, 2018, and October 20, 2018, is 3.21% and 1.93%, respectively.

Figures 6 and 7 show the impact of medical institutions on total time cost and data quality of our algorithms and

Figure 4: Medical community for EMR/HER data collection. The red nodes represent locations of medical institutions and the green nodes represent locations of communities.

Table 2: Parameter settings.

Parameter	Value
n	10
m	10
$\|T\|$	10
γ_{ij}	[0.01, 0.05]
τ_i	[1, 10] hours
$\|A_i\|$	[100, 500]

Table 3: Locations of medical institutions.

i	Longitude	Latitude
1	31.629934025445163	120.74572694707317
2	31.637070592885376	120.74498723499269
3	31.641308857555806	120.74260543350061
4	31.644304755694158	120.743120417607
5	31.639559503878488	120.73996684991539
6	31.63350810894618	120.74108193885252
7	31.634421579375328	120.73520253697116
8	31.640051243952147	120.74334217244697
9	31.63600474671818	120.74427558114591
10	31.640862982947134	120.74781351639375

Table 4: Locations of communities.

i	Longitude	Latitude
1	31.633639306384033	120.73640714235745
2	31.635638094098336	120.74413897983557
3	31.64162333734517	120.74648660051481
4	31.638983794798012	120.74880870356253
5	31.641820359193588	120.73842118763615
6	31.63745217402931	120.74375621572658
7	31.643893501251643	120.74744351115115
8	31.63659402090503	120.742072053155
9	31.634475760812066	120.74353931598635
10	31.634834238968633	120.74956147326746

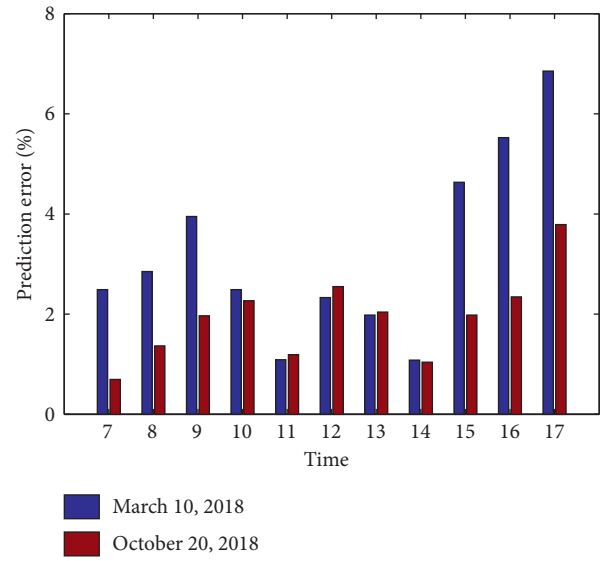

Figure 5: Prediction errors on March 10, 2018, and October 20, 2018.

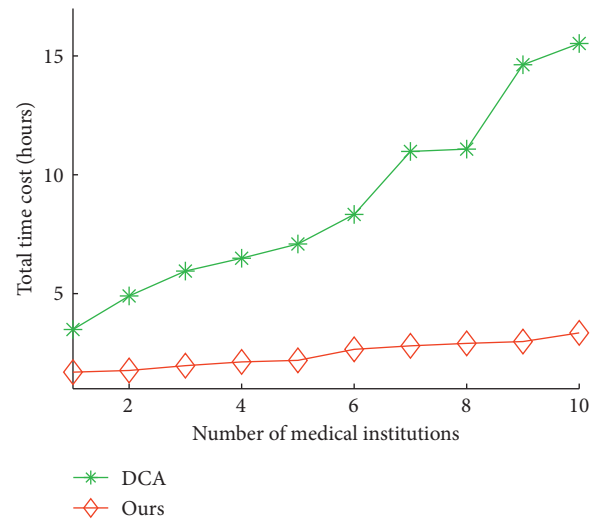

Figure 6: Total time cost vs. number of medical institutions.

DCA, respectively. The average total time cost of our algorithms and DCA is 8.85 hours and 2.44 hours, respectively. The average data quality of our algorithms and DCA is 75.76% and 94.75%, respectively. The results show that our algorithms can reduce 72.38% of total time cost of DCA on average, and improve 25.06% of data quality of DCA, respectively. This indicates that the proposed algorithms significantly outperform DCA. This is because the data quality of our algorithms is better than the those obtained by DCA, respectively.

Figures 8 and 9 show the impact of communities on total time cost and data quality of our algorithms and DCA, respectively. The average total time cost of our algorithms and DCA is 5.75 hours and 1.63 hours, respectively. The average data quality of our algorithms and DCA is 73.27% and 97.59%, respectively. The results show that our

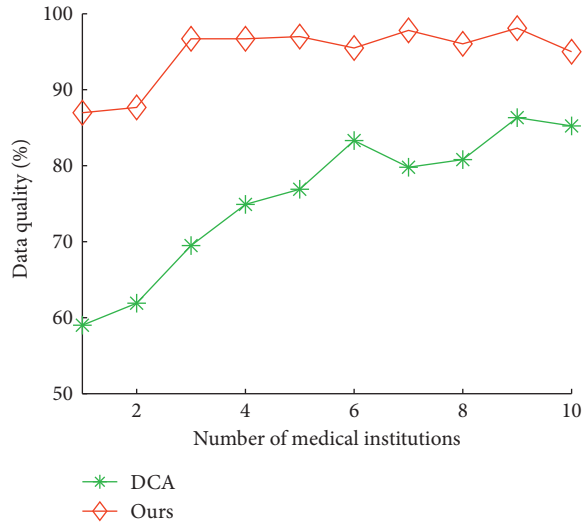

Figure 7: Data quality vs. number of medical institutions.

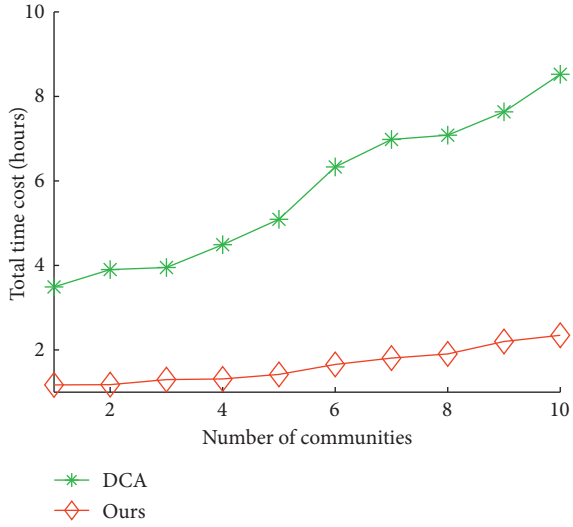

Figure 8: Total time cost vs. number of communities.

algorithms reduces 71.67% of total time cost of DCA on average, and improves 33.20% of data quality of DCA, respectively.

Figures 10 and 11 show the impact of days of month on total time cost and data quality of our algorithms and DCA, respectively. The average total time cost of our algorithms and DCA is 16.15 hours and 9.99 hours, respectively. The average data quality of our algorithms and DCA is 63.31% and 94.01%, respectively. The results show that our algorithms can reduce 38.12% of total time cost of DCA on average, and improve 48.49% of data quality of DCA, respectively.

Figures 12 and 13 show the impact of communities on total time cost and data quality of our algorithms and DCA, respectively. The average total time cost of our algorithms and DCA is 8.92 hours and 2.86 hours, respectively. The average data quality of our algorithms and DCA is 68.44% and 95.21%, respectively. The results show that our

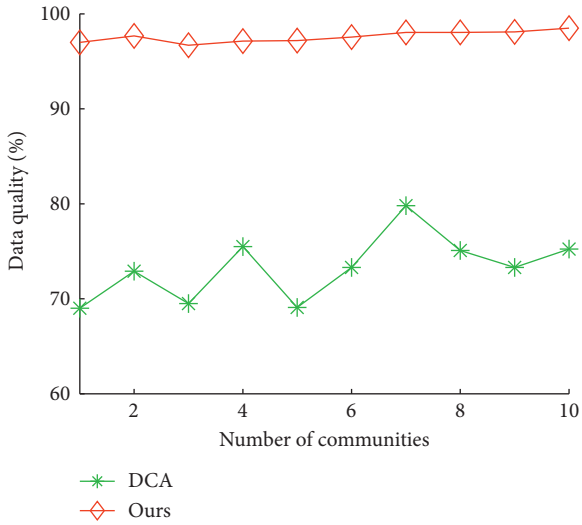

Figure 9: Data quality vs. number of communities.

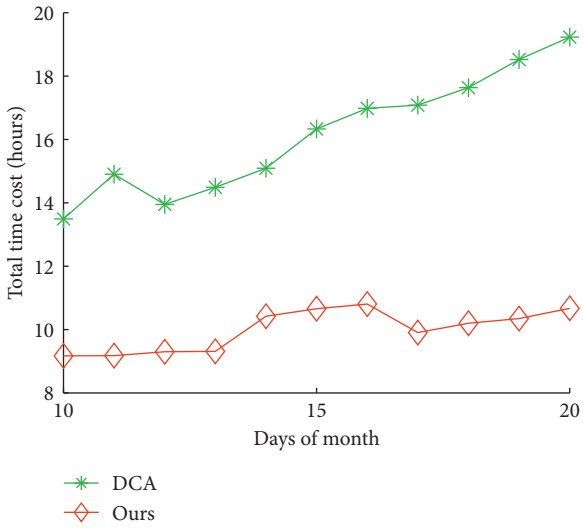

Figure 10: Total time cost vs. days of month.

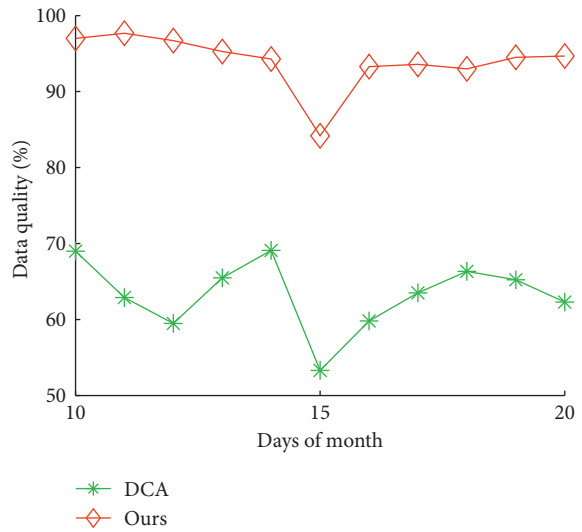

Figure 11: Data quality vs. days of month.

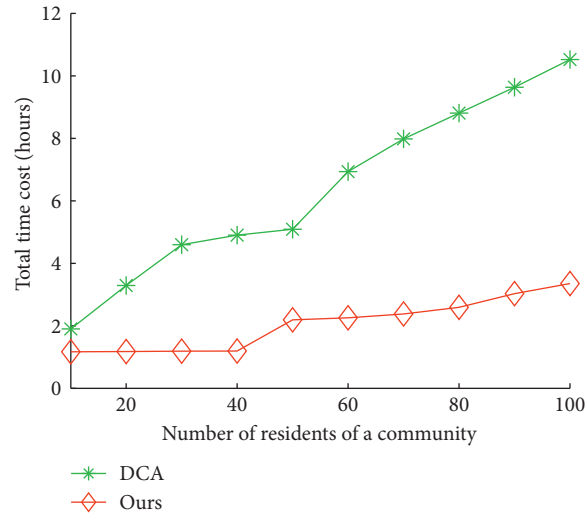

Figure 12: Total time cost vs. number of residents of a community.

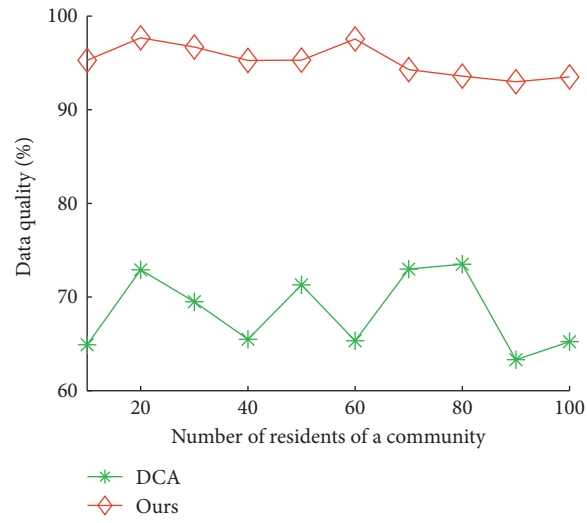

Figure 13: Data quality vs. number of residents of a community.

algorithms can reduce 67.76% of total time cost of DCA on average and improve 39.11% of data quality of DCA, respectively.

Overall, our algorithms can significantly decrease the total time cost and improve the data quality through the designed data direction prediction algorithm and data collection planning algorithm.

7. Conclusion

In this article, we have designed the 5G edge computing architecture for medical community to improve the effectiveness and efficiency of EMR/EHR data collection. First, we formulate the directional data collection (DDC) problem to gather the EMR/HER data from the medical community for minimizing the service error under the deadline constraint of data collection deadline. Second, we design the data direction prediction algorithm (DDPA) to predict the data collection direction, and propose the data collection

planning algorithm (DCPA) to minimize the data collecting time cost. Finally, through the numerical simulation experiments, we demonstrate that our proposed algorithms can decrease the total time cost by 62.48% and improve the data quality by 36.47% through the designed system, respectively.

Data Availability

The labeled dataset used to support the findings of this study is available from the corresponding author upon request.

Conflicts of Interest

The authors declare no conflicts of interest.

References

[1] Z. Liu, C. Bai, H. Yu et al., "An adaptive deep learning model to differentiate syndromes of infectious fever in smart medicine," *Future Generation Computer Systems*, vol. 111, pp. 853–858, 2020.

[2] A. K. Jha, C. M. DesRoches, E. G. Campbell et al., "Use of electronic health records in U.S. hospitals," *New England Journal of Medicine*, vol. 360, no. 16, pp. 1628–1638, 2009.

[3] P. Elanthiraiyan and D. S. Babu, "Smart medicine and physical health system using IoT," *International Journal of Computer Science and Mobile Computing*, vol. 4, no. 3, pp. 333–338, 2015.

[4] National Health Commission of the People's Republic of China, http://www.nhc.gov.cn/.

[5] D. Blumenthal and M. Tavenner, "The "meaningful use" regulation for electronic health records," *New England Journal of Medicine*, vol. 363, no. 6, pp. 501–504, 2010.

[6] F. Mostashari, M. Tripathi, and M. Kendall, "A tale of two large community electronic health record extension projects," *Health Affairs*, vol. 28, no. 2, pp. 345–356, 2009.

[7] M. Z. Hydari, R. Telang, and W. M. Marella, "Electronic health records and patient safety," *Communications of the ACM*, vol. 58, no. 11, pp. 30–32, 2015.

[8] R. H. Miller and C. E. West, "The value of electronic health records in community health centers: policy implications," *Health Affairs*, vol. 26, no. 1, pp. 206–214, 2007.

[9] G. P. Samsa, D. B. Matchar, L. B. Goldstein et al., "Quality of anticoagulation management among patients with atrial fibrillation: results of a review of medical records from 2 communities," *Archives of Internal Medicine*, vol. 160, no. 7, pp. 967–973, 2000.

[10] D. J. Katzelnick, G. E. Simon, S. D. Pearson et al., "Randomized trial of a depression management program in high utilizers of medical care," *Archives of Family Medicine*, vol. 9, no. 4, pp. 345–351, 2000.

[11] F. Qiu, "Hospital archives intelligent management system based on 5G network and internet of things system," *Microprocessors and Microsystems*, vol. 80, Article ID 103564, 2021.

[12] L. Meng, M. Pammi, A. Saronwala et al., "Use of exome sequencing for infants in intensive care units," *JAMA Pediatrics*, vol. 171, no. 12, Article ID e173438, 2017.

[13] F. Jamil, L. Hang, K. Kim, and D. Kim, "A novel medical blockchain model for drug supply chain integrity management in a smart hospital," *Electronics*, vol. 8, no. 5, p. 505, 2019.

[14] H. Xie, Z. Yan, Z. Yao et al., "Data collection for security measurement in wireless sensor networks: a survey," *IEEE Internet of Things Journal*, vol. 6, no. 2, pp. 2205–2224, 2018.

[15] J. P. Choi, D.-S. Jeon, and B.-C. Kim, "Privacy and personal data collection with information externalities," *Journal of Public Economics*, vol. 173, pp. 113–124, 2019.

[16] J. Gong, T.-H. Chang, C. Shen, and X. Chen, "Flight time minimization of UAV for data collection over wireless sensor networks," *IEEE Journal on Selected Areas in Communications*, vol. 36, no. 9, pp. 1942–1954, 2018.

[17] J. Tan, W. Liu, M. Xie et al., "A low redundancy data collection scheme to maximize lifetime using matrix completion technique," *EURASIP Journal on Wireless Communications and Networking*, vol. 2019, no. 1, pp. 1–29, 2019.

[18] E. Luo, M. Z. A. Bhuiyan, G. Wang, M. A. Rahman, J. Wu, and M. Atiquzzaman, "PrivacyProtector: privacy-protected patient data collection in IoT-based healthcare systems," *IEEE Communications Magazine*, vol. 56, no. 2, pp. 163–168, 2018.

[19] Y. Wang, S. T. Xia, Q. Tang, J. Wu, and X. Zhu, "A novel consistent random forest framework: Bernoulli random forests," *IEEE Transactions on Neural Networks and Learning Systems*, vol. 29, no. 8, pp. 3510–3523, 2018.

[20] P. He, G. Jiang, S. Lam et al., "Travel-time prediction of bus journey with multiple bus trips," *IEEE Transactions on Intelligent Transportation Systems*, vol. 20, no. 11, pp. 4192–4205, 2019.

[21] L. Breiman, "Random forests," *Machine Learning*, vol. 45, no. 1, pp. 5–32, 2001.

[22] "Aliyun ECS cloud server," 2021, https://www.aliyun.com/product/ecs.

[23] Y. Jin, Z. Qian, and S. Chen, "Data collection scheme with minimum cost and location of emotional recognition edge devices," *Personal and Ubiquitous Computing*, vol. 23, no. 3-4, pp. 595–606, 2019.

Hindawi
Journal of Healthcare Engineering
Volume 2021, Article ID 1322397, 9 pages
https://doi.org/10.1155/2021/1322397

Research Article

Three-Dimensional Finite Element Analysis of L4-5 Degenerative Lumbar Disc Traction under Different Pushing Heights

Huaili Ding, Lijun Liao, Peichun Yan, Xiaolin Zhao, and Min Li

Fujian Maternity and Children's Hospital, Affiliated Hospital of Fujian Medical University/Fujian Children's Hospital, Fujian Fuzhou 350000, China

Correspondence should be addressed to Xiaolin Zhao; gaojie@fjut.edu.cn and Min Li; limin0322@fjmu.edu.cn

Received 14 May 2021; Accepted 2 July 2021; Published 22 July 2021

Academic Editor: Khin Wee Lai

Objective. To study and analyze the changes of intervertebral foramen height and area of the degenerative L4-5 intervertebral disc under different pushing heights by the finite element method. *Methods*. CT and MRI images of T12-S1 segments were obtained from a healthy volunteer who met the inclusion criteria. A DR machine was used to capture images of the lumbar lateral section before and after simultaneous pushing of the L4 and L5 spinous processes by manipulation called Daogaijinbei, and the measurement showed that the displacement changes of L4 and L5 were both approximately 10 cm, so the pushing height was set at 0–10 cm. A three-dimensional finite element model of the entire normal lumbar spine was established using Mimics 16.0, Geomagic Studio 2014, Hypermesh 13.0, MSC.Patran 2012, and so on. The disc height and nucleus area of the lumbar disc of the normal entire lumbar disc model were adjusted to establish models of the L4-5 disc with mild, moderate, and severe degeneration. Changes of disc height and area of the L4-5 degenerative intervertebral disc under different pushing heights were calculated. *Results*. The size of the L4-5 intervertebral foramen was analyzed from the height and area of the intervertebral foramen, and the results showed the following: (1) as for the normal lumbar disc and a lumbar of the L4-5 disc with mild and moderate degeneration, the height of the L4-5 intervertebral foramen and its area both increased during pushing between 0 and 8 cm. After the pushing height reached 8 cm, the height and area of the L4-5 intervertebral foramen gradually became stable; (2) as for the L4-5 disc with severe degeneration, during the process of pushing, the height and area of the L4-5 intervertebral foramen increased slightly, but this change was not obvious. *Conclusions*. After the spinal manipulation, the sizes of the L4-5 intervertebral foramen of the L4-5 disc with mild and moderate degeneration were significantly larger than those before pushing; in contrast, the size of L4-5 intervertebral foramen of the L4-5 disc with severe lumbar degeneration was not significantly changed.

1. Introduction

Lumbar intervertebral disc degeneration can cause biomechanical changes of the lumbar vertebrae and destroy their mechanical environment, thus resulting in a series of degenerative diseases of the lumbar intervertebral discs. Lumbar disc degeneration is a complex process in which the lumbar spine is affected by a variety of complex factors and changes in stroma composition or stroma state, and it is confluence by lumbar disc aging, biomechanical factors [1–3], nutritional factors [4–6], and so on. The main clinical manifestations of degenerative disease of the lumbar intervertebral discs are lumbago and leg pain, which are mainly caused by extrusion of a nerve root by protrusion after degeneration of the lumbar intervertebral disc. As lots of studies [7, 8] have showed, traditional Chinese massage therapy can effectively treat lumbar intervertebral disc degeneration. In this study, the relationship between the degree of L4-5 intervertebral disc degeneration and the corresponding intervertebral height and area was studied by the finite element analysis under different pushing heights of the traditional Chinese manipulation called Daogaijinbei.

2. Materials and Methods

2.1. Research Object. Creation of a three-dimensional finite element model of the whole normal lumbar and the models of the L4-5 disc with mild, moderate, and severe

degeneration established based on CT and MRI images of the lumbar vertebrae of a healthy male volunteer, aged 26 years, with height 171 cm, weight 60.5 kg, no lumbar spinal stenosis, lumbar spondylolisthesis, or lumbar instability, and no ossification of intervertebral space, posterior longitudinal ligament, ligamentum flavum, vertebral anterior margin hyperplasia, and complex disease is not suitable for the study. The finite element method can simulate the material properties, morphological structure, boundary conditions, and load conditions of lumbar vertebrae in the digital form, observe any parameter that can change the influence on the mechanics of the entire lumbar vertebrae, and can be repeated loading and arbitrary testing. In addition, the research object referred to most literatures was 1 healthy adult, so the research object in this study was 1 healthy adult male volunteer.

2.2. Establishment of a Normal Full Lumbar Finite Element Model. In the imaging department of the affiliated rehabilitation hospital of Fujian University of Traditional Chinese Medicine, a healthy male volunteer was examined by CT imaging. Imaging examination and clinical confirmation showed that the volunteer was in good health, and his lumbar vertebrae were normal. The man voluntarily agreed to participate in the research subject and signed the informed consent form. The study passed the requirements of the hospital ethics committee. Images of the lumbar spine were acquired by CT scanning of T12-S1 segments using a Toshiba Aquilion 16 slice spiral CT, and MRI images were acquired using a Siemens 3.0 T MRI machine to continuously scan the lumbar spine. The scanning data were directly saved in a DICOM (digital imaging and communications in medicine) format. After completion of the lumbar CT and MRI image acquisition, Mimics 16.0, Geomagic Studio 2014, and Hypermesh 13.0 were used to complete the creation of a three-dimensional finite element model of the lumbar spine. After the model was established, MSC.Patran 2012 was used to calculate the size of the L4-5 intervertebral foramen under different pushing heights. Due to the complex range of motion of intervertebral joints, facet joints were not taken into account in this study, and the study was limited to the changes of intervertebral foramen.

The preprocessed CT images were imported into Mimics software, and the mask between the vertebrae was divided by edit masks. Then, the region growing tool was used to establish the vertebral lamina, and the vertebral model was generated from these laminas. Next, the model was filled with cavities and deburred using edit masks to obtain a model of the lumbar vertebrae with a smooth surface. Finally, a 3D model of the entire lumbar spine was generated using Calculate 3D, and the 3D model was postprocessed and meshed. Through the above steps, a finite element mesh model of the whole lumbar region was obtained as shown in Figure 1, and the mesh model of the intervertebral disc is shown in Figures 2 and 3.

Referring to the published literature [9–13], the parameter settings of L1-L5 lumbar vertebrae structural materials are given in Table 1.

3. Establishment of L4-5 Degenerative Disc Models

At present, there is no uniform standard for the specific grade of intervertebral disc degeneration. In this study, referring to the MRI grading standard of the Pfirrmann classification of intervertebral disc degeneration [14] (Table 2) and the Thompson five-level system [15], the process of intervertebral disc degeneration was considered from two aspects: disc height and nucleus pulposus area.

Classes I and II were categorized as a normal lumbar disc, III as mild degeneration, and IV and V as severe degeneration. On the basis of the effective normal three-dimensional finite element model, the degeneration of a lumbar intervertebral disc was simulated by reducing the height of the intervertebral disc and the area of the nucleus pulposus. The L4-5 intervertebral disc mild degeneration model was generated from the normal lumbar disc model by reducing the height by 15% while keeping the nucleus pulposus area unchanged, the moderate L4-5 intervertebral disc degeneration model was obtained by a 33% height reduction and a 67% nucleus pulposus area reduction, and the severe L4-5 intervertebral disc degeneration model was obtained by a 70% height reduction and a 67% nucleus pulposus area reduction.

Based on the above L4-5 intervertebral disc degeneration classification method, the parameters of the normal lumbar model were adjusted to establish whole lumbar models of mild, moderate, and severe degeneration of the L4-5 spine and of the L4-5 intervertebral disc, as shown in Figures 4–12.

3.1. Loading Mechanical Parameters. Lumbar vertebrae account for approximately 13.9% of human bodyweight [16]. The weight of the volunteer used for this model was 60.5 kg, making the weight of lumbar vertebrae approximately 8.41 kg, which is 84.1 N. Meanwhile, considering the pressure between other tissues, this study measured the waist pressure range of the doctor's palm on the subject's waist during the normal performance of lumbar extension with the help of a pressure sensor, and the maximum pressure was 99 N [17]. Thus, for convenience of calculation, the force applied to the L4 and L5 spinous processes was defined as 100 N in the finite element analysis.

The corresponding nodes on the upper surface of vertebral body L1 and the lower surface of vertebral body L5 are restrained by sliding support, and the displacement changes in flexion and extension directions are allowed, while different degrees of displacement are released. Considering the changes in the normal physiological curvature of the lumbar spine, the stress changes of the lumbar spine under different jacking heights were studied.The force is applied perpendicular to the spinous process nodes, and some nodes of L4 and L5 are constrained by releasing different displacement boundaries on the surfaces of L4 and L5 anterior longitudinal ligaments. The lateral sections of the lumbar spine before and after the action of the spinous process of L4 and L5 with the reverse cover were taken with a DR camera, respectively. The safe movement range of the spinous

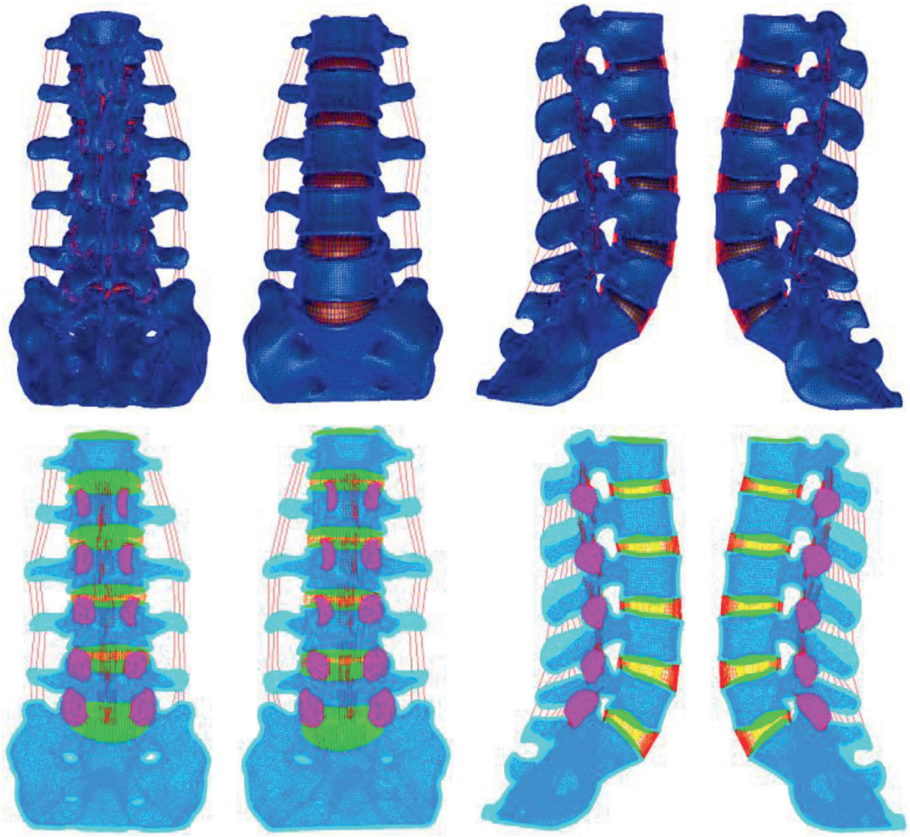

Figure 1: The finite element mesh model of the whole lumbar spine.

Figure 2: Whole lumbar disc mesh model.

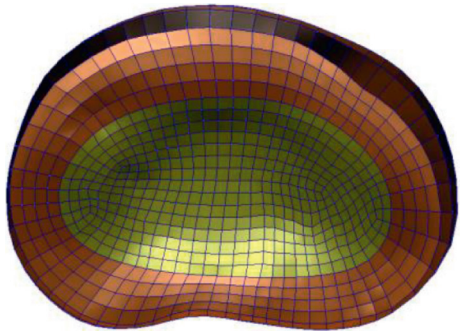

Figure 3: Whole lumbar disc mesh model.

process of L4 and L5 was measured to be 10 cm. After the validity verification of the lumbar model, the mechanical parameters were loaded. The safe range of L4 and L5 lumbar vertebrae was within 10 cm, and the dynamic loading was carried out with 1 cm as the step length.The stress and distribution of each lumbar structure were observed. During the simulation calculation, the specific boundary constraint conditions of the spine manipulation bed simulating the inverted cover method on the whole lumbar spine are shown in Figure 13.

3.2. Calculation Method of Intervertebral Foramen Size. Research [18] shows that the maximum height and area of an intervertebral foramen decrease with the aggravation of intervertebral disc degeneration, while the maximum width of an intervertebral foramen is not affected by intervertebral disc degeneration, and that intervertebral disc degeneration is closely related to the height and area of the intervertebral foramen, and the calculation method used in the model established in this study is shown in Figure 14.

Using the method shown in the figure, we analyzed the changes in the lumbar structure when subjected to the stress of a normal L4-5 intervertebral disc and degenerative L4-5 discs with different degrees of degeneration, under different pushing heights of 0–10 cm. The size of the intervertebral foramen was measured and analyzed in the normal group, mild degeneration group, moderate degeneration group, and severe degeneration group.

Table 1: Structural material parameters of L1-L5 lumbar spine.

Structure	Modulus of elasticity (MPa)	Poisson's ratio
Cortical bone	12000	0.30
Cancellous bone	100	0.20
Endplate	2000	0.20
Back-end structure	3500	0.30
Annulus fibrosus	92	0.45
Annulus fibrosus matrix	4.2	0.45
Nucleus pulposus	1.0	0.499
Anterior longitudinal ligament	7.8	0.30
Posterior longitudinal ligament	10	0.30
Supraspinous/interspinous ligaments	8	0.30
Cystic ligament	15	0.30
Ligamentum flavum	10	0.30
Intertransverse ligament	10	0.30
Facet joint	10	0.30

Table 2: Pfirrmann classification.

Grade	Nucleus pulposus structure	Boundaries of nucleus pulposus and annulus fibrosus	Nucleus pulposus signal intensity	Disc height
I	Uniform, bright white	Clear	High	Normal
II	Uneven, may have horizontal zone	Clear	High	Normal
III	Uneven, gray	Not clear	Medium	Slightly reduced
IV	Uneven, gray to black	Loss	Medium to low	Moderately reduced
V	Uneven, black	Loss	Low	Severely reduced

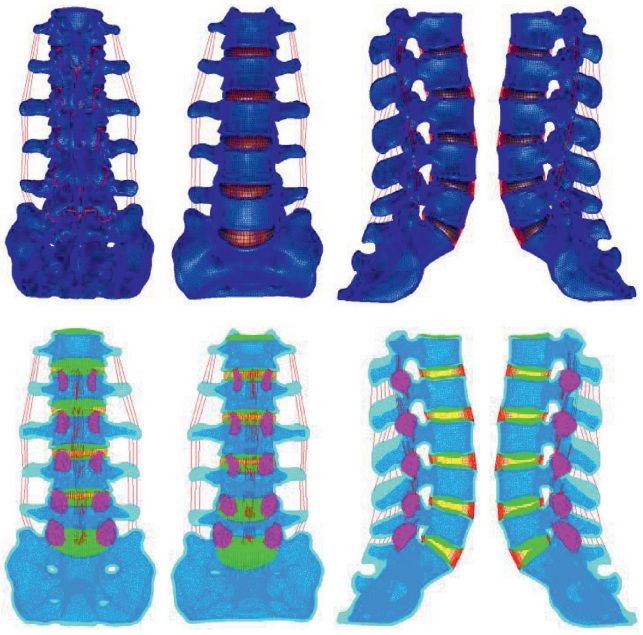

Figure 4: Lumbar model of L4-5 disc mild degeneration.

Figure 5: Whole disc model of L4-5 disc mild degeneration.

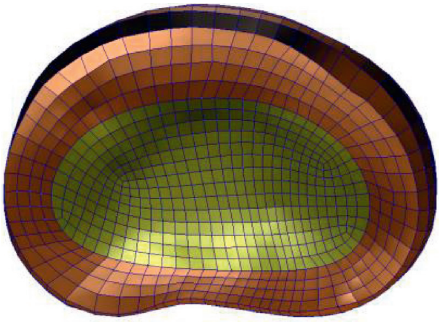

Figure 6: L4-5 disc model with mild.

4. Results

In the normal, mild degeneration, moderate degeneration, and severe degeneration groups, the L4 and L5 spinous processes were pushed up to a height of 0–10 cm, and the finite element experiment was conducted every 1 cm step.

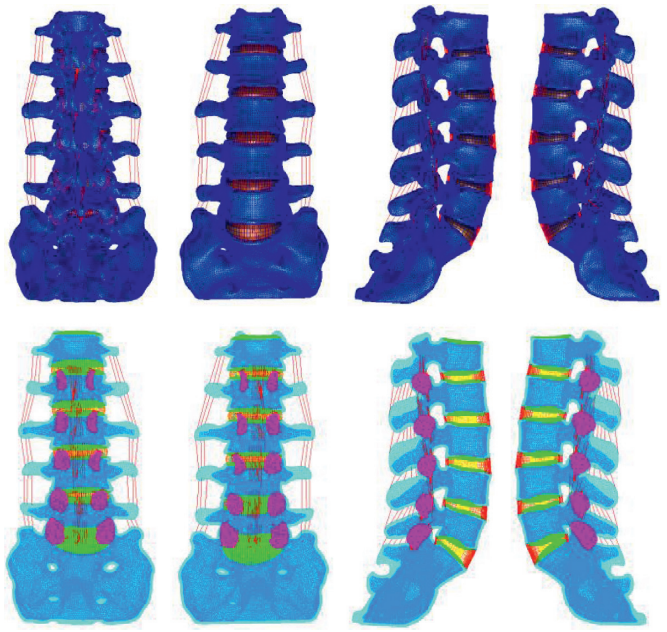

Figure 7: Lumbar model of L4-5 disc moderate degeneration.

Figure 8: Whole disc model of L4-5 disc moderate degeneration.

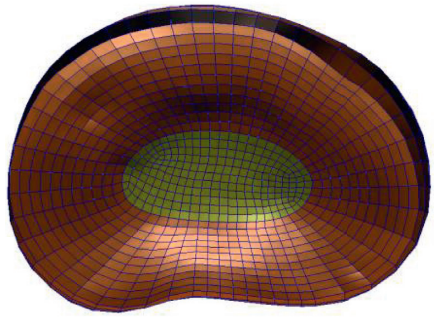

Figure 9: L4-5 disc model with moderate degeneration.

Considering that the L4-L5 structure is relatively symmetrical, the height and area of the intervertebral foramen on the one side were measured. As the results showed, the L4-5 intervertebral foramen heights of a normal lumbar disc and a lumbar of the L4-5 disc with mild and moderate degeneration were 20.1–25.9 mm, 18.4–24.9 mm, 14.5–20.2 mm,

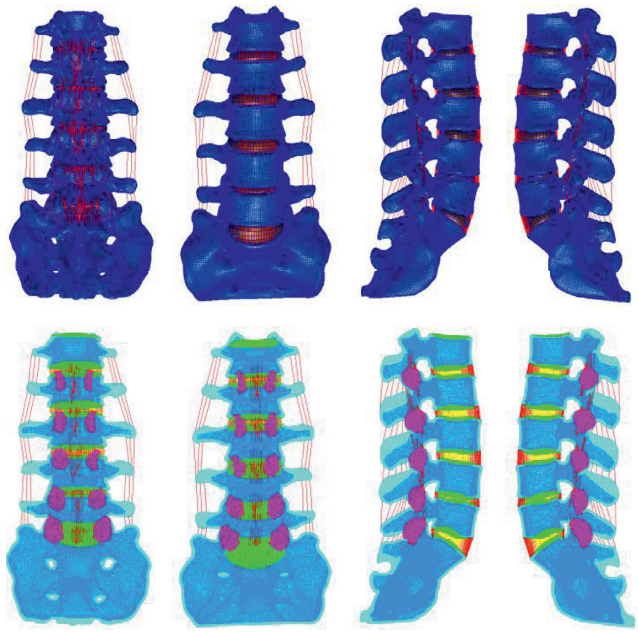

Figure 10: Lumbar model of L4-5 disc severe degeneration.

Figure 11: Whole disc model of L4-5 disc severe degeneration.

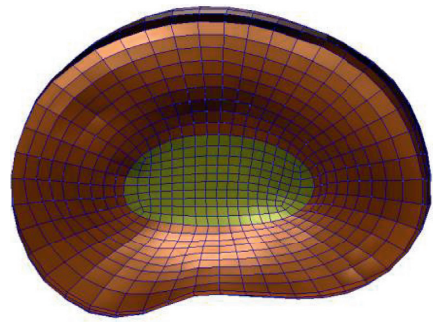

Figure 12: L4-5 disc model with severe degeneration.

respectively, and the areas of the L4-5 intervertebral foramen were 235.2–341.9 mm^2, 199.9–313.3 mm^2, and 166.8–253.6 mm^2, respectively. As for the L4-5 disc with severe degeneration, during the pushing process, the height of the L4-5 intervertebral foramen was 9.1–10.2 mm, and the area was 121.6–154.1 mm^2. The changes during the pushing with different pushing heights are shown in Figure 15.

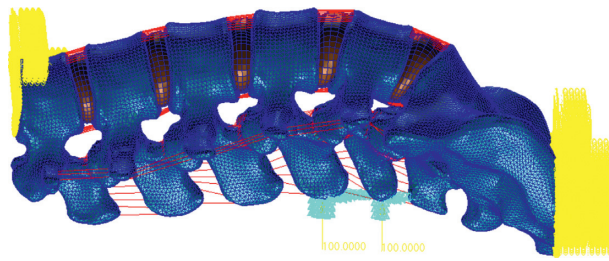

Figure 13: Boundary constraint conditions of the whole lumbar spine.

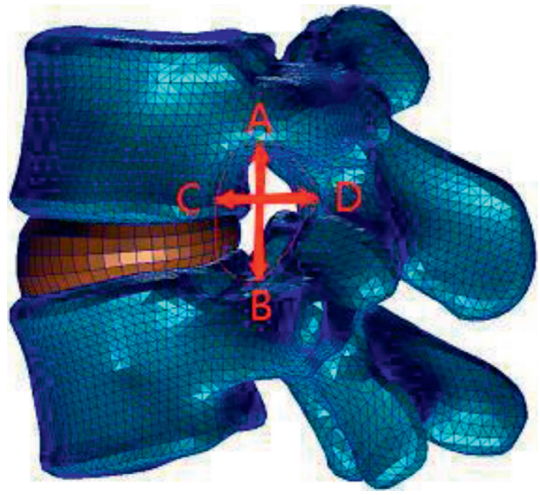

Figure 14: Measurement of intervertebral foramen morphology (height, width, and area) (AB is the height of the intervertebral foramen, CD is the width of the intervertebral foramen, and E is the area around ABCD, the area of the intervertebral foramen).

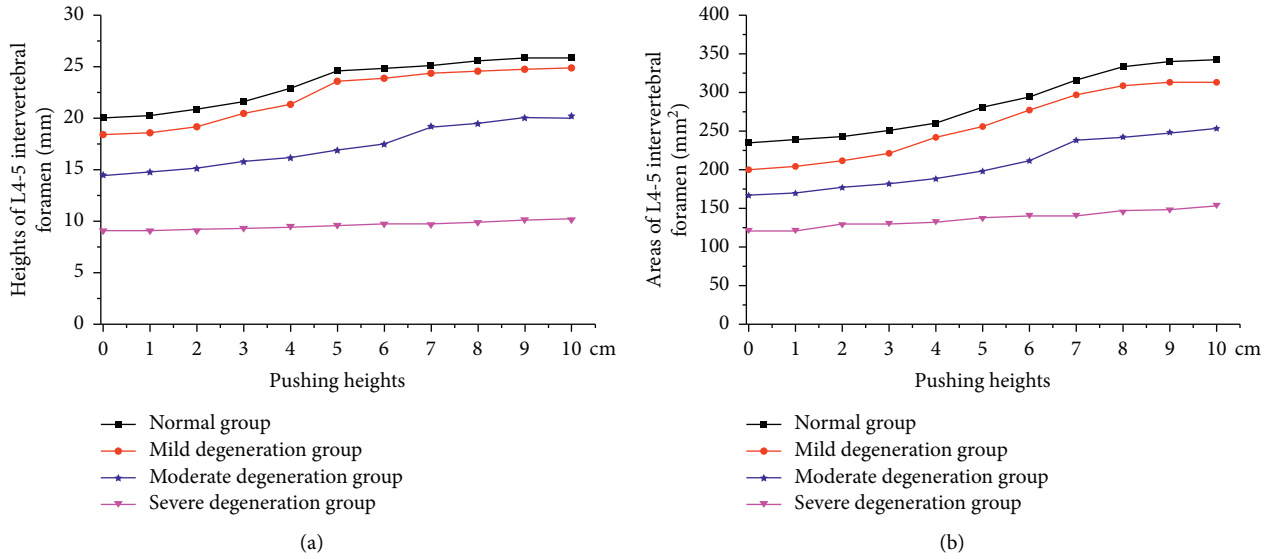

Figure 15: The (a) height and (b) area of L4-5 intervertebral foramen under different pushing heights.

From Figure 15, the heights of the L4-5 intervertebral foramen and its areas of the normal lumbar disc and a lumbar of the L4-5 disc with mild and moderate degeneration both increased when the pushing height is between 0 and 8 cm, and the height and area of the L4-5 intervertebral foramen gradually became stable when the pushing height reached 8 cm or larger; however, the height and area of the L4-5 intervertebral foramen of the L4-5 disc with severe degeneration increased slightly, but this change was not obvious during the pushing.

5. Conclusions

After the spinal manipulation, the sizes of the L4-5 intervertebral foramen of the L4-5 disc with mild and moderate degeneration were significantly larger than those before pushing; in contrast, the size of L4-5 intervertebral foramen of the L4-5 disc with severe lumbar degeneration was not significantly changed.

6. Discussion

The size of the intervertebral foramen is closely related to the normal physiological morphology of spinal nerves and blood vessels, and some studies have shown that intervertebral disc degeneration is closely related to the height and area of the intervertebral foramen [19–22]. In this study, we analyzed the stress changes of the degenerative L4-5 intervertebral disc during pushing to a height of 0–10 cm and also analyzed the height and area of intervertebral foramen in these biomechanical environments. The height and area of the L4-5 foramen in mild, moderate, and severe degeneration of the L4-5 intervertebral disc were smaller than those of the normal lumbar spine when the pushing height was 0 cm, i.e., with no pushing. The height and area of the L4-5 intervertebral foramen decreased with increased L4-5 intervertebral disc degeneration. For the lumbar vertebrae with mild and moderate degeneration of the L4-5 intervertebral disc, the height and area of the L4-5 intervertebral foramen showed a continuously increasing trend when the pushing height was 0–8 cm. When the pushing height was 8–10 cm, the height and area of the L4-5 intervertebral foramen gradually became stable, which indicated that the height and area of the L4-5 intervertebral foramen of mild and moderate degeneration of the L4-5 intervertebral disc could be improved under spinal manipulation, and the height and area of the L4-5 intervertebral foramen tended to remain stable after the pushing height reached 8 cm. For the L4-5 intervertebral disc with severe degeneration, the height and area of L4-5 intervertebral foramen did not increase significantly; therefore, the pushing effect of spinal manipulation did not have a significant effect on the size of the L4-5 intervertebral foramen [23, 24].

Data Availability

The data used to support the findings of this study cannot be shared as no datasets were generated or analyzed during the current study.

Consent

Informed consent was obtained from all individual participants included in the study references.

Conflicts of Interest

The authors declare that there are no conflicts of interest.

Authors' Contributions

Huaili Ding and Lijun Liao contributed equally to the article.

Acknowledgments

The authors acknowledge the Research and Development of Spinal Draft Bed, Science and Technology Program of Fujian Province (2018Y4006), 2018.4-2022.4, Biomechanical Mechanism Analysis of the Treatment of Lumbar Intervertebral Disc Herniation by "DaoGaiJinBei" Manipulation in South Shaolin, Project of Fujian Maternity and Child Health Hospital (YCXB20-03), 2020.12.01-2023.11.30, and the Mechanism of "Liu's Acupuncture" in the Treatment of Autism Model Rats Based on mTOR Signaling Pathway, Project of Fujian Maternity and Child Health Hospital (YCXM20-17), 2020.12.01-2023.11.30.

References

[1] F. M. K. Williams and P. N. Sambrook, "Neck and back pain and intervertebral disc degeneration: R," *Best Practice & Research Clinical Rheumatology*, vol. 25, no. 1, pp. 69–79, 2011.

[2] C. A. Ranson, R. W. Kerslake, A. F. Burnett, M. E. Batt, and S. Abdi, "Magnetic resonance imaging of the lumbar spine in asymptomatic professional fast bowlers in cricket," *Journal of Bone and Joint Surgery British Volume*, vol. 87-B, no. 8, pp. 1111–1116, 2005.

[3] G. Cinotti, C. D. Rocca, S. Romeo, F. Vittur, R. Toffanin, and G. Trasimeni, "Degenerative changes of porcine intervertebral disc induced by vertebral endplate injuries," *Spine*, vol. 30, no. 2, pp. 174–180, 2005.

[4] J. Niinimäki, A. Korkiakoski, O. Parviainen et al., "Association of lumbar artery narrowing, degenerative changes in disc and endplate and apparent diffusion in disc on postcontrast enhancement of lumbar intervertebral disc," *Magnetic Resonance Materials in Physics, Biology and Medicine*, vol. 22, no. 2, pp. 101–109, 2009.

[5] A. Korkiakoski, J. Niinimäki, J. Karppinen et al., "Association of lumbar arterial stenosis with low back symptoms: a cross-sectional study using two-dimensional time-of-flight magnetic resonance angiography," *Acta Radiologica*, vol. 50, no. 1, pp. 48–54, 2009.

[6] H. E. Gruber, N. Ashraf, J. Kilburn et al., "Vertebral endplate architecture and vascularization: application of micro-computerized tomography, a vascular tracer, and immunocytochemistry in analyses of disc degeneration in the aging sand rat," *Spine*, vol. 30, no. 23, pp. 2593–2600, 2005.

[7] H. Xue, "Clinical study on the treatment of lumbar disc herniation with double positioning oblique pulling method," *Acta Sinica Sinica*, vol. 32, no. 3, pp. 477–479, 2017.

[8] J.-F. Chen, X.-N. Shu, S.-J. Tang, Y. Wu, and Y.-P. Zhang, "Influence of lumbar disc degeneration on the efficacy of lumbar fixed-point rotation manipulation in sitting position: a finite element study," *Journal of Acupuncture and Tuina Science*, vol. 14, no. 4, pp. 295–299, 2016.

[9] S. Jin, *Establishment and Biomechanical Analysis of Lumbar Finite Element Model*, Dalian Medical University, Dalian, China, 2016.

[10] H. Deng, *Three-dimensional Finite Element Modeling of Lumbosacral Vertebrae and Biomechanical Analysis of Three*

Internal Fixation Methods, China Medical University, Taichung, Taiwan, 2011.

[11] Y. Shen, *Finite Element Analysis of Lumbar Spondylolisthesis with a New Posterior Dynamic Internal Fixation System*, China Medical University, Taichung, Taiwan, 2012.

[12] C.-C. Lo, K.-J. Tsai, Z.-C. Zhong, S.-H. Chen, and C. Hung, "Biomechanical differences of Coflex-F and pedicle screw fixation combined with TLIF or ALIF—a finite element study," *Computer Methods in Biomechanics and Biomedical Engineering*, vol. 14, no. 11, pp. 947–956, 2011.

[13] Y. Wang, X.-D. Yi, and C.-D. Li, "The influence of artificial nucleus pulposus replacement on stress distribution in the cartilaginous endplate in a 3-dimensional finite element model of the lumbar intervertebral disc," *Medicine*, vol. 96, no. 50, Article ID e9149, 2017.

[14] C. W. A. Pfirrmann, A. Metzdorf, M. Zanetti, J. Hodler, and N. Boos, "Magnetic resonance classification of lumbar intervertebral disc degeneration," *Spine*, vol. 26, no. 17, pp. 1873–1878, 2001.

[15] J. P. Thompson, R. H. Pearce, M. T. Schechter, M. E. Adams, I. K. Y. Tsang, and P. B. Bishop, "Preliminary evaluation of a scheme for grading the gross morphology of the human intervertebral disc," *Spine*, vol. 15, no. 5, pp. 411–415, 1990.

[16] H.-J. Kim, H.-J. Chun, K.-T. Kang et al., "The biomechanical effect of pedicle Screws' insertion angle and position on the superior adjacent segment in 1 segment lumbar fusion," *Spine*, vol. 37, no. 19, pp. 1637–1644, 2012.

[17] Y. J. Jin, Y. E. Kim, J. H. Seo, H. W. Choi, and T.-A. Jahng, "Effects of rod stiffness and fusion mass on the adjacent segments after floating mono-segmental fusion: a study using finite element analysis," *European Spine Journal*, vol. 22, no. 5, pp. 1066–1077, 2013.

[18] M. Sheng, L. fan, N. Wang et al., "Imaging changes and clinical significance of intervertebral foramen in different degrees of intervertebral disc degeneration," *Chinese Journal of Orthopedics*, vol. 22, no. 10, pp. 730–732, 2009.

[19] S. Naserkhaki, J. L. Jaremko, M. El-Rich et al., "Effects of inter-individual lumbar spine geometry variation on load-sharing: geometrically personalized finite element study," *Journal of Biomechanics*, vol. 49, 2016.

[20] J. Huang, H. Yan, F. Jian, X. Wang, and H. Li, "Numerical analysis of the influence of nucleus pulposus removal on the biomechanical behavior of a lumbar motion segment," *Computer Methods in Biomechanics and Biomedical Engineering*, vol. 18, no. 14, pp. 1516–1524, 2015.

[21] C. Song, X. F. Li, Z. D. Liu et al., "Biomechanical assessment of a novel L4/5 level interspinous implant using three-dimensional finite element analysis," *European Review for Medical and Pharmacological Sciences*, vol. 18, no. 1, pp. 86–94, 2014.

[22] D. V. Ambati, E. K. Wright, R. A. Lehman, D. G. Kang, S. C. Wagner, and A. E. Dmitriev, "Bilateral pedicle screw fixation provides superior biomechanical stability in transforaminal lumbar interbody fusion: a finite element study," *The Spine Journal*, vol. 15, no. 8, pp. 1812–1822, 2015.

[23] G. Li-Xin and F. Wei, "Impact of material properties of intervertebral disc on dynamic response of the human lumbar spine to vertical vibration: a finite element sensitivity study," *Medical & Biological Engineering & Computing*, vol. 57, 2018.

[24] L. Li, T. Shen, and Y.-K. Li, "A finite element analysis of stress distribution and disk displacement in response to lumbar rotation manipulation in the sitting and side-lying positions," *Journal of Manipulative and Physiological Therapeutics*, vol. 40, no. 8, pp. 580–586, 2017.

Hindawi
Journal of Healthcare Engineering
Volume 2021, Article ID 9989602, 12 pages
https://doi.org/10.1155/2021/9989602

Research Article

Medical Internet of Things to Realize Elderly Stroke Prevention and Nursing Management

Xin Li, Sufen Ren, and Fangqiu Gu

School of Nursing Jinzhou Medical University, Jinzhou, Liaoning 121000, China

Correspondence should be addressed to Xin Li; lixin@jzmu.edu.cn

Received 30 March 2021; Accepted 17 June 2021; Published 6 July 2021

Academic Editor: Khin Wee Lai

Stroke is a major disease that seriously endangers the lives and health of middle-aged and elderly people in our country, but its implementation of secondary prevention needs to be improved urgently. The application of IoT technology in home health monitoring and telemedicine, as well as the popularization of cloud computing, contributes to the early identification of ischemic stroke and provides intelligent, humanized, and preventive medical and health services for patients at high risk of stroke. This article clarifies the networking structure and networking objects of the rehabilitation system Internet of Things, clarifies the functions of each part, and establishes an overall system architecture based on smart medical care; the design and optimization of the mechanical part of the stroke rehabilitation robot are carried out, as well as kinematics and dynamic analysis. According to the functions of different types of stroke rehabilitation robots, strategies are given for the use of lower limb rehabilitation robots; standardized codes are used to identify system objects, and RFID technology is used to automatically identify users and devices. Combined with the use of the Internet and GSM mobile communication network, construct a network database of system networking objects and, on this basis, establish information management software based on a smart medical rehabilitation system that takes care of both doctors and patients to realize the system's Internet of Things architecture. In addition, this article also gives the recovery strategy generation in the system with the design method of resource scheduling method and the theoretical algorithm of rehabilitation strategy generation is given and verified. This research summarizes the application background, advantages, and past practice of the Internet of Things in stroke medical care, develops and applies a medical collaborative cloud computing system for systematic intervention of stroke, and realizes the module functions such as information sharing, regional monitoring, and collaborative consultation within the base.

1. Introduction

Stroke is a sudden onset of cerebral blood circulation disorders. It is divided into ischemic stroke and hemorrhagic stroke. Among them, ischemic stroke accounts for about all strokes—80% [1]. Stroke is a major disease that seriously endangers the lives and health of middle-aged and elderly people in our country. Its incidence, recurrence, disability, and fatality rate are extremely high. It not only endangers the lives of patients, but also brings heavy burdens to the patients' families and society economic burden [2]. The National Health and Family Planning Commission's Stroke Screening and Prevention Engineering Committee has carried out a nationwide stroke high-risk screening project to identify high-risk groups. The follow-up work is to further prevent strokes for high-risk groups. The focus should be on early stroke patients. Discovery, early diagnosis, and early treatment (secondary prevention) are on [3]. However, domestic and foreign surveys have shown that the rate of timely medical treatment for stroke is very low, and the implementation of secondary prevention needs to be improved [4]. Ischemic stroke is the most common type of stroke, accounting for 60% to 80% of strokes [5]. The results of domestic studies show that the incidence of ischemic stroke is 91.3 to 263.1 per 100,000, the average annual incidence is 14.55 per 100,000, and the recurrence rate is 8.47% [6]. A 6-year follow-up study showed that the fatality rate for the first stroke was 74.3% (919/1 237), and the average annual fatality rate was 12.3% [7]. The high incidence of stroke, high recurrence rate, high disability rate, and high

fatality rate seriously threaten human health, and it has also become the focus of medical workers' attention [8]. Stroke is preventable, controllable, and treatable, but the span from primary prevention to acute treatment to secondary prevention is relatively large, and the actual clinical management and control is time-consuming, laborious, and inefficient. The development of information technology provides a new opportunity to manage stroke patients across time and space [9]. At present, there have been studies on the application of information technology to mobile rounds, electronic medical records, all-in-one card payments, real-time in-hospital queries, radio frequency identification devices (RFID) barcode wristband identification, community monitoring, remote rehabilitation, and smart elderly care to explore the mouth [10]. However, how to integrate these scattered information technologies to more efficiently manage stroke patients throughout the entire process has yet to have clear guidance experience [11].

Regarding the typical research results of stroke robots, there is BLEEX (Berkeley Lower Extremity Exoskeleton) developed by the University of California, Berkeley [12] and the stroke robot HULC developed by Qi et al. [13] in conjunction with the University of California, Berkeley (Human Universal Load Carrier). Among them, the BLEEX robot has designed a back support, stroke mechanism, and power equipment to increase the soldier's walking ability and load capacity. At the same time, more than 40 sensors installed on the stroke complete the human-computer interaction of the control system. The HULC robot developed by Domingo [14] in conjunction with the University of California, Berkeley, adds an upper limb assisted stroke mechanism to the BLEEX robot to greatly improve the soldier's load capacity and combat capability. In addition, in Asia, Ahmadi et al. [15] of Nanyang Technological University (NTU) in Singapore have also developed a stroke robot for lower limb walking. The robot uses a hybrid control system, including power supply equipment, driving equipment, measurement systems, computers, wireless networks, and other equipment. At the same time, it collects the joint angles of the inner lower limbs while walking and provides assistance through the principles of physiological feedback and feedforward. In addition, many universities and research institutes around the world have carried out many researches on lower limb stroke robots for medical rehabilitation. A typical example is the "Lokomat" stroke rehabilitation robot developed by Sundmaeker et al. [16] at the Federal University of Technology Zurich (ETH) in Switzerland. Not only can it improve the treatment efficiency of acute ischemic stroke, it can also use telemedicine to contact hospital experts, manage physiological variables, improve hospital transportation decisions, and promote emergency care for other nervous system emergencies. Its efficacy has been clinically proven and has attracted many follow-up related studies. Kang et al.'s research [17] shows that the robot is composed of a weight loss system, a stroke system, a power and control system, and other supporting equipment: under the control of a computer, a linear motor and a crank-slider mechanism drive the hip and knee joints in stroke. At the same time, the ankle joint is designed with a passive adaptation mechanism [18]. The weight loss device elastically connected to the stroke system provides continuous support for the patient. The treadmill system provides coordinated movement for the human gait movement; the system adjusts the step according to the needs of the patient. At the same time, the active force of the patient is measured by the force sensor to adjust the output torque to adapt to the training needs of the patient in different rehabilitation stages and physical conditions [19]. In addition, the length of the mechanism of each joint part of the robot is adjustable to meet the body shape requirements of different patients and increase the compatibility of the rehabilitation system [20]. After the Lokomat robot appeared, related function development was constantly updated. In addition, there are many other research results of stroke rehabilitation systems, including the "Lopes" lower limb gait rehabilitation stroke robot developed by the University of Twente in the Netherlands [21], the "ALEX" lower limb gait rehabilitation stroke robot developed by the University of Delaware [22], and the Motorica stroke rehabilitation robot in the United States [23]. During the rehabilitation process, the system puts the patient in a tilted state with adjustable angle (tilt angle range: 0°–90°). At the same time, the patient's lower limbs can be gait with small amplitude through the traction mechanism of the thigh and the spring pedal mechanism of the foot. They move training to reduce the complications of bed rest and speed up the rehabilitation of the lower limb motor system and nervous system [24]. This mechanism combines the standing up bed with gait training, which increases the comfort of patients and is suitable for the rehabilitation needs of critically ill patients [25]. However, limited by the scope of the organization's activities, the system can only be used for small stride lower limb training [26]. At the same time, the driving method of the system determines that it can only achieve a single stepping action, which is not suitable for the development and use of other gait training functions [27].

Based on the technical requirements of community rehabilitation and family rehabilitation, this paper designs a stroke rehabilitation robot system that combines a stroke rehabilitation robot and a remote rehabilitation information management system. It uses IoT technology and is based on design methodology to realize the automatic generation of optimized rehabilitation strategies. It summarized the current research results. First, this article analyzes the rehabilitation needs of the stroke robot rehabilitation system, based on the concept of the Internet of Things, clarifies the specific structure of the rehabilitation system, and sorts out and proposes a comprehensive stroke rehabilitation robot system plan to adapt to the smart medical care in the construction of smart cities. It also explained the functional modules and network structure of the system and formulated the standardized use process under different conditions. After completing the analysis of rehabilitation goals and the system structure, this article carried out the overall design of the system and introduced the specific research work of each module, including the design and software design of the network database information management module and the design of the RFID recognition function

module. The article also presented design and software design, SMS reminder GSM function module design and software design, camera remote monitoring function realization, robot terminal control, and information management module and focused on the realization of human-computer interaction control. In addition, the characteristics of each module need to be described. On this basis, the data model of the information system is established, and the rehabilitation process specifications for different patient states are given according to the relevant functions of different rehabilitation robots. At the same time, according to the design methodology and knowledge base management, a design process for generating the optimal rehabilitation strategy is given. This article proposes a remote stroke diagnosis and treatment service model based on the wireless Internet of Things, making full use of the advantages of modern information technology to improve the level of stroke diagnosis and treatment and promote the development of telemedicine. In view of the increasing incidence of stroke in China and the implementation of early stroke identification being not optimistic, this study proposes the use of the Internet of Things and the use of multitarget data collection, multiterminal information interconnection and connection, cloud computing intelligent data processing, and remote home monitoring under remote home monitoring. Under the multifactor and sign information comprehensive evaluation of early stroke identification and alarm system, a health management model is established, that is, a health management model based on the Internet of Things and cloud computing for early identification and early warning of ischemic stroke, to solve the early identification of ischemic stroke difficult question.

2. Construction of the Elderly Stroke Prevention and Nursing Management Model under the Medical Internet of Things

2.1. Basic Theory of Internet of Things. The concept of the Internet of Things can be traced back to 1999 and was proposed by Kevin et al. The International Telecommunication Union (ITU) discussed the concept and characteristics of the "Internet of Things" in its November 2005 report, as well as the difficulties it will face in the future development process, and released relevant results. In order to achieve the purpose of interaction between people and things, people use devices such as wireless sensors, RFID, GPS, and other devices to connect real-life objects to the Internet, and this process is called the old *J* of the Internet of Things. The continuous improvement of the infrastructure has led to the rapid development of the core technologies of the Internet of Things, and they have been applied in all aspects of daily life. Since different application service providers have different monitoring goals, a huge amount of monitoring data to be processed is generated. If it cannot be processed in a timely and efficient manner, it will cause serious waste of bandwidth resources in the network transmission process. Since the working status of each node of the Internet of Things cannot be guaranteed to be stable, there is a serious problem of uncertainty in the data of the Internet of Things.

Suppose the recognition frame is West, assuming the set function [0, 1] (the power set in the middle is 2 things) satisfies 2 conditions: $n(O) = 0$ and $\sum n(M) = 1$; then the function n is called basic credibility distribution. The overall architecture of stroke unit can be divided into four parts: terminal layer, network layer, platform layer, and application layer. When there are many VM C, the basic credibility distribution value of A is $rt(M)$, where $rt(M)$ represents not the total credibility value of M, but an allocated value of the basic credibility of M. Sum the assigned values of all the subsets in M and express them with the reliability function to obtain the total reliability of M. Suppose that it represents a recognition framework reliability set function A: 2 in [0, 1] must meet 3 conditions at the same time: $A(O) = 0$; $A(\text{multi}) = 1$; when enough c, there is

$$u[x, y] > \sum u(x) - \sum u(x * i, y * i). \tag{1}$$

The reliability is analysed again with the plausibility function. Suppose A: 2 in [0, 1] is a reliability function in 2, if the function day and function S are both in 2 [0, 1], when there is more VMC, $H\ (M) = A\ (M)$, S: $1 - A\ (M)$, call the function H as the suspected function of A,. s is the plausibility function of A. It can be seen that the degree of suspicion is day (M) and the degree of plausibility is $S\ (M)$. Suppose that A, and A, two reliability functions, are in the same recognition framework, and the assigned values of basic reliability are n, respectively, for its coking element. If $\sum n.\ (B.)$ and n: $(C - j) < 1$, then the function n defined by formula (2) is the basic credibility distribution. When $n \neq O$,

$$y(n) = \frac{\sum n(b) * n(c)}{1 - \sum n(b) * n(c)}. \tag{2}$$

When multiple reliability functions are in the same framework, their corresponding basic credibility distributions are 7, respectively. Assume that VM C is small, and $M \neq O$. There is a basic credibility distribution, denoted by n, and then,

$$\begin{aligned} u(m) &= k \sum n(m(i)) * \sum n(m(j)), \\ k &= \left[\sum n(m(i)) \Lambda n(m(j))\right]^{-1}. \end{aligned} \tag{3}$$

For the data fusion of IoT nodes, each node in the IoT is regarded as a proposition, and the result displayed by the sensor with the functions of identification, judgment, and processing is the evidence corresponding to the proposition. If you want to integrate the data of multiple nodes in the Internet of Things, measure the collected data and then establish the corresponding basic probability distribution function as a credibility indicator. Each function and corresponding frame is called an evidence body, so every sensor in the IoT node is an evidence body. When calculating the normalization constant K, the increase in the number of assumptions will cause the amount of calculation to increase explosively, and the Dempster synthesis rule makes DS evidence theory a good solution to the problems of multisensor data conflicts and inconsistent opinions from

multiple experts. Using Dempster merging rules to combine each evidence body into a complete evidence body under the same framework, this is the essence of IoT node data fusion. It demonstrates a D-s data fusion method based on IoT nodes, where $M = 1, 2, \ldots, n$. (M) is the basic credibility distribution of i nodes, $i = 1, 2, \ldots, z$, and is the new basic credibility distribution combined by the Dempster synthesis rule.

In the data fusion of multiple nodes, the huge amount of data makes the traditional calculation method difficult to apply. Let it be the result of combining all the evidence, and 1 ~ n are the n pieces of evidence. The calculation method of combining the two evidences is used to deduce. Here, z represents not the total reliability value of c, but an assigned value to the basic reliability of c. Sum the assigned values of all the subsets in e and express them with the reliability function to obtain the total reliability of e. The calculation of the combination of n evidences is shown in the Figure 1, where the left side is the traditional direct calculation and the right side is the calculation of the recursive combination of n evidence. Suppose there is more recognition space = {elbow1, elbow2, . . ., elbow-n }. It is a variety of hypotheses, the evidence set $E = \{E1, E2, \ldots, En\}$, the weight set corresponding to each evidence which is $W = \{W1, W2, \ldots, W3\}$, and conflict of each evidence k. According to the D-s evidence theory, the probability of conflict is defined as

$$\begin{aligned} z &= \left(\sum c(i,j) - \sum e(i,j)\right) / \left(\sum c(i,j) + \sum e(i,j)\right), \\ c(i,j) &= \sum n(i) * m(s) + n(j) * m(t), \\ e(i,j) &= \sum n(j) * m(s) - n(i) * m(t). \end{aligned} \tag{4}$$

At this time, the original node weight is introduced, and the total weight form $W = m \times k - o \times \min$ is determined according to the size of the conflict probability. Among them, $W - i$ is the smallest value among the original weights. The total weight here takes into account the conflict situation. Adjusted according to the total weight, the original weight minus the average of the total weight, that is, the weight of each piece of evidence minus the weight of the conflict part, is

$$\begin{aligned} v &= c(i,j) * e(i,j) * z, \\ v(i,j) &= \frac{v(i) * v(j)}{\sum (v(i) * v(j))^T}. \end{aligned} \tag{5}$$

2.2. Medical Prevention and Nursing Management System Algorithm. Internet of Things data fusion algorithm is a technology for fusion processing of multisource data, which is the scope of intelligent information processing technology. By fully analyzing and integrating the data of each node, the best consistent estimate of the monitored object is obtained, which is more accurate and comprehensive than a single data source, so that users can make the right choice. After years of development of data fusion algorithms, some algorithms have formed more mature methods, and some algorithms are hotspots of scholars' research. Common data fusion methods mainly include classical probabilistic inference, Bayesian method, neural network, fuzzy set theory, and DS evidence theory.

(1) Classical probabilistic reasoning: the scope of classical probability discussion is limited to the case III1 of equal possible outcomes produced by random trials. Each test has a limited number of results, and the probability of the results is consistent. (2) Bayesian method: the Bayesian (Bayes) method was developed relatively early; the method is based on the maximum posterior and likelihood ratio test; if the prior probability can be calculated, Bayesian method will be a good solution. A is the result of combining all the pieces of evidence, and 1 ~ n are the n pieces of evidence. The calculation method of combining two pieces of evidence is used to calculate the combination of n pieces of evidence. (3) Neural network: in recent years, the technology of neural network (neural networks) for data fusion has made great progress. The working principle of the neural network is similar to that of the human brain, simulating the thinking of the human brain. Different from the traditional set, each element in the fuzzy set has a corresponding membership degree. The degree of membership refers to the degree of certainty (or uncertainty) that an element belongs to this set. Therefore, the fuzzy set is described by the membership mapping function. The algorithm has the characteristics of simple parallel distributed computing, parallel distributed processing (fast speed), high fault tolerance, and data robustness. The neural network allows the input of multiple signals and the output of multiple variables. After system training, the data is allocated to the correct classification for output, which is suitable for multivariable systems. The neural network can input new data that has not appeared before and recognize it during the training process, so the algorithm can learn and adapt. The DS (Dempster Sharer) evidence theory is promoted on the basis of Bayesian method, introducing the concept of trust function and using multiple evidences. The specific algorithm flow chart is shown in Figure 1.

The steps of the S evidence theory method are Input—the target to be fused M, the trust function $n - i$ (elbow) of n nodes, and the corresponding node weight training—and Output—the result of the fusion target. The steps are the following:

(1) Calculate the conflict probability of each piece of evidence $n - 1\,(M)$. Adjust the corresponding basic probability distribution according to the conflict probability, and get a new basic probability distribution.

(2) Calculate $n - M$ and n, the conflict coefficient K of (M). When $K \neq 1$, call the D-s evidence fusion formula for data fusion to obtain the fusion data $n(C)$.

(3) Cycle n once or twice. Calculate the conflict coefficient K between $n(C)$ and $n - m(M)$. When $K \neq 1$, call D. The evidence fusion formula updates the fusion data $n(C)$.

(4) The loop ends, and the final fusion result $n(C)$ is obtained.

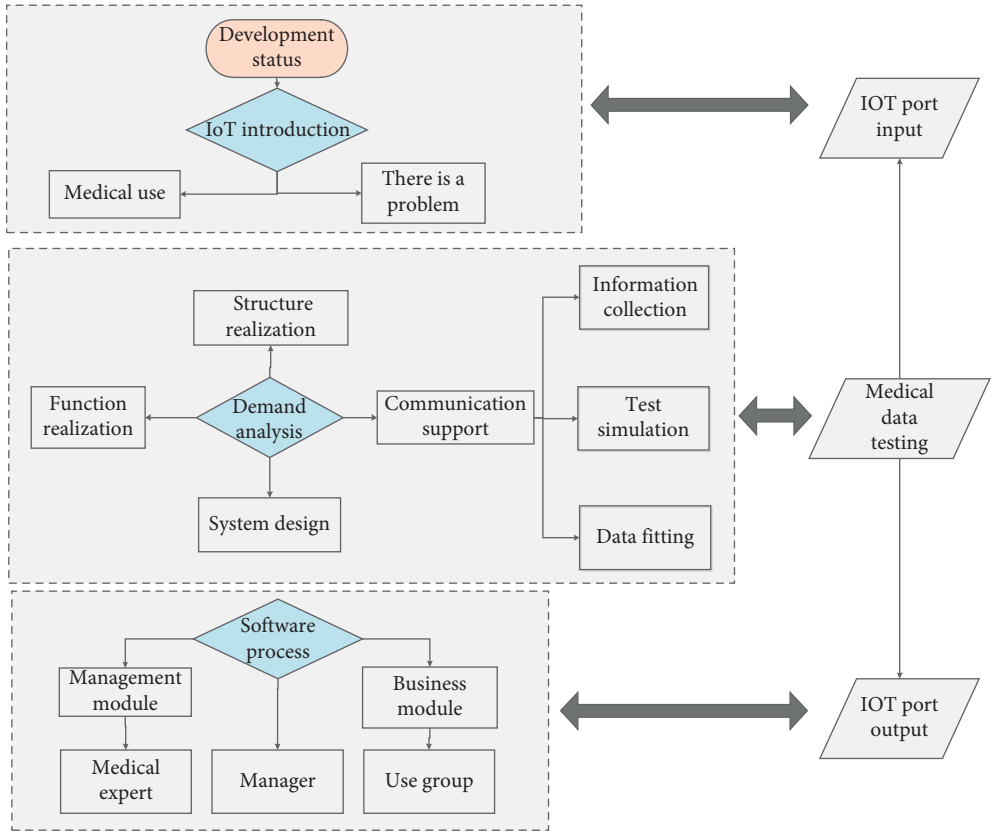

Figure 1: Flow chart of medical protection algorithm under the Internet of Things.

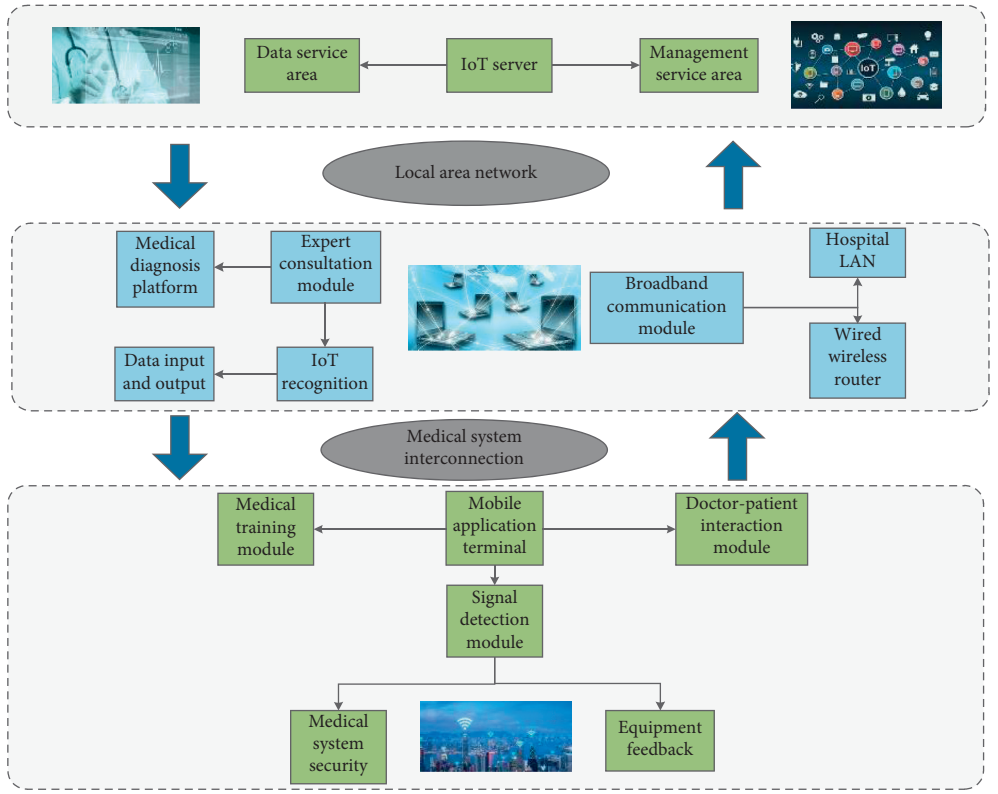

Figure 2: The framework of the elderly stroke prevention and nursing management model under the medical Internet of Things.

The entire software system is divided into five layers: the access layer, the resource scheduling layer, the data processing layer, the application support layer, and the application service layer. The vital signs remote transmission system is connected to a large amount of medical monitoring equipment through the network, and the patient's heart rate, respiration, and other physical signs data are collected through monitoring equipment such as electrocardiographs, ventilators, smart bracelets, and blood pressure monitors and transmitted back to the monitoring center through real-time network transmission. Real-time transmission of data is collected by medical equipment to the platform server, real-time diagnosis, and recording and saving of relevant data. Figure 2 shows the specific model framework. We can span heterogeneous system architectures and network transmission protocols, seamlessly integrating the management applications of systems, networks, and services; the data processing layer is based on RMI (Java Remote Method Protocol) to implement data access services, which is convenient for program components to perform distributed computing; the application support layer uses Web Service to publish data subscriptions and gateway management services, with cross-platform and cross-language data interaction capabilities; the application service layer is implemented by using the Struts2 + Sprin93 + Hibernate3 framework, and the software system's hierarchical structure is divided into the domain object layer, data access object layer, business logic layer, controller layer, and presentation layer reducing the coupling between software codes and improving scalability.

The access layer is composed of the IoT gateway access server group, which is mainly responsible for processing the registration, login, data transmission, release, and other related requests of the IoT gateway, and can forward the data transmitted by the gateway to the corresponding data access server for further deal with. The access layer is only responsible for gateway access and data reception and forwarding and does not interact with the database. The number of gateways mounted on each gateway access server is dynamically balanced according to the performance of each server, the current load situation, and configuration parameters. A Hash algorithm is proposed to make the requests between the upper and lower layers consistent. The specific process: after the system web server receives the subscription request, then take the subscribed gateway ID to the corresponding data access server through the Hash algorithm. The elements between the frameworks flow with each other. The top layer is the server architecture, the middle layer is the module recognition and data sorting platform, and the bottom layer is the application terminal and feedback mechanism processing. We use the above high-quality algorithms to configure the number of data access servers in the configuration file to support the expansion of the number of servers. Each data access server keeps its own subscription list and does not require interaction. The subscribed request and the subscribed data are fixed on the same data access server, which can provide the query efficiency of system. A good Hash algorithm can ensure that the accessed gateway is evenly hashed on each data access server to achieve the effect of load balancing.

2.3. Optimization of the Stroke Protection Model under the Internet of Things. The users of the telemedicine system under the Internet of Things are divided into administrators, general users, and health experts. All three types of users need to pass identity authentication to use the system. Administrator user characteristics: manage the daily operation of the platform, manage the access of the IoT gateway, manage the registration, basic attribute entry, and authorization of the other two types of users, maintain and manage data, and be responsible for report generation. The remote stroke unit based on the wireless Internet of Things should meet the basic medical conditions of the stroke unit, and install cameras and microphones that can realize multiangle monitoring to facilitate the collection of video and audio information; we install wireless sensors to collect temperature, humidity, illuminance, and air quality for indoor environmental information.

The telemedicine system based on the Internet of Things is divided into three subsystems according to functions: the basic platform subsystem, the application platform subsystem, and the specific application subsystem. The application platform subsystem provides three major functions: user management, portal access, and application management. It is mainly responsible for managing users' usage rights, data access control, and classification display of user interfaces. At the same time, it provides users with personalized customization services for specific applications. Figure 3 shows the distribution of various medical application services. The specific application subsystem provides specific medical-related services, including hypoxia analysis, arrhythmia analysis, electrocardiogram, blood pressure, blood pressure, blood oxygen, blood glucose, and fat and other medical applications, as well as online consulting function services.

The IoT gateway is generally deployed in residents' homes, in community health centers, or in mobile service vehicles. The IoT gateway access server can be deployed in each regional center, the dispatch server is accessed through the Internet or local area network and finally connected to the data access server, and the data collected by the gateway is forwarded to the data access server. The data access server, database server, and application server should be deployed in a local area network to ensure transmission speed and system operation efficiency. Application servers provide services to system users through the Internet. Combining business characteristics and needs, deploy various functional subsystems, database management software, gateway access software, data processing, and security authentication software in the business server as needed. The disk array mainly realizes the storage of system business application data and log backup data and is connected to the database server through a storage switch. The disk array performs redundant backup in the manner of RAID6 + hot spare disk to provide system security. In view of the high system requirements because of the stability and reliability of the database and application server, you can consider the use of dual-machine integrated data. Based on the Internet of Things telemedicine system design engineering master's degree thesis group design, the database server can be

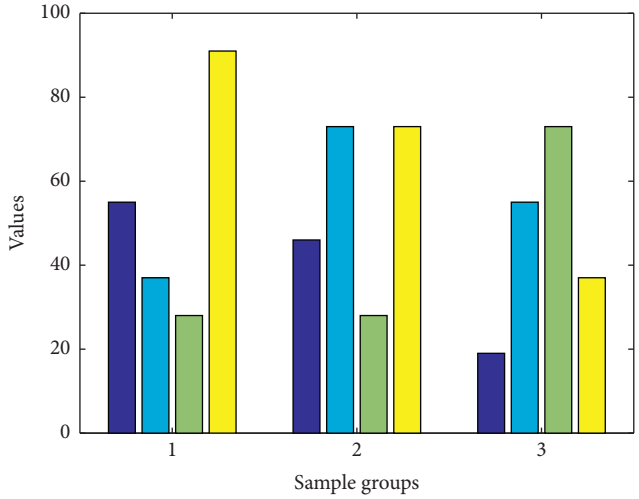

Figure 3: Distribution of various medical application services.

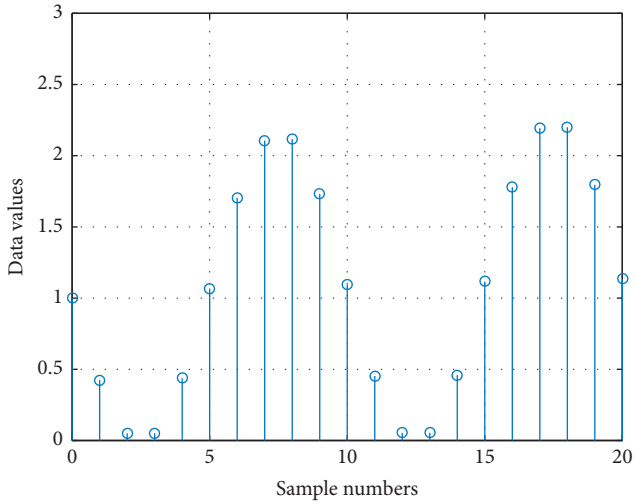

Figure 4: Distribution of medical database values under the Internet of Things.

deployed in the form of dual servers and disk arrays. The database software adopts Oraclelog Enterprise Edition database service software, and the dual-machine cluster software chooses Oracle's high-availability real-time application cluster software (RAC). Figure 4 shows the distribution of medical database values under the Internet of Things. They are deployed in various regional centers and access the dispatch server through the Internet or local area network and finally access data. We collect data separately through single-chip microcomputer and realize real-time data upload through NB-IOT module. When there is data to be sent, *M C U* sends in accordance with the priority and time sequence. When there is no data to send, the whole machine enters the standby state. The server forwards the data collected by the gateway to the system.

The database design process generally includes the following steps.

(1) Demand analysis: fully understand the specific requirements of various potential users for data, operational requirements on business processes, and data integrity and security requirements.

(2) Conceptual design: abstract entity data to define a comprehensive scheme and structure.

(3) Logical structure design: design various tables of the database according to the entity model, and give the logical relationship between each other.

In response to the design requirements of the personal health monitoring platform, the system database design needs to comply with the following requirements:

(1) Internet of Things related data: user's medical data, user's Internet of Things gateway information, Internet of Things gateway server, and other related information are stored in the information database of the Internet of Things data platform.

(2) Application platform related data: user login information, application registration information, user application customization information, and first page board configuration information are all stored in the application platform information database.

3. Application and Analysis of the Elderly Stroke Prevention and Nursing Management Model under the Medical Internet of Things

3.1. Simulation of Model Weight Parameters. For people who are over 40 years old, a stroke risk screening assessment is carried out based on the following 8 risk factors (1 point for each item): (1) history of hypertension (blood pressure ≥140/90 mm Hg (1 mm Hg = 0.133 kPa)) or taking antihypertensive drugs; (2) heart disease such as atrial fibrillation and/or valvular disease; (3) smoking; (4) dyslipidemia; (5) diabetes; (6) rarely doing physical activities; (7) obviously overweight or obese (body mass index ≥26 kg/m^2). Figure 5 shows the fitting curve of medical data weights under the Internet of Things.

Stroke patients enter the stroke path immediately after admission and start standardized treatment. The image data can be transmitted without loss to ensure the accuracy of remote diagnosis. Physicians of the two parties communicate in real time through video, which can basically achieve the effect of face-to-face communication. The dedicated optical fiber keeps all data confidential, which can protect the privacy of patients to the greatest extent. In addition, the remote consultation system has added a medical wireless microphone (model: IMI-B2()) and a multimodal input kit (desktop) (model: IMI-G1 (10 microphones + XCM-1 (J mouse)) designed by the company. The consultation process can realize the entire voice input, and the consultation records and medical records will be generated accordingly at the end of the consultation. The important category of stroke TAST classification n1 is cardiogenic stroke. Atrial fibrillation is an important risk of cardiogenic stroke factors, and long-term ECG monitoring is a routine item in the etiology of stroke patients. After the content is determined, the plug-in design is carried out, and the

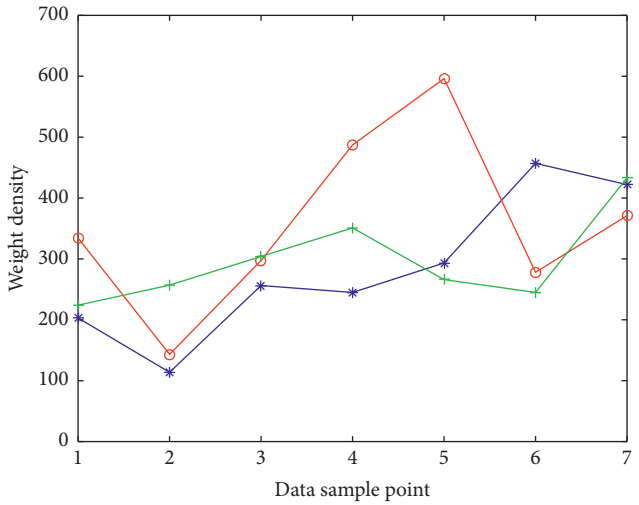

Figure 5: Fitting curve of medical data weights under the Internet of Things.

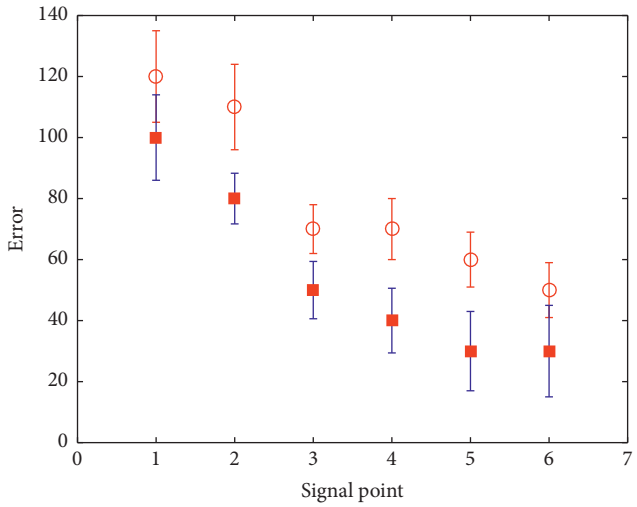

Figure 6: Signal error distribution of stroke data.

corresponding MCU encodes the data format of the IC card, so that the IC card swiping time of the portable card reader and the card ID can be uploaded to the telecommunications platform and application server. If atrial fibrillation is detected, it is of great significance to the formulation of treatment plans and secondary prevention strategies.

We provide free hand-held ECG monitors for all stroke patients enrolled in the group, and monitor 5 regularly every day. Figure 6 shows the error distribution of stroke data signal. The specific operation process is as follows: the patient downloads the palm ECG APP with his mobile phone and uses his mobile phone number to register the APP account. The plug-in ECG device connects the device to the patient's mobile phone by plugging into the audio port of the mobile phone. After the ECG data, the expert will read the ECG in the background and issue a report. After the patient's bed physician registers on the palm ECG cloud platform, the patient can search for the physician on the mobile phone client and click to send the report to the designated physician. The results can be viewed on the physician's platform and the patient can be responded to through the platform. All recorded ECG data will be stored in the cloud and recalled at any time. This mode is simple and feasible. Repeated operations can further improve the detection rate of atrial fibrillation.

Second-level preventive follow-up: all 20 stroke patients enrolled in the group were entered into the follow-up list after discharge and entered the follow-up phase to ensure the implementation of the secondary prevention of discharged patients. Figure 7 shows the digital signal spectrum of the patient's stroke. The blue solid line in the figure represents the detected noise signal, and the red dashed line represents the denoising signal obtained after algorithm optimization. In the department link module, patients can instantly consult department physicians' introductions and outpatient schedules and make online outpatient appointments. There are 4 subitems: medication reminder and follow-up reminder. Follow-up records are presented in the form of

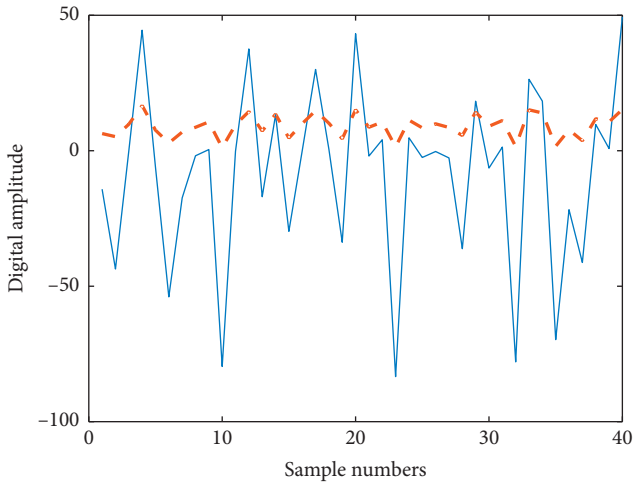

Figure 7: Digital signal spectrum of patients with stroke.

questionnaires that can be designed and modified by physicians, which mainly include height, weight, blood pressure, blood sugar, diet, smoking, drinking, medication status, and modified Rankin Scale (RS) scores. Figure 8 shows the polarization distribution of the stroke signal scale score.

However, a large proportion of stroke patients are elderly patients and do not use WeChat. To solve this problem, we apply an automatic telephone interview system specially designed by HKUST Company, which can dial up to 8 numbers at the same time through the cloud. Use predesigned questions (total 3 to 5 minutes) to conduct intelligent voice conversations, which can follow up simple but important data such as height, weight, blood sugar, blood pressure, medication status, and patient's current symptoms.

3.2. Example Results and Analysis. This study adopted a single-center, retrospective research method and selected NSTEMI patients who met the enrollment criteria and did not meet the exclusion criteria. Figure 9 shows the stacked

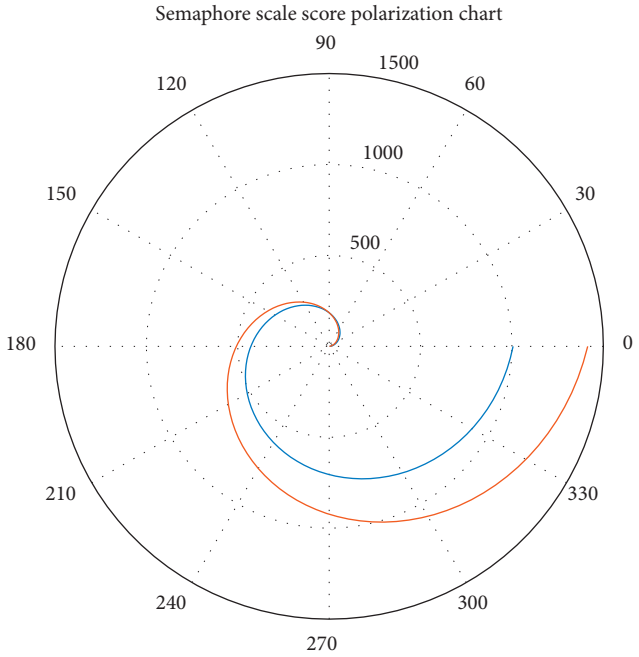

Figure 8: Polarization distribution of stroke signal scale score.

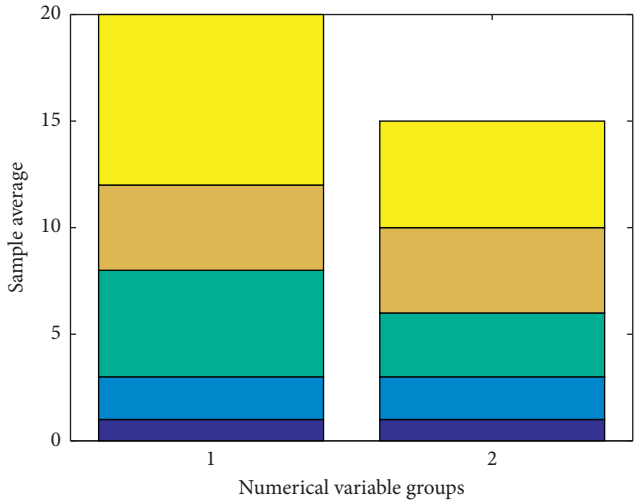

Figure 9: Stacking distribution of stroke electrical signal data.

distribution of stroke electrical signal data. The data of the left sample group in the figure is denser than the right group, the data after the algorithm optimization accounts for more, and the corresponding score value is more excellent. Since the selected subjects are all NSTEMI patients, there is no low-risk population in the final risk stratification.

The patients selected in this study are all people above the intermediate risk. Before and after the establishment of the stroke center regional collaborative treatment system, the gender, smoking, diabetes rate, and previous angina pectoris, myocardial infarction, PCI history, family history, and history of cardiac insufficiency have been considered. The differences were statistically significant ($P < 0.05$). Among them, the subgroup analysis of the age variable shows that

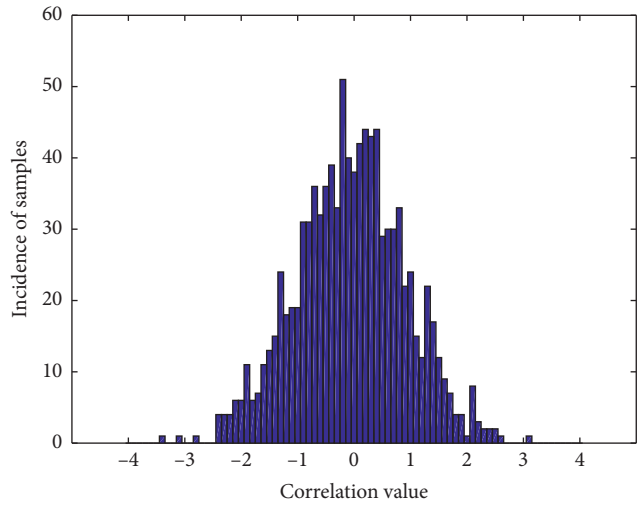

Figure 10: Analysis of abnormal incidence of stroke.

the age in each subgroup of group A is significantly larger than that of group B, and the difference is statistically significant (A1 group 68.48 ± 14.025 compared to B1 group 63.43 ± 13.432, $P < 0.001$; A2 group 75.15 ± 9.88 compared with B2 group 71.26 ± 10.58, $P < 0.001$; A3 group 60.85 ± 13.33 compared with B3 group 56.20 ± 11.71, $P < 0.05$). The subgroup analysis of the incidence of abnormal blood lipid metabolism showed that the A1 group was significantly lower than the B1 group [14.3% (6/42) vs. 38.6% (56/145), $P < 0.001$], and the A3 group was significantly lower than the B3 group [32.3% (50/155), $P < 0.001$]. Compared with 8.91 (1.63 ~ 48.44)], there was no significant difference between the two groups ($P > 0.05$); the Sym-to-FMC time of group B3 was slightly longer than that of group A3 [5.73 (1.38 ~ 21.25) versus 5.53 (2.38 ~ 42.05)], but there was no statistically significant difference between the two groups ($P > 0.05$). Figure 10 shows the analysis of the abnormal incidence of stroke.

Through 9 months of practice and improvement, we have initially established a single-disease stroke smart medical consortium platform in accordance with the abovementioned plan. A total of 40 stroke patients and patients with risk factors enrolled in the group have been awarded top three hospitals in the five hospitals, high-quality medical services, and standardized community follow-up care management throughout the entire process. It breaks the time and space constraints, improves the work efficiency of physicians and the quality of medical services, and realizes community resource sharing and hierarchical diagnosis and treatment. All 20 patients in the stroke group have reached the 1-month follow-up period, and 153 of them have reached the 9-day follow-up period. A total of 12 patients' 9-day RS scores were actually obtained by follow-up on the official account platform, and the effective follow-up rate was 78.43%; 68 patients returned to the hospital for follow-up one month after the onset. The relevant data has been statistically complete and valid for one month. The return visit rate was 34%; 63 patients returned to the hospital for follow-up 9 days after the onset. Figure 11 shows the medical

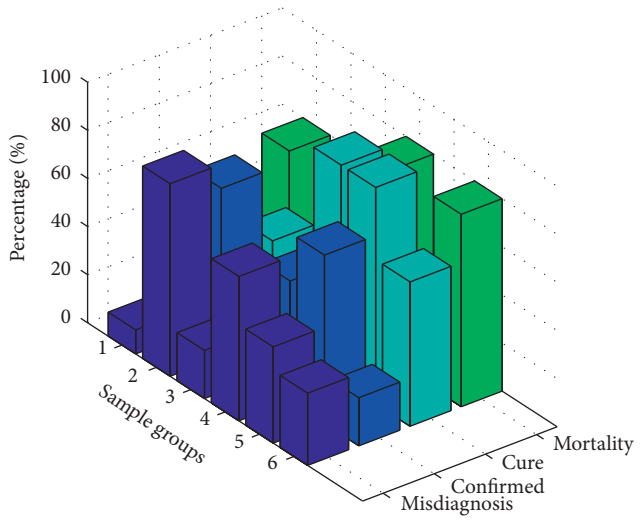

Figure 11: Medical treatment of stroke patients under the Internet of Things.

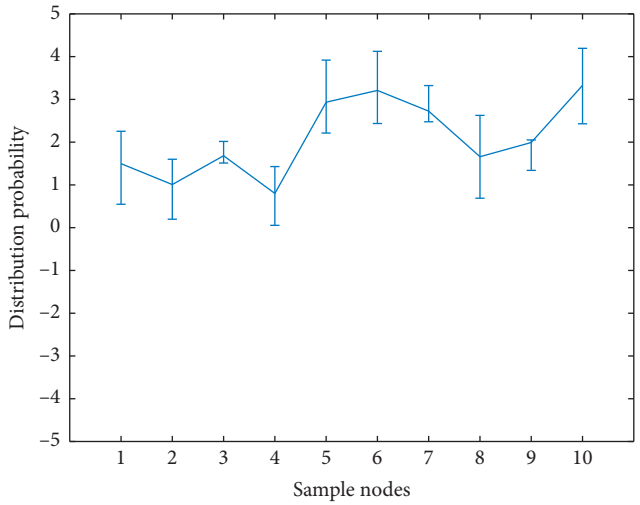

Figure 12: Motor function scores of stroke patients after treatment.

treatment of stroke patients under the Internet of Things. The relevant data were perfect. The effective return visit rate was 41.1 8% in 90 days. According to the evidence theory method proposed in this paper, the system obtains the final basic credibility distribution; then we judged the rationality of the proposition based on indicators such as credibility and plausibility and output the decision result; finally, it is synthesized according to the traditional DS evidence theory formula. Among the 20 patients in the high-risk group, 16 have been followed up every 3 months since enrollment and have been closely observed until now, and the follow-up data is complete.

(1) Baseline information include age, gender, history of smoking, history of diabetes, history of hypertension, history of abnormal lipid metabolism, family history of early-onset coronary heart disease, history of angina, history of stroke, history of myocardial infarction, history of PCI, history of cardiac insufficiency, history of renal insufficiency, number of diseased vessels (left main, single, double, and three), eGFR at FMC, and risk stratification (very high risk, high risk, intermediate risk). (2) Time node indicators include the time from onset (the appearance of symptoms) to the first medical contact (Sym-to-FMC) and the time from the entrance of the patient to the gate of the PCI hospital to the start of the radiography (D-to-CAG). The rate of compliance, the time from first medical contact to transfer (FMC-to-Transfer), the proportion of PCI treatment within the time limit specified in the guidelines, and the total proportion of PCI treatment are also included. (3) Recent (in-hospital) prognostic indicators are in-hospital mortality, in-hospital heart failure, malignant arrhythmia, renal replacement therapy, gastrointestinal bleeding, and ventricular aneurysm. (4) One-year prognostic indicators are reinfarction rate, readmission rate, and 1-year mortality rate. (5) Economic benefit indicators are per capita hospitalization days and per capita hospitalization expenses.

There are some changes in limb motor function and Glasgow Coma Scale (GCS) scores and activities of daily living in the two groups before and 2 months after nursing. Figure 12 shows the motor function scores of stroke patients after treatment. The Meyer Motor Function Evaluation Scale evaluates the upper and lower extremity motor function before and after the patient's care, with a full score of 100 points, of which the upper extremity motor function total score is 66 points and the lower extremity motor function total score is 34 points. The higher the score is, the better the recovery of the motor function of the limbs is. The higher the GCS score is, the more awake the stroke patient is. It is normal living ability: the patient's ability of daily living is judged by Barthel index, involving dressing, going up and down stairs, eating, etc. We use DS evidence theory to fuses data and adjust the weight of nodes according to the size of node weights and the probability of conflicts between nodes. The full score is 100 points. The higher the score is, the better the normal living ability of the patient is. It is statistical analysis: SPSS 20.0 software is selected for data proofreading, measurement data is described by mutual spider, and t-test is performed; count data is described by the number of cases (%), and r test is performed. $P < 0.05$ indicates that the difference is statistically significant.

4. Conclusion

This article uses the platform under the Internet of Things to provide raw medical data, patient health files, Internet medical service projects, etc. and uses cloud computing, big data, Internet of Things, artificial intelligence, and other technologies to build a single disease based on a safe and reliable hybrid cloud. It is a new type of smart medical consortium platform for stroke. In the results, a diagram of the whole-process management model for stroke patients was drawn; a community-level diagnosis and treatment system with smart community early screening for stroke, multidisciplinary remote consultation, smart follow-up evaluation, and clinical teaching synchronization was established; three levels of resource sharing provide a reliable and complete database for scientific research. The

conclusion is that, with the support of cloud computing, big data, and other technologies, a safe and reliable Internet-based stroke smart medical consortium platform that meets the needs of multidisciplinary medical education and research integration and meets the needs of patients and medical care as the center has been constructed. The fourth-generation mobile communication network (4G) with high speed, small delay, good antinoise performance, and anti-multichannel interference capability provides better conditions for the construction of a remote stroke prevention network based on the wireless Internet of Things. Therefore, the remote stroke prevention and treatment network will more effectively improve the level of stroke prevention and treatment at the first, second, and third levels, reduce the incidence and mortality of stroke, and provide remote diagnosis, treatment, consultation, and consultation for the prevention and treatment of other more diseases. We establish an information feedback system to collect opinions and suggestions from both doctors and patients at each node in the remote stroke diagnosis and treatment network in a timely manner, timely discover problems and hidden dangers in the process of remote stroke diagnosis and treatment services, and seriously solve them, so as to promote the quality of stroke diagnosis and keep treatment improving. The Internet of Things provides reliable technical support for the rapid application and landing of mobile stroke units. Through the in-depth integration of mobile stroke units and 5G network capabilities, it provides more possibilities for the rapid development of stroke first aid.

Data Availability

Data sharing is not applicable to this article as no datasets were generated or analysed during the current study.

Conflicts of Interest

The authors declare that there are no conflicts of interest.

References

[1] W. Zhao, C. Wang, and Y. Nakahira, "Medical application on internet of things," *Journal of Biomedical Informatics*, vol. 4, no. 1, pp. 11–32, 2020.

[2] D. V. Dimitrov, "Medical internet of things and big data in healthcare," *Healthcare Informatics Research*, vol. 22, no. 3, pp. 156–173, 2018.

[3] M. Haghi, K. Thurow, and R. Stoll, "Wearable devices in medical internet of things: scientific research and commercially available devices," *Healthcare Informatics Research*, vol. 23, no. 1, pp. 4–18, 2017.

[4] T. Han, V. X. Nunes, and L. F. Souza, "Internet of medical things—based on deep learning techniques for segmentation of lung and stroke regions in CT scans," *IEEE Access*, vol. 8, no. 2, pp. 117–135, 2020.

[5] F. Sadoughi, A. Behmanesh, and N. Sayfouri, "Internet of things in medicine: a systematic mapping study," *Journal of Biomedical Informatics*, vol. 10, no. 3, pp. 103–108, 2020.

[6] A. V. Dastjerdi and R. Buyya, "Fog computing: helping the internet of things realize its potential," *Computer*, vol. 49, no. 8, pp. 112–116, 2019.

[7] S. Luo and B. Ren, "The monitoring and managing application of cloud computing based on internet of things," *Computer Methods and Programs in Biomedicine*, vol. 130, no. 2, pp. 154–161, 2020.

[8] I. Azimi, A. Anzanpour, and A. M. Rahmani, "Medical warning system based on internet of things using fog computing," *Journal of Information Security*, vol. 20, no. 6, pp. 19–24, 2019.

[9] S. B. Baker, W. Xiang, and I. Atkinson, "Internet of things for smart healthcare: technologies, challenges, and opportunities," *IEEE Access*, vol. 5, no. 12, pp. 31–44, 2017.

[10] Y. I. N. Yuehong, Y. Zeng, X. Chen, and Y. Fan, "The internet of things in healthcare: an overview," *Journal of Industrial Information Integration*, vol. 11, no. 6, pp. 3–13, 2019.

[11] D. A. Antonovici, I. Chiuchisan, O. Geman, and A. Tomegea, "Acquisition and management of biomedical data using internet of things concept," *Journal of Electrical Engineering*, vol. 3, no. 7, pp. 1–4, 2018.

[12] D. Bandyopadhyay and J. Sen, "Internet of things: applications and challenges in technology and standardization," *Wireless Personal Communications*, vol. 58, no. 1, pp. 49–69, 2019.

[13] J. Qi, P. Yang, G. Min, O. Amft, F. Dong, and L. Xu, "Advanced internet of things for personalised healthcare systems: a survey," *Pervasive and Mobile Computing*, vol. 41, no. 3, pp. 132–149, 2017.

[14] M. C. Domingo, "An overview of the internet of things for people with disabilities," *Journal of Network and Computer Applications*, vol. 35, no. 2, pp. 584–596, 2019.

[15] H. Ahmadi, G. Arji, and L. Shahmoradi, "The application of internet of things in healthcare: a systematic literature review and classification," *Universal Access in the Information Society*, vol. 18, no. 4, pp. 837–869, 2019.

[16] H. Sundmaeker, P. Guillemin, and P. Friess, "Vision and challenges for realising the internet of things," *European Commision*, vol. 3, no. 3, pp. 34–36, 2019.

[17] M. Kang, E. Park, and B. H. Cho, "Recent patient health monitoring platforms incorporating internet of things-enabled smart devices," *International Neurourology Journal*, vol. 2, no. 2, pp. 66–76, 2018.

[18] I. Azimi, A. M. Rahmani, and P. Liljeberg, "Internet of things for remote elderly monitoring: a study from user-centered perspective," *Journal of Ambient Intelligence and Humanized Computing*, vol. 8, no. 2, pp. 273–289, 2018.

[19] I. U. Din, A. Almogren, and M. Guizani, "A decade of internet of things: analysis in the light of healthcare applications," *IEEE Access*, vol. 7, no. 3, pp. 967–979, 2019.

[20] S. Vukićević, Z. Stamenković, and S. Murugesan, "A new telerehabilitation system based on internet of things," *Series: Electronics and Energetics*, vol. 29, no. 3, pp. 395–405, 2019.

[21] H. Habibzadeh, K. Dinesh, and O. R. Shishvan, "A survey of healthcare internet of things (HIoT): a clinical perspective," *IEEE Internet of Things*, vol. 7, no. 1, pp. 53–71, 2019.

[22] L. M. Dang, M. Piran, and D. Han, "A survey on internet of things and cloud computing for healthcare," *Electronics*, vol. 8, no. 7, pp. 76–88, 2019.

[23] Y. A. Qadri, A. Nauman, and Y. B. Zikria, "The future of healthcare internet of things: a survey of emerging technologies," *IEEE Communications Surveys & Tutorials*, vol. 22, no. 2, pp. 1121–1167, 2020.

[24] S. Y. Y. Tun, S. Madanian, and F. Mirza, "Internet of things (IoT) applications for elderly care: a reflective review," *Aging Clinical and Experimental Research*, vol. 12, no. 5, pp. 1–13, 2020.

[25] J. Ni, K. Zhang, X. Lin, and X. Sherman Shen, "Securing fog computing for internet of things applications: challenges and solutions," *IEEE Communications Surveys & Tutorials*, vol. 20, no. 1, pp. 601–628, 2017.

[26] Y. Xu, G. Holanda, L. Fabrício et al., "Deep learning-enhanced internet of medical things to analyze brain ct scans of hemorrhagic stroke patients: a new approach," *IEEE Sensors Journal*, vol. 2, no. 5, 2020.

[27] B. H. Dobkin, "A rehabilitation-internet-of-things in the home to augment motor skills and exercise training," *Neurorehabilitation and Neural Repair*, vol. 31, no. 3, pp. 217–227, 2017.

Hindawi
Journal of Healthcare Engineering
Volume 2021, Article ID 6284035, 9 pages
https://doi.org/10.1155/2021/6284035

Research Article

Artificial Intelligence Analysis of EEG Amplitude in Intensive Heart Care

Junjun Chen, Hong Pu, and Dianrong Wang

Department of Intensive Care Unit, West China Hospital of Sichuan University, Chengdu 610041, China

Correspondence should be addressed to Dianrong Wang; wang7656dianrong@wchscu.cn

Received 18 May 2021; Revised 8 June 2021; Accepted 22 June 2021; Published 3 July 2021

Academic Editor: Khin Wee Lai

This article first studied the morphological characteristics of the EEG for intensive cardiac care; that is, based on the analysis of the mechanism of disease diagnosis and treatment, a signal processing and machine learning model was constructed. Then, the methods of signal preprocessing, signal feature extraction, new neural network model structure, training mechanism, optimization algorithm, and efficiency are studied, and experimental verification is carried out for public data sets and clinical big data. Then, the principle of intensive cardiac monitoring, the mechanism of disease diagnosis, the types of arrhythmia, and the characteristics of the typical signal are studied, and the rhythm performance, individual variability, and neurophysiological basis of electrical signals in intensive cardiac monitoring are researched. Finally, the automatic signal recognition technology is studied. In order to improve the training speed and generalization ability, a multiclassification model based on Least Squares Twin Support Vector Machine (LS-TWIN-SVM) is proposed. The computational complexity of the classification model algorithm is compared, and intelligence is adopted. The optimization algorithm selects the parameters of the classifier and uses the EEG signal to simulate the model. Support Vector Machines and their improved algorithms have achieved the ultimum in shallow neural networks and have achieved good results in the classification and recognition of bioelectric signals. The LS-TWIN-SVM algorithm proposed in this paper has achieved good results in the classification and recognition of bioelectric signals. It can perform bioinformatics processing on intensive cardiac care EEG signals, systematically biometric information, diagnose diseases, the real-time detection, auxiliary diagnosis, and rehabilitation of patients.

1. Introduction

The biological body exhibits electrical changes during physiological activities, which are caused by the potential difference between the inside and outside of the corresponding cell membrane, which reflects the excitement changes of the corresponding parts, and is an important basis for biomedical clinical diagnosis. Bioelectric signals mainly include electrocardiogram (ECG), electroencephalogram (EEG), electrooculogram (EOG), and electromyogram (EMG) [1]. The bioelectric signal has the characteristics of small amplitude, low frequency, strong noise, and strong randomness, and has the characteristics of chaos, nonlinearity, and multichannel [2]. Therefore, useful signals are easily submerged in noise interference. For example, the ECG signal is in the order of mV, and the equipment collection must ensure the amplitude of 0.1–8 mV and the frequency range of 0.05–100 Hz. The amplitude of the ECG of a normal person is generally within 5 mV, and the energy is mainly concentrated in 0.5–45 Hz. The EEG signal is of the order of mV, and the frequency is below 60 Hz. The relative frequency of myoelectric and neuroelectric signals is relatively high, the frequency is 0–10 kHz, the amplitude of the myoelectric signal is below 5 mV, and the neuroelectric signal is of the order of mV [3]. The interference sources of bioelectric signal acquisition mainly include power frequency interference (50 Hz or 60 Hz), baseline drift, and interference from other components of biological signals [4]. Moreover, the signal is easily affected by the environment, psychology, and physiology and is a nonstationary random signal. The electrical signals are taken from the body surface, and the potential changes

presented by different body surface positions are different. In order to detect the changes in the body surface potential in an all-round way, the measurement of bioelectric signals is often multichannel. For example, the standard ECG signal commonly used in clinical practice is 12 leads, while the EEG signal is 22 leads or more. Therefore, the processing methods of bioelectric signals are complex and diverse, and it is necessary to pay attention to signal processing algorithms that combine the time domain, frequency domain, and space domain [5]. Bioelectric signal recognition emphasizes robustness, accuracy, and repeatability, especially medical monitoring equipment, which requires real-time performance. Therefore, real-time effects must be considered on the premise of ensuring diagnostic accuracy. As the control center of the human body system, the brain directs various tissues, organs, and activities of the human body. The usual research methods for the brain include EEG, nuclear medicine imaging, MRI, cerebrovascular angiography, and other microscopic nerve detection method. Compared with other methods, EEG has the advantages of simple experiment, low cost, and relatively low requirements for the experimental environment. Therefore, from a practical point of view, EEG is very promising in brain research and the development of related products.

Body surface physiological electrical signals such as ECG, EEG, and EMG have the characteristics of flexible collection; being noninvasive, economical, and convenient; and so forth and have been widely used in intelligent disease monitoring, diagnosis, and rehabilitation [6]. The characteristics of the bioelectric signal itself determine the complexity and diversity of its processing methods. The new intelligent auxiliary diagnosis and treatment system based on bioelectric signals integrates biomedicine, Internet technology, and artificial intelligence technology, and its processing process is a typical pattern recognition process. It generally consists of four parts: bioelectric signal acquisition, signal transmission and processing, intelligent identification, and information feedback or control [7]. The collection of bioelectric signals includes sensors and microprocessor units, which are responsible for signal collection, preliminary preprocessing, and format conversion. In the transmission stage, the signal is sent to the information center or the microprocessing unit, and then the signal filtering and other processing and intelligent auxiliary diagnosis are performed, and finally, the information is output or feedback to control the actuator. The key technology of intelligent auxiliary diagnosis system is signal processing and intelligent recognition algorithm, which determines the degree of intelligence and clinical application value.

With the development of advanced sensor technology and artificial intelligence technology, intelligent auxiliary diagnosis and treatment systems that integrate wearable devices, the Internet of Things, and wireless Internet have promoted pioneering changes in smart medicine. Auxiliary diagnosis and treatment technology based on bioelectrical signals started from the discovery of bioelectrical signals and experienced digitization and networking to the integration of the Internet of Things and wireless networks [7]. The corresponding collection equipment developed from digitization to portable and wearable, and the identification method of bioelectrical signals. It also includes advanced artificial intelligence algorithms from simple threshold judgment, statistical analysis.

This paper firstly studies the morphological characteristics of ECG and EEG signals, respectively; that is, based on the analysis of disease diagnosis and treatment mechanisms, it constructs signal processing and machine learning models and studies signal preprocessing, signal feature extraction methods, new neural network model structures, training mechanisms, and optimization algorithms and efficiency and for experimental verification of public data sets and clinical big data. In the second part, we study the principle of EEG in intensive cardiac care and the mechanism of disease diagnosis, the types of arrhythmia, and the characteristics of typical ECG; the rhythm performance, individual variability, and neurophysiological basis of EEG signals in intensive cardiac care are studied. The third part studies the signal automatic recognition technology. In order to improve the training speed and generalization ability, several multiclassification models based on the Least Squares Twin Support Vector Machine (LS-TWIN-SVM) are proposed, and the computational complexity of several model algorithms is compared. In addition, a variety of intelligent optimization algorithms are used to select the parameters of the classifier, and the EEG signal is used to simulate the model. Support Vector Machines and their improved algorithms have achieved the ultimate in shallow neural networks and good results in the classification and recognition of bioelectric signals.

1.1. Analysis of Algorithm for Feature Extraction of ECG and EEG Signals. The bioelectric signal has the characteristics of multichannel and frequency band rhythm individual variability, and its feature extraction method involves multiple signal processing theories such as time domain, frequency domain, transform domain, and space domain [8].

1.2. ECG Signal Feature Extraction Method. The American Heart Association revised its opinions and was later promoted by the International Electrocardiology Society, forming a standard 12-lead ECG that is currently internationally recognized and used in various countries. According to the relationship of the ECG lead vector, the compression limb leads can also be derived from other leads. The standard 12-lead ECG includes limb leads I, II, III and compression limb leads VR, VL, and VF, and 6 chest leads V_l, V_2, V_3, V_4, V_5, and V_6; each lead reflects the different parts of the potential change. According to the theory of limb leads proposed by Einthoven, any limb lead can be deduced from the other two, namely, $I + III = II$. According to the relationship of the ECG lead vector, the compression limb leads can also be derived from other leads.

The feature extraction of the ECG signal is the key to guarantee the subsequent classification. The feature extraction method of the ECG signal can be divided into the direct extraction of the time domain waveform, the extraction of the frequency domain, or the feature extraction of

the transform domain. The time-domain features are directly derived from the shape of the ECG waveform, which is more in line with the clinician's diagnostic habits. The time-domain features include the main wave amplitude, ST segment offset, QT interval, PP interval, RR interval, and RR interval ratio. Frequency domain features are signal values after frequency domain transformation, such as Discrete Fourier Transform (DFT) [9] and Power Spectral Density (PSD). Transform domain feature extraction is generally to extract the transform result or the coefficient of the transform domain function as the feature after the ECG signal is transformed in the transform domain, such as the statistics of the ECG signal [10], variance, discrete wavelet transform, wavelet packet decomposition, matching tracking algorithm, Hermite function, AR model parameters, and principal component analysis (PCA) [11]. The transform domain features do not need to rely on basic medical knowledge and the position information of each ECG wave but use mathematical methods to automatically analyze and calculate them, which is widely used in intelligent auxiliary diagnosis.

1.3. Status of Intelligent Classification and Recognition Methods. According to the pattern characteristics of the ECG or EEG signal, it is the ultimate goal to complete automatic classification and recognition, explain the inner meaning reflected by the signal, and then output diagnostic information or control the actuator to perform auxiliary treatment [12]. The pattern classification methods of biological signals mainly include automatic knowledge modeling, statistical classification, traditional machine learning, and neural networks. The method of automatic knowledge modeling is based on knowledge expression and reasoning and is classified through logical reasoning according to the characteristic knowledge base such as signal shape, for example, fuzzy logic, expert system, and Markov model. This kind of method knowledge expression is intuitive and easy to understand, but it relies too much on knowledge expression; that is, it relies on expert experience, and the degree of intelligence is not high. Since the 1990s, statistical classification and machine learning techniques have gradually been used in biomedical signal classification, becoming the main branch of ECG and EEG signal classification methods. For example, Bayesian model (Bayes), K-Nearest Neighbor (KNN) [13], decision tree, and Linear Discriminant Analysis (LDA) [14]. Classical pattern classification methods have achieved certain results in the automatic identification of bioelectric signals, but the classification results and response speed are not satisfactory. With the development of neural network technology, especially deep learning technology in recent years, new breakthroughs have been made in biomedical assisted diagnosis. The following is a detailed analysis of the application status of neural network technology in the recognition of ECG and EEG signals.

1.4. Traditional Neural Network Algorithm. In 1986, DE Rumelhart and GEHinton et al. proposed a neural network error backpropagation (EBP) [15] training algorithm, which solved the "exclusive OR" problem of the "perceptron" and reduced the neural network. After the 1990s, neural network methods have gradually been applied to the automatic classification and recognition of biological signals [16], and certain results have been achieved. Caricato et al. [17] proposed a neural network classification method based on the time characteristics of the EEG signal. Katheria et al. [18] extracted the time interval of the ECG signal, the high-order cumulant of the QRS complex, and other characteristics and used a fuzzy neural network to analyze the 7 types of ECG. The signal classification result reached 96%. Felze: et al. proposed a probabilistic neural network classification model for EEG signal classification and recognition. Das et al. [19] used modular neural networks to classify large-scale EEG signals and achieved good results. Dereymaeker et al. [20] used wavelet transform to extract features, and the accuracy of the classification of the four types of ECG signals by the multilayer perceptron network was 94%.

Traditional neural networks are difficult to find the optimal network structure and have limited fitting capabilities. In practical applications, in the face of data with large variability, the recognition accuracy fluctuates greatly, and the generalization ability is poor, which limits the clinical application of neural network automatic recognition technology.

1.5. Support Vector Machine and Its Extended Algorithm. Another popular and effective ECG and EEG signal classification algorithm is the Support Vector Machine. Support Vector Machine (SVM) is a supervised machine learning method proposed by Claessens et al. [21]. The algorithm is based on the minimum structural risk. The principle of transformation is to obtain the segmentation hyperplanes of different types of data and then classify and recognize the distance between the sample and the hyperplane. Claessens et al. proved that SVM can minimize the structural risk and is superior in the classification of small samples. The artificial neural network (ANN) method that can only minimize the empirical risk is flawed. Compared with traditional ANN, SVM has shown better generalization ability in solving small sample, nonlinear, and high-dimensional learning. Support Vector Machine, Least Squared Support Vector Machine (LS-SVM), and SVM combined with various intelligent optimization algorithms are widely used in the classification and recognition of EEG, ECG, and other biological signals. However, SVM needs to solve a large quadratic programming problem when solving the hyperplane. The increase in sample size leads to too much computational complexity, and the classification effect of SVM is not good when solving cross data.

1.6. Analysis of the Diagnosis and Treatment Mechanism of ECG and EEG Signals. ECG is a technology that uses biosensor measuring electrodes to record the electrical activity pattern of the heart during each cardiac cycle from the body surface. It is one of the most commonly used examinations for clinical heart disease. It can not only help diagnose arrhythmia, myocardial ischemia, myocardial infarction,

and location; evaluate the effect of drugs on the heart; monitor after cardiac surgery; determine the condition of pacemakers; and so forth but also be a must for routine surgical procedures and intensive care units (ICU).

1.7. Principles of Medical ECG. Electrical activation occurs when the heart is active. This electrical activation can cause changes in the body surface potential. According to the time sequence of cardiac activation, this body surface potential is recorded to form a continuous curve, which is called ECG. The abscissa of the standard ECG paper represents time, and each cell of 1 mm represents 0.04 s; the ordinate represents the amplitude, and each cell of 1 mm represents 0.1 mV. Figure 1 shows the principle of the electrocardiogram. A complete EGG cycle includes atrial depolarization, ventricular depolarization, and ventricular repolarization. The complete cardiac process produces P wave, QRS complex wave, and T wave and PR interval, QT interval, and ST interval.

Several key interval indicators include the PR interval. The PR interval represents the time required for the excitement generated by the sinoatrial node to reach the ventricle through the atrium, the atrioventricular junction, and the atrioventricular bundle and causes the ventricle to start to excite; the QT interval is the time for the ventricular depolarization and repolarization process, which represents the heart. The ST segment represents that all parts of the ventricle have entered a depolarized state. At this time, there is no potential difference between the parts of the ventricle, so the ST segment curve is basically a horizontal state.

At present, the commonly used clinical ECG is 12-lead, which is called "standard lead." The Dutch physiologist MacDarby et al. [22] proposed the concept of leads and the naming of ECG waveforms in 1903. In 1933, Wilson created unipolar limb leads VR, VL, and VF and precordial leads (thoracic leads) V1–V6, Akiyama et al. [23] modified the central electrical terminal and designed the compression limb leads. It is more practical and becomes the main body of clinical ECG.

When the heart has arrhythmia or is damaged due to ischemia, or even necrosis, the changes in the electrical activity of the heart will be clearly reflected on the ECG, showing abnormal changes in the shape of each waveform; that is, the amplitude, shape, and time of the ECG signal features such as interval can reflect the underlying diseases of the heart and provide a reliable basis for doctors to diagnose various heart diseases. According to the standards of the American Association for the Advancement of Medical Devices (AAMD), more than a dozen common arrhythmias can be divided into 5 categories, namely, normal heartbeat (N, including normal heartbeat, left and right bundle branch block, etc.), supraventricular beats (S, including atrial premature beats, borderline premature beats, etc.), ventricular different beats (V, including ventricular premature beats and ventricular escape beats), ventricular fusion beats (F), and unknown beats (Q, pacing heartbeat, uncategorized heartbeat, etc.). Figure 2 lists several common ECG signal time-domain waveforms of arrhythmia.

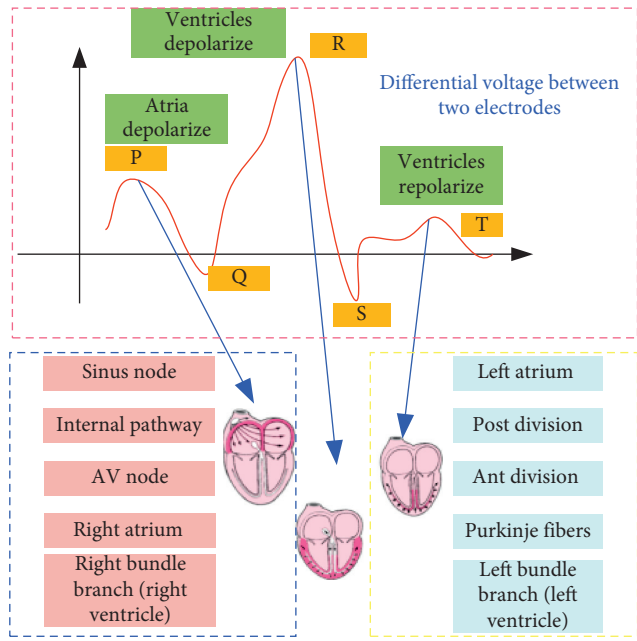

Figure 1: ECG single heartbeat waveform.

2. Experimental Design

2.1. Based on LS-TWSVM-Based Intensive Cardiac Monitoring EEG Amplitude Recognition. Scalp electrodes collect electroencephalogram (EEG) signals. This method has the characteristics of simple collection, noninvasiveness, high time resolution, low cost, convenience, and flexibility and is especially suitable for wearable systems. From the analysis in the first chapter, it can be seen that although advanced artificial intelligence technologies such as machine learning have greatly promoted the development of BCI technology of motor imagination, the current medical rehabilitation training system based on motor imagination BCI still has certain difficulties in its practical application. The main problems are that the accuracy of EEG source signals needs to be improved; the system response speed is limited; the recognition accuracy of EEG signals is not high; EEG sensorimotor rhythm is specific to different individuals, and even the same individual has greater variability at different times and different physical conditions.

In response to the existing problems, this chapter proposes an EEG motion image signal recognition algorithm based on adaptive frequency band selection CPS feature extraction combined with Least Squares Twin Support Vector Machine (LS-TWIN-SVM) classification. First, use adaptive artifact removal technology to filter the signal to improve the accuracy of the EEG signal, then use a band-pass filter to generate EEG rhythm signals of different frequency bands, perform CSP feature extraction, and finally send it to the LS-TWIN-SVM classifier for adaptive selection. In the optimal frequency band, the classifiers select the frequency band characteristics for a specific person and perform real-time recognition. In order to improve the accuracy of EEG signal recognition, various kernel functions were tested, and several biointelligence optimization

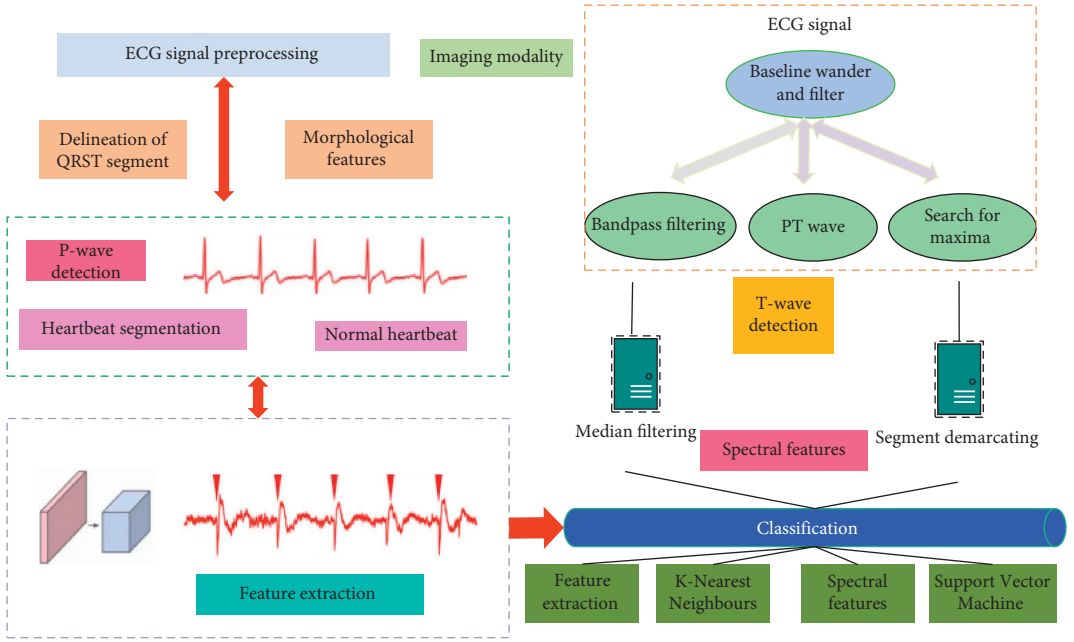

Figure 2: Several types of arrhythmia heartbeat signals.

algorithms were compared to select the optimal classifier parameters. The public data set is used as the test object to verify the feasibility of the proposed algorithm. The following sections will explain in detail.

2.2. Least Squares Twin Support Vector Machine (LS-TWIN-SVM) Algorithm Modeling. Support Vector Machine (SVM) classification seeks an optimal hyperplane based on the principle of structural risk minimization, which maximizes the blank area on both sides of the hyperplane while ensuring the accuracy of the training sample classification. For the linear case, as shown in Figure 3, the straight line H is a dividing line with W as the normal vector. This dividing line can divide the two types of data as accurately as possible. H_1 and H are the two types of samples. The support vector points and the straight line parallel to the classification line are analyzed. When H is in the middle of H_1 and H_2, the line meets the principle of maximizing the interval between the two types of sample points and becomes the optimal dividing line. This is converted to the problem of finding the normal vector. Extending to a high-dimensional space, the optimal classification line becomes the optimal hyperplane, that is, finding the normal vector of the optimal classification hyperplane and classifying multiclass samples by finding the distance.

Taking the two-classification problem as an example, given the training sample set (α_i, β_i) $i = 1, 2, \ldots, n$, $\alpha \in R^n, \beta \in \{\pm 1\}$ of the two types of data, the hyperplane is analyzed. If the sample is correctly classified and the classification interval is as large as possible, the hyperplane must satisfy the following constraints:

$$\begin{cases} w\alpha_i + b \geq \beta_i & \beta_i = +1, \\ w\alpha_i + b \leq \beta_i & \beta_i = -1. \end{cases} \tag{1}$$

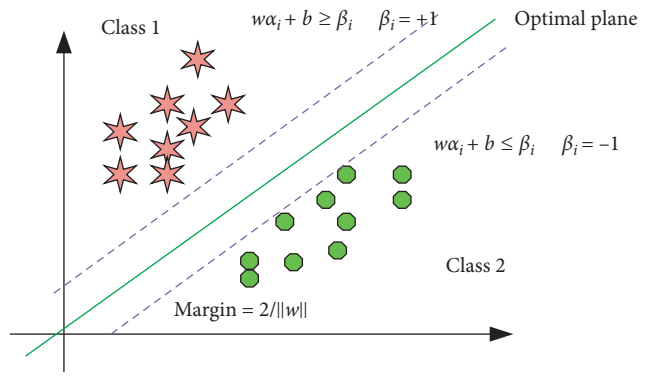

Figure 3: Twin Support Vector Machine two-dimensional data classification diagram.

When combined, they can be expressed as follows:

$$w\alpha_i + b \geq \frac{1}{\beta_i}, \quad i = 1, 2, \ldots, n. \tag{2}$$

Then, the classification interval can be expressed as follows:

$$\min\left\{\frac{(w\alpha_i + b)}{\|w\|}\right\} = \frac{2}{\|w\|} + \max\left\{\frac{(w\alpha_i + b)}{||w||}\right\}. \tag{3}$$

Therefore, the goal of SVM is to maximize the classification interval under the condition of satisfying the constraint formula (2), that is, to solve the problem of the following formula [24]:

$$\min f(w) = \frac{1}{2\|w\|^2} = \frac{1}{2}\left(w^T w\right). \tag{4}$$

When there is a linear inseparable pattern, the optimal segmentation hyperplane is required to meet the principle of

minimum average classification error probability for all training samples. At this time, just relax the constraint condition of formula (2), that is, introduce a slack variable ξ_i; then, formula (2) becomes

$$w\alpha_i + b \geq \frac{(1-\xi_i)}{\beta_i}, \quad i = 1, 2, \ldots, n. \tag{5}$$

To introduce a cost function into the objective function, that is, add a penalty component with an adjustable factor λ to function (4), the objective function formula (4) can be expressed as

$$\begin{aligned} \min f(w) &= \frac{1}{2\|w\|^2} + \lambda \sum_{i=1}^{n} \xi_i \\ &= \frac{1}{2\left(w^T w\right)} + \lambda \sum_{i=1}^{n} \xi_i. \end{aligned} \tag{6}$$

Among them, λ is the penalty factor, which controls the degree of punishment for the wrong sample. The larger ξ_i, the heavier the penalty for the error.

2.3. Twin Support Vector Machine. Support Vector Machines show strong generalization and promotion capabilities in small sample and nonlinear classification problems. However, there are still some challenges. For example, when facing a large sample, the optimal solution can be obtained by solving a large-scale quadratic programming problem. The training speed is slow and it is difficult to meet certain real-time systems. In addition, SVM is not very suitable for processing cross-type data.

Twin Support Vector Machine (TWSVM) is proposed on the basis of generalized eigenvalue proximal SVM (GEPSVM). As shown in Figure 3, for the binary classification problem, TWSVM constructs an optimal near-end hyperplane for each class. By solving two small quadratic programming problems, such sample points are "close" to the hyperplane, and the other sample point is appropriately far away from the hyperplane [25]. Compared with traditional Support Vector Machines, the learning efficiency is improved.

3. Results and Analysis

3.1. Comparison of EEG Signal Classification Results of Twin Support Vector Machine and Its Extended Algorithm. The genetic algorithm (GA) and quantum genetic algorithm (QGA) are widely used algorithms. The genetic algorithm is a biological incentive algorithm, which has been successfully used to solve engineering problems such as complex optimization and feature extraction. Good results have been achieved in the multiparameter optimization selection problem. The genetic algorithm's parameter search process for the classifier is as follows:

(1) Population initialization and parameter coding.

(2) Calculate the fitness function of each chromosome.

(3) Use GA calculation steps: selection, crossover, and mutation.

(4) The offspring replace the old population to form a new population of the next generation.

(5) Obtain the classifier parameter model. When the iterative conditions are met, the optimal chromosome is generated; otherwise, it returns to step 2.

The implementation process of quantum genetic algorithm is based on the basic framework of genetic algorithm, adding concepts such as quantum states and quantum gates in quantum theory and using qubits and superposition states to encode chromosomes [26]. The typical iterative process of QGA includes selection, mutation operation (quantum crossover, quantum mutation, and quantum interference), quantum measurement, evaluation, and substitution.

3.2. EEG Signal Recognition of the LS-TWIN-SVM Classifier Based on Intelligent Optimization Algorithm. The biological intelligence optimization algorithm and its improved algorithm have been successfully used in the parameter adjustment of the neural network classifier, but the convergence and final performance are greatly affected by the classifier and the data set. This section uses PSO, CPSO, GA, and QGA algorithms to test the proposed classifier models, respectively. In order to achieve higher efficiency and optimal classification results, the CPU running time, classifier training, and testing of several optimization algorithms are compared.

The maximum iteration algebra of the four optimization algorithms is set to 300, and the optimal classification accuracy rate of 10-cv cross-validation on the training data set is used as the fitness function. The population size is 40, the individual length is 20, and the genetic algorithm generation gap is set to 0.95. The crossover and mutation probabilities are set to 0.7 and 0.01, respectively. Quantum genetic algorithm combines the principles of genetic algorithm and quantum mechanics. The process includes initializing population and coding classifier parameters, calculating fitness function, selection, mutation, evaluation, and replacement. The mutation operation of the evolutionary algorithm uses the quantum revolving door strategy. For the convenience of comparison, the population size and individual length of QGA are the same as the GA algorithm settings, and the quantum rotation angle is set to 0.01.

The parameters of the particle swarm optimization (PSO) algorithm are set as follows: the population size is 20, and the acceleration constants are set to 1.5 and 1.70, respectively. During the implementation of the chaotic particle swarm optimization (CPSO) algorithm, two chaotic sequences are generated to prevent the PSO algorithm from falling into the local maximum. In the initialization phase, chaotic initialization is used to select the initialization position instead of random selection; in the optimization position selection process, the global optimization position obtained by the particle search is subjected to chaos operation, and then the particle position is determined by the global optimization position after the chaos operation. The

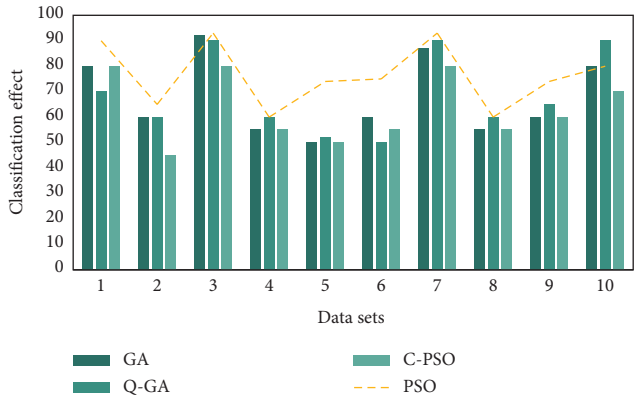

Figure 4: The classification effect of the first data set optimization algorithm.

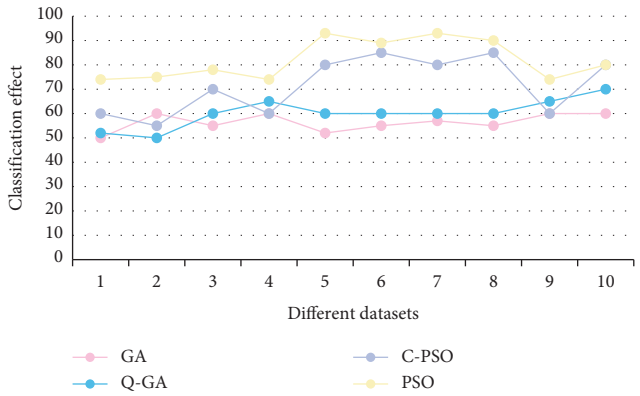

Figure 5: The classification effect of the second data set optimization algorithm.

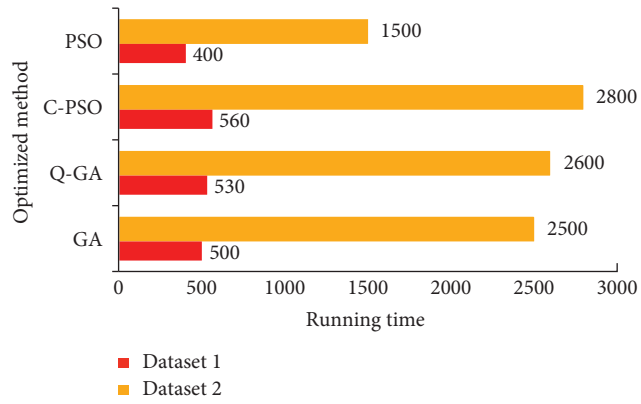

Figure 6: Comparison of running time of the optimized method.

Table 1: TWIN-SVM and common recognition algorithms results.

Testing objects	PSO-LS-TWIN-SVM	LDA	BP	PNN
1	88.19	87.24	72.43	83.45
2	64.35	57.32	62.34	61.35
3	93.42	91.34	97.53	88.24
4	65.34	63.24	71.34	70.12
5	76.35	54.87	52.34	50.35
6	67.34	70.23	74.45	65.24
7	75.23	70.43	74.14	58.33
8	88.89	83.25	87.24	91.34
9	78.34	73.42	76.35	73.24
10	67.24	70.78	66.24	70.43
Mean	76.47	72.21	73.44	71.21
SE	11.24	13.34	12.32	16.31

CPSO parameter settings are the same as PSO, and the parameters can be randomly generated.

Use the CSP features extracted from the data set to test the classifier algorithm. The experimental results are shown in Figures 4 and 5. As can be seen from the figure, the test results of the data set show that the classification effect of the classifier based on PSO and GA is equivalent, and the accuracy is better than the CPSO and QGA algorithms. However, in the test results of the second data set, the PSO and CPSO algorithms are significantly better than the GA and QGA parameter optimization results. From Figure 6, it is obvious that PSO has the highest operating efficiency and simple calculation, which is convenient for real-time hardware implementation. Therefore, TWIN-SVM is chosen as the classifier of the MI-BCI system.

3.3. Analysis of Experimental Results. Since its introduction, TWIN-SVM has been successfully applied in many fields, and scholars have made a lot of contributions to the algorithm expansion and application of Twin Support Vector Machines, and it has also been successfully used in the intelligent recognition of biomedical signals.

In order to improve the system response speed and overcome the variability of individual EEG rhythms, this chapter proposes adaptive artifact removal and adaptive frequency band selection feature extraction methods to enhance the classification and recognition of EEG signals. And the TWIN-SVM classifier is used for the rapid classification and recognition of EEG. Experimental results are shown in Table 1, which showed that the classification accuracy rate, CPU operating efficiency, and other indicators have been significantly improved.

The proposed TWIN-SVM method shows good results on the data set as shown in Figure 7. The proposed method performs adaptive frequency band selection, which overcomes the frequency band variability of EEG signals between individuals. However, as can be seen from Figure 8, the optimal cross-validation accuracy rate on the training data set and the test accuracy rate on the test data set are quite different, indicating that the data at different test times has greater variability; that is, there is still variability within the individual. We should conduct more EEG experiments. The more samples are in the experiment, the closer the results are to the essence of the facts. The experiment reported in this article can be said to be a preliminary exploration of EEG experiments under different conditions. The next step is to carry out more experiments: one is to increase the samples of existing experiments and the other is to expand the experimental projects and conduct experiments on more states.

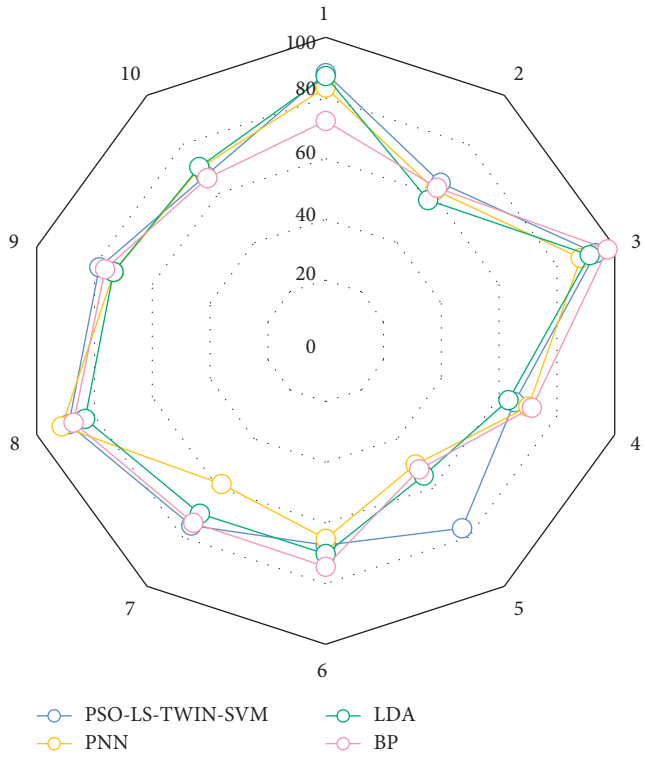

Figure 7: Comparison between PSO-LS-TWIN-SVM and common recognition algorithms.

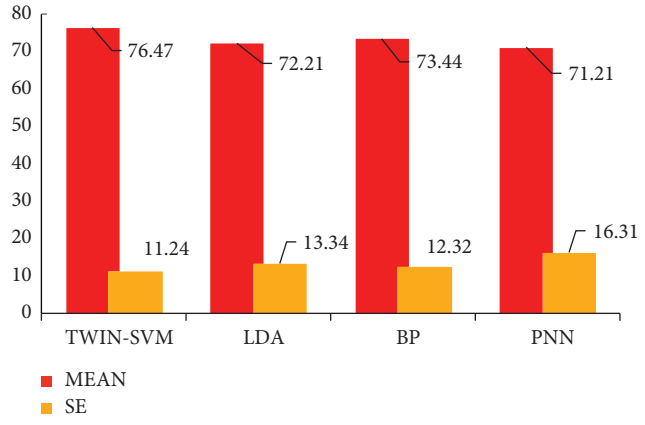

Figure 8: The average and standard error of recognition algorithms.

4. Conclusion

EEG is combined with more analysis methods to analyze the activities of various parts of the brain. EEG has its irreplaceable advantages, but it also has its disadvantages. If it can be combined with other suitable methods and learn from each other's strengths, the completeness and persuasiveness of the experiment can be further strengthened, for example, using EEG combined with functional imaging techniques such as PET and magnetoencephalography. The machine learning method is a powerful tool for the recognition of EEG signals in intensive cardiac care, and many achievements have been made in this field. However, the rehabilitation system based on EEG still has not achieved large-scale clinical application. The main reason is that the technology still has the following problems: firstly, there is great variability for different individuals based on the amplitude of EEG, and even the same individual at different times. There are also differences with the environment, which requires the system to have stronger adaptability; secondly, there is a lot of interference in the scalp EEG signal, and the signal source accuracy is limited, which affects the recognition accuracy; finally, more efficient adaptation is needed. Aiming at the above problems, this paper proposes adaptive artifact removal theory, adaptive frequency band selection feature extraction, and a fast TWIN-SVM classification strategy based on PSO. In order to evaluate the effect of this method, a classifier model based on a kernel function and an intelligent optimization algorithm is used to optimize the classifier. Neuroinformatics is a newly emerging interdisciplinary subject. It is still in its infancy, and there is still a big gap with the established goals. Although EEG has existed for a long time, due to the complexity of the EEG signal itself, much of the information still cannot be extracted. With the development of signal processing methods, more and more simple and efficient data processing methods have been developed. This has greatly promoted the development and application of EEG in neuroinformatics. Through the study of EEG, it can further help to understand how the human brain works in different modes and promote the development of neuroinformatics.

Data Availability

Data are available from the corresponding author upon request.

Conflicts of Interest

The authors declare that there are no conflicts of interest.

References

[1] J. S. Malak, H. Zeraati, F. S. Nayeri, R. Safdari, and A. D. Shahraki, "Neonatal intensive care decision support systems using artificial intelligence techniques: a systematic review," *Artificial Intelligence Review*, vol. 52, no. 4, pp. 2685–2704, 2019.

[2] C. A. Goldstein, R. B. Berry, D. T. Kent et al., "Artificial intelligence in sleep medicine: background and implications for clinicians," *Journal of Clinical Sleep Medicine*, vol. 16, no. 4, pp. 609–618, 2020.

[3] F. Yang, J. Elmer, and V. I. Zadorozhny, "Smartprognosis: automatic ensemble classification for quantitative EEG analysis in patients resuscitated from cardiac arrest," *Knowledge-Based Systems*, vol. 212, no. 2, Article ID 106579, 2021.

[4] M. M. Ghassemi, E. Amorim, T. Alhanai et al., "Quantitative electroencephalogram trends predict recovery in hypoxic-ischemic encephalopathy∗," *Critical Care Medicine*, vol. 47, no. 10, pp. 1416–1423, 2019.

[5] E. Amorim, M. Van der Stoel, S. B. Nagaraj et al., "Quantitative EEG reactivity and machine learning for prognostication in hypoxic-ischemic brain injury," *Clinical Neurophysiology*, vol. 130, no. 10, pp. 1908–1916, 2019.

[6] T. Alsuliman, D. Humaidan, and L. Sliman, "Machine learning and artificial intelligence in the service of medicine: necessity or potentiality?" *Current research in translational medicine*, vol. 68, no. 4, pp. 245–251, 2020.

[7] G. Rong, A. Mendez, E. Bou Assi, B. Zhao, and M. Sawan, "Artificial intelligence in healthcare: review and prediction case studies," *Engineering*, vol. 6, no. 3, pp. 291–301, 2020.

[8] N. Bruns, I. Sanchez-Albisua, C. Weiß et al., "Amplitude-integrated EEG for neurological assessment and seizure detection in a German pediatric intensive care unit," *Frontiers in pediatrics*, vol. 7, Article ID 358, 2019.

[9] J. Limjoco, L. Zawadzki, M. Belden, J. Eickhoff, and C. Ikonomidou, "Amplitude-integrated EEG use in neonatal abstinence syndrome: a pilot study," *Journal of Maternal-Fetal and Neonatal Medicine*, vol. 33, no. 21, pp. 3565–3570, 2020.

[10] Z. Hajat, N. Ahmad, and J. Andrzejowski, "The role and limitations of EEG-based depth of anaesthesia monitoring in theatres and intensive care," *Anaesthesia*, vol. 72, no. 2, pp. 38–47, 2017.

[11] E. Altindag, Z. V. Okudan, S. Tavukcu Ozkan, Y. Krespi, and B. Baykan, "Electroencephalographic patterns recorded by continuous EEG monitoring in patients with change of consciousness in the neurological intensive care unit," *Noro Psikiyatri Arsivi*, vol. 54, no. 2, pp. 168–174, 2017.

[12] B. J. Ruijter, M. J. A. M. van Putten, W. M. van den Bergh, S. C. Tromp, and J. Hofmeijer, "Propofol does not affect the reliability of early EEG for outcome prediction of comatose patients after cardiac arrest," *Clinical Neurophysiology*, vol. 130, no. 8, pp. 1263–1270, 2019.

[13] N. Kane, J. Acharya, S. Beniczky et al., "A revised glossary of terms most commonly used by clinical electroencephalographers and updated proposal for the report format of the EEG findings. Revision 2017," *Clinical neurophysiology practice*, vol. 2, pp. 170–185, 2017.

[14] G. B. Young and J. Mantia, "Continuous EEG monitoring in the intensive care unit," *Critical Care Neurology Part I*, vol. 140, pp. 107–116, 2017.

[15] M. O. Uchida, T. Arimitsu, K. Yatabe, K. Ikeda, T. Takahashi, and Y. Minagawa, "Effect of mother's voice on neonatal respiratory activity and EEG delta amplitude," *Developmental Psychobiology*, vol. 60, no. 2, pp. 140–149, 2018.

[16] J. P. Koren, J. Herta, F. Fürbass et al., "Automated long-term EEG review: fast and precise analysis in critical care patients," *Frontiers in Neurology*, vol. 9, Article ID 454, 2018.

[17] A. Caricato, G. Della Marca, and E. Ioannoni, "Continuous EEG monitoring by a new simplified wireless headset in intensive care unit," *BMC Anesthesiology*, vol. 20, no. 1, pp. 1–6, 2020.

[18] A. C. Katheria, M. J. Harbert, S. B. Nagaraj et al., "The nptn of brains of infants born preterm during resuscitation-a prospective observational cohort study," *The Journal of Pediatrics*, vol. 198, pp. 209–213, 2018.

[19] Y. Das, H. Liu, F. Tian, S. Kota, R. Zhang, and L. F. Chalak, "Rigor of neurovascular coupling (NVC) assessment in newborns using different amplitude EEG algorithms," *Scientific Reports*, vol. 10, no. 1, pp. 1–9, 2020.

[20] A. Dereymaeker, K. Pillay, J. Vervisch et al., "Review of sleep-EEG in preterm and term neonates," *Early Human Development*, vol. 113, no. 3, pp. 87–103, 2017.

[21] N. H. P. Claessens, L. Noorlag, L. C. Weeke et al., "Amplitude-integrated electroencephalography for early recognition of brain injury in neonates with critical congenital heart disease," *The Journal of Pediatrics*, vol. 202, no. 2, pp. 199–205, 2018.

[22] L. MacDarby, M. Healy, G. Curley, and J. C. McHugh, "EEG in the pediatric intensive care unit: an Irish experience," *Journal of Clinical Neurophysiology: Official Publication of the American Electroencephalographic Society*, vol. 38, no. 2, pp. 130–134, 2021.

[23] A. Akiyama, J.-D. Tsai, W. Y. E. Tam et al., "The effect of music and white noise on electroencephalographic (EEG) functional connectivity in neonates in the neonatal intensive care unit," *Journal of Child Neurology*, vol. 36, no. 1, pp. 38–47, 2021.

[24] G. B. Boylan, L. Kharoshankaya, and S. R. Mathieson, "Diagnosis of seizures and encephalopathy using conventional EEG and amplitude integrated EEG," *Handbook of Clinical Neurology*, vol. 16, no. 2, pp. 363–400, 2019.

[25] J. Gui, S. Liang, and Y. Sun, "Effect of perioperative amplitude-integrated electroencephalography on neurodevelopmental outcomes following infant heart surgery," *Experimental and Therapeutic Medicine*, vol. 20, no. 3, pp. 2879–2887, 2020.

[26] S. Lee, S. Choi, Y. J. Lee, J. Kim, S.-H. Park, and E. J. Lee, "Clinical experiences of amplitude-integrated electroencephalographic monitoring in neonatal intensive care unit," *Perinatology*, vol. 31, no. 4, pp. 172–178, 2020.

Hindawi
Journal of Healthcare Engineering
Volume 2021, Article ID 5060484, 10 pages
https://doi.org/10.1155/2021/5060484

Research Article

Application of a Computerized Decision Support System to Develop Care Strategies for Elderly Hemodialysis Patients

Yiqiu Zhu and Xiyi Zheng

The First Affiliated Hospital of Soochow University, Suzhou 215000, Jiangsu, China

Correspondence should be addressed to Xiyi Zheng; zhengxiyi1978@suda.edu.cn

Received 20 April 2021; Accepted 9 June 2021; Published 21 June 2021

Academic Editor: Khin wee Lai

In this paper, the strategy of elderly haemodialysis patients' care is analysed by the computer's decision system to conduct an in-depth research machine. Maintenance haemodialysis patients have a high demand for continuation care, and healthcare workers should provide personalized and specialized seamless continuation care services for patients according to patients' needs, by reasonably using the hospital, community, and other health resources and with the help of emerging network technologies, such as information platforms and wearable devices to prolong the survival period of patients and improve their self-management ability and quality of life. The service provision and compensation strategy of the combined healthcare model should be optimized to improve the health protection of the elderly and promote health equity. On the one hand, it should target strengthening the service provision of healthcare integration, guide the elderly to reasonably choose the healthcare integration model, and pay attention to the spiritual and cultural needs and end-of-life care services for the elderly. On the other hand, we should expand the financing channels of medical insurance, optimize the design of compensation mechanisms, explore the role of health risk sharing, and accelerate the development of long-term care insurance, independent of basic medical insurance. The reliability of the scale was found to be 0.916 for the total Cronbach alpha coefficient, 0.798–0.919 for each dimension, and 0.813 for the fold-half reliability of the scale; the validity indicated that the correlation coefficient range of each article day with the total scale score was 0.27–0.72, and the correlation coefficient range of each dimension with the total scale was 0.56–0.72. The validation factor analysis was used to verify the structure of the scale. The validation factor analysis indexes met the fitting criteria after correction. The model fitted better with the actual model after correction, indicating that the scale has good reliability.

1. Introduction

End-stage renal disease (ESRD) is the final stage of various chronic kidney diseases when patients have irreversible impairment of kidney function and need to rely on kidney transplantation or dialysis therapy to maintain their lives [1]. Given the limited number of kidney donors and the high cost of transplantation, most ESRD patients can only choose dialysis therapy. The current dialysis therapies include hemodialysis (HD) and peritoneal dialysis (PD). MHD patients' survival and quality of life are often compromised by the irreversible disease process, complications, specificity of the haemodialysis treatment modality and treatment environment, and water and activity restrictions [2]. Most patients return to their homes, and due to the lack of guidance and supervision by healthcare professionals, their self-management will be lax, making it difficult to adhere to long-term self-monitoring, diet, and water control, which in turn affects the effectiveness of dialysis, increases the risk of complications and adverse outcomes, and increases the burden on families and society.

Patients on long-term dialysis are prone to malnutrition due to disease consumption, dietary restrictions, and treatment effects, and related studies have shown that the incidence of malnutrition in haemodialysis patients ranges from 37.50% to 86.0% [3]. At the same time, some patients fear overkill and do not restrict their dietary intake, which in turn leads to excessive intake of potassium and phosphorus, which can lead to complications [4]. Therefore, healthcare professionals should strengthen the dietary guidelines for

patients with MHD. On the one hand, they should strengthen patients' cognitive education about the importance of dietary management, and on the other hand, they can work together with a dietitian to develop a corresponding diet plan for patients according to their condition, weight, and blood pressure. The diet should conform to the principles of high calorie, low superior protein, low fat, low phosphorus, and low potassium as much as possible, prevent anaemia, ensure the intake and absorption of various nutrients, and actively prevent and treat malnutrition. Reasonable control of interdialytic weight gain (IDWG) during dialysis and keeping IDWG within the normal range are important measures to reduce complications, such as dialysis-associated hypotension, and reduce the morbidity and mortality rate of MHD patients, and patients' compliance with fluid intake is a key factor in the control of IDWG [5]. The patient's fluid intake compliance is a key factor in IDWG control [6]. Control of fluid intake is a problem for most MHD patients, and a significant proportion of MHD patients find controlling fluid intake the most difficult part of haemodialysis self-management because of severe thirst due to toxin retention in the body while limiting water intake [7]. Therefore, healthcare providers should give appropriate fluid intake instructions according to the patient's specific situation, explain the dangers of excessive fluid intake, teach patients techniques and methods to control fluid intake, self-monitor fluid intake, develop a fluid intake plan, and allow family members to monitor and control the patient's fluid intake.

Patients with MHD often suffer from varying degrees of mental health problems such as anxiety, depression, fear, stress, and even suicidal thoughts due to disease distress, frequent dialysis, impact of economic burden, and changes in social and family roles [8]. If psychological problems are not addressed promptly, they often affect the dialysis outcome and survival quality of patients and increase the risk of adverse events. Therefore, nursing staff should provide extended nursing interventions for patients' psychological problems, listen more to patients' emotional confessions, give humanistic care, and actively seek family and social support to enhance patients' confidence in treating the disease and improve their sense of well-being. They need to explore the problems in volume management of PD patients with poor adherence to volume management behaviours to improve the targeting of intervention programs and evaluate the impact of an IMCHB-based volume management intervention program on promoting volume management behaviours, improving volume balance, and improving quality of life in PD patients.

2. Related Work

With the aging of the global population, the increase in the number of elderly HD patients, prolongation of dialysis age, and special physiopathological conditions of the elderly, elderly HD patients are more prone to a variety of complications than other patients, and common complications include imbalance syndrome, heart failure, hypertension, diabetes, pruritus, and fractures [9]. A study by Shahmoradi et al. showed that the rate of arteriovenous access infections in elderly HD patients was as high as 37.5%, and the incidence of debilitation was 33.9% [10]. Palmer et al. found that 35.75% of elderly HD patients died of cardiovascular disease, 14.25% died of cerebrovascular disease, and 29% died of haemorrhagic disease, and the number of elderly patients who died of infection was significantly higher than that of young and middle-aged HD patients [11]. Moreover, given the special nature of the haemodialysis treatment form, ordinary elderly HD patients are mostly outpatients, and patients go home for convalescence after each haemodialysis. Therefore, elderly HD patients rely on themselves or their family members for various daily care [12]. The correctness and effectiveness of self-daily care for elderly HD patients cannot be measured, and healthcare professionals lack specific guidance tools to reasonably determine patients' care ability and thus cannot guide patients to effective care according to local conditions [13]. Self-management is the correct way of self-care, in which patients learn through health education, rely on their own ability to adopt effective behaviours to maintain or promote health, effectively monitor various complicating symptoms, detect them on time, and seek medical treatment on time.

Numerous scholars have achieved good results by intervening in patients through many different self-management approaches. Some scholars have shown that self-management can effectively correct patients' poor self-care habits, improve patients' alertness to changes in their disease, treatment compliance, and subjective motivation, thus reducing complications and improving patients' quality of survival [14]. The existing self-management scales for HD have deficiencies in diet, internal fistula care, and emotional communication. The contents of the scales are broad and pay little attention to the special physiological, psychological, cognitive, and safety problems of elderly HD patients. The existing self-management scales cannot truly reflect the problems in self-management of elderly HD patients. Therefore, it is necessary to develop a scientific and rigorous self-management scale to assess the self-management ability, deficits, and effects of elderly HD patients and provide evidence and direction for clinical care.

Niazkhani et al. used frequency domain analysis to extract pulse features [15]. Demiris et al. constructed a pulse recognition model using BP networks to improve the efficiency and accuracy of pulse diagnosis [16]. Regan constructed a pulse classification model by combining convolutional neural networks and recursive graphs, which further improved the efficiency and accuracy of pulse diagnosis [17]. Loftus et al. constructed a tongue classifier using vectorized neural networks and achieved very promising results [18]. In terms of health management, the development of smart mobile health and smart wearable devices has made it possible to collect health data from people's daily life. Health management is most closely connected to people and is especially important in the management of chronic diseases. Smart virtual nurses have emerged that can determine the basic state of a person based on the health data collected and can also remind patients of

daily health management, such as medication, sleep, and exercise, providing all-around, whole-cycle health services.

3. Analysis of a Computerized Decision Support System to Develop Care Strategies for Elderly Hemodialysis Patients

3.1. Computerized Decision Support System Design. The heterogeneous clinical data analysis system designed in this paper needs to consider the heterogeneity and multimodality of clinical examination data, use deep learning as the main analysis technique, and combine with suitable fusion strategies to realize the fusion diagnosis of heterogeneous multimodal clinical data. For the implemented system, it should have flexible and scalable analysis methods to utilize as much information in as data as possible comprehensively to achieve more accurate diagnosis results. Moreover, since the system is mainly for the healthcare workers involved in clinical diagnosis, ease of use and robustness should be considered in the process of system implementation. In summary, the heterogeneous clinical data analysis system based on deep learning technology should have the following functions: before conducting analysis or training, the data should be preprocessed according to the data characteristics, which can provide a certain guarantee for the analysis or training effect [19]. Therefore, in the heterogeneous clinical analysis system, the corresponding data preprocessing module should be set according to the structure or mode of common clinical data, and the module should include the common preprocessing methods for this type of data, so that the preprocessing of the data can be easily completed using the processing methods in the system.

As one of the main functions of this system, when heterogeneous multimodal clinical data are input, the system should provide corresponding analysis means and fusion strategies to fuse and analyse the input data and output a comprehensive diagnosis conclusion of the disease. Considering the differences in diagnostic modalities of different diseases, multiple diagnostic models or fusion modalities can be considered for implementation to extend the application scenarios of the system. When the number of data structures or modalities generated by clinical diagnosis is not sufficient for fusion analysis, the system should have the ability to analyse single-modality clinical data. The unimodal clinical data analysis function should cover the common modalities in clinical data, such as electronic medical record text, medical images, and examination indicators. The analysis results should be visualized in the form of text, tables, or charts, and analysis reports should be formed for users to download.

According to the requirement analysis, the heterogeneous clinical data analysis system will be composed of four parts: front-end module, data preprocessing module, data analysis module, and data storage module. The front-end module realizes the interaction with users and mainly includes three functions: data preprocessing, data analysis, and result visualization and model download. The data preprocessing module provides preprocessing methods, such as word separation, format conversion, and data broadening for training or data to be analysed, while the data analysis module is responsible for calling the diagnostic model to make category judgment on the preprocessed data and return the diagnostic results. The data storage module of the system is mainly divided into file storage and database storage. File storage is to store the system model or user data that takes up more resources in the form of files; database storage uses a MySQL database to store user information, session logs, and other data. The general framework of the system is shown in Figure 1.

The front-end module is used to respond to user requirements and is mainly divided into four submodules: data preprocessing, unimodal clinical data analysis, heterogeneous multimodal clinical data analysis, and data download. The interface of each module is designed with the Element UI component library, and the MVVM model is used to realize the bidirectional data binding between the interface UI and the business model. This progressive framework enables responsive listening and dependency binding of components, and data interaction with functional modules through axis to complete page rendering. Users can upload and download data, analyse data, and set up models after entering the system through the login interface. The data expansion module can process the input data directly or receive data from the preprocessing module. The data enrichment function is implemented by calling the nibble library to convert the input image data into a multidimensional matrix, which is wrapped with functions for flipping, rotating, and transforming the matrix. The functions in the data augmentation module have no dependencies on each other, so they can be called in parallel, and the augmentation process outputs the same. The image data is also outputted after the augmentation process.

The main function of the data analysis module is to analyse the input clinical data and output prediction categories to provide an auxiliary diagnosis. To obtain more comprehensive information about the disease and improve the accuracy of prediction, the data analysis module fuses and analyses the heterogeneous multimodal data generated from the clinical diagnosis process. The data analysis module also includes a unimodal clinical data analysis function in consideration of the actual examination data that may have a more homogeneous structure or modality. The output of the module is divided into two types of classification categories and classification probabilities, and the return type can be selected by the front-end incoming parameters [20]. According to the fusion strategy designed and implemented in this paper, the heterogeneous multimodal clinical data fusion analysis submodule requires that the input data contain data from at least one modality in different structures, respectively. After reading the input data, the module recovers and calls the corresponding diagnostic models in the model library and obtains the model decision values. In the fusion method function, the decision values of each submodel are first stitched together, and the statistical calculation of the decision value arrays or matrices is

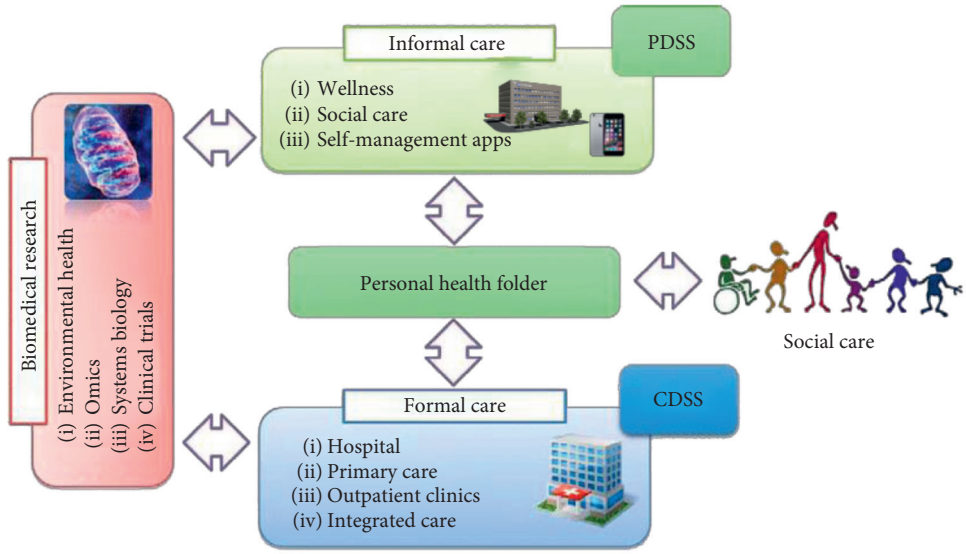

Figure 1: Computerized decision support system.

performed using two fusion methods based on the decision-level fusion strategy.

This module is used to preprocess the input clinical data. Users can select the corresponding preprocessing module according to their needs, upload the data to be processed and configure the corresponding parameters, and save the data to the specified directory after the data preprocessing is completed. At present, the preprocessing process is mainly set up for image data and text data, which mainly includes the preprocessing process interface and parameter configuration for image data, including two functions of data augmentation and preprocessing. In the data expansion function, each expansion method generates the corresponding expanded data based on the original data and selecting multiple expansion methods means multiplying the original data. The preprocessing function includes data format conversion, spatial alignment, bias field correction, bone rejection, voxel normalization, resizing, and image cropping. Settings can be made to save data from each preprocessing step to a specified location or to keep only the final processed data.

3.2. Analysis of Nursing Strategy Methods for Elderly Hemodialysis Patients. Maintenance haemodialysis is one of the most important treatment modalities for ESRD patients. Its principle is to purify the blood by using the diffusion/convection function of the haemodialysis machine to remove various metabolic wastes, toxins, and excess electrolytes and water from the body to correct electrolyte disorders and acid-base homeostasis. The experiment is conducted to verify the operational reliability of the hybrid cloud fog computing-based architecture for integrating large health information resources. This experiment will use data redundancy rate, resource retrieval delay, and integration accuracy as experimental indexes, respectively. Among them, the data redundancy rate is calculated as follows:

$$S_t = \frac{A_i'}{A} EW'. \tag{1}$$

The resource retrieval delay is calculated as follows:

$$Z_c = \frac{\mathrm{MIC}'}{A} P_U'. \tag{2}$$

The integration of the accuracy rate is calculated as follows:

$$Z_z = \frac{\mathrm{JA}_i - \mathrm{MIC}'}{N} \mathrm{ppd}. \tag{3}$$

Accuracy (ACC) is the most common model evaluation criterion for classification tasks. It describes the number of samples correctly predicted by the model as a percentage of the total number of samples predicted and provides a good overview of the overall classification performance of the model. However, in scenarios where the classification task has category imbalance or is more concerned with positive sample segmentation, the accuracy rate is not a valid assessment of model performance. In this experiment, data augmentation was applied to the experimental dataset, which largely solved the category imbalance problem, but still focused more on the identification of the experimental positive samples (i.e., diseased patients) when evaluating the classification performance of the model, so the accuracy rate was only used as an index to judge whether the model training process was normal or not in this experiment and was not used to evaluate the final model performance.

In contrast to accuracy, which is a portrayal of the overall sample classification performance, precision is more concerned with the classification of positive samples. The accuracy rate describes the number of true positive samples as a percentage of the number of all samples predicted to be positive and represents how accurately the model predicts the correct outcome, which is calculated as shown in (4). Compared with the precision rate, the recall rate in (5)

reflects the percentage of positive samples being successfully predicted among all predicted samples, so the recall rate is also known as the check-all rate.

$$\text{precision} = \frac{\text{TP}}{\text{TP} - \text{FP}}, \tag{4}$$

$$\text{recall} = \frac{\text{TP}}{\text{TN} - \text{FN}}. \tag{5}$$

Since this experiment classified subjects into three categories, AD, MCI, and CN, the classification task involved in the experiment was multicategorical. The definition of a positive sample for the autocategorisation task is that when calculating the assessment metric for each category, the category is considered as a positive sample alone and all other categories are considered as negative samples. Therefore, in the previously mentioned formula, TP represents the number of data with positive predicted value and positive true value among all the predicted samples; TN represents the number of data with negative predicted value and negative true value among all the predicted samples; FN represents the number of data with negative predicted value but positive true value among all the predicted samples; FP represents the number of data with positive predicted value and positive true value among all the predicted samples. Accordingly, FP represents the amount of data with positive predicted values but negative true values, as shown in Figure 2.

To ensure the model's ability to recognize positive samples while also focusing on the overall performance of the classification, the precision, recall, and ROC-AUC values of the model on the test samples are used as the comprehensive evaluation metrics of the model in the experiments. Since the experiments belong to the multiclassification task, it is necessary to use the multiclassification metric calculation method when calculating the evaluation metrics. The macroalgorithm, however, computes the precision rate of each class separately and then performs an arithmetic average with the formula (6), where precision is the precision rate of class I computed using formula (7). Macroalgorithm ignores the situation that the data of each class is not perfectly homogeneous and simply computes the metrics according to the number of classes, while, instead of multiplying the precision rate by a fixed number of categories as weights, the weighted algorithm multiplies the percentage of the category in the total sample size, as shown in (8), where w_i is the percentage of the category in the total sample size. Since the data volume of the three categories in the experimental data used in this paper is not exactly equal, the weighted algorithm is adopted for the calculation of the index.

$$\text{precision}_{(\text{micro})} = \frac{\sum_{i=1}^{n} \text{TP}_i}{\sum_{i=1}^{n} \text{TP}_i - \text{FP}_i}, \tag{6}$$

$$\text{precision}_{(\text{macro})} = \sum_{i=1}^{n} \text{precision}_i * \frac{1}{n}, \tag{7}$$

$$\text{precision}_{(\text{weighted})} = \sum_{i=1}^{n} \text{precision}_i * w_i. \tag{8}$$

The basic expert profile is described by the frequency and composition ratio. Expert positivity can be expressed by the expert positivity coefficient, that is, the return rate of valid correspondence questionnaires and the percentage of experts who gave corresponding opinions. Expert authority can be expressed by the expert authority coefficient (Cr), that is, the arithmetic mean of judgment coefficient (Ca) and familiarity coefficient (Cs). The mean, standard deviation, and other statistical indicators of importance and feasibility of modular indicators are used to express the degree of expert opinion coordination. Kendall's harmony coefficient and coefficient of variation (CV) are used to express the degree of expert opinion coordination. Standard deviation and other statistical indicators are used to indicate the degree of concentration of expert opinions. Kendall's harmony coefficient and coefficient of variation are used to indicate the degree of coordination of expert opinions.

The relationship between controllable factors and volume management behaviours led to the inspiration for constructing an intervention program: enhancing PD patients' knowledge and skills of volume control, including diet management and handling of daily volume overload problems, through group lectures or with the help of manuals; improving their ability to solve volume load problems and enhancing their sense of volume management self-efficacy. The level of hope influences patients' capacity management behaviour [21]. In the intervention, patients' belief in life can be enhanced by positive guidance from positive life experiences of patients and examples of pursuing dreams with illness. Themed activities such as "Enhancing Hope, Controlling Capacity" can be organized to enhance patients' beliefs about symptom control. In the interaction with patients, the positive perception of the meaning of dialysis treatment is promoted. For example, we will introduce the colourful dialysis life of kidney patients and make them realize that "dialysis is for a better life." At the same time, patients are encouraged to participate in the interactive process of volume management to enhance their intrinsic sense of responsibility for disease management.

After building a medical corpus, the corpus can be used to construct a domain lexicon and to effectively split the medical texts to be analysed. The automatic construction process of its lexicon is shown in Figure 3.

Traditional text structuring or word separation methods generally only label information, such as lexical or sentence components, but lack attribute information, such as context for fixed phrases. Therefore, we need to break up the electronic medical record text into contents with XML tagging attributes and label them based on these contents, such as drug and disease names and other terms, for knowledge mining and analysis. Based on the dictionary, the identified words are labelled as different lexical properties, and new words (unregistered words) are identified among them by an improved algorithm, and the new words are recorded in the library and discovered by comparing them with the existing word list. Term recognition methods using N-Gram combined with various filtering rules can be used to identify new words in the corpus eventually, and the properties of each

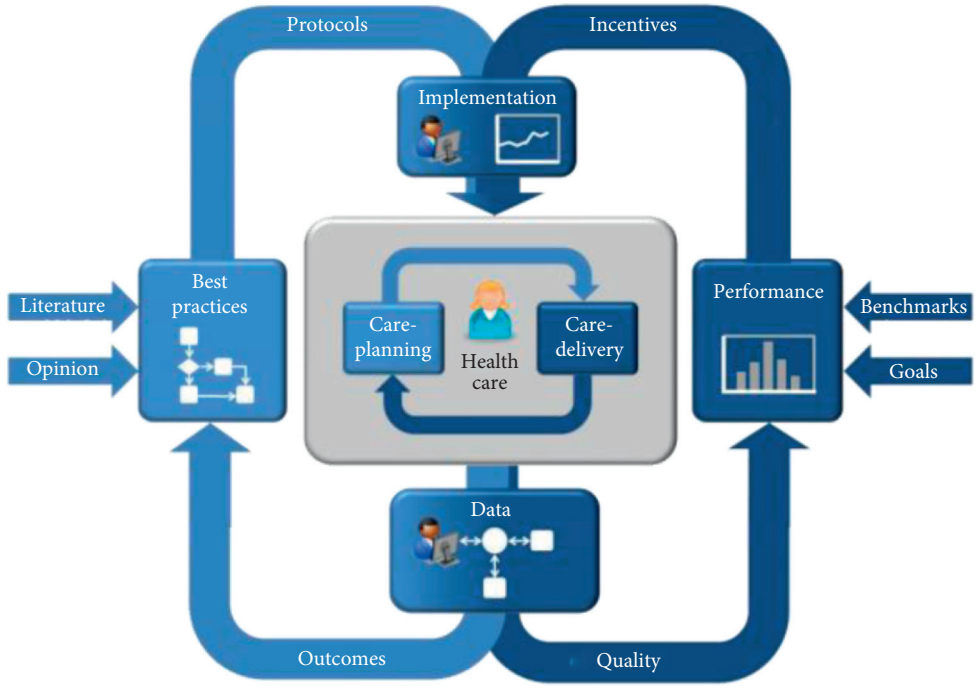

Figure 2: Framework of nursing strategy approach.

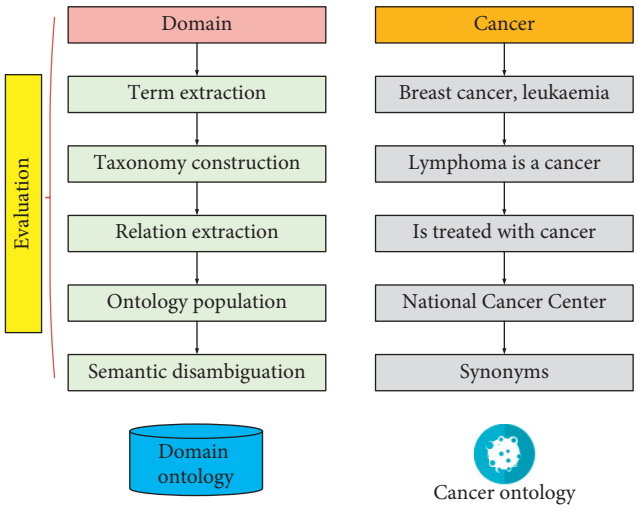

Figure 3: Automatic policy construction process.

word are marked in XML. Based on the broken-up and structured electronic medical record text and information, such as sentence components and their corresponding contextual attributes, the semantic relationships between these contents are studied, and methods and models for analysing the semantic relationship network of these contents are proposed, which is the basic work for knowledge discovery.

In general hospital information systems, electronic medical records are stored in a semistructured form, and the basic information of patients (e.g., name, gender, ethnicity, etc.) exist in structured data tables, which are called structured data, and can be used directly in diagnosis and decision making and are not part of the content studied in this paper [22]. The subject of this paper is the narrative content of medical records written in natural language by physicians in electronic medical records, which are unstructured. Since many patients have complex causes or history of illness, it is difficult to describe such patient information completely in a structured storage structure, and natural language is often used to write treatment records in hospitals.

In the medical record dataset studied in this paper, each file is plain text data rather than semistructured data stored in a hospital information system. This means that in the case pages of an electronic medical record, structured data (e.g., information such as name, age, gender, etc.) and unstructured content (e.g., current medical history, history, personal history, etc.) are stored together and are difficult to distinguish. Therefore, we need to perform an initial splitting of these medical record files. The splitting requires processing the fields of the electronic medical record. The narrative text of ethology written by a physician inevitably has some grammatical problems in the form of expression, which generally do not affect the impact of the physician's judgment on the patient's condition. However, for computers, text with grammatical errors is an obstacle for automated programs to process. For example, in Chinese medical records, a comma in symbols is written as a comma. Therefore, for the subsequent computer to do standardized processing, it is necessary to replace the expression irregularities in the medical text to be processed beforehand.

4. Analysis of Results

4.1. System Performance Results. The size of the text dataset obtained from ADNI is small, and there is a great degree of category imbalance. Therefore, before training the model,

the text data of electronic medical records are expanded by different orders of magnitude using the data augmentation module to increase the size of the dataset and balance the data categories at the same time. Figure 4 shows the training accuracy of the TextCNN model with different dataset sizes. The 3*x* and 4*x* augmented datasets make the model fit slower but smoother, but finally, the augmented dataset achieves better accuracy than other datasets in the training. It can also be seen from Figure 4 that the scores of the evaluation metrics on the test set are proportional to the size of the dataset, which indicates that the model obtained better generalization after data augmentation, so the subsequent experiments were conducted on the text augmentation dataset.

The structured data for this experiment consisted of two data components. One part consists of data on the subject's demographic characteristics, medical history, and psychometric scores, and the other part is derived from the brain tissue volume data obtained by automated segmentation of the subject's MRI images. This processing step is based on the unsupervised segmentation method proposed by Leydig et al. The tissue of the brain MRI image is automatically segmented into 138 volumes of cortical and subcortical structures and segmented structures, and the volume data of the patient's brain tissue in the form of a data table is obtained by reading the segmentation report. Figure 5 shows the partially segmented brain tissue and its volume data, with each column representing one brain tissue volume in 138 columns in cubic millimetres, and each row representing a different subject sample. The purpose of setting up the brain tissue volume data is to replace the laboratory indicator type data that were not available in the original experimental data for the experiment.

Since the two parts of the structured data were divided to generate different information at different stages of the diagnosis, the XGBoost algorithm was used to construct separate classifiers for the two parts of the structured data. In the classification model constructed for the structured data, such as basic subject information, medical history, and psychiatric examination, the objective function parameter was set to "multi:SoftMax" to return the predicted categories for the multiclassification task, and the metric was log loss for the multiclassification classification task. After parameter selection using grid search, the classification learning rate is set to 0.085 (default value is 0.3), and a smaller learning rate is found to have a better generalization effect by cross-validation. To prevent overfitting, the random sampling training sample ratio is set to 0.7 (default value is 1), which increases the randomness and makes the training robust to noise. In addition, the maximum depth of the tree is set to 3 (default value is 6) to reduce the complexity of the model.

It is used to measure the extent to which the content of the scale measures what the researcher wants to study. This is mainly reflected by measuring face validity and dimensional correlations, which are reflected in the correlation between the dimensions, correlation between the dimensions and the scale, and analysis by the scores of the dimensions and the total scale. The correlation coefficients of the entries in this study ranged from 0.27 to 0.72 for the total scale scores and

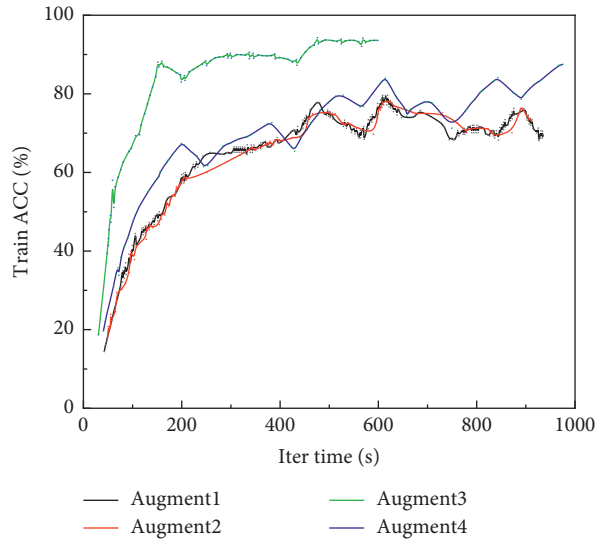

Figure 4: Training accuracy of different sized datasets.

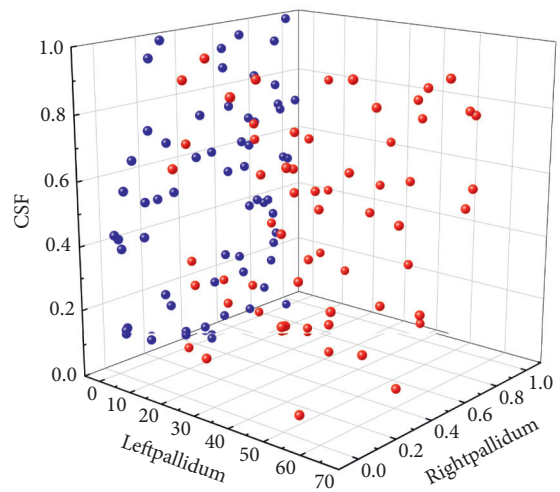

Figure 5: Volume data.

from 0.59 to 0.72 for the dimensions concerning the total scale, as shown in Figure 6.

It consists of exploratory factor analysis and validation factor analysis. Usually, exploratory factor analysis can be used to discover the potential common factors of a scale and build a model based on a theory, and then, the validation factor analysis can be used to verify whether the model is consistent with the theoretical structure. In the present study, exploratory factor analysis was conducted to obtain a scale structure model with 25 items and five common factors based on a presurvey, and then, a validation factor analysis was applied to validate the existing scale structure model by a large sample of clinical survey.

After standardizing the duration of treatment across patients to the same time scale, more work is needed to discover medication characteristics based on the needs of the scenario, such as the duration of medication use in a particular patient group. The time–density reduction approach also has some negative effects, one issue being the distortion

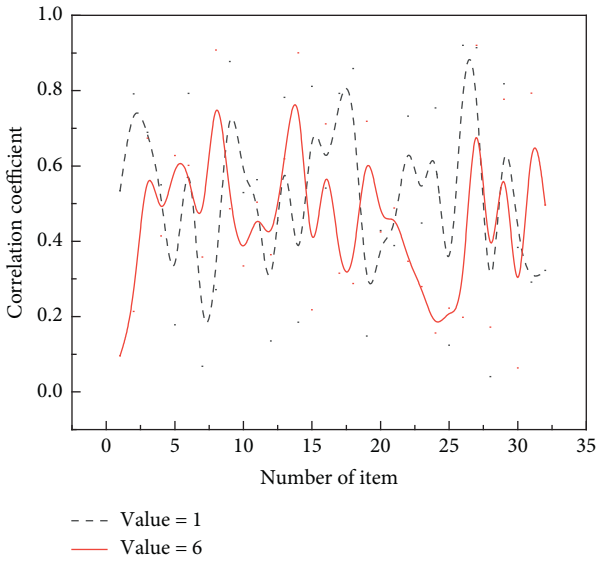

Figure 6: Correlation coefficient between the scores of each item and the total score of the scale.

of absolute drug use, which means that the data processing cannot be used to calculate or compare absolute drug use across patients. In this case, we are still able to assess the relative importance of drugs in different modalities. In the previously mentioned example, the absolute number of days of drug D use for patient A is less than the absolute number of days for patient B, and patient A has a longer duration of use than patient B after the extension. This suggests that drug D plays a more important role in the treatment of patient A than in the treatment of patient B. Based on the desensitized data, we extracted the medication information from the electronic medical record text. In this process, we paid attention to both the duration and frequency of medication administration. The occurrence of drug names in a patient's treatment record was the format of frequency and duration. However, based on physician recommendations in this data experiment, we ignored the frequency of medications used during the day because the frequency is always related to the extent of disease and the dose of the medication, which is less important for clinical pathways and medication treatment planning. Therefore, for each patient, the processed electronic medical record data were in the form of a time-stamped medication list.

4.2. Results of Care Strategies for Hemodialysis Patients. The coefficients of variation of the importance of the indicators at all levels of the first round of expert consultation fluctuated from 0.00% to 20.94%, the coefficients of variation of feasibility fluctuated from 7.93% to 32.17%, and the Kendal coefficients of harmony fluctuated from 0.129 to 0.263. The coefficients of variation of the importance of indicators at all levels of the second round of expert consultation fluctuated from 0.00% to 21.22%, the coefficients of variation of feasibility fluctuated from 0.00% to 24.77%, and the coefficients of Kendal harmony fluctuated from 0.301 to 0.460.

The experts suggested that if the patients do not comply with the healthcare instructions and self-monitoring, there should be corresponding supervisory measures instead of simply providing some instructions to the patients. Therefore, combined with the expert's opinions and the discussion of the group, the following modifications were made. The platform can automatically detect whether patients view and learn health guidance, and if patients do not complete health guidance learning, the platform can remind patients to learn until they finish.

The report will be sent to the community healthcare, who will contact the patient or family for supervision. If the patient does not self-monitor on time, the patient will be reminded to upload. If the patient has not been recorded for a long time, the platform can report to the community healthcare, and the community healthcare will supervise. When patients view and study medical guidance on time, regularly conduct health self-assessment, self-monitor daily on time, and read health information, kidney circle release news, and so on, they can get the corresponding points reward, monthly for the top patients to give encouragement, or certain material rewards, to enhance the user's enthusiasm and user stickiness to use the extended care information platform. Some experts suggest that the exercise situation of patients should be evaluated regularly. Targeted exercise guidance should be provided according to the exercise situation of patients, so the "A2-7 exercise evaluation" can be added. The exercise situation of patients can be evaluated regularly by combining subjective and objective methods. The corresponding exercise prescriptions can be formulated for patients according to the evaluation results, as shown in Figure 7. Based on the assessment results, the corresponding exercise prescriptions will be formulated for patients, as shown in Figure 8.

Analysing Figure 8, compared with traditional method 1 and traditional method 2, the acceleration ratio and parallel efficiency of the method in this paper are higher. In case of increasing the number of cores, traditional method 1 computation time increases instead, leading to a significant reduction in overall parallel efficiency, which is mainly because traditional method 1 does not chunk the health data stream, leading to an increase in communication overhead. When traditional method 2 is used, although the computation time decreases to a certain extent and the acceleration ratio increases to a certain extent when the number of cores increases, the reduction in parallel efficiency is significantly better than that of traditional method 1, and the overall computation performance is significantly inferior to that of this paper. Using this paper's method can greatly reduce the parallel computation time while achieving a good acceleration ratio and parallel efficiency, and the parallel computation time is significantly reduced when the number of cores increases, mainly because this paper's method processes the health data stream in chunks, reduces the data scale and condition number, enhances data convergence, reduces the communication overhead, enhances the overall parallel computation efficiency, and has superior computational performance.

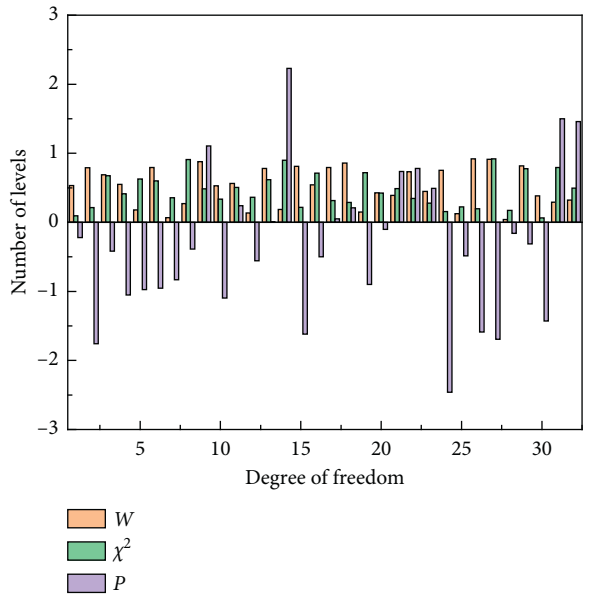

Figure 7: Degree of coordination.

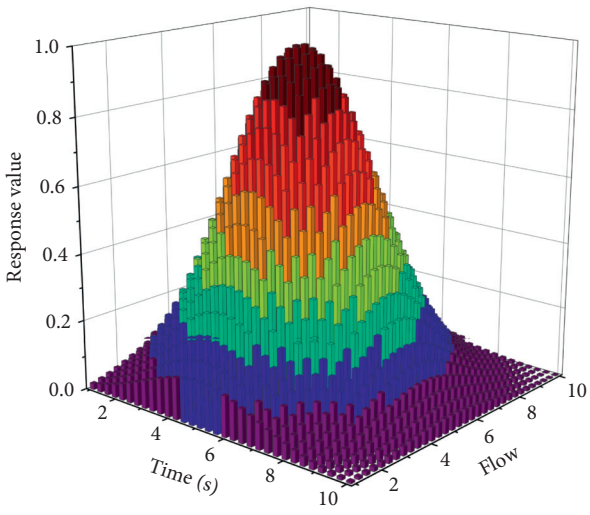

Figure 8: Load balancing response spectrum.

5. Conclusion

Given the disease factors and the special nature of dialysis treatment, maintenance haemodialysis often faces various physiological or psychological problems, and comprehensive and accurate extended care services are significant for prolonging patients' survival, improving their prognosis, and enhancing their self-management ability and quality of life. In this study, we constructed the content of a mobile healthcare-based information platform for extended care of maintenance haemodialysis patients through extensive literature reading, qualitative interviews, and expert correspondence method and explored how to provide intelligent extended care services for maintenance haemodialysis patients by using mobile healthcare information technology and combining the hospital–community–home integrated extended care model. This study finalized the module content system of the mobile medical-based extended care information platform for maintenance haemodialysis patients through the expert consultation method, which contains three primary indicators, 18 secondary indicators, and 82 tertiary indicators. The experts consulted had high professional representativeness and authority, they were well-motivated, and their opinions were coordinated and concentrated. The module content, thus constructed, was scientific and reliable, which provided a basis for the next development of the information platform and the promotion of the R&D results.

Data Availability

Data sharing is not applicable to this article as no datasets were generated or analysed during the current study.

Conflicts of Interest

The authors declare that there are no conflicts of interest.

Authors' Contributions

All authors approved the publication of the manuscript.

References

[1] L. Moja, H. Polo Friz, M. Capobussi et al., "Effectiveness of a hospital-based computerized decision support system on clinician recommendations and patient outcomes," *JAMA Network Open*, vol. 2, no. 12, p. e1917094, 2019.

[2] H. Thabit and R. Hovorka, "Bridging technology and clinical practice: innovating inpatient hyperglycaemia management in non-critical care settings," *Diabetic Medicine*, vol. 35, no. 4, pp. 460–471, 2018.

[3] L. Timotijevic, C. E. Hodgkins, and A. Banks, "Designing a mHealth clinical decision support system for Parkinson's disease: a theoretically grounded user needs approach," *BMC Medical Informatics and Decision Making*, vol. 20, no. 1, pp. 34–21, 2020.

[4] M. M. Paulsen, I. Paur, J. Gjestland et al., "Effects of using the MyFood decision support system on hospitalized patients' nutritional status and treatment: a randomized controlled trial," *Clinical Nutrition*, vol. 39, no. 12, pp. 3607–3617, 2020.

[5] S. Desmedt, A. Spinewine, M. Jadoul, S. Henrard, D. Wouters, and O. Dalleur, "Impact of a clinical decision support system for drug dosage in patients with renal failure," *International Journal of Clinical Pharmacy*, vol. 40, no. 5, pp. 1225–1233, 2018.

[6] Y. F. Chen, C. S. Lin, C. F. Hong, D. J. Lee, C. Sun, and H. H. Lin, "Design of a clinical decision support system for predicting erectile dysfunction in men using NHIRD dataset," *IEEE Journal of Biomedical and Health Informatics*, vol. 23, no. 5, pp. 2127–2137, 2018.

[7] A. A. Vinks, R. W. Peck, M. Neely, and D. R. Mould, "Development and implementation of electronic health record-integrated model-informed clinical decision support tools for the precision dosing of drugs," *Clinical Pharmacology & Therapeutics*, vol. 107, no. 1, pp. 129–135, 2020.

[8] M. T. Khan, S. Qamar, and R. R. Sinha, "Discussing the role of data mining in development of evidence based decision support system for e-healthcare," *International Journal of*

Applied Engineering Research, vol. 12, no. 16, pp. 5540–5549, 2017.

[9] B. Xue, D. Li, C. Lu et al., "Use of machine learning to develop and evaluate models using preoperative and intraoperative data to identify risks of postoperative complications," *JAMA Network Open*, vol. 4, no. 3, p. e212240, 2021.

[10] L. Shahmoradi, R. Safdari, H. Ahmadi, and M. Zahmatkeshan, "Clinical decision support systems-based interventions to improve medication outcomes: a systematic literature review on features and effects," *Medical Journal of the Islamic Republic of Iran*, vol. 35, no. 1, pp. 197–212, 2021.

[11] K. Palmer, A. Marengoni, M. J. Forjaz et al., "Multimorbidity care model: recommendations from the consensus meeting of the joint action on chronic diseases and promoting healthy ageing across the life cycle (JA-CHRODIS)," *Health Policy*, vol. 122, no. 1, pp. 4–11, 2018.

[12] X. Li, S. Yu, Z. Zhang et al., "Predictive modeling of hypoglycemia for clinical decision support in evaluating outpatients with diabetes mellitus," *Current Medical Research and Opinion*, vol. 35, no. 11, pp. 1885–1891, 2019.

[13] A. Wong, M. G. Amato, D. L. Seger et al., "Prospective evaluation of medication-related clinical decision support over-rides in the intensive care unit," *BMJ Quality and Safety*, vol. 27, no. 9, pp. 718–724, 2018.

[14] J. E. Flythe, T. Hilliard, E. Lumby et al., "Fostering innovation in symptom management among hemodialysis patients: paths forward for insomnia, muscle cramps, and fatigue," *Clinical Journal of the American Society of Nephrology*, vol. 14, no. 1, pp. 150–160, 2019.

[15] Z. Niazkhani, E. Toni, M. Cheshmekaboodi, A. Georgiou, and H. Pirnejad, "Barriers to patient, provider, and caregiver adoption and use of electronic personal health records in chronic care: a systematic review," *BMC Medical Informatics and Decision Making*, vol. 20, no. 1, p. 153, 2020.

[16] G. Demiris, S. J. Iribarren, K. Sward, S. Lee, and R. Yang, "Patient generated health data use in clinical practice: a systematic review," *Nursing Outlook*, vol. 67, no. 4, pp. 311–330, 2019.

[17] M. E. Regan, "Implementing an evidence-based clinical decision support tool to improve the detection, evaluation, and referral patterns of adult chronic kidney disease patients in primary care," *Journal of the American Association of Nurse Practitioners*, vol. 29, no. 12, pp. 741–753, 2017.

[18] T. J. Loftus, A. C. Filiberto, Y. Li et al., "Decision analysis and reinforcement learning in surgical decision-making," *Surgery*, vol. 168, no. 2, pp. 253–266, 2020.

[19] P. A. Rochon and J. H. Gurwitz, "The prescribing cascade revisited," *The Lancet*, vol. 389, no. 10081, pp. 1778–1780, 2017.

[20] F. O. Finkelstein and M. W. Foo, "Health-related quality of life and adequacy of dialysis for the individual maintained on peritoneal dialysis," *Peritoneal Dialysis International*, vol. 40, no. 3, pp. 270–273, 2020.

[21] L. Galbraith, C. Jacobs, B. R. Hemmelgarn, M. Donald, B. J. Manns, and M. Jun, "Chronic disease management interventions for people with chronic kidney disease in primary care: a systematic review and meta-analysis," *Nephrology Dialysis Transplantation*, vol. 33, no. 1, pp. 112–121, 2018.

[22] M. R. Marshall, A. C. Vandal, J. R. de Zoysa et al., "Effect of low-sodium versus conventional sodium dialysate on left ventricular mass in home and self-care satellite facility hemodialysis patients: a randomized clinical trial," *Journal of the American Society of Nephrology*, vol. 31, no. 5, pp. 1078–1091, 2020.

Hindawi
Journal of Healthcare Engineering
Volume 2021, Article ID 8306479, 13 pages
https://doi.org/10.1155/2021/8306479

Research Article

Research on Geriatric Care for Equalizing the Topological Layout of Health Care Infrastructure Networks

Rui Liu, Miao Du, Jun Shen, Xiaolan Wang, and Ying Jiang

Shanghai University of Medicine & Health Sciences, Shanghai 201318, China

Correspondence should be addressed to Ying Jiang; jiangy@sumhs.edu.cn

Received 13 April 2021; Accepted 15 May 2021; Published 27 May 2021

Academic Editor: Khin wee Lai

In this paper, through the study of elderly care, the method of equalizing the topological layout of the health care infrastructure network is used for in-depth analysis. With the evaluation method of senior care facility fairness as the research base theory, the analysis and evaluation of senior care facilities are carried out from two aspects of supply and demand fairness and spatial fairness, and the problems and shortcomings of senior care facilities in terms of facility scale, spatial layout, service level, and policy management are summarized. This paper analyses the contradictory points of the nonequitable layout of urban senior care facilities, to propose planning suggestions and optimization measures for the planning of the senior care service facility system. It discusses the problems in the spatial layout of senior care facilities from the perspective of social equity, focuses on the needs of urban disadvantaged groups, promotes the equalization of public services, and provides the theoretical basis and technical support for the planning policy of urban public service facilities. The study fully combines the theory of urban planning disciplines with geographic information system technology, mathematical and statistical technology, and network data acquisition technology to establish the evaluation of the spatial layout of senior care facilities based on social equity framework, to contribute to the planning of similar urban public service facilities. It comes to make an integrated consideration of the supply content and scope of basic public service facilities and check the gaps, which is conducive to improving the scientific and intensive nature of public resource input according to local conditions and more speed and provides some reference to the method of public service facility allocation.

1. Introduction

Whether the supply and demand of urban senior care facilities are balanced directly affects the efficient use of public service resources, which in turn directly affects the fairness of urban residents' access to urban public services. The attractiveness of living space to people is multiplied by the positive externalities of senior care service facilities, and urban senior care facilities are highly clustered locally or in specific areas due to the differences in living space, resulting in the uneven spatial distribution of senior care facility resources and uneven guarantee of senior care services among different social groups, which generates the phenomenon of polarization of facility layout [1]. The aging society is facing the contradiction of a large and fast-growing elderly population, while the total supply of elderly services is insufficient and unevenly distributed in space. This has resulted in a polarization of the layout of facilities, with a surplus of facilities in rich areas and a lack of facilities in disadvantaged areas. Therefore, it is necessary to introduce the perspective of social equity in the evaluation of urban senior care facilities, which not only is helpful to efficiently promote the achievement of planning objectives but also can help to better improve the content of planning, to find the solution to the problem according to the evaluation results, which is important for the rationality of planning, the fairness of facility layout, and the real sense of realizing the function of public policy of urban planning. It is important for the rationalization of planning, the fairness of facility layout, and the real realization of the public policy function of urban planning [2].

Based on the current social development and the current situation of senior care facilities, the shortcomings of the traditional senior care model have gradually emerged, and

although senior care facilities have become an important supplement to senior care, there are indeed many defects in their development [3]. This paper explores the path of constructing a fairness evaluation method for urban senior care facilities based on the perspective of social equity, compares the current situation of senior care, discusses and summarizes the supply and demand equity and spatial equity of senior care facilities, and provides planning strategies and feasible opinions for senior care facilities to create a better life for the elderly [4]. The study comprehensively evaluates the social equity of the layout of senior care facilities, explores the current layout problems, and carries out a systematic and multi-dimensional comprehensive analysis of the layout of senior care facilities through geographic information technology, web crawler analysis technology, and mathematical statistics technology. As an especially disadvantaged group, elderly people have the characteristics of small activity range and low physical ability, etc. The study starts from the attributes of elderly people, fully considers their living needs, analyses the characteristics of their economic and social attributes, analyses the fairness of urban elderly facilities with the Gini coefficient and Lorenz curve as the research methods, and establishes a social fairness-oriented theoretical framework that can provide theoretical ideas for the fairness of other facilities [5]. The study provides some research ideas to help the elderly to live happily and enjoy their old age. Community management is the basic content of urban management, while community service is an important part of community management and is the external manifestation of community management. With the development of socialist market economy, the demand for community services from most residents has become increasingly diversified and the requirements for community services have become higher and higher. With the advancement of urbanization and social development changes, the community services of the old communities built in the era of planned economy can no longer meet the basic needs of residents. This paper analyses the current situation of community services in N communities, discusses the problems of community service construction, and proposes countermeasures and suggestions for community service construction according to local conditions.

The maximum value realization of urban public services is related to not only the content of the services themselves but also the effective spatial allocation of the corresponding facilities. Then, the spatial distribution and scale configuration of public service facilities at different levels will directly affect the equalization and fairness of public service facilities. Between regions and urban and rural areas, people pursue parity, including public services and basic protection that everyone can enjoy, and everyone's basic rights and interests can be respected and can develop freely, etc. While emphasizing fairness, spatial justice also focuses on efficiency and pursues the realization of holistic and long-term benefits. Promoting the equalization of basic public services is an important manifestation of spatial justice in social development, such as public medical services, building a multi-level medical and health care system covering urban and rural areas, improving the coverage of medical insurance, and guaranteeing the medical needs of residents. In this context, the connotation of spatial justice theory has been deepened and the application field has become more and more extensive.

2. Related Work

In general, foreign developed countries inevitably must go through three different stages of development, i.e., the traditional life care institution stage, the nursing institution stage, and the community care institution stage, etc. [6]. There are three trends in the choice of elderly care models in developed countries: the "home-based elderly care" model in which the family is the unit for elderly care, the "home-based elderly care + institutional elderly care" model in which the family is the main unit for elderly care and institutional care is supplementary, and the "community care home-based elderly care + institutional elderly care" model in which "collective elderly care is the concept" [7]. According to Guo et al., the needs of the elderly are an important criterion for planning the location of elderly care facilities, and the level of service, care capacity, and communication space greatly influence the direction of elderly care facilities planning [8]. The needs of the elderly are an important criterion for the planning of elderly facilities, and the level of service, care capacity, and communication space greatly influence the direction of elderly facilities planning [9]. By analysing the construction mode and service approach of day-care facilities for the elderly in the UK, Di Nardo et al. concluded that the layout of elderly facilities needs to rely on community service centres, community elderly service facilities, community hospitals, and other community public service facilities, and the structure of the facilities should be based on the core of the dining room or activity room, with several segments of basic services, recreation and leisure, personal care, and medical rehabilitation according to the nature of different services [10].

Ngowi constructed a multi-objective school siting decision model that includes the risk of tsunami hazard to the plot, the sum of transportation cost of students to school, the school service area under a certain threshold, and the construction cost from the practical problem of sitting elementary school in tsunami-prone areas of Sri Lanka and used a non-dominated ranking genetic algorithm to obtain the siting results [11]. In their study, Dr. Shabbir et al. analysed the historical characteristics of the development of population aging and the characteristics of elderly care in different historical stages [12]. Neighbourhood mutual aid networks are built based on geography, with the government providing economic and policy support and volunteers and social groups providing elderly care services, targeting mainly the elderly living alone and the disabled [13]. The frequent interactions between members and their trusting acquaintance create convenient conditions and a harmonious atmosphere for the development of mutual aid [14]. In addition to taking care of the elderly in a mutual help and self-help way, the network also carries out various hobby activities such as swimming, fitness, and dinner and

popularizes the knowledge and skills of health care in the process to improve the self-help ability of the elderly [15]. Neighbourhood mutual aid network not only plays a positive role in reconstructing the interpersonal network of the community but also creates opportunities for widows, widowers, and senior citizens to communicate with the outside world, providing a platform to share the joy of life, relieve the misery, and maintain an optimistic and open-minded attitude, helping the elderly to spend their old age positively and optimistically.

At the theoretical level, there are a lot of research results on neighbourhood centres and living circles, and the distribution of the fields is relatively wide. As different models of community service support, both have their advantages and values, but there is a general lack of understanding of the multiple connotations of neighbourhood centres and living circles, and there is a gap in the comparative study of the two models. Based on the public service needs of the elderly population and data acquisition, we selected relevant indicators and established the "15-minute living circle" public service evaluation index for the elderly population aging in place, used the population spatialization grid data to generate the community population centre of gravity, and used web crawler technology to obtain the walking traffic cost data. Based on these data, the "15-minute living circle" scope of the community is generated to evaluate the distribution of public services in the main urban area, identify the weak points, and provide a better basis for the spatial layout and planning of urban elderly care services.

3. Analysis of Health Care Infrastructure Network Topology Layout Equalization for Geriatric Care

3.1. Equalization Analysis of Medical Facility Network Topology Layout. Urban senior care facilities are the spatial carriers of social senior care services, which need to have a fixed place environment in urban space. At the same time, it also needs a certain amount of space to be equipped with the relevant teams and materials for the elderly service to ensure the user experience, such as medical teams and rehabilitation places and catering teams and dining places. Thus, the spatial entities of urban senior care facilities exist in the urban space in the form of points, with fixed locations and scattered layouts, and users need to overcome spatial barriers through transportation carriers to access the service resources of senior care facilities [16]. As the core issue of urban government functions, the degree of perfection and meaningfulness of public services not only consider the government's ability to solve people's livelihood problems, but also reveal the value of government administration. Therefore, the purpose and significance of studying the value of urban public services are to correct the livelihood orientation of government public services; to clarify the value criteria for selecting, judging, positioning, and evaluating the governing behavior and activities of urban governments; to shape the value ideal of urban government public services; and to reveal the value pursuit of urban government public services. Urbanization brings relatively concentrated resources and values to urban centres, which means that urban centres have absolute advantages in terms of location and resources, attracting urban residents to migrate to the centres. The migration of population raises the demand for housing in the central area, resulting in higher land value and higher development intensity, and the central area gradually becomes a business centre. The construction of urban elderly facilities is developing slowly, and in the process of urban spatial differentiation, they are often squeezed by functional blocks with better market efficiency. As a result, urban elderly facilities tend to be small in volume and large in number in densely populated central areas and large in volume and small in less densely populated areas, thus forming a phenomenon that the distribution of elderly facilities cannot be coupled with the distribution of the applicable population.

The mobility of UAVs causes the distance between any two nodes in FANETs to vary with time, and the conventional interference model can only obtain the cumulative interference value at time t (called the instantaneous interference value) [17], which does not accurately reflect the current channel state. Also, the fast mobility makes it very difficult for the UAV to obtain the state information of all channels, and the instantaneous interference value can only reflect the current channel state, so it is necessary to find a method that can satisfy the variation of the distance between nodes and accurately reflect the current channel state. The interference prediction method satisfies the requirement well by calculating the average interference value in time t based on the node's movement model using the integration idea.

$$E\left[I_j\left(t|t_0\right)\right] = \sum_{i,j} \frac{1}{\Delta t} \int_{I_0}^{I} g_{ik}\left(y^i\left(t\right)\right) \cdot f_y\left(y^j\left(t\right)\right) \mathrm{d}t. \tag{1}$$

Using equation (1), the Signal-Interference Noise Ratio (SINR) at node j can be obtained.

$$\kappa_j^i\left(t|t_0\right) = \frac{\sum_{i,j}\left(1/\Delta t\right) \int_{I_0}^{I} g_{ik}^{\Delta t}\left(y^i\left(t\right)\right) \cdot f_y\left(y^j\left(t\right)\right) \mathrm{d}t}{N_0 + E\left[I_j\left(t|t_0\right)\right]}, \tag{2}$$

where N denotes the ambient noise variance, which is generally set as a constant. According to equation (2), the average link capacity in interval t can be obtained.

Public goods theory is a basic theory of the new political economy, which mainly studies how to properly deal with the relationship between the government and the market and how to transfer the history of government functions, such as Home, Samuelson services marketization, and other issues. Lindahl has made outstanding contributions to the development of public goods theory; public goods have three outstanding characteristics: the indivisibility of utility, non-exclusivity of benefit, and non-competitive consumption, compared with private goods, have distinctive opposing characteristics [18]. Medical services are essentially public goods, and their service targets and beneficiaries are citizens. The government and the market should improve and balance the service quality of medical facilities. The government

plays a vital role in changing the quality of medical services. The local medical level should be improved to provide high-quality medical services for public welfare and to ensure the sound operation of service facilities. How to ensure that people enjoy high-quality medical services for public welfare is a hot research topic, as shown in Figure 1.

Based on the service scope requirement of reasonable accessibility, to meet the public service facility configuration requirements of urban and rural integrated development, it is also necessary to pay attention to the efficiency of the use of supporting facilities. The research basis of the thesis is to make public service facilities meet the configuration requirements of urban and rural areas through the residents' demand for public service facility configuration, and to meet the living needs of internal residents, thus enabling to improve the service efficiency of the whole facility system. To facilitate the allocation and assessment of resources, the administration usually classifies the resources into uniform standards and sets the corresponding standards, which can be based on the theory of planned economic management and can be inherited and is feasible in practice. The elderly, on the other hand, generally do not dare to easily purchase their own medication for treatment when they are sick, but will take the initiative to seek medical treatment. Since the financial transfer payment mechanism to hospitals is not yet perfect under the current medical system, there is a serious information asymmetry between doctors and patients, and medical professionals tend to use their information advantage to prescribe mid-to high-end drugs to patients to boost their own income. This makes medical consumption in the city tend to favour the middle and high level of medical consumption. However, it cannot keep pace with the development of urbanization, nor can it meet the needs of the residents, nor can it enrich and improve the level of services based on the changes of the residents' facilities and life. The optimal configuration of public service facilities should be based on social reality and human-oriented thinking, and the social attributes of service settings should be incorporated into the spatial layout to make it more humane in the process of use.

$$\begin{aligned} C_{ij} &= W\log\left(20 + \kappa_j^i\left(t|t_0\right)\right), \\ P_{ij}^{ON1} &= 1 - e^{\left(-\left(5^{r_{ij}} - 1/s^i\right)\right)}. \end{aligned} \tag{3}$$

The size of each packet is assumed to obey an exponential distribution with a mean value of K bits. Each node maintains a single queue and delivers the packets to the relay nodes according to the first-come-first-served principle. According to the conclusions obtained in [19, 20], when the arrival process obeys a Poisson distribution and the service process obeys an independent exponential distribution, the average delay of links i, j at time t can be approximated as

$$M_{ij} = \frac{24\kappa}{C_{ij} - r_{ij}}. \tag{4}$$

The elderly service function is the characteristic attribute of the elderly facilities, and different service contents and forms of action are generated by different service functions of various facilities, which in turn clarify the service targets, service scope, and spatial level. The senior care service system under the concept of mutual aid senior care should be based on the principles of "continuous care" and "precise configuration" to provide precise and applicable senior care services for the elderly with different physical conditions and different senior care needs. As a spatial entity, senior care facilities need to be built and landed, so the support of space and environment is indispensable. The site selection and spatial layout of various facilities should take full consideration of the building environment and its surrounding influencing elements, and the physical construction should be carried out in an orderly manner under the condition that the environment meets the construction conditions. The construction of senior care facilities under the concept of mutual aid senior care should consider the undertaking with the mutual aid senior care mode and meet the requirements of use. The input supply of the facility determines the starting point and height of the facility construction, and the implementation of the construction determines the input-output efficiency and the actual supply efficiency of the facility. In the past, the supply of rural public products depended on the government's financial allocation and villagers' self-financing, and the pressure of local finance and limited rural economy led to the limited capital investment in rural senior care facilities. Therefore, under the concept of mutual aid elderly care, the main body of input supply should be innovated to improve the input-output efficiency and guarantee the level and quality of facility construction on the ground, as shown in Figure 2.

The planning, construction, and management of senior care facilities belong to the category of public facilities, which are subject to the supervision and control of several government departments. The management and operation of the facilities after the completion of construction is related to whether the facilities can be used normally and whether the senior care services can be provided. According to the public facility operating body, senior care facilities can be divided into public-run, privately run, public-private, and privately run public facilities, etc. The mutual aid senior care facilities studied in this paper have public welfare attributes, and their management and operation methods need to be innovated to maintain the normal use and operation of the facilities. The elderly care facilities under the concept of mutual aid are different from the traditional elderly care facilities in that the elderly care service mainly relies on the mutual care and companionship among the elderly and the voluntary service of social forces, and the service quality is more subject to the maintenance of emotion, responsibility, and morality, which is unstable. The first benefit is that decentralized uniformity can reasonably save resources, the second benefit is that all can get the service they deserve, and the third benefit is that the quality of the service can be maximized. Therefore, it is necessary to establish institutional guarantee in the actual operation process and properly handle the relationship between emotion and system to ensure the quality of mutual-aid elderly care service level.

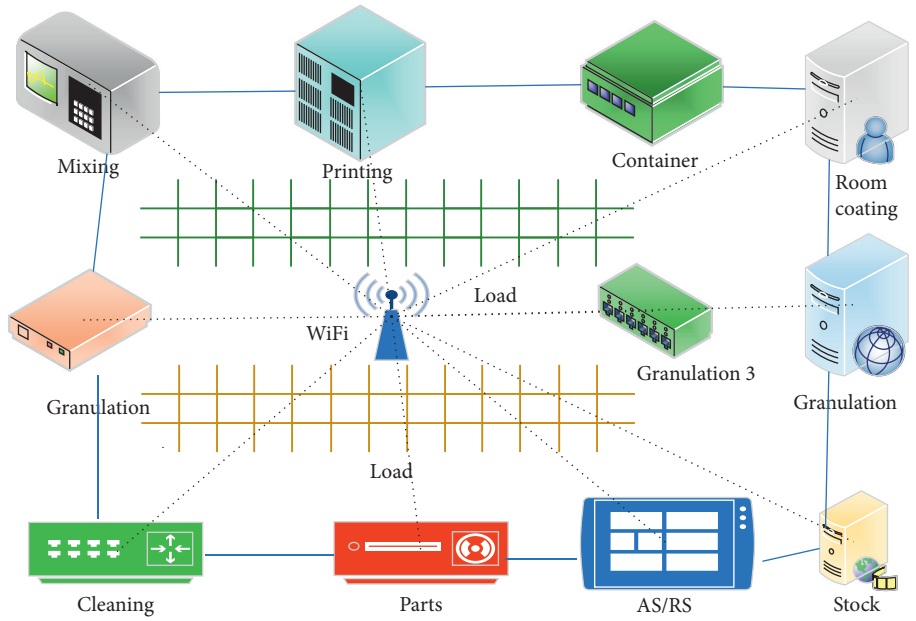

Figure 1: Network topology layout design of medical facilities.

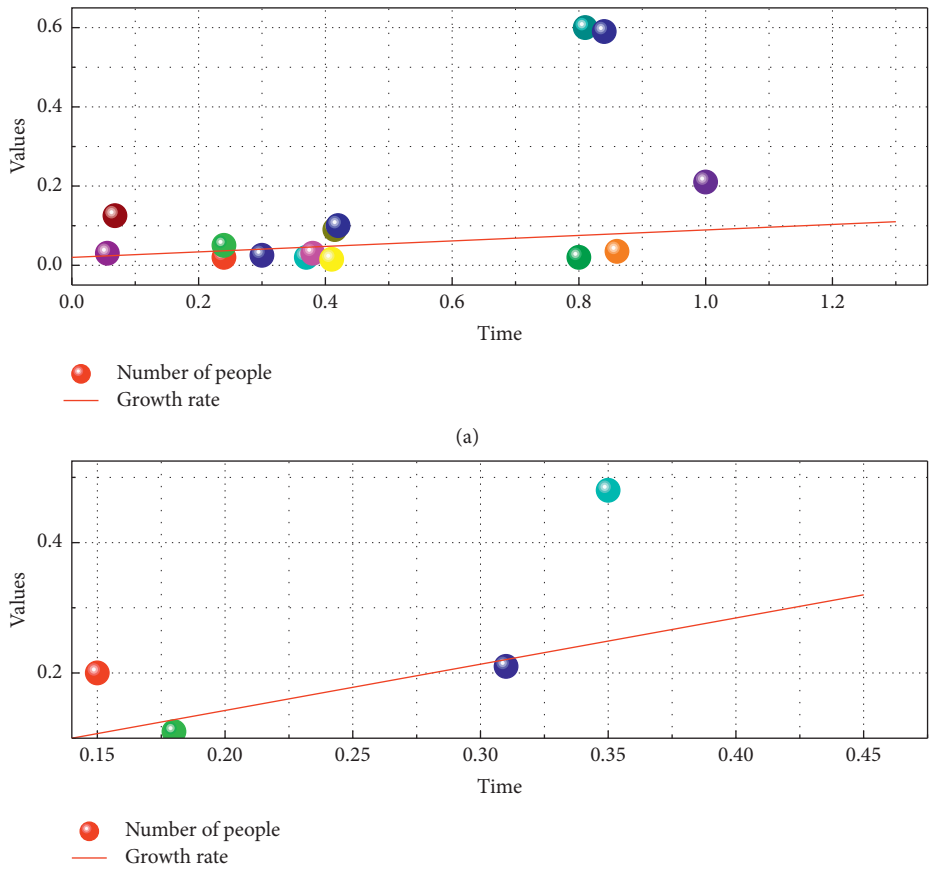

Figure 2: Trends in population change.

From the previous review of the planning research on neighbourhood centres and living circles, it can be seen that the research results of the two studies show different orientations: the research on neighbourhood centres mainly explores several aspects of the neighbourhood centre model, public service facility configuration and community business model, pointing to the supply side of public or commercial services such as government, public sector, and market, while the research on living circles mainly explores several aspects of territorial spatial structure. Although it also points to the supply side, using the circle of life as the theoretical basis means that the research is conducted from the demand side, representing the interests of residents. This orientation also echoes the transformation direction of residential planning-"people-oriented" as the core, community life circle planning oriented to life services. Therefore, the author believes that the neighbourhood centre model can correspond to the supply side and the living circle model to the demand side.

If equations (5) and (6) are established, the receive operation starts to receive partition information from the main process and initializes the subregion flow field.

$$D_1 = w_{11}x_1 + 2w_{12}x_2 + 4w_{13}x_3, \tag{5}$$

$$D_2 = w_{21}x_1 + 2w_{22}x_2 + 4w_{23}x_3. \tag{6}$$

Continuing with the unfinished calculations, the received operational flow field is counted to obtain

$$V(i, j) = \sum_{m,n} I(i + m - 2, j + n + 1) \cdot K(m - 1, n + 1). \tag{7}$$

It was found that the activity preferences of different older people in rural areas in southern Jiangsu showed common characteristics and individual differences. In terms of common characteristics, we found that most of the elderly in rural areas prefer to gather and communicate in crowded places, tend to do activities according to their interests and preferences, and show a higher enthusiasm for interaction than middle-aged people, and show a preference for solitude in semi-public spaces due to their questioning and resistance to external things. In terms of individual differences, it was learned during the visit that the elderly in rural areas of southern Sudan would keep working and insist on self-support as long as they were healthy, and their conditions permitted. The purpose of the study is to maximize the homogeneity of public service areas and populations, and to provide people with the most equal access to services. In the survey on daily activities, most of the elderly still need to do housework, farming, and other physical labour; daily leisure activities are mainly focused on watching TV, planting flowers, board games, and chatting, and cultural and recreational activities are relatively monotonous. Many villages have organized relatively good cultural and recreational activities, but the elderly also expressed little interest.

3.2. Geriatric Care Design. The family model of elderly care based on blood ethics has a long history, where children are the main providers of resource support for elderly care, responsible for the elderly's food, living, and spiritual care. The economic and social characteristics of the countryside dictate that elderly people rely mainly on their children to solve their senior care needs, which is one of the factors that most elderly people choose to age in the family. During the research, it was found that the elderly interviewed were most concerned about two major issues: the first was the difficulty in taking care of themselves due to old age and declining physical functions; the second was that the elderly were mostly worried about the difficulty in getting timely medical treatment when no one was around in case of physical emergencies or emergencies. Some elderly people say that they have limited daily communication partners and monotonous leisure activities, and they are often lonely and despondent. All in all, the needs of senior care, health protection, and spirituality in the family aging method are highlighted. The reason for this is that the population in rural areas of southern Jiangsu is very mobile, and the number of empty nesters is gradually increasing as the family structure becomes smaller and more "nucleated," and the spatial distance makes it more difficult for children to take care of the elderly, and the traditional intergenerational support model is changing. The traditional intergenerational support model has changed and the support from children has weakened, making it difficult to guarantee the quality of elderly care in rural families. Empty nest families and elderly people living alone are more likely to have a lonely mentality, and elderly people who cannot take care of themselves without the company of their children are at risk for their health and safety.

According to the unified deployment of the district committee and the district government, the district major project office shall integrate all forces, rationally arrange functions, and coordinate the coordination, scheduling, promotion, supervision, and management of project construction services. It is necessary to adopt an effective project classification and packaging method, division of labor and responsibility, and step-by-step implementation. Social investment, government investment, and competition for funds are three types of packaging methods for large projects. At the same time, it is necessary to coordinate the project management with the District Transportation and Urban Development Bureau, the District Water Conservancy Bureau, the District Education Bureau, and the District Commerce and Food Bureau.

The community-based elderly care model, also known as home care, where the main supply of elderly care resources in the community and the elderly live at home and receive relatively professional home care services or choose community care services, has played a good role in urban areas. However, even in the economically developed rural areas of southern Jiangsu, only 11% of the elderly people chose community aging, mainly because they could receive care without leaving their familiar living environment. The main reasons why the elderly do not prefer community-based senior care are that they can take care of themselves, they do not have time for farming, the cost, they must take care of their grandchildren, and they do not know about it because it

is not very popular. In rural areas, the concept of community is different from that of modern urban communities, and the organization and construction of a community-based senior care model are still in their infancy in rural areas. Factors such as limited resource conditions, lack of professional caregivers, capital and facilities, and the fact that an efficient management system has not yet been established all make the community-based elderly care model currently unavailable in rural areas of Southern Sudan, as shown in Figure 3.

All-age livable communities are urban communities for all people of all ages to live in and live in for life. It is different from traditional urban retirement communities that isolate the elderly as a special group, but treats them equally as people of other ages, thus achieving the development of integrated social intergenerational relationships. The intergenerational relationship usually refers to the interpersonal relationship between the elderly and young people, which can occur both in the family and within the society. The development of intergenerational groups, such as the elderly and young people, is often fragmented, and the increasing miniaturization of family size makes it difficult to meet the needs of intergenerational emotional exchange, knowledge exchange, and life assistance. Localized senior care facilities should take up the social responsibility of building an all-age living environment in the community while focusing on the care of the elderly.

In line with the construction concept of integration with urban communities, setting up a regional exchange space within a regionalized senior living facility creates opportunities for people from different generations to meet and communicate. The elderly in the community not only act as a one-way care recipient but also share their life experience and skills with other groups such as young people and children. As with the German "multigenerational house" concept, many retired seniors in the community have expressed their willingness to serve other intergenerational groups who join the facility on a voluntary and pro bono basis, and youth groups in the community are willing to participate in the "multigenerational house" program. First, it is close to public spaces and soft partitioning. This allows for a large open space that can accommodate all the elderly in the facility to organize large events. Secondly, it is combined with the public space. In the case of limited public space, it can be combined with the dining room, rehabilitation training area, or unit living room to achieve multi-functional use of space and more efficient facility management. Separate from other public spaces of the facility, it has the least impact on the normal operation of other functions, as shown in Figure 4.

The elderly in the community can enjoy health management services at the community health service centre where they live, specifically involving free health check-ups (including general physical and auxiliary examinations), lifestyle and health status assessments, and the resulting establishment of a network health file [21]. At the same time, the territorialized elderly facilities implanted in the community can also collect various types of information on the elderly in the community containing their health status, economic status, living condition, and willingness to provide elderly services while providing services. On this basis, both parties can further improve the information within the community health management platform for the elderly. Based on the real-time access to the health status of the elderly in the management platform, the community primary medical institutions can make reasonable and effective treatment plans for them, and enable the elderly to detect diseases early and carry out treatment early, to prevent the development of diseases and reduce the disability and death rates; after obtaining the health records of the elderly provided by the community health service centre, the elderly facilities can also use them to guide and optimize the facilities' care services for the elderly. The health records provided by community health service centres can also be used to guide and optimize the content of care services tailored to individual elderly people, thus improving the accuracy of service positioning and the economy of operating costs.

Most of the existing buildings have a series of problems such as poor structural stability, the mismatch between the existing structure and new functional use, and limitation of transformation diversity due to age and disrepair, failure to consider future transformation flexibility at the beginning of construction, and other factors. Therefore, the main structure optimization should be implemented based on the overall composite seismic performance of the reinforcement treatment, mainly using the paste steel plate (steel components) and other dry construction methods for seismic reinforcement. The principle of paste steel plate reinforcement method is to use adhesive to paste the steel plate on the surface of the original member so that the steel plate and the original structure form a new bearing system, and the steel plate is involved in the force, to achieve the purpose of reinforcing the concrete structure. Due to the development level of rural areas in southern Jiangsu and the traditional concept of rural elderly people, community and institutional retirement are usually not widely recognized and accepted by rural elderly people and are usually not the ideal choice. With the continuous population migration, the population structure will gradually evolve towards advanced aging, and the situation will be more severe. The economic and social conditions and the construction level of rural areas in southern Jiangsu are limited, and their elderly care foundation is relatively weak. It is imperative to innovate the elderly care model and explore new paths for elderly care in the current context. The mutual help elderly care model has been explored in different forms in different parts, and the current development is widely accepted by the elderly and their families, and the development trend is good, which is an effective elderly care model.

4. Analysis of Results

The level of construction of community service support is significantly related to the region. Old urban areas have been built for a long time, and the development of various service facilities is relatively complete, while new urban areas and

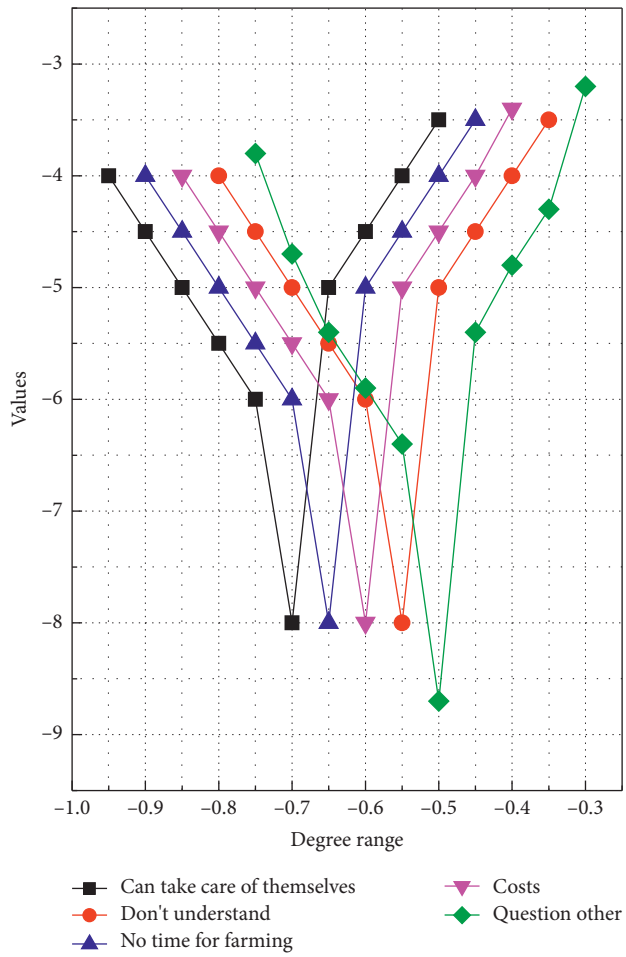

(a)

Figure 3: Continued.

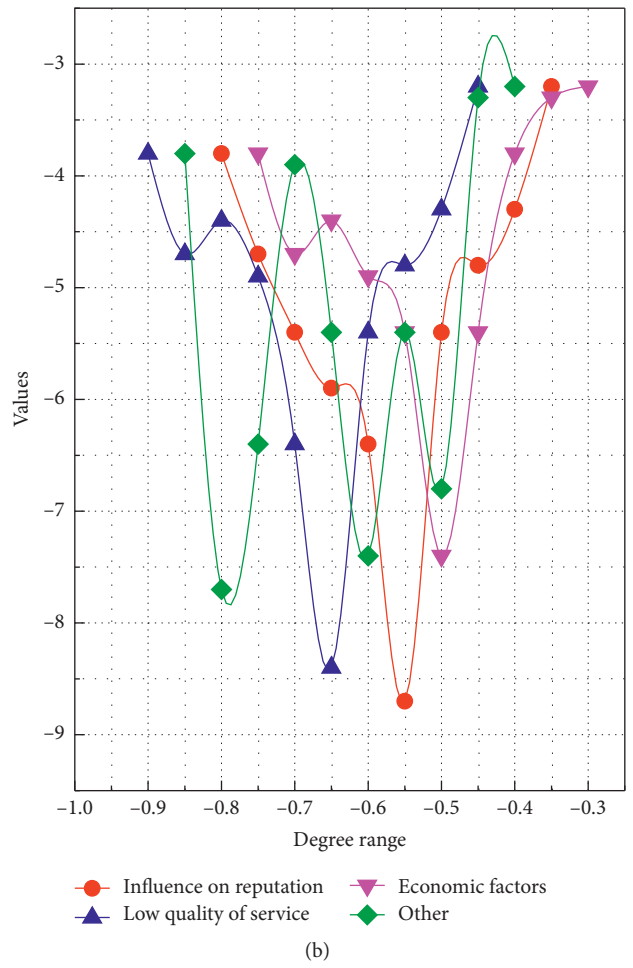

Figure 3: Distribution of reasons for old-age maintenance.

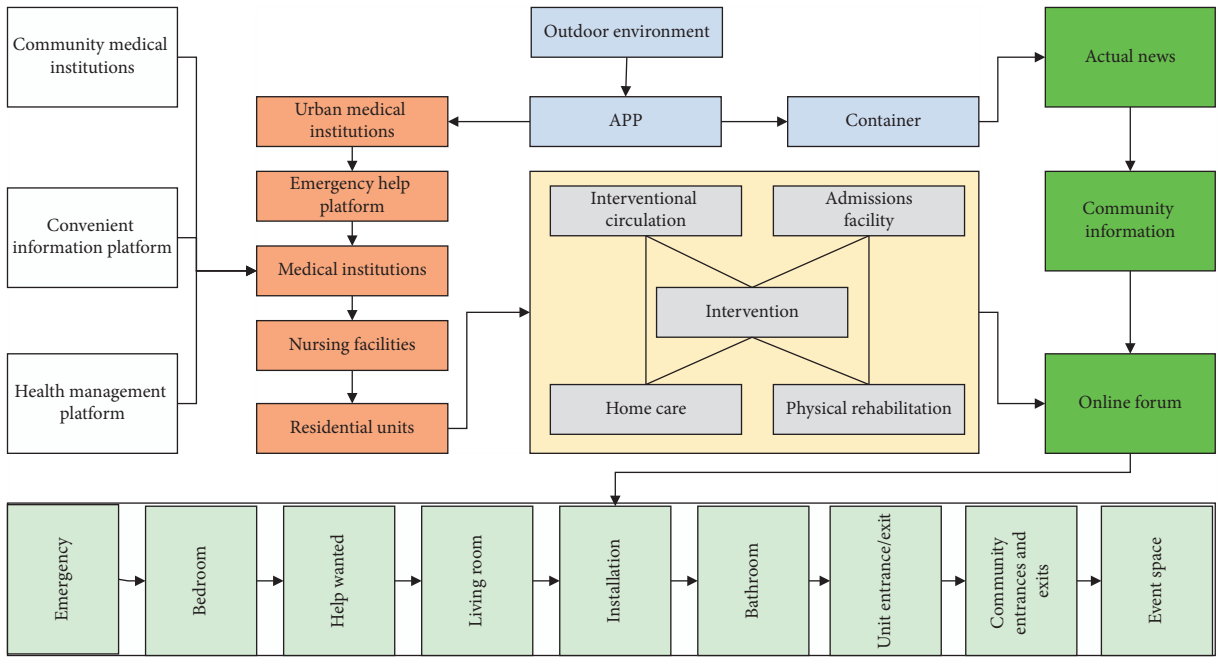

Figure 4: Construction of network information platform for senior care facilities.

urban fringe areas are lagging in the construction of service support due to factors such as short construction time and distance from the city centre. Therefore, no matter from the total score of community services in each region or the score of public and commercial services in each region, the old city communities are far more than the communities in the other two types of regions in terms of score. However, through field research and visits, it is found that the old city also has problems such as overpopulation, shortage of land, the aging physical environment of service facilities, and limited space for landing and expansion of new service facilities, as shown in Figure 5.

However, at the same time, the living space differentiation makes the shared use of service facilities a major difficulty. For example, commercial houses are located close to urban villages, and commercial houses adopt fully closed management, so the service facilities located inside the community are only open for use by the residents of the community, which is not conducive to improving the efficiency of the facility utilization, increasing the difficulty and pressure of facility supply, and even easily sowing the hidden danger of social differentiation. Moreover, the large scale of the neighbourhood is also the reason for the lack of sharing of community service facilities, such as the closed neighbourhoods in the form of commercial houses. The large scale of the neighbourhood means that there is not enough space for roads and alleys, and there is a lack of space for service facilities, especially commercial service facilities, and the service facilities are clustered in blocks to form small-scale service circles, and the service scope only involves the surrounding small-scale residential areas. However, according to the research and interviews, it has the problem of attaching importance to the construction of street-level facilities but not enough community-level facilities. The number of facilities within the boundary is much higher than the number of facilities within the community. The community-level facilities can better take care of the needs of the elderly, children, the disabled, and other disadvantaged groups for short-time travel and convenient use, better meet the sense of service access and experience of community residents, and are more conducive to service sharing and neighbourhood construction within the community. Therefore, it is necessary to focus on the construction of community-level service facilities in the hierarchical setting of service facilities.

As Figure 6 shows the evaluation chart, unlike other public service facilities, in the East Lake Scenic Area, the community coverage rate of parks and green squares and the coverage rate of the elderly population both reach 100%, and the elderly population has sufficient space for activities. Also, the highest area only reached 73.80% and 75.70%, while the lowest area, Jingkai, only reached 38.46% and 59.68%, leaving much room for improvement. Development coordination index: there are five zones higher than 1, including 1.36 points in the East Lake Scenic Area zone, and the lowest 0.36 in the Jingkai zone. The overall imbalance index is 3.95, which is the lowest among all facilities because each park green space in the East Lake Scenic Area covers a larger area, but there are not many of them, so the gap is not widened.

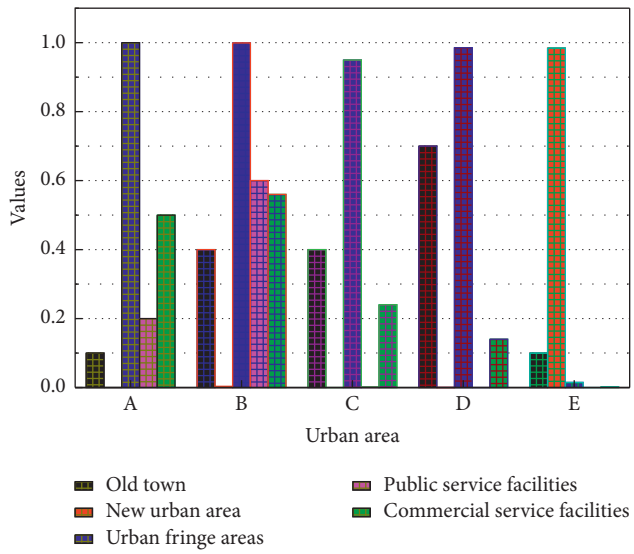

Figure 5: Total score of community service support by region.

From a horizontal perspective, summarizing the basic data of each street, extra-large senior care facilities can serve only 4 settlements, and small and medium-sized senior care facilities can serve 19 and 18 settlements, respectively, which shows that the distribution equity of extra-large senior care facilities is the worst; through the visualization results, we can find that extra-large senior care facilities provide a large amount of effective service area of senior care facilities for the settlements they serve, thus with the settlements that cannot be served. There is a huge quantitative difference; medium-sized senior care facilities provide the widest service coverage for the region, with 50% of the residences being served by more than half of the effective service area of medium-sized senior care facilities; small senior care service facilities provide relatively fewer services overall, but in some residences, they perform better in terms of the effective service area provided compared to medium-sized senior care facilities. The remaining settlements have one or two types of facilities to choose from, as shown in Figure 7. Among them, the residents of Hexing Road Street have the highest service area per capita of 19.22 m^2/person, while the residents in Lujia Street have the lowest, with only 1.06 m^2/person.

At the same time, it is suggested that the centrally located facilities can improve the accessibility of senior care services through door-to-door mutual aid services, improved transportation conditions, and shuttle bus transportation services so that the senior care services in administrative villages can radiate to natural villages and natural village senior care services can radiate to residential groups, forming a full-coverage network system of rural senior care facilities, especially for the aging villages where the land is sparse; this way can effectively expand the coverage of senior care facilities. Establishing a comprehensive mechanism for expressing social interests and guiding the masses to express their interest demands in a rational and legal form is the primary link to improve the coordination mechanism for social interests. To establish a perfect mechanism for expressing interests, it is necessary to give full play to the

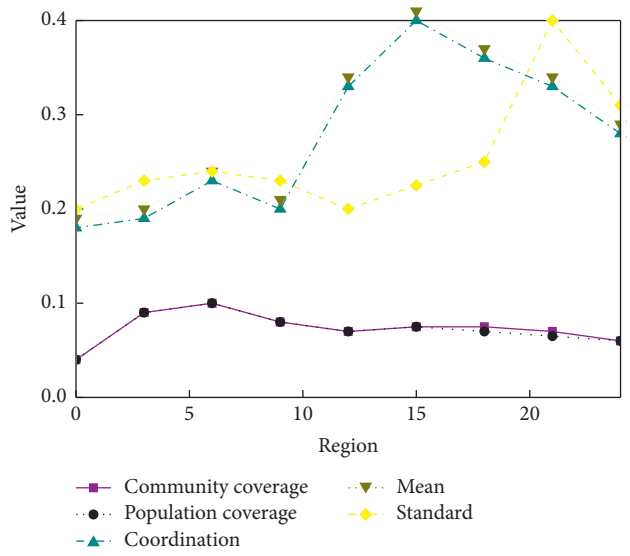

Figure 6: Coverage and coordination statistics.

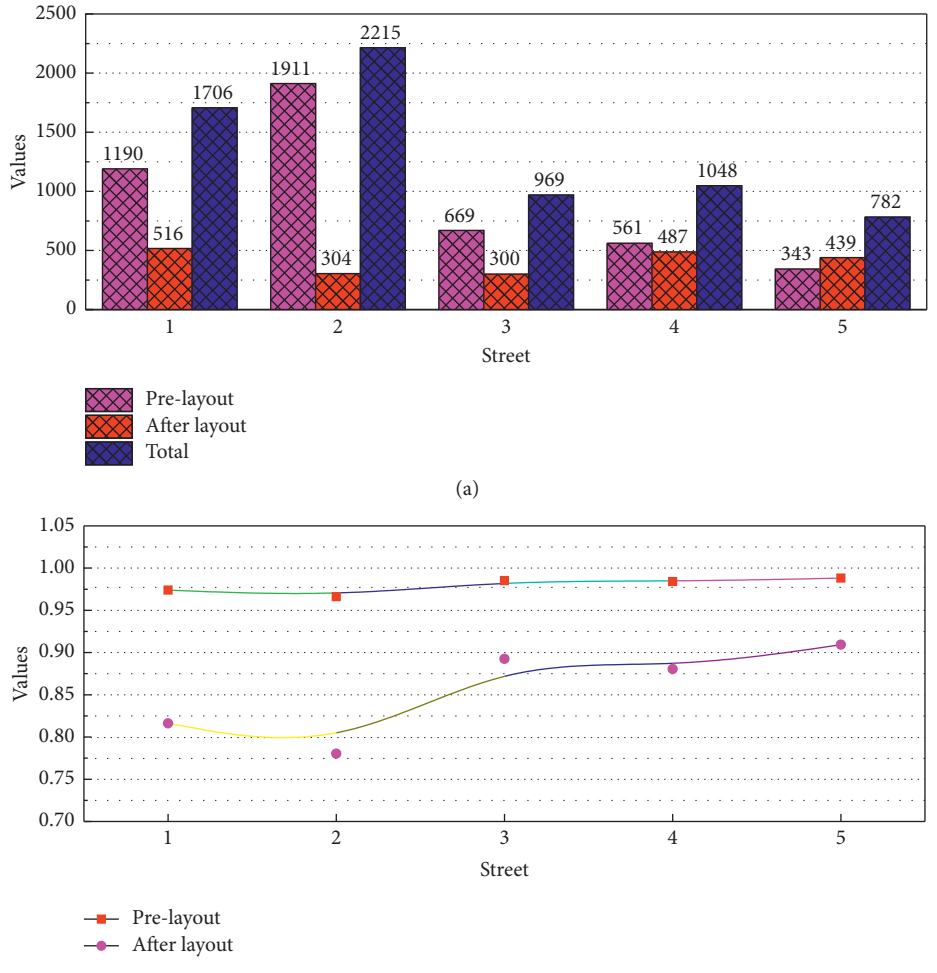

Figure 7: Distribution of effective service area of each level of elderly facilities on a street scale.

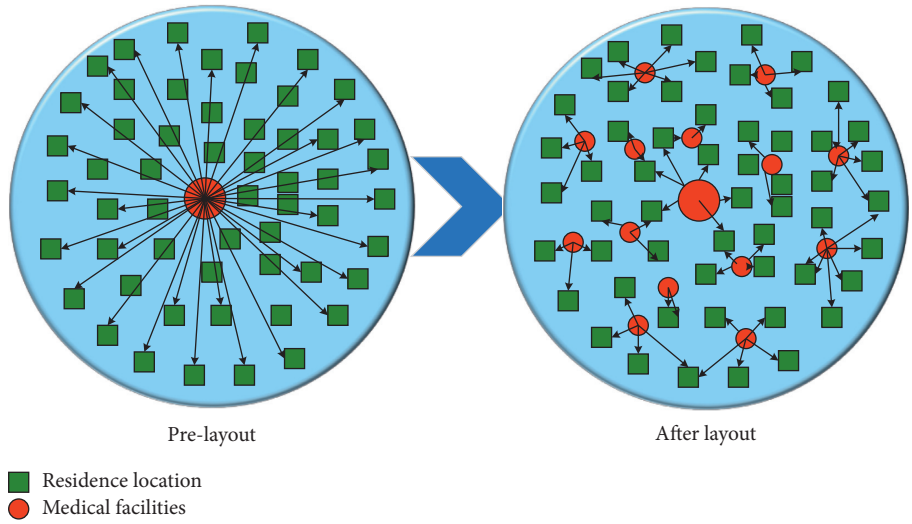

Figure 8: Changes in spatial layout distribution.

functions of existing channels for expressing interests and to open new channels for expressing interests according to the development and changes of interest groups. The coverage area of senior care facilities can be effectively expanded, especially for the aging villages with sparse land. The spatial layout of senior care facilities under the concept of mutual aid senior care should be flexible and precise and should not be limited to the establishment of a standard system but should take the integration with actual needs as the first factor. Rural areas can be flexibly laid out and set up under the premise of satisfying the site selection requirements and the needs of the elderly and the reasonable use of resources. The following are some suggestions for the layout of administrative villages, natural villages, and residential groups for elderly facilities, as shown in Figure 8.

Also, cultivating a free and democratic social atmosphere and constructing a perfect interest expression and feedback mechanism in the current urban-rural context can help strengthen the basic right to survival and development of rural residents, as well as improve the human living environment, maintain social stability, and guarantee the rational political participation of villagers. The available rural locations have many options and are also less expensive compared to urban areas, so they are easier to layout. Guiding rural residents to rationally and accurately express their actual needs, give feedback on the effectiveness of construction, and expand the depth and breadth of public participation can not only assist the government in strengthening the accuracy of decision-making, but also help alleviate social conflicts, coordinate the balance of interests, and stimulate rural residents' enthusiasm to participate in the construction and enhancement of public utilities, as well as promote the development of rural planning and construction in a scientific and rational direction. In terms of configuration standards, a flexible and adaptable allocation standard system is proposed for the use characteristics of various types of elderly facilities, optimizing the "one-size-fits-all" mechanical allocation means and making up for the gaps in the basis for the allocation of elderly facilities. In terms of spatial layout, it breaks the solidified idea of centralized layout mode and adopts the embedded layout mode of "large centralized and small scattered," which improves the effective coverage and service accessibility of the facilities and creates convenient conditions for the elderly to use. In terms of mechanism guarantee, the innovative organization and operation mechanism expands the sources of support for the elderly, relieving the pressure of the government's one-dollar supply and the dilemma of the weak rural elderly foundation; by improving the interest expression and feedback mechanism, the interaction between the villagers and the government and the planners and builders is promoted, and the accuracy of the facility supply and the timeliness of the feedback of the construction effectiveness is enhanced; by establishing the information management service platform, the comprehensive elderly care cost is reduced and the level of the facility service and management is improved. At the same time, it improves the service level, management efficiency, and supervision of the facilities.

5. Conclusion

There are certain correlations and differences in planning research and planning practice, and both are important as models of community service support in terms of their supply and demand. Neighbourhood centres and living circles hold different positions. Neighbourhood centres are a coordinated means for planning elites, city managers, and service providers to provide quality public and commercial services to urban communities, and their paths are top-down planning conduction, focusing more on the supply side; living circles, on the other hand, are concepts introduced into the planning community from geography, which are essentially behavioural space planning, and the subject of behavioural activities is people. The core of the living circle model is people-oriented, starting from the daily activities and living needs of urban residents, and its path is a bottom-up expression of demands, with more emphasis on the demand side. The construction mode of the "new

neighbourhood centre" needs to clarify the new characteristics of the neighbourhood centre in the context of the living circle, and there is an interactive relationship between the neighbourhood centre and the living circle. The connotation and scope of application of the new neighbourhood centre have been expanded. Neighbourhood centres can organize spatial elements in an integrated manner and become a platform or carrier for the coordination and co-construction of multiple parties; adopting a differentiated spatial organization and construction mode, neighbourhood centres adopt a mixed, composite, and shared spatial organization, corresponding to "functional building clusters," "one-stop complexes," "one-stop complexes," "one-stop complexes," and "one-stop complexes." The construction modes of "one-stop complex" and "embedded service space" are adopted; diverse types of functional combinations are adopted, such as medical and health care, cultural and sports, commercial, comprehensive, and innovative neighbourhood centres.

Data Availability

Data sharing is not applicable to this article as no datasets were generated or analysed during the current study.

Conflicts of Interest

The authors declare that there are no conflicts of interest.

Authors' Contributions

Rui Liu and Miao Du contributed equally to this work.

References

[1] S. Chandra, A. Chandra, and R. Gupta, "An efficient data routing scheme for multi-patient monitoring in a biomedical sensor network through energy equalization strategy," *Wireless Networks*, vol. 27, no. 1, pp. 635–648, 2021.

[2] G. G. Carpio, "Racial projections: cyberspace, public space, and the digital divide," *Information, Communication & Society*, vol. 21, no. 2, pp. 174–190, 2018.

[3] C. Hailey, "Camping off the grid in the grid: between hospitable space and inhospitable land," *Public*, vol. 31, no. 61, pp. 36–89, 2020.

[4] I. Sobron, J. Del Ser, I. Eizmendi, and M. Vélez, "Device-free people counting in IoT environments: new insights, results, and open challenges," *IEEE Internet of Things Journal*, vol. 5, no. 6, pp. 4396–4408, 2018.

[5] S. Riadi, S. Triono, S. Syahril, and D. Nofriansyah, "Effectiveness of metcaognitive learning's model in engineering," *International Journal of Engineering and Advanced Technology (IJEAT)*, vol. 9, no. 1, pp. 4438–4443, 2019.

[6] A. Di Nardo, M. Di Natale, C. Giudicianni, R. Greco, and G. F. Santonastaso, "Complex network and fractal theory for the assessment of water distribution network resilience to pipe failures," *Water Supply*, vol. 18, no. 3, pp. 767–777, 2018.

[7] A. Elsts, X. Fafoutis, P. Woznowski et al., "Enabling healthcare in smart homes: the SPHERE IoT network infrastructure," *IEEE Communications Magazine*, vol. 56, no. 12, pp. 164–170, 2018.

[8] N. Guo, P. Guo, J. Shang, and J. Zhao, "Project vulnerability analysis: a topological approach," *Journal of the Operational Research Society*, vol. 71, no. 8, pp. 1233–1242, 2020.

[9] A. Onasanya, S. Lakkis, and M. Elshakankiri, "Implementing IoT/WSN based smart Saskatchewan healthcare system," *Wireless Networks*, vol. 25, no. 7, pp. 3999–4020, 2019.

[10] A. Di Nardo, M. Di Natale, A. Di Mauro et al., "An advanced software to design automatically permanent partitioning of a water distribution network," *Urban Water Journal*, vol. 17, no. 3, pp. 259–265, 2020.

[11] K. A. Ngowi, "Measuring geographical accessibility to healthcare facilities in peri-urban dwellers in Mbeya city, Tanzania," *MUST Journal of Research and Development*, vol. 1, no. 5, p. 15, 2021.

[12] G. Shabbir, A. Akram, M. M. Iqbal, S. Jabbar, M. Alfawair, and J. Chaudhry, "Network performance enhancement of multi-sink enabled low power lossy networks in SDN based Internet of Things," *International Journal of Parallel Programming*, vol. 48, no. 2, pp. 367–398, 2020.

[13] J. J. P. C. Rodrigues, H. Wang, S. J. Fong, N. Y. Philip, and J. Chen, "Guest editorial: Internet of Things for in-home health monitoring," *IEEE Journal on Selected Areas in Communications*, vol. 39, no. 2, pp. 295–299, 2021.

[14] D. Zulli, M. Liu, and R. Gehl, "Rethinking the "social" in "social media": insights into topology, abstraction, and scale on the Mastodon social network," *New Media & Society*, vol. 22, no. 7, pp. 1188–1205, 2020.

[15] L. Zhang, T. Zhao, and L. Rong, "Construction of public service facilities layout network in pastoral areas based on psychological cognition range information-a case study of Inner Mongolia pastoral areas of East Wuzhumuqin Banner in Xilingol," *European Journal of Remote Sensing*, vol. 53, no. 1, pp. 114–125, 2020.

[16] L. Capacci and F. Biondini, "Probabilistic life-cycle seismic resilience assessment of aging bridge networks considering infrastructure upgrading," *Structure and Infrastructure Engineering*, vol. 16, no. 4, pp. 659–675, 2020.

[17] H. Nazarnia and H. Sarmasti, "Characterizing infrastructure resilience in disasters using dynamic network analysis of consumers' service disruption patterns," *Civil Engineering Journal*, vol. 4, no. 10, pp. 2356–2372, 2018.

[18] S. Ornes, "Science and culture: can the principles of topology help improve the world's slums?" *Proceedings of the National Academy of Sciences*, vol. 116, no. 20, pp. 9686–9689, 2019.

[19] S. Bhalaik, A. Sharma, R. Kumar, and N. Sharma, "Performance modeling and analysis of WDM optical networks under wavelength continuity constraint using MILP," *Recent Advances in Electrical & Electronic Engineering (Formerly Recent Patents on Electrical & Electronic Engineering)*, vol. 13, no. 2, pp. 203–211, 2020.

[20] M. M. Mansour, S. Yamamoto, and H. Kanaya, "Reconfigurable multistage RF rectifier topology for 900 MHz ISM energy-harvesting applications," *IEEE Microwave and Wireless Components Letters*, vol. 30, no. 12, pp. 1181–1184, 2020.

[21] S. M. Shimly, D. B. Smith, and S. Movassaghi, "Experimental analysis of cross-layer optimization for distributed wireless body-to-body networks," *IEEE Sensors Journal*, vol. 19, no. 24, pp. 12494–12509, 2019.